Technische Universität München

WACKER-Lehrstuhl für Makromolekulare Chemie

# Development of Efficient Catalysts for the $CO_2$/Epoxide Copolymerization Reaction

**Stephan Klaus**

Vollständiger Abdruck der von der Fakultät für Chemie der Technischen Universität München zur Erlangung des akademischen Grades eines

**Doktors der Naturwissenschaften**

genehmigten Dissertation.

| | | |
|---|---|---|
| Vorsitzender: | | Univ.-Prof. Dr. Kai-Olaf Hinrichsen |
| Prüfer der Dissertation: | 1. | Univ.-Prof. Dr. Dr. h.c. Bernhard Rieger |
| | 2. | Univ.-Prof. Dr. Fritz E. Kühn |

Die Dissertation wurde am 14.06.2011 bei der Technischen Universität München eingereicht und durch die Fakultät für Chemie am 11.07.2011 angenommen.

## Danksagung

An dieser Stelle möchte ich mich insbesondere bei Herrn Prof. Dr. Dr. h.c. Bernhard Rieger für die Möglichkeit bedanken, dieses aktuelle, spannende und herausfordernde Promotionsthema bei ihm zu bearbeiten. Ich danke Ihnen für die zahlreichen Diskussionen, hilfreichen Ideen, das große Vertrauen und die gelassene Freiheit, welche mir bei der Bearbeitung dieses Themas stets geholfen haben. Außerdem für die Fähigkeit, Potentiale zu entdecken und einen an den richtigen Stellen zu fördern.

Herrn Dr. Carsten Troll möchte ich für die stets tatkräftige Unterstützung danken, bei Problemen jeglicher Art zu Rat und Tat zu stehen und mit fachlichen Ratschlägen die Arbeit aufzuwerten. Außerdem natürlich all seinen Einsatz dafür, dass der Lehrstuhl stets am Laufen gehalten wird und eine tolle Atmosphäre besteht.

Danke auch an Dr. Sergei Vagin und Dr. Carly Anderson für ihre exzellenten fachlichen Hilfestellungen und die tatkräftige Unterstützung beim Schreiben von Publikationen, sowie all ihr Einsatz für den Lehrstuhl.

Meiner Laborkollegin Naïma Hutter für die tolle und entspannte Atmosphäre im Labor und die vielen lustigen Momente. Natürlich auch allen anderen Stammgästen, die uns mit ihren stetigen Besuchen, Diskussionen und Scherzen auf Trab und bei Laune gehalten haben. Den Labornachbarn, insbesondere Carly Anderson, Timo Anselment, Stefan Weidle und Dominik Lanzinger für ihre Unterstützung, die vielen negativen Bananen, Eisbären und unglaublich abstruse Unterhaltungen und Gedankengänge. Maximilian Lehenmeier und Stefan Kissling, sowie Anna Ott und Peter Deglmann für eine tolle Atmosphäre im Projektteam. Uwe Seeman, Robert Reichardt und Michael Reif und natürlich allen anderen Makros aus dem Lehrstuhl, die stets dafür gesorgt haben, dass man sich auf der Arbeit wohl fühlt.

Meiner Mutter für ihre stetige Unterstützung und dass sie mir immer den Rücken frei gehalten und sich über die Meinung anderer immer hinweg gesetzt hat.

Allen meinen Freunden, die mich im Laufe der letzten Jahre unterstützt und motiviert haben, insbesondere Christian Jung und Christian Mertens für die langjährige Freundschaft, Rebecca Mpe Wirries für ihre unglaubliche Unterstützung und Durchhaltevermögen. Ohne Euch wäre diese Arbeit für mich nicht möglich gewesen.

# 1. Introduction*

## 1.1. Carbon Dioxide Activation into New Products

Crude oil remains the most important chemical feedstock of our times. The importance of fossil fuel resources for mankind becomes clear when its broad areas of usage are fully considered. The utilization of crude oil ranges from energy carrier (fuel) to a suppliant for carbon-containing molecules used in chemical synthesis and as building blocks for polymeric materials. At current rates of consumption, worldwide crude oil reserves are rapidly depleting, thus emphasizing the importance of alternative, renewable carbon-based sources for raw materials.[1-4]

One possible source is $CO_2$, which is released in many combustion processes and is (alongside methane) considered as a main contributor to the so-called Greenhouse Effect.[5-8] Current global $CO_2$ emissions are estimated to exceed 30 billion tons each year.[9] One long considered strategy to reduce atmospheric $CO_2$ content is CCS (Carbon Capture and Storage), which is assumed to considerably diminish the $CO_2$ concentration *via* storage.[10-12] Intense research activities in this area indicate promising results in near future, however the thought of retaining huge $CO_2$ reservoirs is not very appealing. As global warming is thought to principally result from excessive combustion of fossil fuels, emphasis should be placed upon restricting $CO_2$ emissions rather than processing excess $CO_2$ after its generation. Independent of such environmental considerations, the chemical utilization of excess $CO_2$ is an important topic.

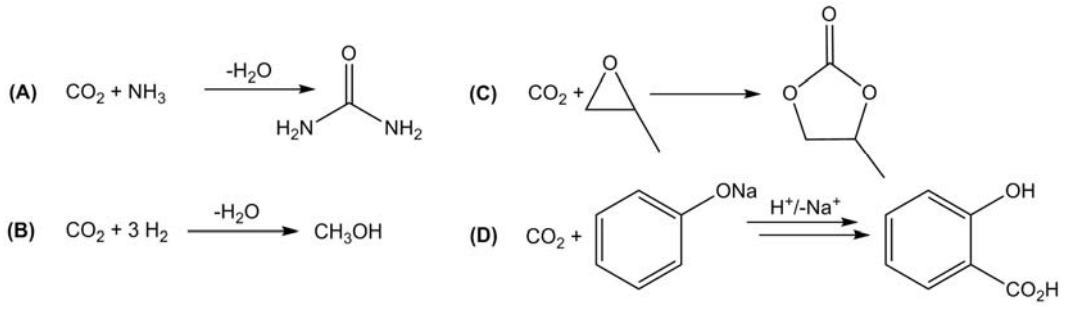


**Scheme 1.** Utilization of $CO_2$ as a C1-feedstock for chemical reactions; A: synthesis of urea (146 x $10^6$ t/a); B: methanol (6 x $10^6$ t/a); C: cyclic carbonate (0.040 x $10^6$ t/a), D: salicylic acid (0.060 x $10^6$ t/a)[13-15]

* This introduction and the Chapter Catalyst Systems for $CO_2$/Epoxide Copolymerization have been published with slight variations in the special issue "Industrial Chemistry" of Coordination Chemistry Reviews.[16] By courtesy of Elsevier.

A significantly more meaningful strategy is the utilization of abundant, non-toxic and non-flammable $CO_2$ as a C1-feedstock for chemical reactions,[13-15, 17-19] however the thermodynamic stability of $CO_2$ has thus far precluded its usage as widespread chemical reagent. Methods to overcome the high energy barriers are based upon reduction, oxidative coupling with unsaturated compounds on low valency metal complexes and increasing electrophilicity of the carbonyl carbon.[20-21] Specifically, the reaction of $CO_2$ with highly reactive substrates, such as epoxides, affords valuable materials which can be produced on industrially relevant scales.[22-26]

The use of $CO_2$ as a chemical feedstock will never be able to compensate emission-based $CO_2$, however this strategy potentially provides access to high-value products from a non-toxic, renewable and low-cost resource. Current examples of the industrial utilization of $CO_2$ include the large-scale production of urea, salicyclic acid and several carbonate-based materials (Scheme 1). A further large-scale industrial application of $CO_2$ potentially lies in the production of the biodegradable thermoplastics poly(propylene carbonate) (PPC, Scheme 2A) and poly(cyclohexene carbonate) (PCHC, Scheme 2B).

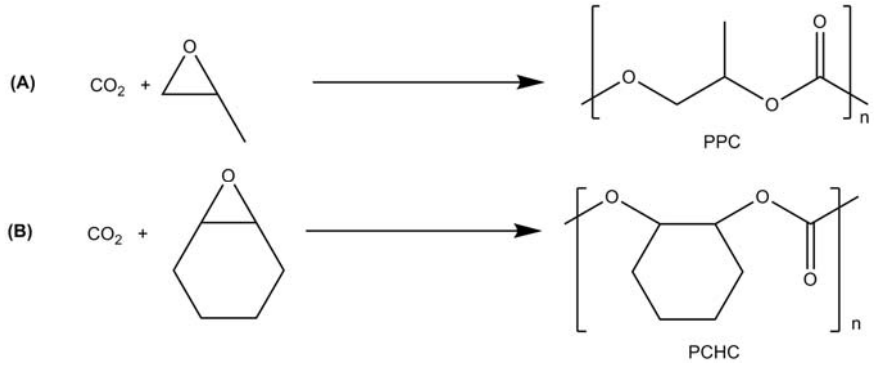


**Scheme 2.** Alternating copolymerization of propylene oxide (PO) (A) and cyclohexene oxide (CHO) (B) with $CO_2$.

The usage of $CO_2$ in this manner could substitute the environmentally malign industrial synthesis involving polycondensation of *trans*-diols (*e.g. Bis*phenol-A) with highly toxic phosgene by utilizing the energy rich three-membered, highly ring-strained oxiranes to react with $CO_2$.

The outstanding properties of polycarbonates such as strength, lightness, durability, biodegradability, heat resistance, easy processability, high transparency and good electrical insulation render these materials of high industrial importance with applications in the

automotive, electronics, optical media, glazing and sheeting industries as well as the medical and healthcare sectors.

## 1.2. First Steps in Copolymerization of Carbon Dioxide and Epoxides

The complete historical development of this area has been comprehensively reviewed by others and the interested reader is directed to these publications.[25-32] The copolymerization of $CO_2$ with epoxides has been known since 1969 when Inoue *et al*. combined $ZnEt_2$, water, $CO_2$ and PO to yield a small quantity of polymeric material.[33-34] The subsequent investigations in this area were frequently frustrated by low catalytic activities and the formation of undesired by-products such as cyclic carbonates and/or high degrees of ether linkages in the polymer chains. Furthermore, many systems that show polymer formation with the CHO/$CO_2$ system, only yield cyclic carbonate or show no conversion at all with PO/$CO_2$ as monomers.

Shortly after the initial discovery from Inoue *et al.* the effect of dihydric molecules (*e.g.* resorcinol[35], dicarboxylic acids[36] and primary amines[37]) in combination with $ZnEt_2$ was studied on the copolymerization of $CO_2$ and PO. In 1976-77 Kuran *et al.* developed new catalyst systems with trihydric phenols such as pyrogallol and 4-bromopyrogallol.[38-39] The first catalytic observations (PO/$CO_2$) with these systems suggested that monoprotic molecules such as alcohols and secondary amines exclusively yield cyclic propylene carbonate (cPC) whereas di- and tri-protic species yield PPC.[39-43] In order to overcome the low activities generally encountered, Soga *et al.* synthesized the first well-defined heterogeneous catalyst system from a $Zn(OH)_2$/glutaric acid mixture for the copolymerization of $CO_2$ and PO.[41]

The first homogeneous single-site catalyst was developed by Inoue *et al.* in 1986, comprising a tetraphenylporphyrin ligand (tpp) with an aluminum metal center (Figure 1A).[44]

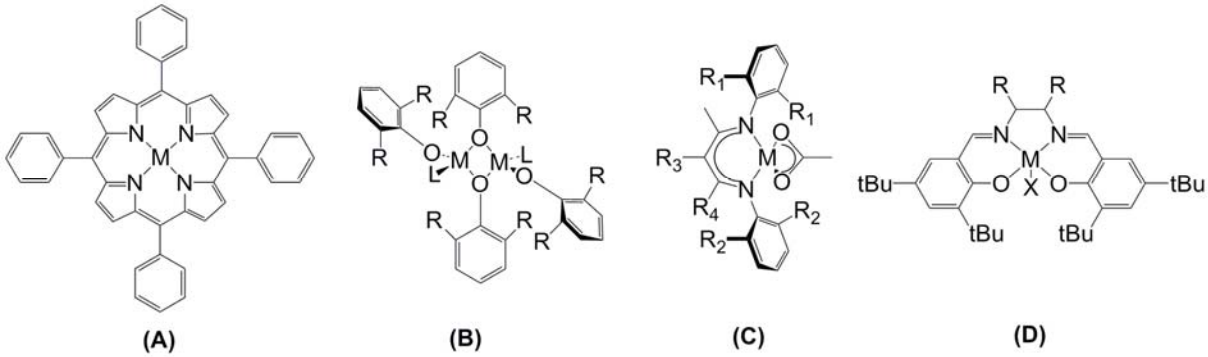


**Figure 1.** Representative homogeneous single-site catalysts for epoxide/$CO_2$ copolymerization (A: porphyrin system, B: phenoxides system, C: β-diiminate system, D: salen system)

In 1995 a series of discrete zinc phenoxide derivatives as catalysts were synthesized by Darensbourg *et al.* These catalysts demonstrated moderate activities for PO/$CO_2$ copolymerization with approximately 10 % polyether content even under high $CO_2$ pressures (55 bar) (Figure 1B).[45-47] With modification of the substituents on the phenoxide ligands, catalytic activities varied only slightly.

The first breakthrough which lead to a more systematic catalyst design was the exploration of β-diiminate zinc catalysts (BDI) in CHO/$CO_2$ copolymerization by Coates *et al*.,[48-49] where minor variations in the electronic and steric character of the BDI ligand framework showed dramatic changes in catalytic activity (Figure 1C). Moreover the BDI catalysts could be tailored to achieve high activities in PO/$CO_2$ copolymerizations.[50] To date, salen-type systems (Figure 1D) have received the most attention for $CO_2$/epoxide copolymerization.[28] All of the above-detailed complex categories will be reviewed in the following chapters.

## 2. **Catalyst Systems for Carbon Dioxide/Epoxide Copolymerization**

The development of active $CO_2$/epoxide copolymerization catalysts resembles in many aspects the early advances in alkene polymerization with the first active catalyst systems being heterogeneous in nature. Although the composition of these heterogeneous catalysts is often ambiguous and the active sites poorly defined, they are nonetheless employed industrially for the production of polycarbonates. Indeed, the majority of commercial PPC is produced with the use of the heterogeneous zinc glutarate system (Chapter 2.2. Heterogeneous Catalyst Systems). In this system, the Zn-Zn distances are typically between 4.6 - 4.8 Å and the variation of these values in homologous catalyst structures is probably reflected in lower activities. This indicates that the spatial distance between two metal centers is crucial for significant copolymerization activity and that the directed design of homogeneous systems containing a defined metal-metal distance would raise observed activity levels.

Whilst there remains an industrial reliance on heterogeneous systems, homogeneous catalysts are still subject to intense study, not least because their soluble nature permits *in-situ* examination of the polymerization mechanisms. It is for this reason that homogeneous catalysts remain the subject of intense research activity. The determination of their solution state behavior facilitates the design of improved catalysts with enhanced efficiency. These topics form the scope of this introduction which comprises four main sections.

The first part gives an overview of the copolymerization pathways that are encountered in $CO_2$/epoxide copolymerization.

The second part provides a resume about the well-investigated but, from a mechanistic point of view, poorly understood zinc dicarboxylates and concludes with mechanistic considerations.

The third part focuses on traditional homogeneous catalysts and the progress made to date with these systems. The main ligand families covered are porphyrins, phenoxides, β-diiminates and salens, which are covered in their respective chapters. Several of these studies imply that multi-site catalysts or binary systems are required to deliver alternating copolymers from $CO_2$ and epoxides.

In the final part of this introduction, the most recent advances and new strategies to circumvent the problems that have been uncovered with the traditional catalyst systems are outlined. Here the focus lies on the development of new dinuclear and binary linked catalyst

systems that are able to initiate a cooperative mechanism in $CO_2$/epoxide copolymerizations. Furthermore the strategy of immobilizing homogeneous systems on substrates is reviewed. For a convenient comparison of the different catalytic systems, the productivity is given as Turn-Over-Number (TON) in mol/mol and the activity as Turn-Over-Frequency (TOF) in TON $h^{-1}$. In cases where it is relevant, the selectivity towards copolymerization and the corresponding quality of the produced polymer is given.

## 2.1. Mechanistic Aspects of Carbon Dioxide/Epoxide Copolymerization

### 2.1.1. Copolymerization Mechanism

Despite intense research activities in the area of $CO_2$/epoxide copolymerization, a profound understanding of the underlying mechanisms is still lacking and thus, this field is under continual investigation and review. Homogeneous catalysts of the form $L_nMX$ generally contain only one specific active-site, which can easily be tailored by modifying either the ligand framework ($L_n$), the catalytically active metal center (M) or the initiating group (X). The mechanistic aspects of the initiation step of $L_nMX$ complexes is currently a highly active field of research, with a number of different mechanisms being proposed. The possible mechanism pathways are described with a model salen-complex (Scheme 3).

**Reaction pathway A** involves two metal complexes and an intermolecular interaction of two active sites (Scheme 3A). In a theoretical study conducted by Rieger *et al.*, chain growth was predicted to take place *via* attack of a metal-bound alkyl carbonate on a metal-coordinated epoxide.[51] Such a bimolecular process has also been observed by Jacobsen *et al*. for the asymmetric ring-opening of epoxides.[52-54] Other investigations have indicated a bimetallic initiation, followed by a monometallic propagation step.[55-58] The bimetallic pathway generally is thought to occur in the absence of cocatalysts at low epoxide/catalyst loadings and is rate-dependent on the Lewis acidity of the metal center as well as the nucleophilicity of the axial ligand X and therefore upon the type of the catalytic system. For example, mechanistic studies conducted by Chisholm *et al*. with metal-porphyrin systems strongly indicate that the initiation step is monometallic.[59]

**Reaction pathway B** involves an intramolecular attack of the nucleophile on the pre-coordinated epoxide, which formally is comparable with an associative ligand exchange

mechanism (Scheme 3B). In the monometallic pathway, a nucleophile (Nu) ring-opens the epoxide at the least hindered C-O bond (even though some regio-irregularity is always observed). As both X and Nu can serve as initiator groups, they are both generally integrated into the polymer chain as end groups. Such a mechanism is, however, rather unlikely as the corresponding transition state in commonly applied metal complexes is thermodynamically unfavorable.

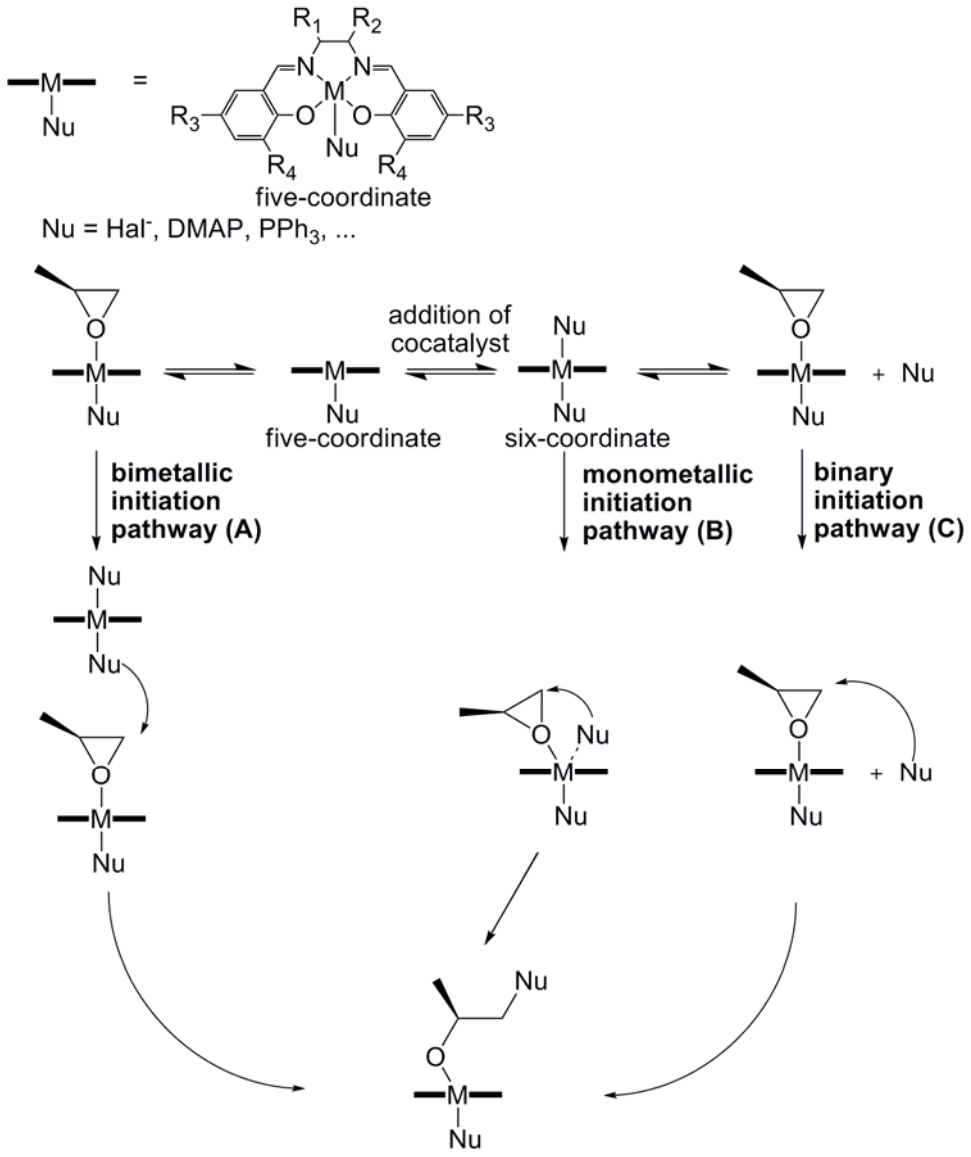


**Scheme 3.** Initiation mechanisms for a generalized salen-complex: bimetallic pathway (A), monometallic pathway (B), binary pathway (C)

**Reaction pathway C** involves the interaction of a binary catalyst/cocatalyst system, where the added nucleophile adopts the role of attacking the pre-coordinated epoxide (Scheme 3C). The abundance of investigations on such binary systems have shown that the addition

of a nucleophilic cocatalyst can significantly improve the activity and selectivity even at low $CO_2$ pressures and/or elevated temperatures depending on the nature of the added nucleophile.[31, 60-77]

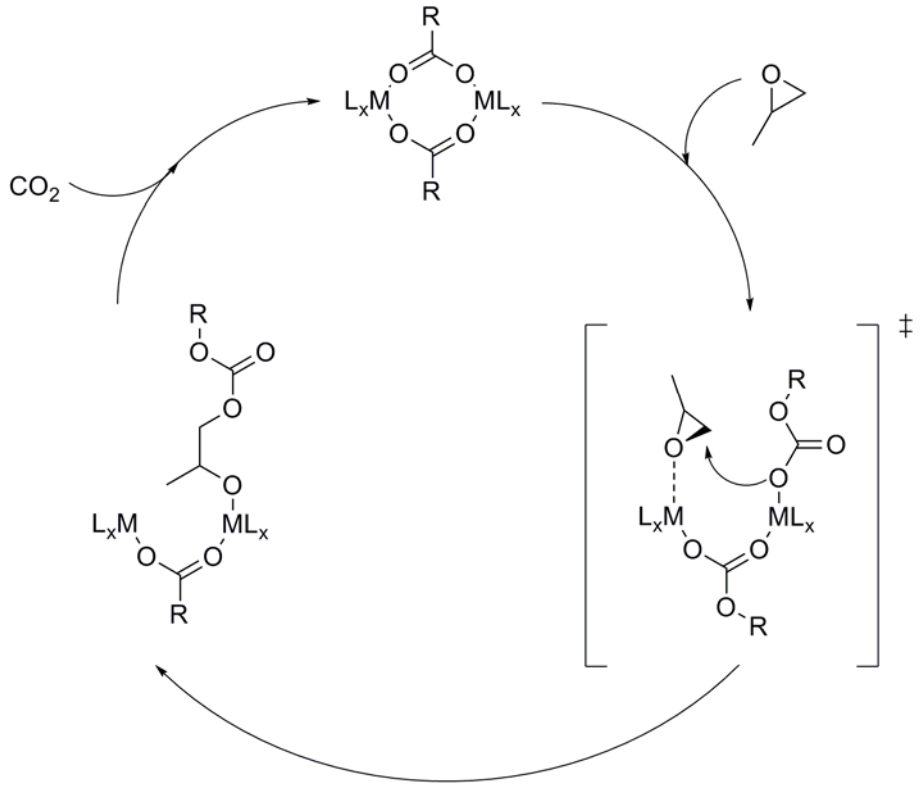


**Scheme 4.** Bimetallic catalytic mechanism for $CO_2$/PO copolymerization

A catalytic cycle for the bimetallic formation of polycarbonate is presented in Scheme 4. As shown by Coates *et al.* the rate determining step is the incorporation of the epoxide.[78] The key step in the catalytic cycle is the ring-opening of the epoxide as a result of the nucleophilic attack by a carbonate end-group. However the carbonate group is a very weak nucleophile, such that the epoxide must be pre-coordinated and pre-activated by a Lewis acid, which may be another metal center or cocatalyst. Following the ring-opening of the epoxide, $CO_2$ is inserted into the metal-alkoxy bond. These iterative insertions are repeated in further catalytic cycle thus leading to the formation of the copolymer.

Homogeneous systems were considered to follow a cooperative (bimetallic or binary) pathway in many early publications.[23, 25, 40, 79-82] This explains the loss in activity at higher dilutions, which are often observed with such systems. The above-shown mechanistic considerations lead to the conclusion that two interacting species need to be in spatial proximity to achieve high catalytic activity. Therefore new strategies in $CO_2$/epoxide

copolymerization increasingly focus on dinuclear and binary linked systems (Chapter 2.4.1 - 2.4.2).

### 2.1.2. Factors Influencing Copolymerization

Beside self-evident parameters as temperature, pressure and catalyst/cocatalyst concentration, several other factors must be taken into consideration in the copolymerization of $CO_2$ and epoxides:

- viscosity and dilution problems

A major drawback which limits polymer yields is the viscosity of polymerization mixtures at higher monomer conversions. During the copolymerization process, the viscosity of the reaction medium increases with polymer formation and diffusion of the monomer to the active catalyst site is therefore impeded. Higher solvent contents can facilitate monomer diffusion; however activities have a propensity to drop at high catalyst dilutions, principally due to an overall decrease of monomer concentration and due to the spatial separation of two potentially interacting species. The combination of two metal centers or linkage of two binary components into one ligand framework can counter this effect (Chapter 2.4.1 – 2.4.2).

- side reactions

Side reactions typically occur when epoxides are consecutively inserted into the growing polymer chain or through the production of cyclic carbonate *via* a back-biting pathway (Scheme 5). The consecutive insertion of two $CO_2$ molecules has never been observed as this is strongly disfavored from a thermodynamic perspective.[27]

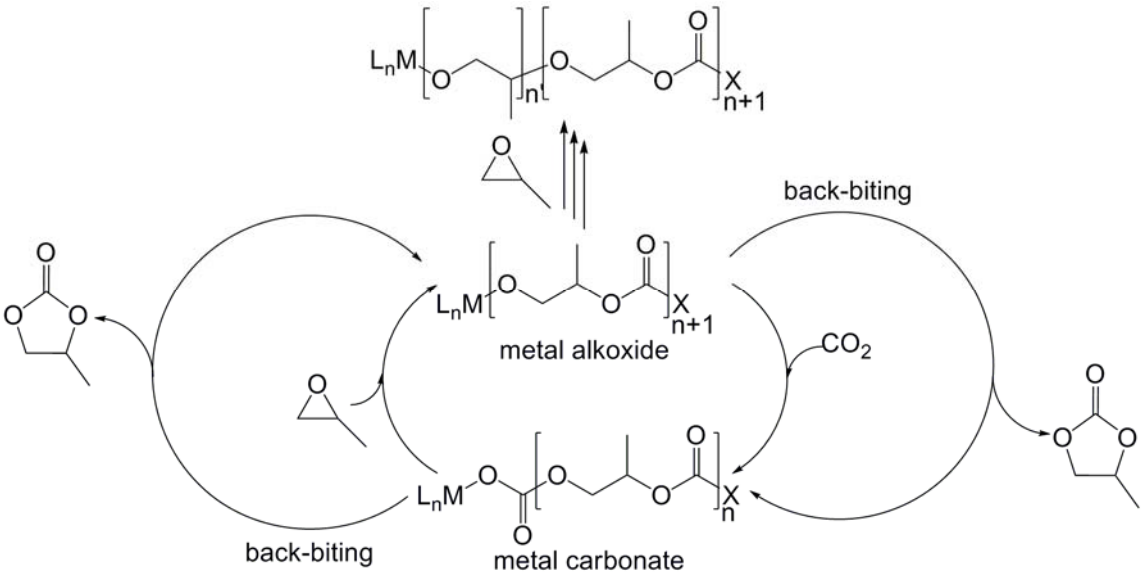


**Scheme 5.** Side product: polyether formation through consecutive PO insertions, formation of cyclic carbonate through chain back-biting

One advantage of two adjacent interacting species in cooperative catalysis is the constant contact of the polymer chain to an active metal center during the reaction. Therefore the so-called back-biting reaction is suppressed and depolymerization is minimized. This back-biting can occur from an anionic carbonate group or an anionic alkoxide chain end (Scheme 6).[51]

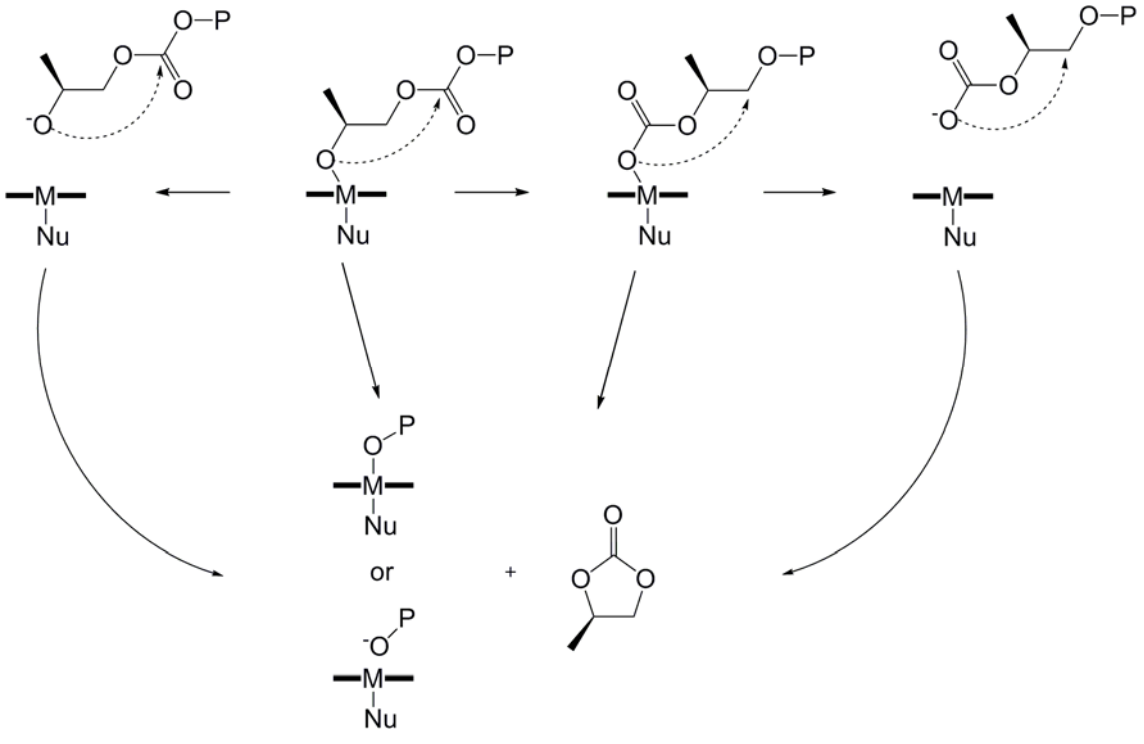


**Scheme 6.** Chain back-biting mechanism[51]

Factors enhancing the back-biting and cyclic carbonate content include higher temperatures and cocatalysts that help dissociate the growing polymer chain from the metal center.

- chain transfer

Any traces of water, alcohol and acid in the polymerization medium can initiate a chain transfer, which results in lower molecular weights than theoretically calculated.[83-85] The minor contribution of a consecutive back-biting mechanism and the release of the by-product cyclic carbonate has been previously discussed.[85] However, the protonated chain-end is considered to be insufficiently nucleophilic for the back-biting event to take place.[83] Although the copolymerization reagents are generally dried, molecular weights and PDI usually differ from those expected, an effect which has to be accounted for in this field of chemistry.

## 2.2. Heterogeneous Catalyst Systems

### 2.2.1. Zinc dicarboxylates

Even though huge steps in homogeneous catalysis have been made over the last years, the traditional heterogeneous zinc dicarboxylate systems remain industrially relevant as they are easy to prepare and handle, non-toxic and economically viable. An excellent set of reviews on this topic has been published.[27-29, 86] This introduction therefore summarizes the most recent findings for heterogeneous systems with particular emphasis upon polymerization mechanisms on heterogeneous surfaces and directions for future catalyst development.

Despite the numerous advantages of the heterogeneous zinc carboxylate system, the exact nature of the catalytically active species is still unknown, which renders systematic modifications of the system difficult.

The zinc glutarate (ZnGA) system, comprising Zn and glutaric acid, has been subject to the most intensive studies. There are several ways to prepare ZnGA, namely by the introduction of different Zn sources (*e.g.* ZnO, $Zn(OH)_2$, $Zn(OAc)_2$, $Zn(NO_3)_2$, $Zn(ClO_4)_2$, $ZnEt_2$) and carboxylate sources (*e.g.* glutaric acid, anhydride, methyl ester, glutaronitrile).[36, 41, 87-89] Although the same product structure is found for all synthetic strategies (X-ray powder

diffraction studies) [87-90], activities can vary considerably. The standard procedure combining zinc oxide and glutaric acid affords ZnGA with the highest activity.[88]

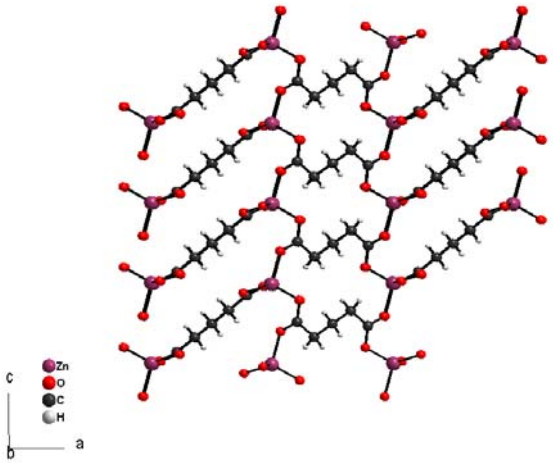


**Figure 2.** Crystal structure of ZnGA; view along *b*-axis including the material porosity[91-92]

The molecular structure of ZnGA has only recently been elucidated[91-92] and consists of a unique structure type with four carboxyl groups coordinating one Zn center with the glutarate ligands in either a bent or an extended conformation (Figure 2). This particular conformation leads to the formation of two metallacycles A and B that introduce a porosity which is not conducive for monomer diffusion.[87] These investigations showed that overall activity is restricted to the outer surface of the ZnGA-particles

Strategies to increase the activity were therefore focused on increasing the ZnGA surface area [90, 93] by one of four methods:

- variation of stirring procedure: magnetic or mechanic
- post-modification: ball-milling or ultrasonic preparation
- introduction of additives: substrates with high surface area
- addition of growth controllers: block copolymers or monoacids

Each of these strategies has been tested in the literature and shown to enhance activity, although the desired high activities that have been realized for several homogeneous catalysts have not been achieved with ZnGA to date. Indeed, Coates *et al*. categorized

catalyst systems by their catalytic activity (low TOF < 5 $h^{-1}$, moderate TOF between 5 and 200 $h^{-1}$, high TOF > 200 $h^{-1}$; all values given in mol epoxide converted / mol catalyst · time interval) and heterogeneous catalysts still remain in the lower region of this scale.[27]

A supported ZnGA on montmorillonite was obtained by a solution procedure and showed a slightly increased activity (TOF = 5.51 $h^{-1}$) compared to more standard procedures (TOF ≈ 3.00 $h^{-1}$).[94] Introduction of templates, such as amphiphilic block copolymers, during the synthesis of ZnGA can slightly increase the activity, presumably due to the inhibition of agglomeration (before: TON = 64 g/g, TOF = 3.06 $h^{-1}$; after: TON = 83 g/g, TOF = 3.97 $h^{-1}$).[87, 95] The different stirring methods (magnetic, mechanical) and particulary the ultrasonic preparation of ZnGA considerably increase the efficiency, thus yielding the highest activity achieved for a zinc carboxylate system [90, 96]. Regeneration of zinc carboxylate catalysts after complete polymerization gave less product than the freshly synthesized catalyst.[97] The influence of traces of water, ethanol, remaining residues of unreacted glutaric acid or other proton donors as chain transfer agents upon catalytic activity have already been suggested.[85]

With regards to the surface constitution of the carboxylate catalysts, the active species is still unidentified. MALDI-TOF mass spectrometric studies have shown that the copolymer is terminated by an OH group, thereby indicating that Zn-OH groups are the active initiating species in the ZnGA system (Figure 3).[85, 98] In an early work, Inoue *et al.* combined diethyl zinc and glutaric acid to yield a ZnGA with very low activity,[36] presumably due to the presence of ethyl groups at Zn (which are known to react sluggishly with epoxide and $CO_2$) [39, 48, 99]. However, post-activation of the surface-situated Zn-ethyl species with $SO_2$ leads to ethyl-sulfinato groups and a considerable increase in activity, achieving activities approaching the best known for ZnGA to date (Figure 3).[100]

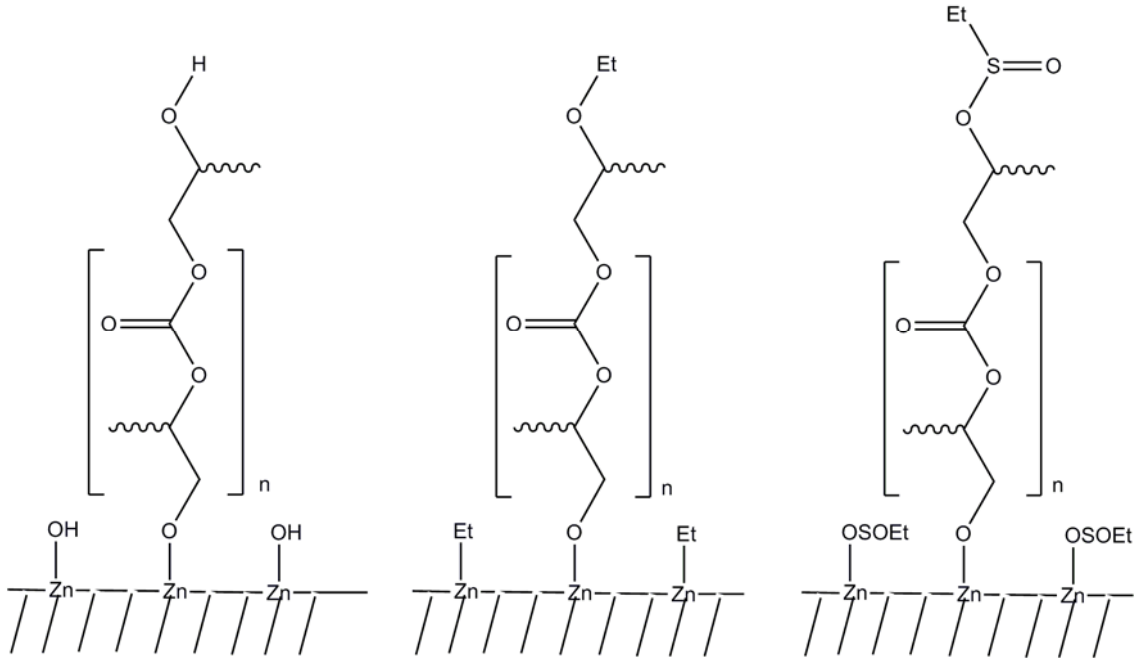


**Figure 3.** Initiator groups ZnOH, $ZnEt_2$ and $Zn(SO_2Et)$ on the surface of heterogeneous zinc dicarboxylates and associated polymer end-groups

Another aspect often and ambivalently discussed is the crystallinity of the resulting Zn-containing materials, as it seems that amorphous catalysts are less active than their highly crystalline counterparts.[87-90, 93, 101-102] However, the crystallinity of the catalyst prepared from $ZnEt_2$ is less than that of a catalyst prepared by the standard procedure with ZnO,[87] but a higher surface area and potentially better initiator groups on the surface are probably responsible for the higher activity.

Other investigations have introduced various dicarboxylic acids, derivatives of zinc glutarate and mixtures of di- or mono-acids with variable success.[87, 93, 103] In particular the substitution of glutaric acid by derivatives with other functionalities in the hydrocarbon chain (*e.g.* 2-ketoglutaric acid, 3,3-dimethylglutaric acid, diglycolic acid) afforded materials with no appreciable activity, presumably due to different solid-state constitutions and associated variations of the local environment around the Zn center.[87, 100, 104]

Further attempts to form active heterogeneous Zn-containing systems were based on the exchange of glutaric acid for its higher or lower homologues. It was long thought that the zinc carboxylate system with glutaric acid (GA, $C_5$) was the only system with a considerably high activity for copolymerization, whereas other variants such as succinic acid (SA, $C_4$), adipic acid (AA, $C_6$) or pimelic acid (PA, $C_7$) were presumed to be inactive (Figure 4). However, recent reports have demonstrated that ZnAA[105-106] (TOF = 5.65 $h^{-1}$) and ZnPA[102]

(TOF = 5.20 $h^{-1}$) show similar activities to ZnGA when appropriately treated. Adipic acid is of particular interest as this is a large-scale industrial product.

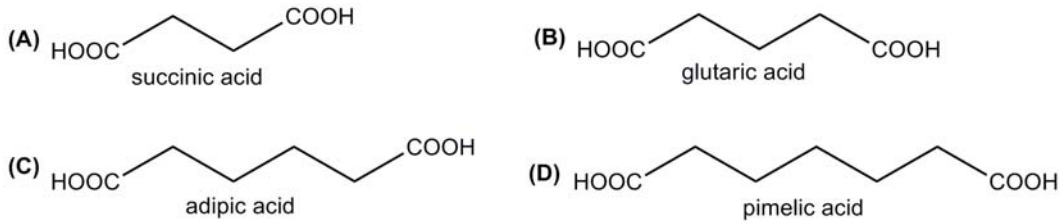


**Figure 4.** Various dicarboxylic acids used in the synthesis of heterogeneous catalyst systems

Interestingly the same trend of activity for analogous structures of ZnGA is observed when the functionalization route with $ZnEt_2$, followed by $SO_2$ activation, is employed. Almost no activity is observed for ZnSA (TOF = 0.07 $h^{-1}$), whereas the activity slightly decreases in the order of ZnGA (TOF = 6.17 $h^{-1}$) > ZnAA (TOF = 5.18 $h^{-1}$) > ZnPA (TOF = 4.50 $h^{-1}$).[100]

These results indicate that the activity of heterogeneous zinc dicarboxylate systems of this type is dependent on a defined spatial structure which is influenced by the dicarboxylic acid used. Of these systems, only the solid state structures of ZnGA and ZnSA[107-108] have been reported so far. In the structure of ZnSA, the necessary Zn-Zn distance is only found on one of the main *hkl*-indiced plains, whereas for ZnGA, the corresponding distance of 4.6 – 4.8 Å is found on each main *hkl* plain (Figure 5). From the molecular structures of ZnSA and ZnGA, it can be concluded that at least two zinc centers in close spatial conformation need to be present for copolymerization activity.

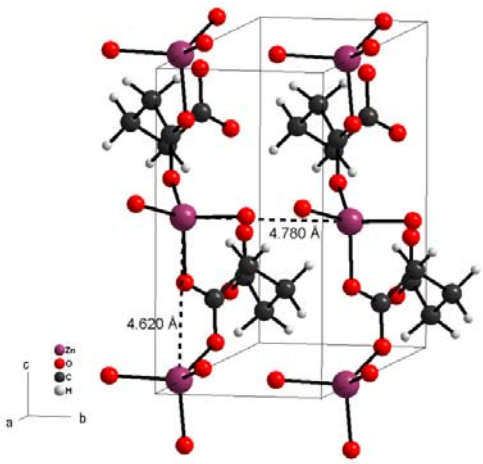


**Figure 5.** Representative metal distances in zinc glutarate (Zn-Zn distance = 4.6 – 4.8 Å)

The optimal Zn-Zn distance for $CO_2$/epoxide copolymerization is assumed to lie between 3 – 5 Å, as can also be deduced from investigations with homogeneous systems (c.f. following chapters). These results strongly indicate that for heterogeneous systems a very specific metal-metal distance is required for high copolymerization activities. However the activities with such systems are restricted due to a restrained surface and diffusion limitations. Therefore, new strategies have to focus on homogeneous systems that comprise two metal centers or a cooperative binary linked ligand system.

## 2.3. Traditional Homogeneous Catalyst Systems

### 2.3.1. Porphyrin Systems

Shortly after the first tetraphenylporphyrin ligand (tpp) with an aluminum metal center was developed, trials with the addition of cocatalysts were reported (Figure 6). Porphyrin (tpp)AlCl catalysts, in conjunction with quaternary organic salts or triphenylphosphine, are active at ambient temperature and relatively high catalyst loadings with low TOFs. Following these results, Kruper and Dellar investigated the activity of (tpp)CrX (X = Cl, Br, OAc) complexes (in addition to 4-10 equivalents of nitrogen donors such as *N*-methylimidazole (*N*-MeIm) or (4-dimethylamino)pyridine (DMAP)) which predominantly yield copolymer with the CHO/$CO_2$ system, but only cyclic carbonate with PO/$CO_2$.[109-111] The DMAP cocatalyst fulfils two roles; firstly the amine labilizes the metal–X bond and secondly it promotes insertion of $CO_2$ into the metal–OR bond.[59]

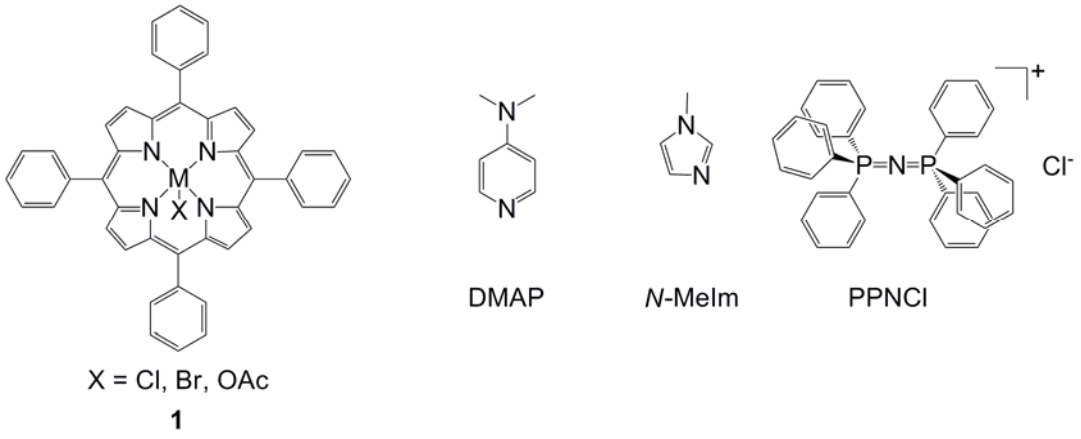


**Figure 6.** Representative structure of the porphyrin system and commonly used cocatalysts

Whilst cobalt-porphyrin systems have been traditionally overlooked in favor of other metal-containing systems, Wang and co-workers have shown through a series of experiments that the (tpp)CoCl/cocatalyst system is indeed active in the PO/$CO_2$ copolymerization. Furthermore they demonstrated that the efficiency of this binary system decreases with the exchange of cocatalyst in the order PPNCl > $Bu_4NCl$ > $Et_4NBr$ ~ $Bu_4NBr$ >> $Bu_4NI$.[112] This work directly challenged the assumption that Co-porphyrins demonstrate low activity (as a result of the reduced Lewis acidity of the cobalt center in these complexes).[113] Also (tpp)CoCl complexes, in association with DMAP[114] and phenyltrimethylammonium tribromide[115] are efficient systems for the catalytic coupling of $CO_2$ and PO, affording cyclic carbonate. Without cocatalyst, the effect of the substituent X in (tpp)CoX on the catalytic activity decreases in the order Cl ~ Br > I >> OAc (with the (tpp)CoOAc system being completely inactive for PPC formation).

These new developments with porphyrin systems give a strong indication for a favorable cooperative mechanism in $CO_2$/epoxide copolymerization which is highly dependent on the catalyst and cocatalyst combination used.

### 2.3.2. Phenoxide Systems

The discovery in 1986 of the first soluble and therefore well-characterized aryl-oxide zinc complex initiated the development of a new family of complexes[116] which have been demonstrated to be active catalysts for epoxide/$CO_2$ copolymerizations.

Numerous investigations have shown that the activity of these complexes is linked to the substitution pattern of the aryl ligand framework and the “base” ligand present at the metal center. The exchange of Zn for other metals (*e.g.* Cd)[117] demonstrated a loss in activity. However, Zn-containing systems have demonstrated the highest activities.

The effect of ligand substitution on CHO/$CO_2$ copolymerization was demonstrated with monomeric Zn complexes bearing different substituents (R) in the *ortho*-position of the aryl rings (**2a-d**, Figure 7). For early investigations on phenoxides, no TOF values were given and therefore values in this chapter are reported in g polymer/g Zn. The R group significantly affects the catalyst efficiency, where the yield increases with decreasing substituent size (477 g/g (*i*Pr), 602 g/g (Ph), 677 g/g (*t*Bu), 1441 g/g (Me)).[46]

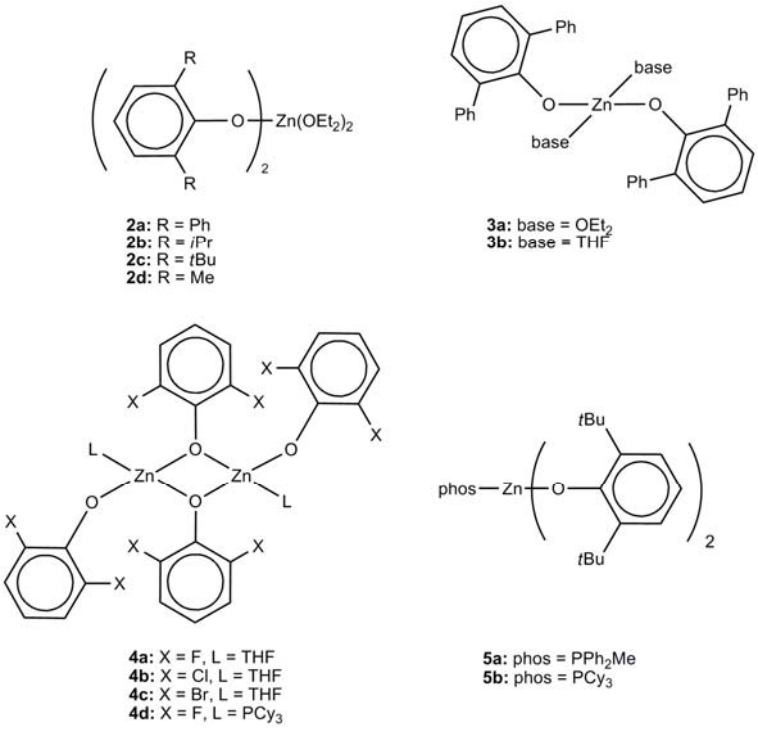


**Figure 7.** Active phenoxide systems for $CO_2$/epoxide copolymerizations[45-47, 118-119]

Dimeric phenoxide complexes of the type **3** (Figure 7) have shown activities around 88 g/g in CHO/$CO_2$ copolymerizations, whereas no copolymer formation was observed for the PO/$CO_2$ system. However, complex **3a** is an active system for the terpolymerization of CHO, PO and $CO_2$ with moderate incorporation of PO (*ca*. 20 %).[45]

The introduction of halides in the *ortho*-position of the aryl rings increases the activity of the correspondent catalyst in the order Br < Cl < F (Figure 7, **4a-c**).[47, 118] The authors attribute this trend to a decrease in electron density at the metal center, which reflects the increased electronegativity of the substituted halide, thereby increasing the binding ability of the metal center to the epoxide. This emphasizes that epoxide activation is generally more important $CO_2$ insertion in complexes of this nature.

Analysis of the polymer with $^{19}$F NMR spectroscopy demonstrated the presence of different F-containing environments in the polymer. This indicates that the initiation mechanism occurs *via* nucleophilic addition of the zinc-bound phenoxide to the first monomer (Scheme 7).[118]

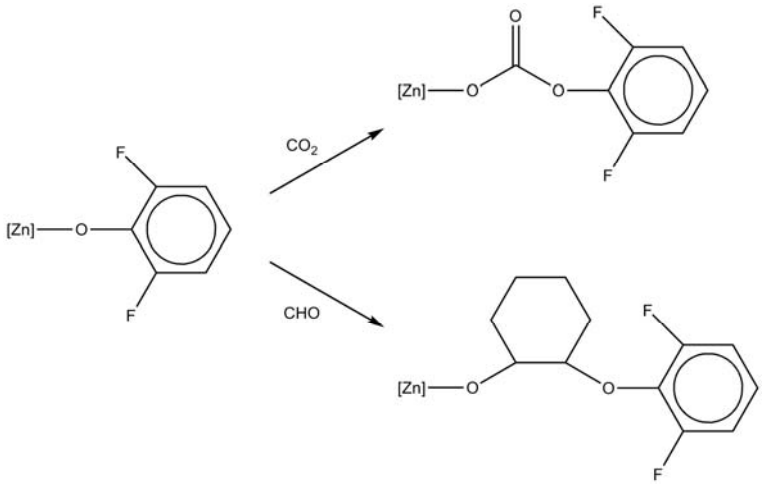


**Scheme 7.** Initiation step in fluoro-phenolate Zn complexes[118]

Replacement of the labile $Et_2O$ and THF bases in Zn-phenolate complexes of the type **3** and **4a-c** has a pronounced impact on the complex activities, as the phosphine can irreversibly bind to the active metal site (**4d**).[118] However the introduction of phosphine donors such as $PPh_2Me$ (**5a**) and $PCy_3$ (**5b**) in monometallic Zn phenolate complexes increases the percentage of polymeric carbonate linkages without loss of catalytic activity. This demonstrates that two adjacent coordination sites are needed for consecutive epoxide insertions.[119]

Mechanistic investigations with Zn-phenoxide complexes of this type have long been frustrated due to the lack of a spectroscopic probe suitable for Zn systems. It is for this reason that early mechanistic studies focused on Cd complexes as these analogous compounds are active for epoxide/$CO_2$ copolymerizations (albeit with lower activities than their respective Zn complexes) and adopt similar geometries to the analogous Zn complexes [118-119].

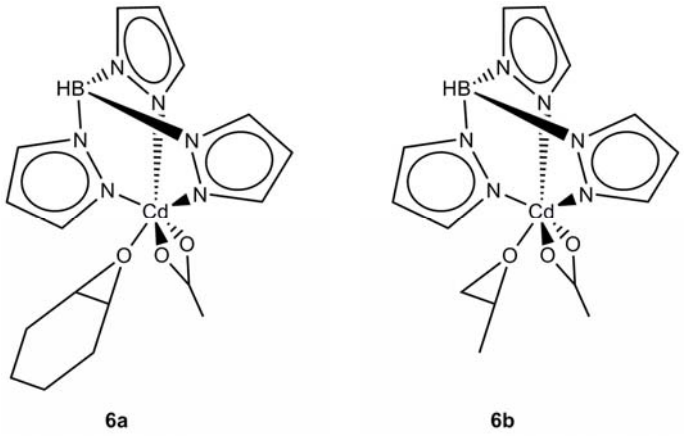


**Figure 8.** Cd model complexes for epoxide insertions[120]

$^{113}$Cd NMR spectroscopic investigations with $L_nCd(THF)(acetate)$ demonstrated that the labile THF ligands in these systems can be easily replaced by a CHO (**6a**) or PO (**6b**) molecule.[120] In both cases the epoxide was weakly bound to the Cd-center and solution-state equilibrium studies permitted the determination of the thermodynamic parameters for epoxide insertion. The complexes with coordinated PO and CHO were both crystallographically characterized and therefore represent the first isolated intermediates in the initiation step of $CO_2$/CHO and $CO_2$/PO copolymerizations with metal carboxylate complexes.[121]

By the combination of experimental Zn studies and their related Cd systems, it has been determined that both mono- and bimetallic Zn-phenoxides have the potential to produce high molecular weight PCHC. Unfortunately, copolymerizations with PO and $CO_2$ remain challenging and progress with these systems been frustrated by low activities and a propensity for chain back-biting to form cPC. However successful terpolymerizations of PO/CHO/$CO_2$ have demonstrated that Zn-phenoxides have great potential in this area to produce novel mixed polycarbonate materials.

### 2.3.3. β-Diiminate Systems (BDI)

#### 2.3.3.1. Influence of Ligand Framework

β-Diiminate ligands have recently gained considerable attention in the areas of coordination chemistry as well as in $CO_2$/epoxide chemistry.[122] The sterically demanding environment of BDI ligands inhibits *bis*-ligation of the complexed metals, allowing the BDI metal system to retain free coordination sites crucial for any catalytic process. The structure of the BDI ligand

framework lends itself towards variation of both steric and electronic properties. This versatility is a helpful tool in understanding the underlying mechanisms of $CO_2$/epoxide copolymerization.

Over the years, a broad range of BDI catalysts has been developed (Figure 9). These generally incorporate a Zn metal center and demonstrate copolymerization activities at relatively low pressures (7 bar $CO_2$) and moderate temperatures (< 50°C).[48-50, 78, 123-126] The majority of these catalysts are only active for CHO/$CO_2$ copolymerization but adjustment of the reaction conditions can significantly modify the selectivity towards PO, with a reduced temperature generally increasing the polymeric carbonate over cyclic carbonate ratio.[50, 98, 127]

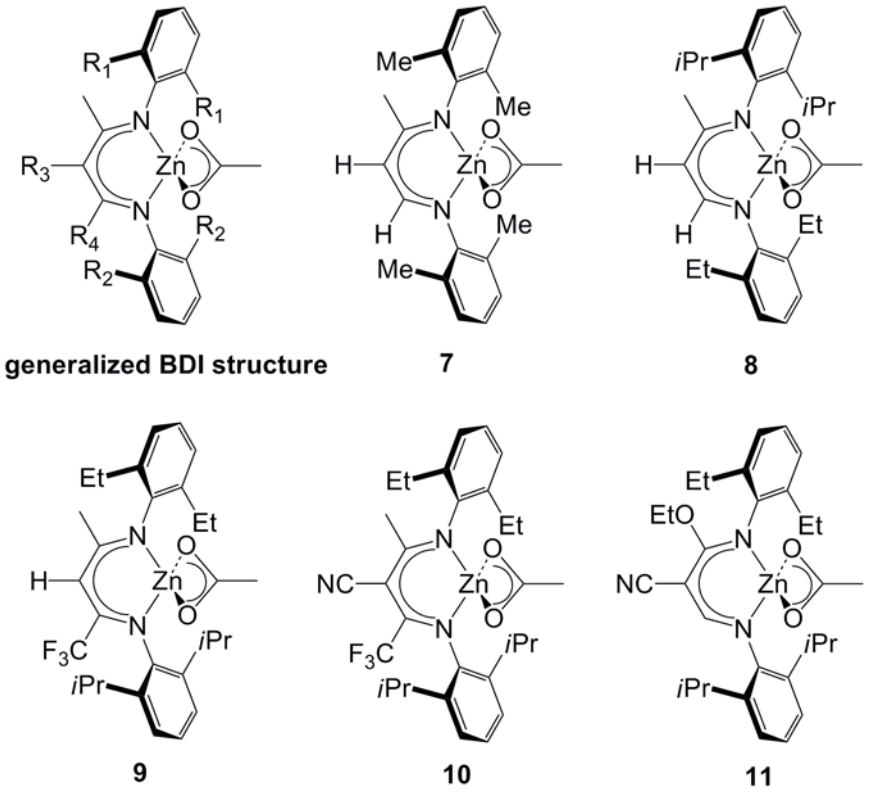


**Figure 9.** Generalized β-diiminate (BDI) ligand framework and representative catalysts for epoxide/$CO_2$ copolymerization

Minor modifications of the *N*-aryl ligands ($R_1$, $R_2$) significantly influence the catalytic activity. Methyl-substituted BDI ligands are inactive (**7**, TOF = 0 $h^{-1}$), whereas the incorporation of ethyl and isopropyl substituents at the *N*-aryl ring enhance the activity towards CHO/$CO_2$ copolymerization (**8**, TOF = 729 $h^{-1}$).[78, 123, 128] Symmetrical ligands, where $R_1$ and $R_2$ are either Et or *i*Pr are inactive for both cPC and PPC formation.[50] The introduction of an

unsymmetrical ligand framework and electron-withdrawing groups on the diimine backbone (*e.g.* $R_3$ or $R_4$ = CN, $CF_3$) considerably enhance the activity, especially towards PO (**9**, TOF = 424 $h^{-1}$).[49-50, 128-129] Nevertheless, it should be mentioned that the incorporation of more electron-withdrawing groups results in inactivity of the catalyst, presumably due to the high Lewis acidity of the metal center which results in a very strong, irreversible Zn-epoxide bond (**10**). Other modifications of the backbone, such as utilization of the aminoamidoacrylate **11** and amidoimidomalonate pattern only slightly modulate the catalytic efficiency (**11**, TOF = 158 $h^{-1}$).[127, 129-130]

#### 2.3.3.2. Bimetallic Considerations

Most reports only consider dimeric BDI species as being the active complex for $CO_2$/epoxide copolymerization. In the dimeric state the two metal centers are held in close proximity to each other by bridging anionic ligands, thus permitting facile interaction to form the respective polycarbonate. Molecular structure investigations have shown that, in the solid state, most β-diiminate complexes are dimeric. However, in solution a monomer-dimer equilibrium exists, being highly dependent on temperature as well as on catalyst concentration and steric properties of the ligand.[48, 78, 123, 126, 129] Dilution of the system by addition of monomer or an inert solvent shifts the position of equilibrium to the monomeric side, resulting in a reduced catalyst activity. At very low catalyst concentration, the equilibrium is completely shifted to the monomeric side and almost no catalytic activity is observed.[131-132] However at high catalyst concentrations, the epoxide conversion is limited due to resulting viscosity problems.[67, 131-132]

The possibility of some contribution from a monometallic mechanism with these catalysts cannot be discounted. Zn-BDI derivatives comprising sterically encumbering initiators, such as O*t*Bu or $OSiPh_3$, retain their monomeric form in both the solid and solution state. The monomeric complex **12** however is effective (but exhibits lower activities than the dimeric complexes) for the copolymerization of CHO and $CO_2$ (Figure 10).[133-134] In such monomeric catalyst species, the initial ring-opening step involving the bulky alkoxide initiators presumably proceeds *via* a monometallic transition state.

In other catalytic systems, the metal-metal distances differ from complex to complex but are generally found in the range of 3-5 Å.[50, 78, 129] For dimeric BDI complexes the distance

between the two metal centers is flexible and the system is able to adjust the metal-metal distance necessary for copolymerization.

The metal-metal distance as well as the monomer-dimer equilibrium can be controlled by the *ortho*-substituents of the *N*-aryl ring, with more sterically congested complexes having increased zinc-zinc separations in the solid state (Figure 10). Furthermore, the aggregatory state in solution shows a monomer-dimer equilibrium which is strongly influenced by the *N*-aryl substituents. Finally the nature of the bridging ligand influences the monomer-dimer equilibrium.

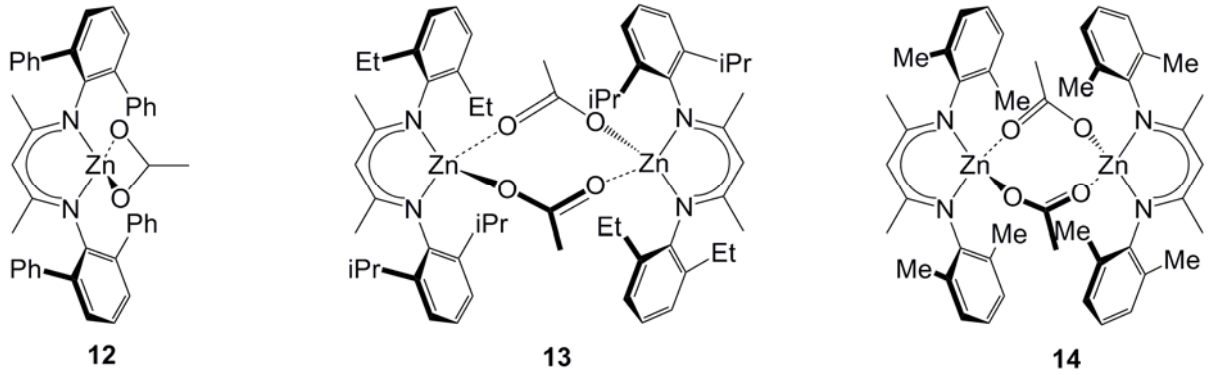


**Figure 10.** Monomeric complex **12** incapable of dimerization (generally considered as unreactive), loosely bound dimeric complex **13** (highly reactive), tightly bound dimeric complex **14** (unreactive)[78, 123, 133-134]

The introduction of bulky groups on the *N*-aryl substituents in BDI frameworks (Ph, 4-*t*Bu-Ph) affords predominantly monomeric complexes in solution which consequently exhibit lower activities than their dimeric counterparts. Asymmetrically substituted complexes with moderately bulky *i*Pr- and Et groups **13** exist in a loosely bound dimeric form and are effective catalysts for alternating $CO_2$/CHO copolymerization. Exchange of the *i*Pr substituent for a less bulky Me-group on the *N*-aryl ring leads to more tightly bound dimers **14** which are completely unreactive for copolymerization.[78, 123] Studies imply that the monomer/dimer equilibrium can be shifted by temperature with the dimeric complex being present at lower temperatures.[78, 135] Kinetic studies with different BDI complexes show that the copolymerization follows a zero-order in $CO_2$, a first-order in epoxide and a 1.0 to 1.8 order dependence in total metal.[78] Therefore, variations in ligand sterics and electronics,

alongside polymerization temperature, play a major role in discriminating one catalytic pathway over other alternatives.

### 2.3.3.3. Influence of Initiating Group

The activity of the catalytic system can be modified and examined by the introduction of initiating groups. For instance, acetate serves as an initiating group which mimics $CO_2$. Mechanistic studies have revealed that the epoxide is attacked by the metal-acetate bond in the initial step of the copolymerization.[78] Complexes with alkoxide groups[123] and ethylsulfinato groups[99] as initiators exhibit comparable or slightly enhanced activities, respectively (Figure 11, **16**).

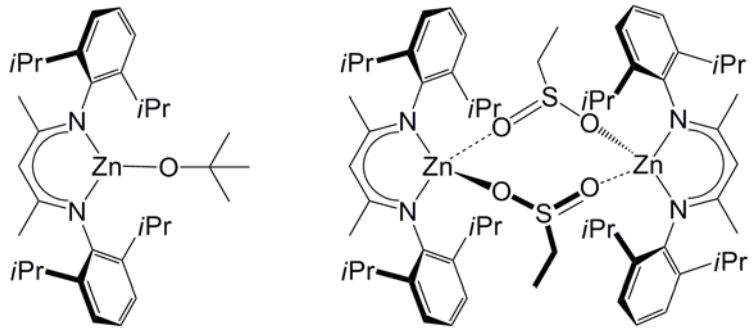


**Figure 11.** BDI complex with bulky *i*Pr groups: monomeric **15** and ethylsulfinato-bridged dimeric form **16** [99, 123]

In general the order of catalytic activity of BDI-Zn complexes of the general formula $L_nZnX$ with different initiation groups decreases with X = $SO_2Et$ > O*i*Pr > OMe > OAc, where the order of reactivity is the opposite of the order of the leaving ability of the initiation groups.[99, 136] The bimodal distribution in GPC elugrams leads to the assumption that, for the ethylsulfinato complexes, a monomer-dimer equilibrium is also present in which the two species possess different activities/polymerization rates, thus leading to different molecular weights in the obtained polymer.[99]

### 2.3.3.4. Influence of Metal Center

The Lewis acidity of the metal center and its steric and electronic environment is of major importance for the activity of a complex. The introduction of Cu and Mg into BDI frameworks affords inactive systems for $CO_2$/epoxide copolymerization.[134, 137] By contrast, rare earth metal complexes (Ln = La, Y) show some activity (Figure 12, **17**, TOF = 12.7 $h^{-1}$) which is rather low in comparison to the most active zinc- and chromium-based catalyst systems.[138-139]

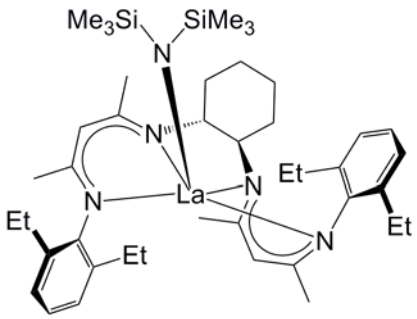


**17**

**Figure 12.** Lanthanoid-based quadridentate BDI complex [138-139]

Molecular structure and solubility studies suggest that only the monomeric species is present in these complexes in the solid state as well as in solution and therefore a monometallic mechanism is prevalent. However, blind tests with the precursors $Y[N(SiMe_3)_2]_3$ (TOF = 8.9 $h^{-1}$) and $La[N(SiMe_3)_2]_3$ (TOF = 0.86 $h^{-1}$) show that these complexes are also active for copolymerization reactions. These experiments show that to date the most successful BDI systems are still Zn-based.

The findings with BDI system over recent years strongly imply a bimetallic mechanism in $CO_2$/epoxide copolymerization. The system is strongly influenced by modifications in the ligand framework, the initiator group, the bridging ligand and the incorporated metal center. New strategies therefore have focused on the development of dinuclear BDI and BDI-like structures (Chapter 2.4.1).

### 2.3.4. Salen Systems

The salen system represents the most investigated homogeneous system for $CO_2$/epoxide copolymerization and considerable developments have been made with this system. An excellent and extensive review on (salen)MX catalyst systems has been provided by Darensbourg in 2007.[28] This chapter of this introduction focuses on the newest developments and advances in the field of (salen)MX catalysts and only repeats data reported previously if necessary for a more in-depth understanding.

Although the first generation of salen catalysts demonstrated lower activities than representative BDI-Zn[50] (TOF = 160 $h^{-1}$, PPC = 71 %) catalysts (*vide supra*), they introduced several advantages such as high polymer selectivity as well as excellent regioselectivity. Moreover, the copolymerization with salen complexes typically proceeds under mild temperatures and pressures.

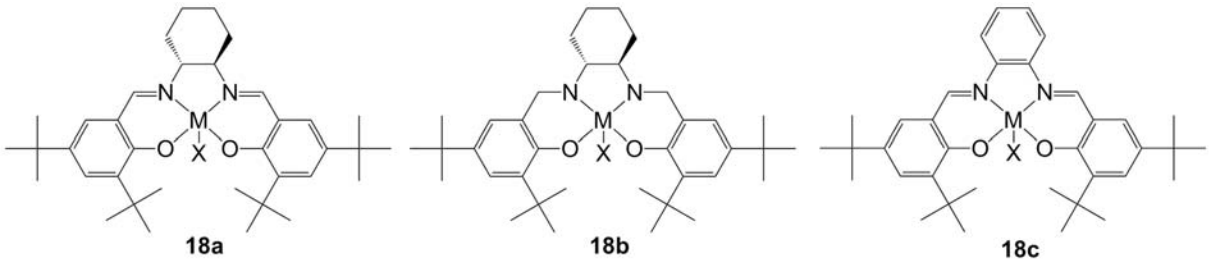


**Figure 13.** Representative (salen)MX (**18a**), (salan)MX (**18b**) and (salphen)MX (**18c**) complex

Initial investigations focused on Cr as the incorporated metal center, but recently the (salen)CoX complex system has garnered more attention (Figure 13, **18a**).[55-56, 61-62, 65, 68, 140] The first cobalt catalyst **18a** with M = Co and X = OAc was reported by Coates *et al.* in 2003 and produced PPC with 99 % carbonate content at TOFs around 70 $h^{-1}$.[68] In addition to exchange of the metal center, simple changes to the axial group X of (salen)MX complexes drastically affect the PPC/cPC selectivity, which emphasizes the potential effect of cocatalyst addition (*e.g.* PPNCl, DMAP, *N*-MeIm, Figure 14).[55, 61-62] For example, addition of substoichiometric PPNCl amounts to complex **18a** with M = Co and X = pentafluorobenzoate increases the activity up to TOFs of 620 $h^{-1}$.[55] From GPC analyses, it was concluded in this work that one copolymer chain is produced from one complex, whereas upon addition of cocatalyst, two copolymer chains are formed per metal center.

In general, the ideal ionic cocatalyst for high activities and selectivities consists of a bulky cation, which is demonstrated to decrease in the order $[PPN]^+ > [n\text{Hept}_4\text{N}]^+ > [n\text{Bu}_4\text{N}]^+ > [n\text{Et}_4\text{N}]^+$ and an anion with poor leaving group ability, where $Cl^- > Br^- > I^- > ClO_4^-$.[62] For neutral cocatalysts, bulky Lewis bases (*e.g.* DMAP) are preferred over their less sterically hindered counterparts (*e.g. N*-MeIm), as such bases render the catalyst system completely inactive due to their tight bonding to the metal center, which hinders effective epoxide binding and activation.

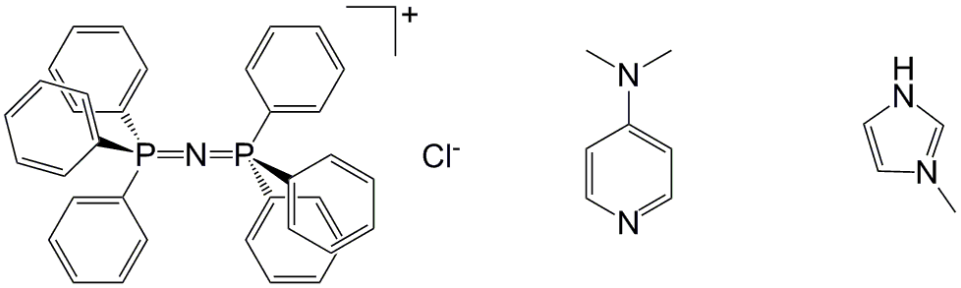


**Figure 14.** Frequently used cocatalysts PPNCl, DMAP and *N*-MeIm

Studies conducted by Rieger *et al.* have shown that traditional (salphen)-Cr(III) complexes **18c** only gave activity in combination with DMAP, whereas reactions in the absence of cocatalyst showed no activity, neither producing PPC nor cPC.[74] At higher cocatalyst concentrations however, the polymer chain end is in a coordination equilibrium with the cocatalyst and is detached from the metal center, which promotes depolymerization through back-biting.[71] This effect is attributed to a reduced activation barrier, which facilitates backbiting. Therefore not more than one or two equivalents of ionic cocatalysts should be added during copolymerization if a high polymer content is desired in the end-product.

The cocatalyst can also give both a positive and a negative effect on the overall rate of copolymerization.[75] The initiation time is generally lengthened due to competitive insertion with epoxide at the metal-site *trans* to the nucleophile, which leads to an induction period. This effect is much more pronounced for (salen)MX-systems **18a** than for the corresponding saturated (salan)MX-systems **18b**.[60] Meanwhile the propagation is enhanced considerably and as a result, accelerated overall activities can be observed.[60, 74-75, 77] The combination of (salan)MX-complexes in conjunction with (neutral) cocatalysts efficiently enhances the catalytic activity as well as the regio- and stereo-selectivity of the alternating

copolymerization of $CO_2$ and PO.[60, 77] This effect is attributed to the $sp^3$ hybridized amino donors in the salan ligand, the resulting reduced Lewis acidity of the metal center and the facilitated reversible epoxide/cocatalyst binding. It was also proposed that the salan-ligand system is conformationally much more flexible than its rigid and planar salen counterpart. Therefore a penta-coordinate complex is formed, in which one vacant coordination site can be found in an equatorial or an axial position of the coordination octahedral.[60] The reduced nucleophilicity of the metal center and the coordinative flexibility could both facilitate dissociation and re-association of the cocatalyst and the growing polymer chain, thereby increasing back-biting, but simultaneously considerably enhancing the activity.[51, 60, 77]

During copolymerization, the Lewis base coordinates to the (salen)MX metal center in the axial position (*trans* to the propagating species) forming the resulting complex (salen)M-XNu, which results in an improved electronic environment for propagation. The (salen)M-X can also be ligated by corresponding epoxides or coordinating solvents such as THF.[54, 141] The competitive equilibrium between (salen)MX-epoxide and (salen)MX-Nu is shifted depending on the catalyst/cocatalyst/epoxide ratio and can have profound effects on the PPC/cPC (respectively PCHC/CHC) ratio and overall activity, with an excess of cocatalyst generally leading to reduced activity and higher PC (respectively CHC) content.[31, 58, 66, 71, 74] In the presence of very strongly coordinating nucleophiles, the ligation process is irreversible and subsequent exchange by epoxide is precluded.

These conclusions, in addition to the observations from related homogeneous systems, have recently lead to reports of binary linked salen systems which are reviewed later in this introduction (Chapter 2.4.3. Dinuclear Salen System).

## 2.4. New Strategies with Homogeneous Catalyst Systems

### 2.4.1. Dinuclear BDI Catalysts and Similar Systems

As indicated in the previously discussed BDI catalysts, a bimetallic mechanism is needed for enhanced activities in $CO_2$/epoxide copolymerizations. It is for this reason that dinuclear BDI and BDI-like systems have been developed over the last years.

In 1999 Nozaki *et al.* used diethyl zinc and a chiral amino alcohol (*S*)-diphenyl(pyrroridin-2-yl)methanol (Scheme 8) for the copolymerizations of cyclohexene, cyclopentene and *cis*-butene oxide with $CO_2$, respectively.[142] These copolymerizations were carried out under 30 bar $CO_2$ using equimolar ratios of diethyl zinc to amino alcohol. The resulting copolymers were the first alternating polycarbonates with isotactic units up to 70 %.

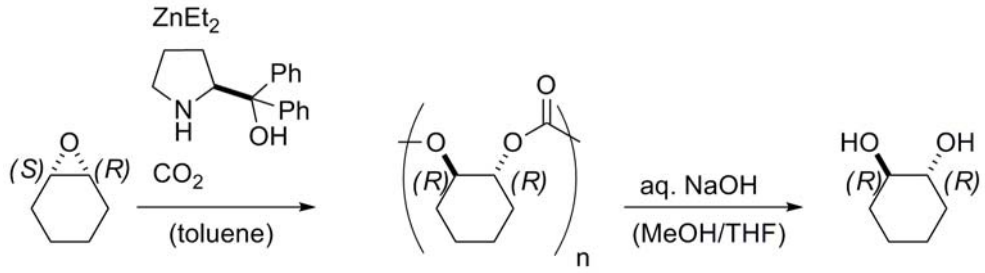


**Scheme 8.** Chiral amino alcohol complex[142]

The hydrolysis of the copolymers with aqueous NaOH leads to the corresponding diols. In the case of CHO the *meso*-cyclohexane diol was not obtained, which clearly confirmed $S_N2$-type ring opening of the epoxide. The *trans*-cyclohexane diol yielded an enantiomeric excess of up to 70 % (*R*,*R*)-cyclohexane diol.

In a further work in 2003, Nozaki and coworkers crystallized the desired complex **19** from the synthesis of diethyl zinc and (*S*)-diphenyl(pyrroridin-2-yl)methanol (Figure 15).[143] The obtained catalyst adopts a dimeric structure with the two zinc centers adopting a distorted tetrahedral geometry. The zinc-zinc distance in this catalyst was determined to be 3.00 Å.

The copolymerization reaction of CHO and $CO_2$ was performed in toluene at 40 °C and yields perfectly alternating polycarbonate. However the isotactic ratio never exceeded 50 % and was therefore lower than in the previous report. The MALDI-TOF mass spectrum showed a series of peaks, which could be attributed to copolymers initiated by the amino alcohol ligand. Therefore presumably the enantiomerically pure ligand dissociates from the active metal site and the chiral information around the zinc center is lost. To overcome this

problem, ethanol was added to the reaction mixture, which lead to the formation of new Zn-OR moieties. These new Zn-alkoxide groups could initiate the copolymerization, whereas ethyl groups were unable to initiate the reaction.

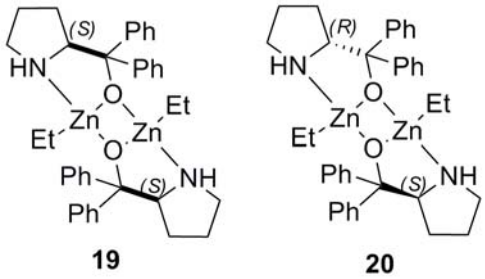


**Figure 15.** Dinuclear homo- and hetero-chiral zinc complexes[143]

The MALDI-TOF mass spectrum of these polymers showed a series of peaks with an ethoxy-end group and an increased isotactic ratio in the polymer of 75 %. Several different alcohols were tested in the *in-situ* initiation for the copolymerization, with a higher nucleophilicity of the alkoxide species leading to better copolymerization results.

Nozaki and coworkers used the *R*- and *S*- enantiomer of the ligands to form a hetero-chiral complex (Figure 15, **20**).[144] This catalyst is less active than those previously reported, however the complex indicated an asymmetric amplification, which is the first reported for the copolymerization process. However no TOF values were given for this kind of catalyst.

In 2003 Coates *et al.* introduced a new type of ligand for dinuclear structures.[126] The β-oxo-*δ*-diimine (BODDI) ligands can be coordinated with diethyl zinc to form a dinuclear complex. The reaction of these complexes with acetic acid affords zinc acetate systems (Figure 16, **21**) which are potentially active in the copolymerization of $CO_2$, but corresponding experiments have not been reported.

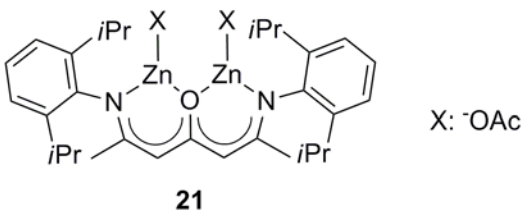


**Figure 16.** Dinuclear BODDI catalyst (resonance structures not shown)[126]

In 2005 Ding and coworkers used Trost's intramolecular dinuclear zinc complex for the copolymerization of CHO and $CO_2$ (Figure 17, **22**).[145] The catalyst was prepared *in situ* by complexation of the ligand with $ZnEt_2$ and the copolymerization reaction carried out under 30 bar $CO_2$ in toluene at 80 °C and a catalyst/CHO loading of 1:500. The TOFs at these conditions were around 140 $h^{-1}$ and the conversion and selectivity for poly(cyclohexene carbonate) up to 99 %.

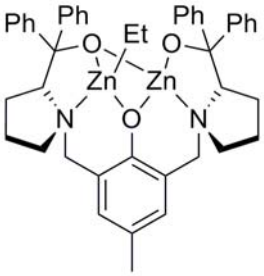


**22**

**Figure 17.** Dinuclear Trost complex[145]

The dinuclear Zn catalysts **22** were also highly active in diluted solutions and retained their selectivity even under very low $CO_2$ pressures (*i.e.* 1 bar), even though the activities decreased to 3 $h^{-1}$. It should be noted that the analogous Mg complex was also active in CHO/$CO_2$ copolymerization.[146]

By substitution of the prolinol framework, varied ligand structures were tested in copolymerization reactions. Electron donating groups lead to a decrease in epoxide conversion, however the introduction of electron withdrawing groups promoted consecutive epoxide insertions, yielding a polymer with a high degree of polyether linkages.

In 2005 Lee *et al.* reacted the anilido-aldimine ligands with dimethyl zinc and subsequently with $SO_2$ to generate "closed" and "open" dinuclear zinc complexes for the copolymerization (Figure 18, **23** and **24**).[131] A combination of NMR spectroscopic studies at varying temperatures and X-ray crystallographic analysis demonstrated the dinuclear nature of these catalysts, with zinc-zinc distances of 4.88 Å and 4.69 Å for the "open" and "closed" structure, respectively. The distances are in the same range as the previously reported β-diketiminato ethyl sulfinato zinc complexes (4.98 Å).[99]

These dinuclear catalysts are highly active for the copolymerization of CHO and $CO_2$ even under highly diluted conditions (catalyst/CHO = 1:17 000) and showed TOFs of up to 200 $h^{-1}$ with molecular weights of up to 280 000 g/mol and a carbonate content around 90 %. The copolymerization activity is very sensitive to the nature of the *ortho*-substituents of the aromatic moiety and the "open" catalyst is active, whereas the "closed" is completely inactive. The difference in efficiency is probably due to the better access to the metal centers in the "open" structure.

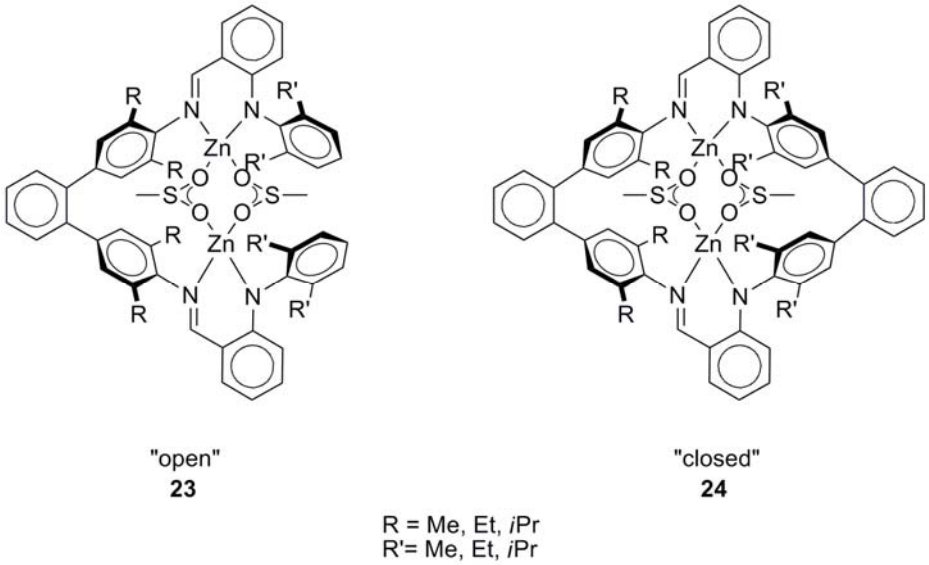


**Figure 18.** "Open" and "closed" dinuclear zinc complexes[131]

In 2006 *Lee et al.* prepared fluorinated anilido-aldimine ligands, which through complexation with dimethyl zinc afforded dinuclear complexes.[147] Reaction of these complexes with $SO_2$ converts the complexes into active catalysts for the copolymerization of CHO and $CO_2$ (Figure 19, **25**).

The Zn-Zn separation of compound **25** is slightly smaller (about 4.82 Å), compared to the non-fluorinated complex. Again, copolymerization reactions can be carried out, with the highest TOF of 2860 $h^{-1}$ being obtained at high dilutions (catalyst/CHO = 1:50 000).

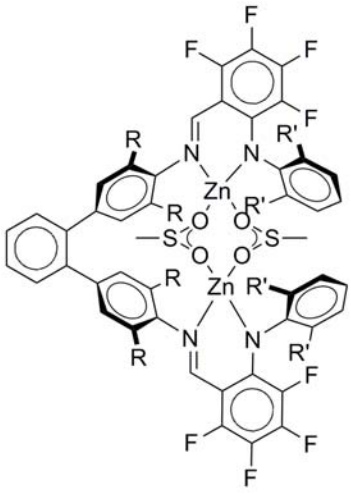


**25**

**Figure 19.** Fluorinated dinuclear zinc complex[147]

The electron-withdrawing fluorine groups presumably influence the Lewis acidity of the metal center, thereby increasing its $CO_2$/epoxide binding strength. At the same time the system is less sensitive to chain transfer agents, due the reduced basicity of the ligand nitrogen donors. As a drawback, the percentage of carbonate linkages is lower for the fluorinated than for the non-fluorinated system, which is attributed to the increased reaction speed and the lowered selectivity.

Limberg, Hultzsch and coworkers reported in 2007 xanthdim ligands which afforded dinuclear zinc complexes after complexation with diethyl zinc (Figure 20, **26** and **27**).[148] Zn-Zn distances of 4.92 Å and 5.60 Å were reported for the fluorinated and non-fluorinated complexes, respectively. The ligand structure allows the parallel orientation of two metal centers, in comparison to the above-mentioned dinuclear structures in which they are generally orientated face to face.

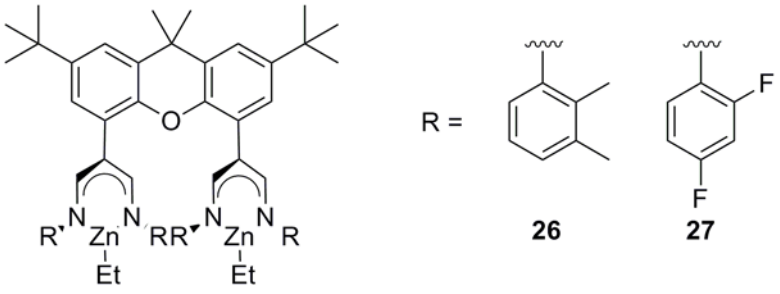


**26** **27**

**Figure 20.** Dinuclear xanthdim complexes[148]

The reaction of the zinc ethyl moieties in the dinuclear xanthdim complexes with $SO_2$ was unsuccessful due to the formation of oligomeric or polymeric coordination species. However the complexes comprising zinc ethyl groups were tested successfully in the copolymerization of CHO and $CO_2$. In traditional mononuclear BDI complexes the ethyl groups are not able to bridge two monomers to form an active dimer. However this unfavorable dimerization with ethyl groups can be overcome by activation with $SO_2$, which affords an active dimeric system with bridging ethylsulfinato-groups.[99] However, for complexes **26** and **27** the dinuclear nature implies an activity even with non-activated ZnEt moieties.

The non-fluorinated catalysts lead to poly(cyclohexene carbonate) with a relatively low content of carbonate linkages (50 %). This problem could be overcome by dilution of the reaction mixture with toluene which increases the content of the carbonate groups (up to 91 %) with a low TOF of 9 $h^{-1}$. The fluorinated complex mainly affords polyether formation (8 % carbonate linkages), the reason for this being the higher Lewis acidity of the metal center and therefore the accelerated ring opening of the epoxide.[148] The experiments show that these dinuclear xanthdim catalysts with parallel BDI-type ligands are only moderately active, which is attributed to overcrowding of the reaction pocket.[148]

Harder and coworkers used bridged β-diiminato ligands for the preparation of dinuclear zinc and calcium complexes (Figure 21).[149] The zinc complexes were all characterized by X-ray crystal diffraction, with the Zn-Zn distances for the 1,4-phenylene, 1,3-phenylene and 2,6-pyridylene complexes being 8.17 Å, 6.10 Å and 3.79 Å, respectively.

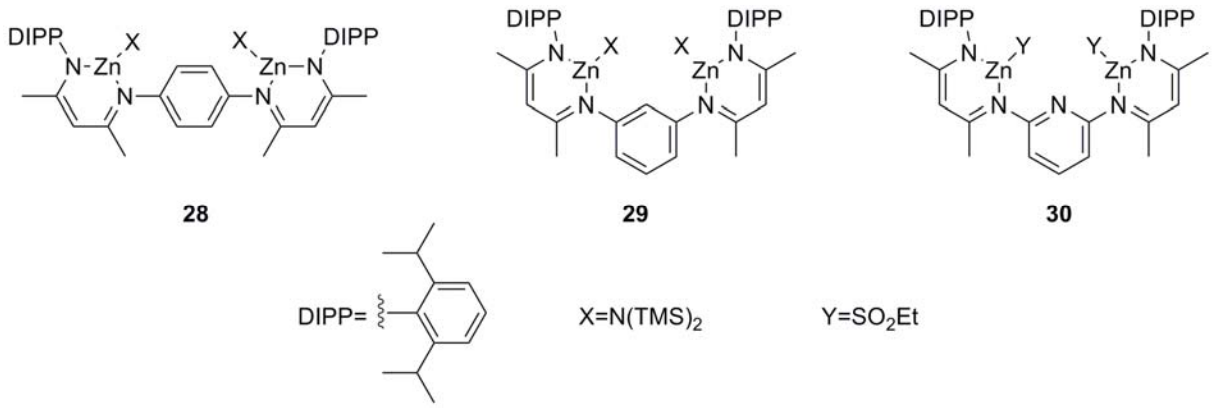


**Figure 21.** Bridged dinuclear Zn-BDI complexes[149]

Again, the proposed bimetallic mechanism is an important aspect of such dinuclear zinc catalysts. Dinuclear *para*-$(ZnEt)_2$ **28** and *meta*-$(ZnEt)_2$ **29** complexes initiate CHO/$CO_2$

copolymerization without $SO_2$ activation, a trend which has already been reported for the previously mentioned xanthdim catalysts **26** and **27**.

The activity is considerably higher for the *meta*-$(ZnEt)_2$ complex **29** (TOF = 129 $h^{-1}$) than for the *para*-$(ZnEt)_2$ complex **28** (TOF = 36 $h^{-1}$), presumably because the zinc-zinc distance in the *meta*-substituted ligand is much more suitable for the copolymerization. This illustrates the importance of a controlled metal-metal distance in these catalyst systems. Activation with $SO_2$ increases the activity of *meta*-$(ZnSO_2Et)_2$ (TOF = 181 $h^{-1}$) and a three-fold dilution raises the activity even further (TOF = 262 $h^{-1}$) delivering polymer with a molecular weight of up to 100 000 g/mol and 99 % carbonate linkages.

Complex **30**, which comprises a pyridine fragment in the center of the ligand framework is inactive, presumably due to the presence of the heterocyclic *N*-atom. This alters the complex conformation or coordinates to the Zn atoms thereby reducing its Lewis acidity, thus inhibiting CHO coordination and subsequent ring-opening.

In 2009 Williams *et al.* reported a dinuclear zinc catalyst with a reduced Robson-type ligand structure for the copolymerization of CHO and $CO_2$ (Figure 22, **31**),[150] with an acetate group initiator the zinc centers and the Zn-Zn distance being in the range of 3.11 Å.[151]

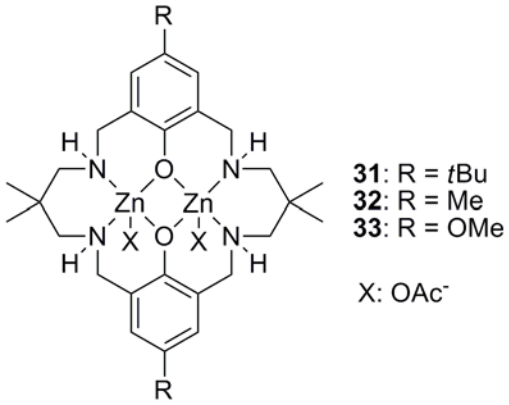


**Figure 22.** Dinuclear Robson-type complexes[150-151]

Copolymerization reactions can be carried out with **31** at pressures as low as 1 bar $CO_2$, with activities and TOFs up to 25 $h^{-1}$ and a high copolymer to cyclic carbonate ratio (TOF = 140 $h^{-1}$ at 10 bar $CO_2$). Room temperature NMR spectra of this complex showed broad resonances, whilst in higher temperature measurements, the peaks coalesce to observable resonances. This behavior indicates a fluxional complex structure in the solution state.

In further work, Williams and coworkers altered the substituents in the *para*-position of the phenolic moieties (Figure 22, **31** - **33**).[151] Introduction of a methyl **32** or methoxy group **33** in the *para*-position of the aryl backbone of the ligand moderately decreases activity in the copolymerization of CHO and $CO_2$ (**32**: TOF = 8.3 $h^{-1}$, **33**: TOF = 6 $h^{-1}$). This effect is associated with the lower Lewis acidity of the metal center and a decreased binding and activation of epoxide and $CO_2$.

In 2010 Williams *et al.* used the same ligand structure for the synthesis of dinuclear cobalt and iron complexes for the copolymerization of CHO and $CO_2$ (Fig. 23, **34a-c**).[152] Complexes comprising cobalt acetate centers were selected for these studies in order to compare the complexes with the previously reported zinc catalysts. Complexation was achieved by reaction of the ligand with cobalt(II) acetate which affords the desired Co(II) compound **34a** with a TOF of 410 $h^{-1}$ at 1 bar $CO_2$. The subsequent aerial oxidation leads to a mixed valency Co(II)/Co(III) complex **34b** with a slightly increased TOF of 480 $h^{-1}$ at this pressure and a TOF of 1700 $h^{-1}$ at 10 bar.

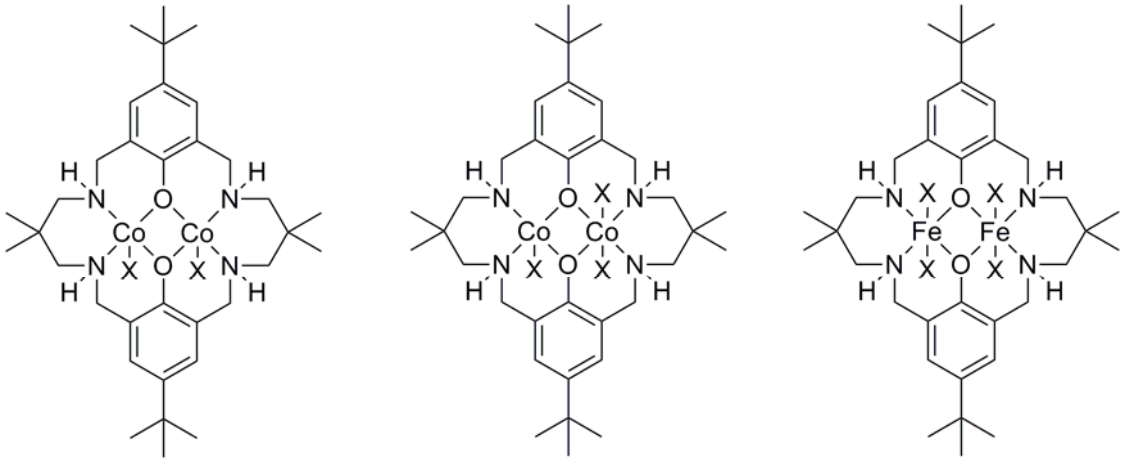


**Figure 23.** Dinuclear Robson-type complex with Co- and Fe-centers[152-153]

The Co-Co distances in **34a** and **34b** are close to 3 Å. Copolymerizations of CHO and $CO_2$ under 1 bar $CO_2$ pressure and at 80 °C demonstrate activities of an order of magnitude greater than those of the zinc analogues (TOF up to 172 $h^{-1}$). Additionally the selectivity of the cobalt catalysts (1 % cyclic carbonate) for the polymer formation is higher than that of the zinc complexes (4 % cyclic carbonate). The activity of these complexes at low pressures is attributed to the coordinative flexibility of the ligand system. Furthermore, the two closely

linked metal centers facilitate a bidentate carboxylate binding mode, thus lowering the energy barrier for $CO_2$ insertion. The higher activity of the cobalt catalysts is attributed to the enhanced nucleophilicity of the metal-bound carbonate group and thus better incorporation of the epoxide.

Recently, Williams *et al.* reported two iron(III) centers in this ligand framework and the corresponding copolymerization data (Fig. 23, **34c**).[153] This system was able to produce copolymer with CHO/$CO_2$ and demonstrated a TOF of 107 $h^{-1}$ at 80°C, 10 bar and a [Fe]/[CHO] ratio of 1000. The system did not yield copolymer with PO, but introduction of one equivalent PPNCl per Fe-center allowed the conversion of PO into cyclic propylene carbonate with TOFs around 25 $h^{-1}$.

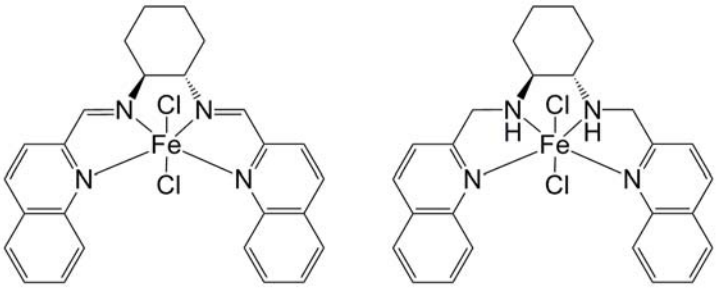


**Figure 24.** Mononuclear tetraamine-iron complexes[154]

Independently, Rieger *et al.* recently reported a mononuclear Fe-system that shows similar behavior toward PO and produces cyclic propylene carbonate in relatively high yields (Fig. 24, **35a - b**).[154] Preliminary experiments also indicate the copolymer formation with CHO/$CO_2$ and a strong dependence on the cocatalyst system. These works show for the first time that $CO_2$/epoxides can be copolymerized into polycarbonates *via* iron-complexes. In close future, this could allow an ecological as well as economical favorable alternative to the preferentially used toxic metals cobalt and chromium.

These reports all indicate that future work should focus on dinuclear ligand structures or binary linked systems as presented in the next chapter, especially when factors such as high dilutions and temperatures are considered.

### 2.4.2. Binary Linked Salen Systems

In order to increase the activity of the previously investigated salen complexes, different aspects have been addressed. As discussed previously (*vide supra*), a binary or a dinuclear catalytic system is presumably needed for $CO_2$/epoxide copolymerization with high activities. At the same time higher catalyst dilutions are needed to overcome diffusion limitations and enhance TON, and therefore TOF values. At such high dilutions, all associative processes are disfavored by the mass action law. The probability of formation of an active species by interaction of two catalyst molecules or a catalyst and a cocatalyst molecule is therefore decreased and activities tend to drop.

In order to overcome the low activities typically observed at low catalyst concentrations, new strategies are centered on tethering the cocatalyst to the same ligand framework. In this way, even at high dilutions, the interacting species remain in close proximity and these systems therefore retain their activity.

Nozaki *et al.* synthesized a piperidinium end-capped (salen)Co(III) complex which copolymerizes PO and $CO_2$ without the generation of cyclic propylene carbonate (cPC) with a TOF of 254 $h^{-1}$ (Scheme 9).[83]

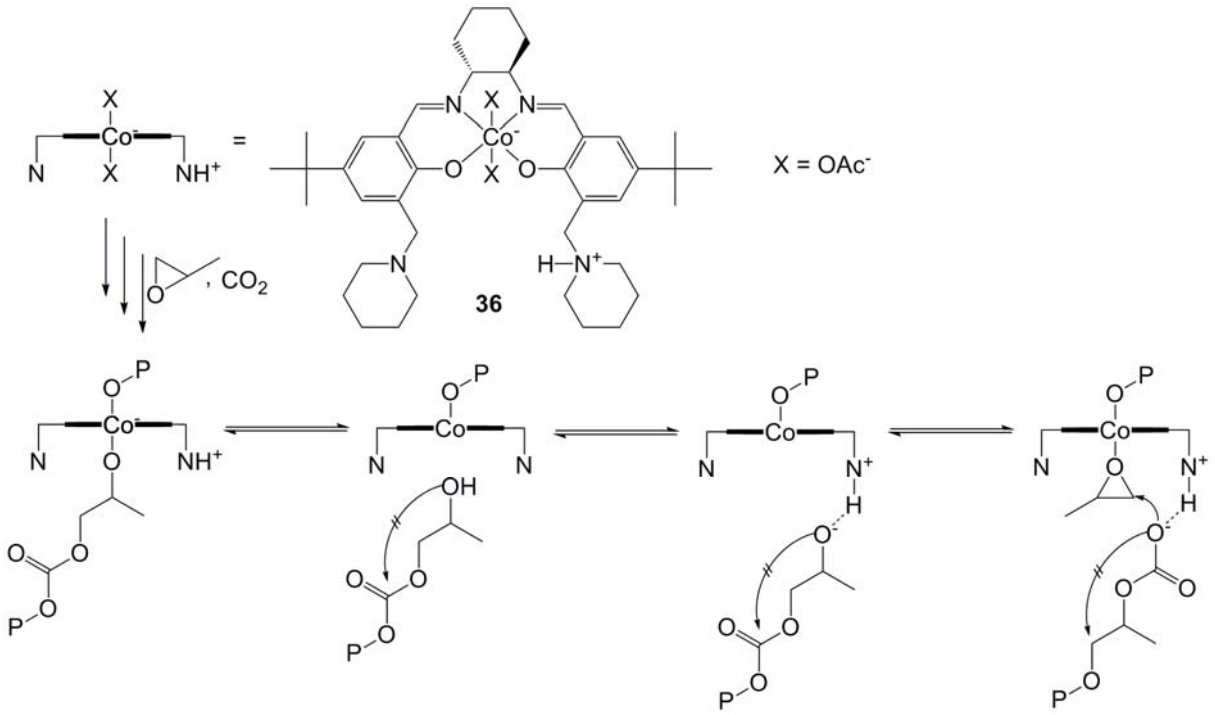


**Scheme 9.** Piperidinium end-capped (salen)Co(III)[83]

The high polymer selectivity observed with **36** is presumably achieved due to the piperidinium arm, which inhibits the formation of cyclic carbonate by protonation of the anionic propagating species when it dissociates from the metal center.

This protonation leads to a reduced nucleophilicity of the chain-end and hinders chain back-biting, a process leading to cyclic carbonate formation. Therefore the [epoxide]/[catalyst] ratio can be raised to 6500 and the polymerization temperature can be increased to 60°C, whereupon activities reach TOF = 600 $h^{-1}$ and a high PPC/cPC ratio is retained. Complete epoxide conversion could be achieved by addition of solvents such as DME (1,2-dimethoxyethane), toluene or dichloromethane. In this way, the polymerization mixtures become less viscous and diffusion of the monomers to the active site is retained. Another advantage of this system is that following complete monomer consumption, another monomer feedstock (*e.g.* 1-hexene oxide) can be added resulting in the formation of block terpolymers.

A similar strategy has been employed in related salen-type systems. A quaternary ammonium cation has been anchored on the salen ligand framework **39** resulting in higher activities, higher PPC/cPC content and the possibility of terpolymerizing CHO, PO and $CO_2$ (Figure 25).[155-158]

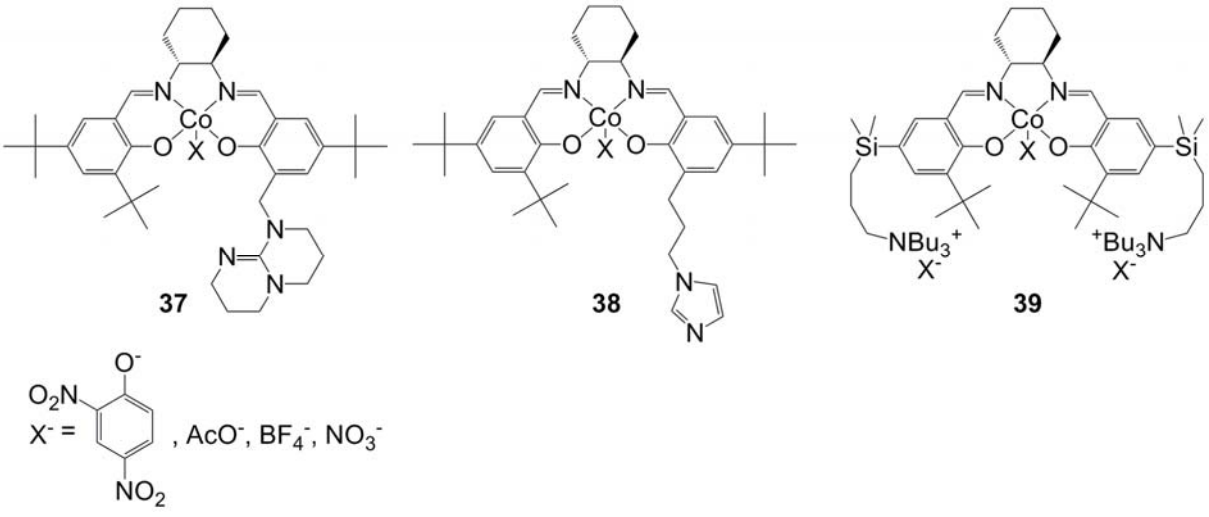


**Figure 25.** Representative (salen)Co(III) complexes with tethered sterically hindered organic bases and quaternary ammonium salts[155-158]

In contrast to the piperidinium-anchored catalyst **36** reported above, inhibition of back-biting occurs due to higher coulombic interactions of the growing chain with the catalyst

molecule **39** as a whole. Therefore the polymer is considered to not diffuse to any great distance from the active metal site in complexes **39**. Additionally the nucleophilicity of the anionic chain end is decreased through interaction with the positively charged groups. In this way the activity of quaternary ammonium salt anchored (salen)CoX remains high (**37**, X = OAc, TOF = 7100 $h^{-1}$; **38**, X = $NO_3$, TOF = 7 $h^{-1}$; **39**, X = 2,4-dinitrophenoxy: TOF = 3500 $h^{-1}$) even at high [monomer]/[catalyst] ratios of > 25 000 and high temperatures > 80°C. The copolymers produced have a molecular weight of around 50 000 – 100 000 g/mol and narrow PDI's around 1.3. At such conditions the traditional binary systems comprising (salen)CoX and PPNCl produce only cyclic carbonate or are completely inactive.

A considerable improvement to these anchored motifs was made by Lee *et al.*, who included four (or more) quaternary ammonium groups attached to the salen framework (Figure 26, **40** - **42**).[159-161]

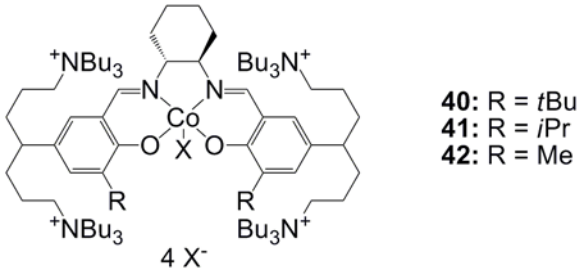


**Figure 26.** Salen with four anchored ammonium salt units[159-161]

This anchoring strategy gives rise to a catalyst which is able to be recovered after copolymerization whilst retaining its activity. At the same time, the catalyst residues can be removed from the produced polymer in a simple manner. In contrast to other salen systems, such binary linked complexes are strongly influenced by the nature of the *ortho*-substituent in the salicylaldimine moiety. The highest TOFs were achieved with a methyl substituted salen **42** and four anchored ammonium salt units; 25 % PO conversion was observed in 15 minutes at [PO]/[cat] ratio of 25 000 which corresponds to TOF = 26 000 $h^{-1}$, a PPC/cPC selectivity of greater than 99 % and a carbonate content above 99 %.[159] The TON and TOF could be considerably improved by increasing the reaction time at higher PO/catalyst loadings of up to 100 000 (TOF = 22 000 $h^{-1}$, TON = 22 000). At such high TONs, the copolymer produced has a molecular weight of 285 000 g/mol (PPC/cPC selectivity 96 %) and the cobalt level in the isolated polymer reaches 26 ppm and can even be lowered by

separating the residual cobalt complex by filtration of the polymerization mixture through a short pad of silica gel. The salen complex can be recovered and reactivated with 2,4-dinitrophenol and exhibits a comparable catalytic performance.

The authors propose that in this type of catalyst, the imino-nitrogens do not coordinate to the metal center, instead the counter anions of the quaternary ammonium cations ligate the cobalt (in this case 2,4-dinitrophenolate, DNP) (Figure 27).[161] As a result, the tetradentate coordination of regular salen systems shifts into an unusual bidentate coordination mode, which is presumably responsible for the high activity (Figure 26, **43** and **44**). Introduction of bulkier aryl substituents such as *t*Bu (**40**) or *i*Pr (**41**) prevent the bidentate coordination in favor of tetradentate coordination. As a result the activities drop, thus emphasizing the importance of a bidentate binding mode for this catalyst system. The tethered cationic side arms hold the cocatalyst anions respectively the anionic chain ends in the coordination sphere of the metal center, thus allowing rapid and efficient copolymerization. The growth of the polymer chains commences from the DNP initiator in the catalysts and hence all the polymer chains contain a DNP end group. However a bimodal distribution is found in GPC elugrams, a certain amount being initiated by DNP, the rest showing initiation *via* hydroxyl groups that result from chain-transfer reactions with water. However as DNPs are highly explosive in the dry state, new catalysts with inexpensive anions (*e.g.* 4-nitrophenolate, 2,4-dichlorophenolate) that replace the hazardous DNP have been investigated.[161]

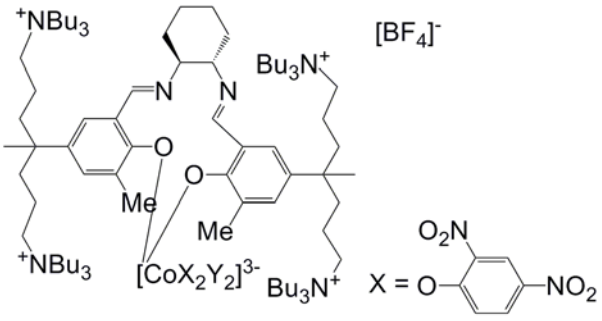


**43:** (Y = X)
**44:** (Y = X...H...X)

**Figure 27.** Unusual binding mode of binary linked salen complexes[161]

Another strategy to separate the catalyst after copolymerization has been investigated by Darensbourg *et al.* The salen derivative **45** contains two polyisobutylated (PIB) phenol

groups and is phase-selectively soluble in the heptane phase of a heptane/DMF or similar mixtures (Figure 28).[162]

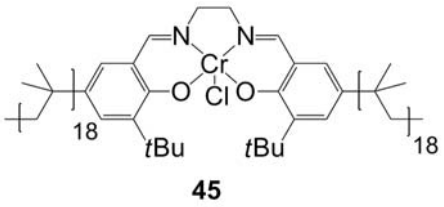


**45**

**Figure 28.** Polyisobutylene supported salen Cr(III) complex[162]

Complex **45** could be completely separated from the polymer by extraction after copolymerization at 80°C, 35 bar $CO_2$. The same initial rates of polymerization were observed as for Cr(salen) complexes without PIB-anchors. Recycling of the catalyst however lead to a 20-30 % reduction in polymerization activity, presumably due to acidolysis of the Cr(III) center from the PIB-salen complex.

The addition of cocatalysts to traditional salen complexes can considerably influence the efficiency of the system. Through tethering of cocatalyst functionalities to the salen ligand framework, the activity and selectivity towards polymerization can therefore be increased by a factor of several orders of magnitudes in comparison to earlier systems indicating a potentially successful direction for future catalyst development.

### 2.4.3. Dinuclear Salen Systems

Jacobsen *et al.* suggested that the activity of catalyst $CO_2$/epoxide copolymerization can be increased by utilization of flexibly linked dinuclear species and prepared bifunctional salen complexes.[52, 163] Other early experiments reported a combined gas-phase and solution-phase study of mono- and dinuclear (salen)$Cr^{III}$ complexes, which suggested the important role of dinuclear species in the homopolymerization of epoxides.[164]

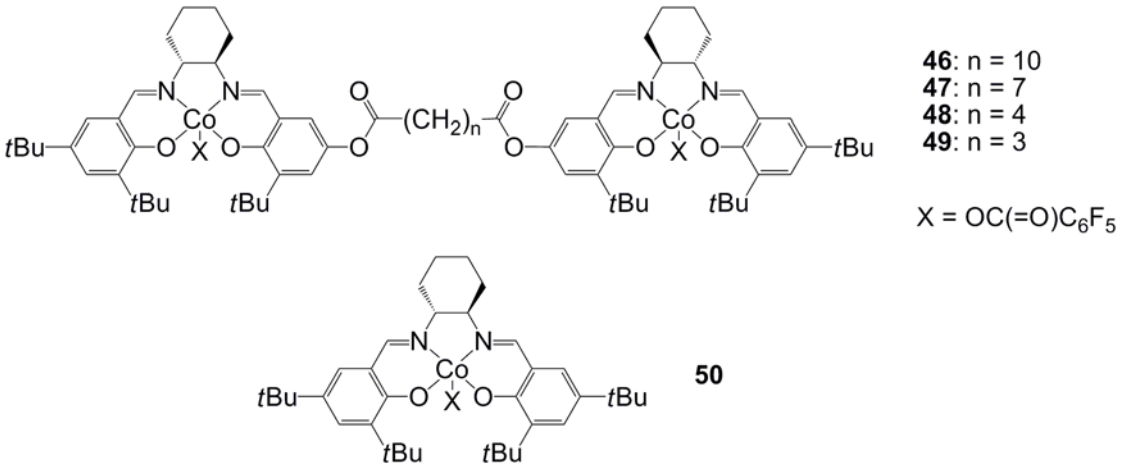


**Figure 29.** Mono- and dinuclear salen(Co) complexes[165]

In 2010, Nozaki *et al.* further investigated this system and synthesized a series of complexes with different spacer lengths (Fig. 29, **46-49**).[165] Copolymerization experiments under 53 bar and at 22 °C in 2 hours with a [PO]/[Co] ratio of 1000 indicated the optimal spacer length to be n = 4 (**48,** TOF = 180 $h^{-1}$), in comparison to n = 10 (**46**, TOF = 150 $h^{-1}$), n = 7 (**47**, TOF = 130 $h^{-1}$) and n = 3 (**49**, TOF = 140 $h^{-1}$). The racemic mixture of the mononuclear catalyst **50** shows a comparable activity at such copolymerization conditions (TOF = 100 $h^{-1}$). It should be noted that the optimal distance between two metal centers not only accelerates the alternating copolymerization, but also the homopolymerization of PO, which results in a somewhat lower content of carbonate linkages in the resulting polymer.

The main characteristic of the dinuclear cobalt complex however was the retention of catalytic activity even under low concentrations [PO]/[Co] = 3000 (*e.g.* for **48**, TOF = 150 $h^{-1}$), whereas the efficiency of the mononuclear complex **50** decreases (TOF = 20 $h^{-1}$) under such conditions. Addition of 0.5 equivalent PPNCl cocatalyst further increased the activity of the dinuclear system (**48**, TOF = 1280 $h^{-1}$), as well as that of the mononuclear system (**50**, TOF = 1180 $h^{-1}$). This indicates, as previously discussed that in presence of cocatalysts a binary mechanism is in state, which is independent of the dinuclearity of the system. Therefore activity and selectivity can easily improved by controlling the amount and nature of added cocatalyst.

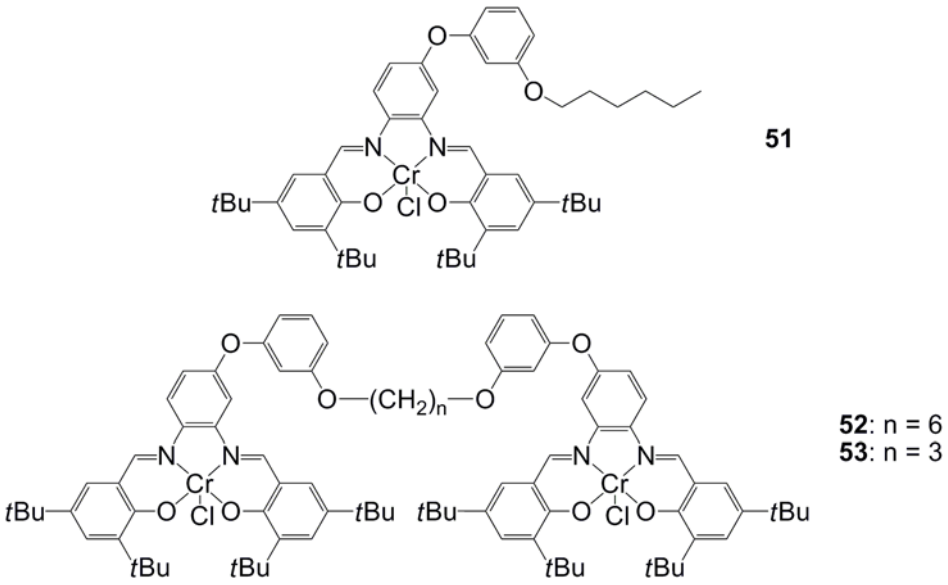


**Figure 30.** Mono- and dinuclear salphen(Cr) complexes[166]

In 2010, a similar study was independently conducted by Rieger *et al.* A new synthetic route allowed the preparation of dinuclear salphen(Cr) complexes with different linker lengths (Fig. 30, **52-53**).[166] Even though such systems generally show a slightly lower activity than salen systems, the same trend upon dilution is observed. Complex **52** with a spacer length of n = 6 shows a TOF of up to 49 $h^{-1}$ at copolymerization conditions of 40 bar and 60 °C, with a [PO]/[Cr] ratio of 2000. At a [PO]/[Cr] ratio of 20 000, the TOF even increases to 82 $h^{-1}$. In contrast, the activity of the mononuclear complex **51** drops from TOF = 67 $h^{-1}$ to TOF = 7 $h^{-1}$ upon dilution.

These investigation strongly indicate the copolymerization of $CO_2$ and epoxides to proceed *via* a bimetallic mechanism.

### 2.4.4. Immobilized Salen and BDI Systems

Immobilization of catalysts to a surface provides an effective means to recover and regenerate the catalyst after copolymerization. Immobilization of Zn-BDI catalysts for the copolymerization of epoxides and $CO_2$ onto silica materials (mesoporous SBA-15 and controlled-pore glass (CPG)) (Figure 31, **54**) gave moderate polymerization activities in comparison with their homogeneous analogues, presumably as a result of pore diffusion effects.[167] Recovery and potential regeneration of the catalyst were not reported.

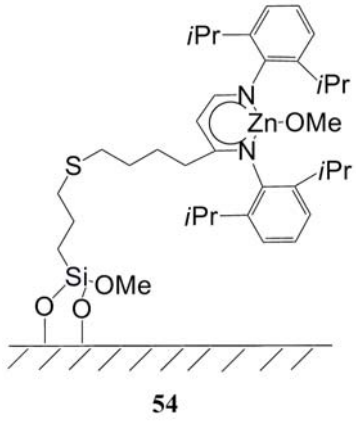


54

**Figure 31.** Immobilized BDI complexes[167]

García *et al.* described recyclable salen(Cr)Cl and salen(Al)X derivatives which were covalently anchored to a silicon polymer-support *via* a linker (Figure 32, **55** and **56**) but only exhibited activity towards cyclic carbonate production from styrene oxide.[53, 168-169]

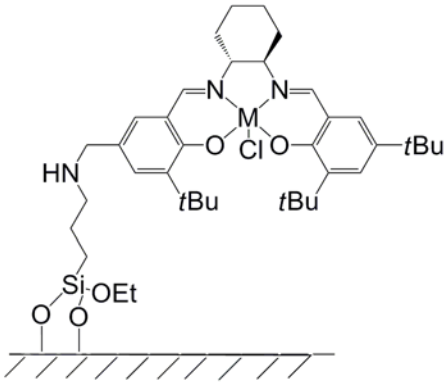


**55:** M = Cr
**56:** M = Al

**Figure 32.** Silica supported Cr- and Al-salen complexes[53, 168-169]

# 3. **Motivation**

As depicted in the introduction, a lot of catalyst systems and strategies have been developed in recent years for the $CO_2$/epoxide copolymerization reaction. Even though the copolymerization is known for 40 years, this chemistry is lacking efficient, economical and selective catalysts. This work focuses on the synthesis and development of efficient, untoxic and low-cost catalysts for the copolymerization.

The main part of this work concentrates on the development of highly active heterogeneous zinc dicarboxylates, which are industrially used for the large-scale polycarbonate production. The work focuses on logical enhancements of the system by increasing the surface area and modification of the active surface species. The results are substantiated by mechanistic considerations and theoretical calculations.

In the second part, homogeneous flexibly linked dinuclear salphen complexes are investigated in both their catalytic efficiency and the underlying polymerization mechanisms. Kinetic investigations corroborate the widely discussed bimetallic mechanism of such salen-like complexes.

In the third part, iron-containing complexes are described that allow the effective coupling of $CO_2$ and epoxides and open the route to an unproblematic polycarbonate production with untoxic metals.

Each of the three parts contains an own discussion and conclusion section, which give a summary of the results of each subject treated in this work. A complete conclusion, summarizing the most important results of all three parts, is given at the end of this work.

# 4. Results and Discussion

## 4.1. Heterogeneous Zinc Dicarboxylates

As described in Chapter 2.2, heterogeneous zinc dicarboxylates allow the industrial production of polycarbonates. Meanwhile, a series of effective homogeneous catalysts has been developed, which however involve disadvantages such as difficult synthesis processes, high production and separation costs and a high toxicity. Therefore, the majority of commercial polypropylene carbonate (PPC) is produced with the use of zinc glutarate. Such a heterogeneous process for the polycarbonate production is desirable, as the zinc dicarboxylates can easily be prepared and handled, are non-toxic and economically viable.

However, in over 30 years of research, the efficiency of zinc dicarboxylates could not be improved significantly. So far, the exact nature of the catalytically active species remains unknown, which renders systematic modifications of the system difficult. Furthermore, a huge activity difference between zinc glutarate and its lower homologue zinc succinate exists, which could not been explained so far.

In this work, several strategies for the enhancement of the catalytic activity were developed and investigated. Furthermore, a detailed investigation of the underlying copolymerization mechanisms on heterogeneous catalysts was conducted. Copolymerization mechanisms on zinc dicarboxylates have not been reported so far. In this work, the system is supposed to copolymerize in a bimetallic fashion (Chapter 2.1.1, Scheme 4).

All activities (turn-over frequencies; TOF) in this Chapter are given in “g polymer per mol metal center per hour” to allow a better comparison of the systems treated, whereas activities of homogeneous systems in all other Chapters are given in “mol polymer per mol metal center per hour”.

### 4.1.1. Synthesis Procedures

In order to investigate the zinc dicarboxylate system in its completeness, it is necessary to address all aspects of the material. Zinc dicarboxylates can be synthesized *via* several different procedures, which all allow to address one particular material property (Figure 33).

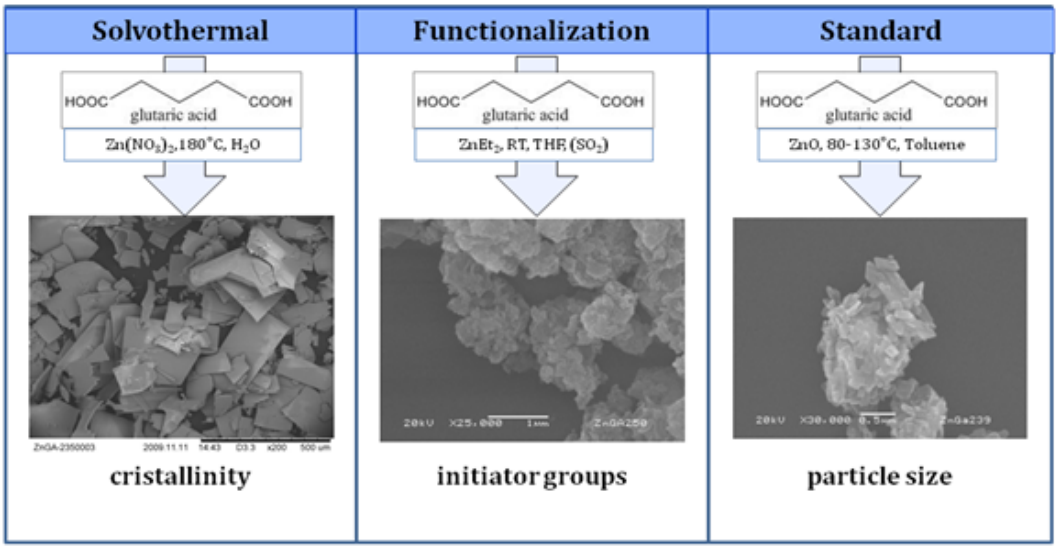


**Figure 33.** Synthesis routes to zinc glutarate, SEM pictures and the material properties that can be addressed.

The most common and convenient route enables the rapid formation of small crystalline particles *via* a slurry reaction. The dicarboxylic acid is added altogether with zinc oxide and stirred for several hours in toluene at 80 °C. The correspondent zinc dicarboxylates forms and precipitates in almost quantitative yields. The product gained *via* this procedure is – for reasons of simplicity and comparability – denominated as *standard* zinc glutarate with a rounded activity of 300 $g \cdot mol^{-1} \cdot h^{-1}$ (corresponds to ≈ 3 $mol \cdot mol^{-1} \cdot h^{-1}$). The benefit of the standard procedure is the rather easy alteration of the synthesis parameters as well as the unproblematic addition of templating chemicals. This allows an easy modification of the particle properties and sizes of the gained zinc dicarboxylate.

The second procedure involves a solvothermal (in this case: hydrothermal) process. The dicarboxylic acid and zinc nitrate are dissolved in water, closed into a high pressure reaction vessel and heated to 180 °C. The drawbacks of this procedure are the rather long reaction times, which prevent an industrial utilization. In return, the solvothermal synthesis route allows to produce highly crystalline and large particles that can easily be analyzed (*e.g.*

crystal structure through X-ray diffraction) and processed (*e.g.* down-sizing through ball-milling).

The third procedure allows the modification of active surface sites. In the functionalization route, dicarboxylic acid is combined with dialkyl zinc (*e.g.* $ZnMe_2$, $ZnEt_2$, $ZnPh_2$) in THF to yield zinc dicarboxylate with surface Zn-alkyl species that can be altered with other chemicals (*e.g.* alcohols, $SO_2$, …). In this way, the surface groups that will initiate the copolymerization of $CO_2$ and epoxides can be exchanged and compared.

All of these synthesis procedures have been used in this work and will be discussed in more detail where relevant. In general, the best investigated system with glutaric acid, namely zinc glutarate, is considered for discussion. This is why mainly zinc glutarate will be found in the following chapters. Other zinc dicarboxylates are only treated in the corresponding chapter, where they are substantial for a complete (mechanistic) understanding.

### 4.1.2. Influence of Water on Activity

As described in the introduction (Chapter 2.1.2, Factors Influencing Copolymerization), water is commonly considered as an undesired intoxicant of catalysts. In the best case, the catalysts undergo a chain transfer mechanism, leading to uncontrollable activities, molecular weights and PDIs. In the worst case, the catalyst completely loses its activity due to irreversible binding of water to the active sites. In any case, water is an aspect that has to be considered, especially when it comes to industrial applications, where identical polycarbonates need to be synthesized in every production cycle, but also when different catalytic systems are tested and copolymerization experiments are performed in lab-scale. In general, this means that catalysts and reagents (especially propylene oxide) have to be accurately dried in order to gain comparable and reproducible results.

However, an understanding of the influence of different water contents on the copolymerization efficiency of zinc dicarboxylates is of major importance, especially from an industrial perspective. An elaborated investigation of the influence of water has so far not been conducted. Therefore a set of copolymerization reactions were performed in which the water content was continuously increased from 0 % (no water per metal center) to 50 % (one water molecule per two metal centers) (Figure 34). The complete set of results can be found in the corresponding experimental section (Chapter 7.1.6. Copolymerization with Different Water Contents).

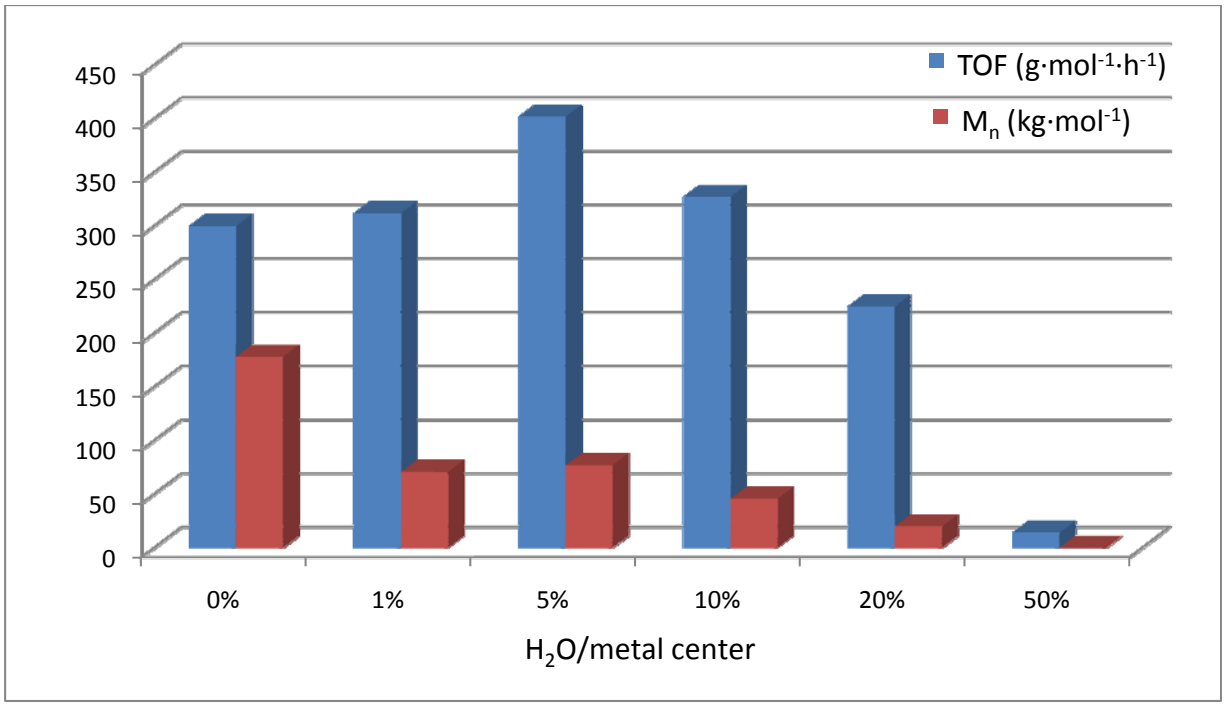


**Figure 34.** Influence of water content during copolymerization on activity and molecular weight.

Interestingly, the activity initially increases up to a water content of 5 %. This can probably be explained when taking into consideration the chain transfer mechanism. When this mechanism occurs, a growing polymer chain is cleaved from the active site and a new initiator group is created that is again able to initiate copolymerization. By this way, more but shorter polymer chains are formed and the overall viscosity during copolymerization is lowered, allowing for better monomer diffusion to the active sites and a higher catalyst performance.

With increasing water content, the activity rapidly drops as expected, due to irreversible binding to the active sites. At the same time, molecular weights decrease (due to the chain transfer mechanism) and the amount of cyclic carbonate increases (due to back-biting of the cleaved polymer chain ends).

Having defined the influence of water on copolymerization, it becomes clear that the catalysts, the propylene oxide, the $CO_2$ and all other eventual chemicals taking part in the polymerization reaction need to be carefully purified and dried to allow the comparability and reproducibility of experimental results. This is an important aspect of the copolymerization reaction, which has to be addressed both in lab-scale as well as in industrial scale.

## 4.2. Modification of Zinc Glutarate / Improvement of Activity

Having eliminated the main contributors to side-reactions, one can now focus on the development of efficient catalysts for the $CO_2$/epoxide copolymerization reaction. In order to enhance the activity of zinc glutarate, there exist mainly three different procedures. Initial strategies were focused on increasing the ZnGA surface area by one of four methods (stirring procedure, post-modification, additives, growth controllers) (Figure 35).[90, 93]

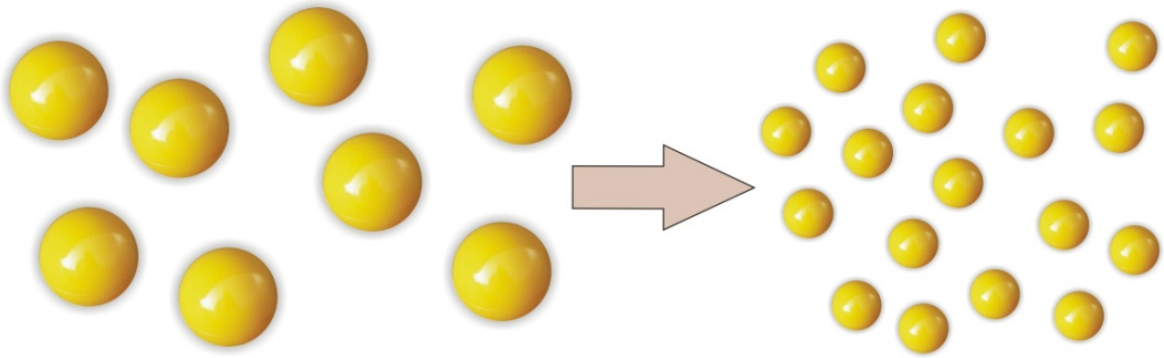

**Figure 35.** Increase of surface area (and activity) *via* down-sizing the material.

Each of these strategies has been tested in literature and shown to enhance activity, although the desired high activities that have been realized for several homogeneous catalysts have not been achieved with zinc dicarboxylates to date.[87, 90, 94-97] Therefore the different modification routes were further – and in a more structured way – investigated in this work.

### 4.2.1. Addition of Substrates during Synthesis

In a first attempt, highly disperse silica gel was added during the standard synthesis procedure of zinc glutarate. The underlying motivation was that the added silica gel with its high surface area would act as substrate on which the zinc glutarate would form with a similarly high surface area.

Indeed, it can be seen that the activity of zinc glutarate increases with increasing silica gel amount (Table 1, Entries 2 – 3). However, a control reaction (standard ZnGA and $SiO_2$ added during the copolymerization experiment) lead to comparable results (Table 1, Entries 4 - 5). Apparently the silica gel does not act as substrate, but has another role during copolymerization. One potential reason could be that the silica gel absorbs any residual water, therefore limiting its negative influence on catalyst efficiency (c.f. Chapter 2.1.2, Factors Influencing Copolymerization).

**Table 1.** Activity of zinc glutarate synthesized with different amounts of highly disperse silica gel as substrate.[a]

| Entry | catalyst | TON[b] | TOF[c] | % PPC[d] | $M_n$[e] | $M_w/M_n$[e] |
|---|---|---|---|---|---|---|
| 1 | standard ZnGA | 5876 | 294 | 95 | 72 | 4.1 |
| 2 | ZnGA (20 % $SiO_2$) | 6482 | 324 | 88 | 41 | 4.6 |
| 3 | ZnGA (50 % $SiO_2$) | 10671 | 534 | 65 | 49 | 4.8 |
| 4 | standard ZnGA + 20 % $SiO_2$ | 8680 | 434 | 83 | 58 | 4.1 |
| 5 | standard ZnGA + 50 % $SiO_2$ | 8288 | 414 | 79 | 73 | 4.5 |

[a] Polymerization conditions: 0.5 mmol cat, 150 mmol PO, 80°C, 20h, 40 bar, 500 rpm. [b] Turnover number in g polymer per mol of zinc. [c] Turnover frequency in g polymer per mol of zinc per hour. [d] Estimated by $^1$H NMR spectroscopy. [e] Determined by GPC, calibrated with polystyrene standard in THF, $M_n$ given in kg/mol

In order to gain a better understanding of the influence of silica gel onto the synthesis of zinc glutarate, high resolution SEM- and TEM-pictures were taken (Figure 36). It is apparent that zinc glutarate grows completely independent of the added substrate. In other words, the crystallization of zinc glutarate can only hardly be controlled *via* additives. It seems that zinc dicarboxylates always tend to crystallize in a platelet-shaped manner, independently of the reaction conditions. As a side-notice, also the addition of block-copolymers as structuring

agent during the synthesis will presumably not alter the way of crystallization, but only limits the degree of agglomeration therefore leading to more accessible reaction sites and higher activities.[87, 104]

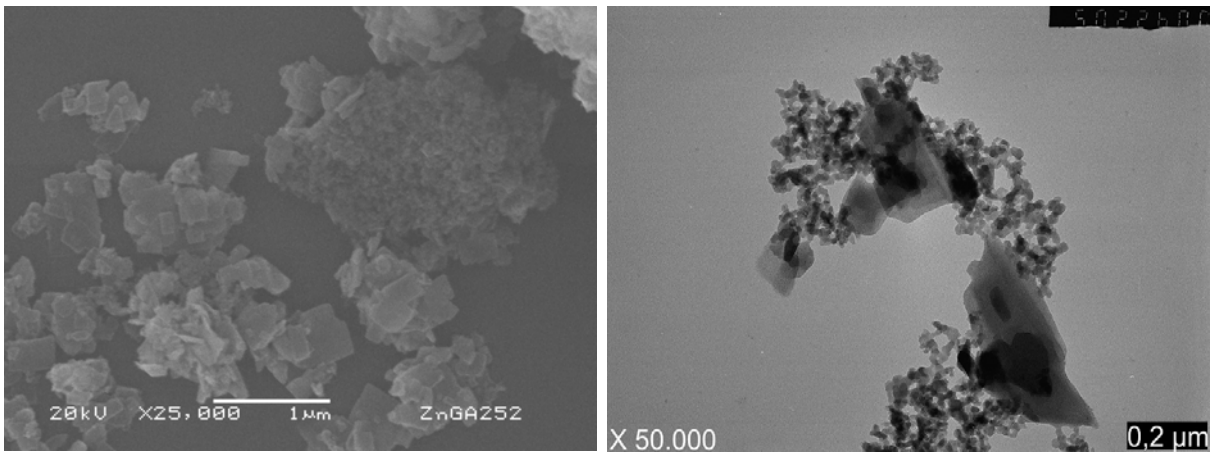


**Figure 36.** SEM- (left) and TEM-picture (right) of zinc glutarate synthesized with highly disperse siliga gel as substrate.

This renders the supporting of zinc dicarboxylates onto another material rather difficult. One possible strategy however could be the addition of a substrate material with a comparable crystal structure to that of zinc glutarate (space group P2/c), on which the catalyst preferentially grows.

### 4.2.2. Addition of Growth Controllers during Synthesis

Another strategy to enhance the efficiency of zinc glutarate involves the addition of growth controllers during the standard synthesis of zinc glutarate. When dicarboxylic acid is partially exchanged by a monocarboxylic acid (*e.g.* valeric acid, $CH_3$-$(CH_2)_3$-COOH), after incorporation of the monoacid, growth into that direction is suppressed. Therefore the average particle size gets smaller with increasing monoacid content. Indeed, the activity of zinc glutarate with added valeric acid increases with increasing monoacid content (Table 2). However, the activities rapidly converge to a maximum at about 450 $g \cdot mol^{-1} \cdot h^{-1}$, limiting the potential of this procedure.

**Table 2.** Activity of zinc glutarate synthesized with different amounts of valeric acid as growth controller.[a]

| entry | catalyst | TON[b] | TOF[c] | % PPC[d] | $M_n$[e] | $M_w/M_n$[e] | Surface[f] |
|---|---|---|---|---|---|---|---|
| 1 | standard ZnGA | 5876 | 294 | 95 | 72 | 4.5 | 15 |
| 2 | ZnGA (10 % VA) | 8084 | 404 | 81 | 57 | 4.8 | 16 |
| 3 | ZnGA (20 % VA) | 8500 | 425 | 94 | 87 | 5.3 | 20 |
| 4 | ZnGA (50 % VA) | 9064 | 453 | 90 | 91 | 2.5 | 35 |

[a] Polymerization conditions: 0.5 mmol cat, 150 mmol PO, 80°C, 20h, 40 bar, 500 rpm. [b] Turnover number in g polymer per mol of zinc. [c] Turnover frequency in g polymer per mol of zinc per hour. [d] Estimated by $^1$H NMR spectroscopy. [e] Determined by GPC, calibrated with polystyrene standard in THF, $M_n$ given in kg/mol, [f] Determined by BET-measurements with nitrogen, given in $m^2/g$.

In order to gain further insight into the effect of monoacid incorporation, BET-measurements (Table 2) as well as high resolution SEM- (Figure 37) and TEM-pictures (Figure 38) were taken. The absorption isotherms show that the surface area increases with increasing monoacid content. However, the activity does not increase by the same factor. Probably, the high content of valeric acid hinders the perfect crystallization of zinc glutarate, rendering the material less active overall.

Another reason could be that the particles formed *via* the standard procedure are already "close" in size to the unit cell. The SEM- and TEM-pictures show that there is no observable morphology change and that the crystal sizes are comparable. In all cases, thin platelets with

the dimensions of less than 1 µm x 1 µm and a thickness of less than 200 nm are formed. This means that the potential of further down-sizing the material (and thereby increasing the surface area and activity) is strongly limited. Addition of a higher content of monoacid will not substantially modify the particle size formed.

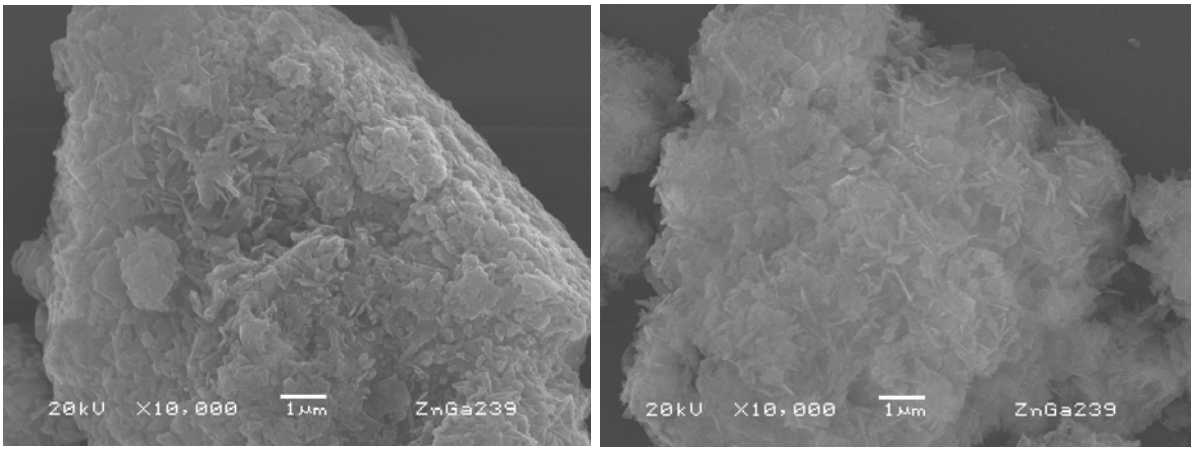


**Figure 37.** SEM-pictures of standard zinc glutarate (left) and zinc glutarate with 10 % valeric acid (right)

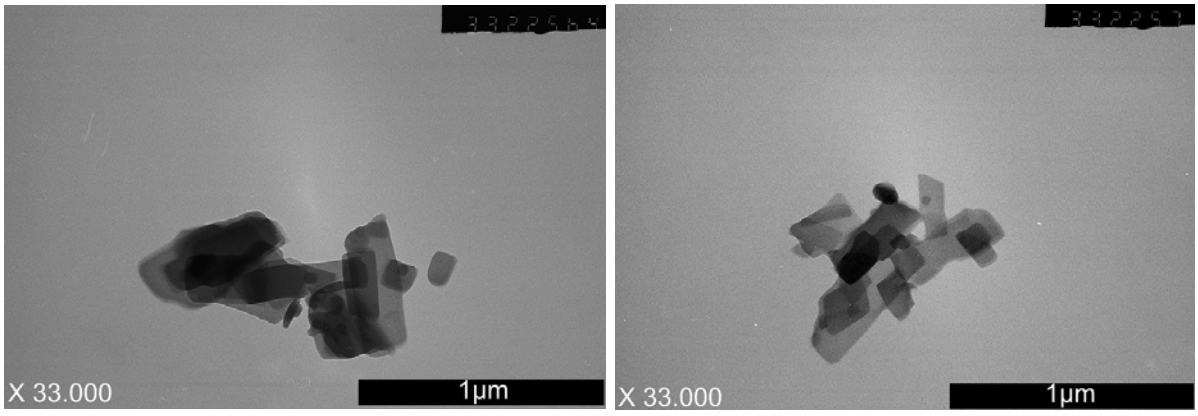


**Figure 38.** TEM-pictures of standard zinc glutarate (left) and zinc glutarate with 10 % valeric acid (right)

The addition of growth controllers to the synthesis of zinc dicarboxylate particles is therefore limited in its potential and leads to only slightly more active catalysts for the copolymerization reaction.

### 4.2.3. Post-treatment of Zinc dicarboxylates

As shown in the last chapters, the zinc dicarboxylate system is rather intolerant to logical modifications, which could lead to a substantial enhancement of the catalytic activity. None of the strategies tested in literature (stirring procedure, post-modification, additives, growth controllers), neither the strategies employed in this work lead to the efficiency needed for an industrially relevant and upscalable process.

This and the lacking knowledge about polymerization mechanisms on heterogeneous zinc dicarboxylates prompted us to investigate not only the already characterized solid state structure of zinc glutarate (ZnGA) and zinc-succinate (ZnSA), but also of their higher homologues zinc-adipate (ZnAA) and zinc-pimelate (ZnPA).

In order to get decent crystals for a structure determination, the synthetic route *via* hydrothermal treatment was used. For this purpose, the corresponding zinc-nitrate together with dicarboxylic acid and water is introduced into a glass-autoclave and heated to 180 °C. After several hours at this temperature, the glass vessel is interstratified with streaks that eventually form the crystalline particles after one to thirty days, depending on the dicarboxylic acid used. Even though this procedure generally suffers from low yields, highly crystalline particles can be gathered in all cases. Several of these crystals were collected for structure determination; the rest was grinded for 4 hours *via* a ball-mill in an inert argon atmosphere.

In order to minimize abrasion during the grinding-procedure, an abrasion resistant $ZrO_2$-beaker and $ZrO_2$-balls were used. The received powder was immediately transferred to a glovebox and the correspondent amount of the received powder weighed for $CO_2$/PO copolymerization experiments (Table 3, Entries 1-4). However, very low activities were achieved with this material.

This inefficiency of the ball-milled zinc dicarboxylates is supposed to result from inactive Zn-species on the newly generated surface. As the treatment was conducted in an inert argon atmosphere, no water molecules or other reagents could react with the Zn-species on the newly created faces. However post-treatment of the material with water and thorough drying in a vacuum-oven at 130 °C (to anticipate any chain transfer reaction with residual water) allowed us to activate the material. Indeed, the post-modified material shows a largely increased activity toward PO/$CO_2$ copolymerization (Table 3, Entries 5-8). This effect

is ascribed to the generation of ZnOH-groups on the surface, which then show an activity for the polymerization.

**Table 3.** Propylene oxide (PO)/$CO_2$ copolymerization results[a] with ball-milled zinc dicarboxylates

| entry | catalyst | TON[d] | TOF[e] | % PPC[f] | $M_n$[g] | $M_w/M_n$[g] |
|---|---|---|---|---|---|---|
| 1 | ZnSA[b] | 374 | 19 | 82 | 12 | 12.4 |
| 2 | ZnGA[b] | 1160 | 58 | 94 | 54 | 4.6 |
| 3 | ZnAA[b] | 867 | 43 | 94 | 38 | 4.8 |
| 4 | ZnPA[b] | 1107 | 55 | 95 | 52 | 4.1 |
| 5 | ZnSA[c] | 600 | 30 | 83 | 33 | 11.1 |
| 6 | ZnGA[c] | 7146 | 357 | 96 | 103 | 2.8 |
| 7 | ZnAA[c] | 6431 | 322 | 96 | 82 | 3.2 |
| 8 | ZnPA[c] | 4264 | 213 | 95 | 78 | 3.4 |

[a] Polymerization conditions: 0,5 mmol cat, 150 mmol PO, 80 °C, 20h, 40 bar $CO_2$ (initial pressure), 500 rpm. [b] not activated. [c] activated. [d] Turnover number in g polymer per mol of zinc. [e] Turnover frequency in g polymer per mol of zinc per hour. [f] Estimated by $^1$H NMR spectroscopy. [g] Determined by GPC, calibrated with polystyrene standard in THF, $M_n$ given in kg/mol.

To further determine the effect of grinding and post-activation, a series of different ball-milling intervals with the system ZnGA was investigated. In this series, the crystalline ZnGA particles from the hydrothermal synthesis were ball-milled for 10 min, 30 min, 1h, 2h and 4h respectively in an inert argon atmosphere and copolymerization experiments conducted with the resulting materials (Table 4, Entries 2 - 6). Copolymerization experiments with the untreated ZnGA yielded no product at all; the material obtained *via* hydrothermal synthesis route is constituted of big crystals with almost no surface area (Table 4, Entry 1). Additionally, the grinded material was post-activated the same way as previously described with water, then thoroughly dried and used in copolymerization (Table 4, Entries 7-11). For a better comparison, a copolymerization experiment with standard ZnGA (from ZnO and

glutaric acid) was realized using the same conditions (Table 4, Entry 12). The activity of ZnGA formed *via* standard procedure corresponds with TOF ≈ 300 $h^{-1}$ to that of ZnGA currently reported in literature.[36, 41, 87-89]

**Table 4.** Propylene oxide (PO)/$CO_2$ copolymerization results[a] with different ball-milling times of zinc glutarate

| entry | time of BM | TON[d] | TOF[e] | % PPC[f] | $M_n$[g] | $M_w/M_n$[g] |
|---|---|---|---|---|---|---|
| 1 | 0 min | 0 | 0 | / | / | / |
| 2 | 10 min[b] | 1080 | 54 | 94 | 48 | 3.7 |
| 3 | 30 min[b] | 1548 | 77 | 93 | 23 | 4.4 |
| 4 | 1 h[b] | 1432 | 72 | 93 | 18 | 8.2 |
| 5 | 2 h[b] | 1348 | 67 | 92 | 13 | 5.9 |
| 6 | 4 h[b] | 2108 | 105 | 94 | 43 | 4.9 |
| 7 | 10 min[c] | 1056 | 53 | 94 | 24 | 4.3 |
| 8 | 30 min[c] | 1416 | 71 | 94 | 43 | 4.6 |
| 9 | 1 h[c] | 1744 | 87 | 93 | 23 | 6.3 |
| 10 | 2 h[c] | 2932 | 147 | 95 | 45 | 4.0 |
| 11 | 4 h[c] | 7146 | 357 | 96 | 103 | 2.8 |
| 12 | standard | 5876 | 294 | 95 | 72 | 4.5 |

[a] Polymerization conditions: 0,5 mmol cat, 150 mmol PO, 80 °C, 20h, 40 bar, 500 rpm. [b] not activated. [c] activated. [d] Turnover number in g polymer per mol of zinc. [e] Turnover frequency in g polymer per mol of zinc per hour. [f] Estimated by $^1$H NMR spectroscopy. [g] Determined by GPC, calibrated with polystyrene standard in THF, $M_n$ given in kg/mol.

Ball-milling of ZnGA without post-activation leads to almost no improvement in activity. Non-activated material shows the same efficiency for copolymerization, independent of the previous grinding interval, which can be attributed to the lack of initiator groups on the surface. Again, post-activation with water leads to active material which shows the expected correlation of grinding time and activity. For a better comparison, a graphical presentation of the activities shown in Table 4 is given in Figure 39.

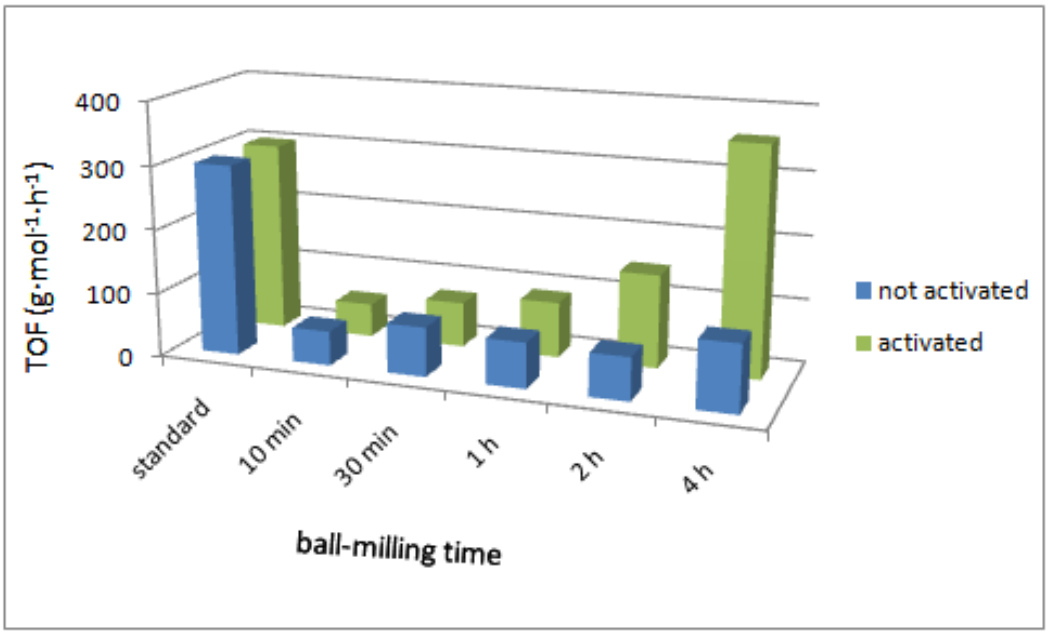


**Figure 39.** Graphical presentation of the correlation between ball-milling time, activity and the influence of post-activation.

From the activity data given in Table 3, it is apparent that all zinc dicarboxylates except ZnSA show a comparable activity for PO/$CO_2$-copolymerization. Indeed, ZnGA, ZnAA and ZnPA exhibit a comparable efficiency in their activated (TOF ≈ 50 $h^{-1}$) as well as in their non-activated state (TOF ≈ 300 $h^{-1}$). However, the activity of the ball-milled ZnSA (TOF = 19 $h^{-1}$) and post-activated ZnSA (TOF = 30 $h^{-1}$) does not change to the same degree as for ZnGA and its higher homologues. The underlying reason for this behavior is examined in the following chapters.

### 4.2.4. Comparison of Surface Area and Particle Size

In order to further investigate the correlation between grinding and activity, the surface areas of the ball-milled samples and the reference (standard) sample were determined *via* BET-measurements ($N_2$) and the particle sizes compared in high-resolution SEM- respectively TEM-pictures.

The ZnGA synthesized *via* standard procedure has a surface area of 15.2 $m^2/g$, the samples that were ball-milled for 4 hours show a surface area of 8.9 $m^2/g$ (ZnSA), 14.9 $m^2/g$ (ZnGA), 9.6 $m^2/g$ (ZnAA) and 8.5 $m^2/g$ (ZnPA) respectively. These results show that all materials have

a surface area of approximately 10 - 15 $m^2/g$ and no microporosity at all, confirming that the copolymerization only takes place on the outer surface of zinc dicarboxylates. As the surface area of all four catalysts lies in the same range, it cannot the decisive factor for the activity difference between ZnSA and its higher homologues.

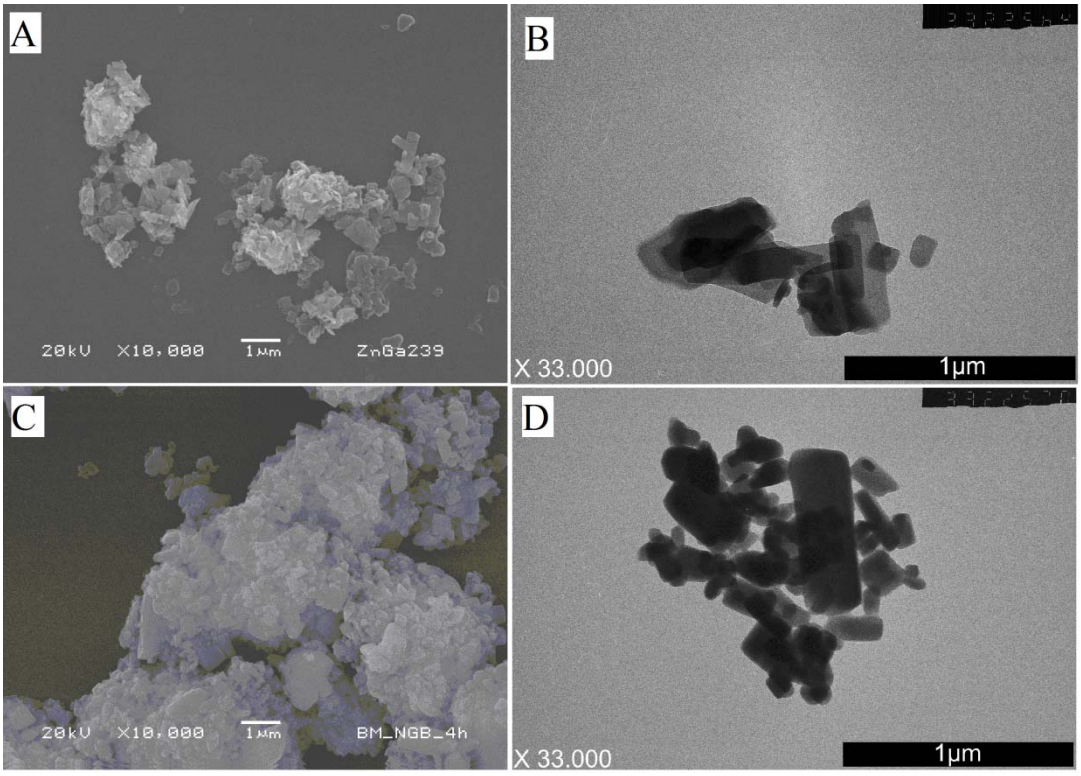


**Figure 40.** High-resolution SEM- and TEM-pictures of standard ZnGA (A, B) and ball-milled ZnGA (ball-milling interval: 4h) (C,D).

Additionally, high-resolution SEM- and TEM-pictures of the material were taken (Figure 40, A-D). This allowed us to compare the morphology and particle size of the resulting materials. The TEM-pictures indicate that the ball-milling of the crystalline particles for 4 hours delivers ZnGA platelets with approximately the same particle size (and therefore surface area and activity, Table 4 Entry 11) as for the material synthesized with the standard procedure (Table 4, Entry 12).

Further ball-milling would presumably only show a marginal effect on activity, as the particle size of the resulting material after 4 hours of ball-milling is already situated at the lower end (< 1 µm) of what ball-mills are capable to treat. The same size of crystal sizes can be found

when synthesizing zinc dicarboxylates *via* the standard procedure (c.f. Chapter 4.2.2. Addition of Growth Controllers during Synthesis), where thin platelets with the dimensions of less than 1 µm x 1 µm and a thickness of less than 200 nm are formed. As a side-notice, this observation also gives a good hint on why logical modifications of the zinc dicarboxylates only lead to a marginal effect in its efficiency. All strategies investigated so far to increase the activity were based on the increase of its surface area (stirring procedure, post-modification, additives, growth controllers). It becomes obvious that all of these strategies are limited due to the limitations in further down-sizing the material. Efficient catalysts for the copolymerization reaction presumably have to be based on homogeneous systems.

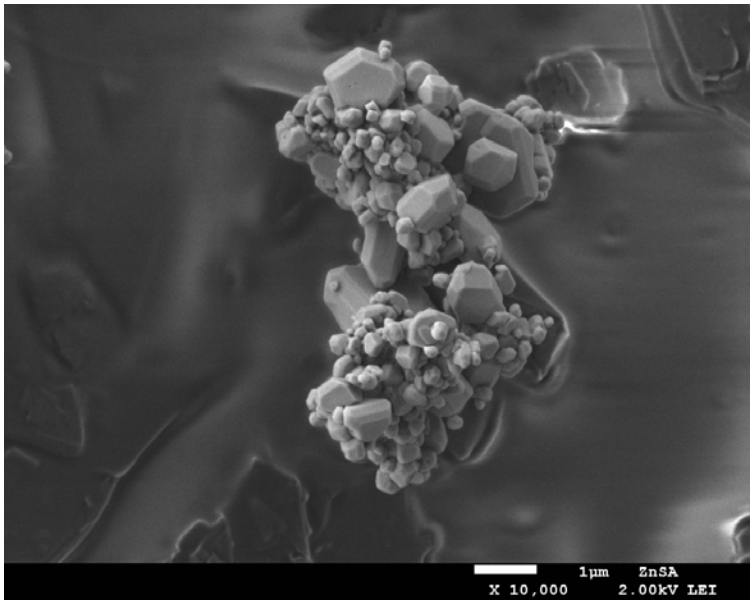


**Figure 41.** SEM-picture of zinc-succinate that has been ball-milled for 4 hours. The particle size is situated in the same range as for ball-milled ZnGA.

In conclusion, the surface area, the particle size and the morphology of ZnSA (Figure 41) is comparable to that of ZnGA. The reason for the activity difference between ZnSA and its higher homologues must therefore be attributed to a different solid state structure of ZnSA, which does not provide the active surface species that are necessary for copolymerization.

### 4.2.5. Investigation of the Solid State Structure

To get a better insight into the difference between ZnSA and its higher homologues and the effect of the surface constitution, the solid state structures of the different zinc dicarboxylates have to be compared. In two independent attempts, the molecular structure of ZnSA has been reported.[108, 170] Considerable variations in the solid state structure of ZnSA are observed, which presumably arise from the different synthetic conditions employed. However, in this work, only the synthesis of the monoclinic C2-symmetric structure of ZnSA could be achieved (Figure 42, A). The solid state structure of ZnGA has been verified as described in literature (Figure 42, B). The two structures of ZnSA and ZnGA vary considerably, which makes a clear statement about the active species difficult. In order to get a complete insight into the inefficiency of ZnSA compared to the other zinc dicarboxylates, the solid state structure of ZnAA and ZnPA was also determined (Figure 42, C and D). The crystalline particles for structure determination were taken from the hydrothermal synthesis route and their orientation, respectively growth direction determined (Figure 43).

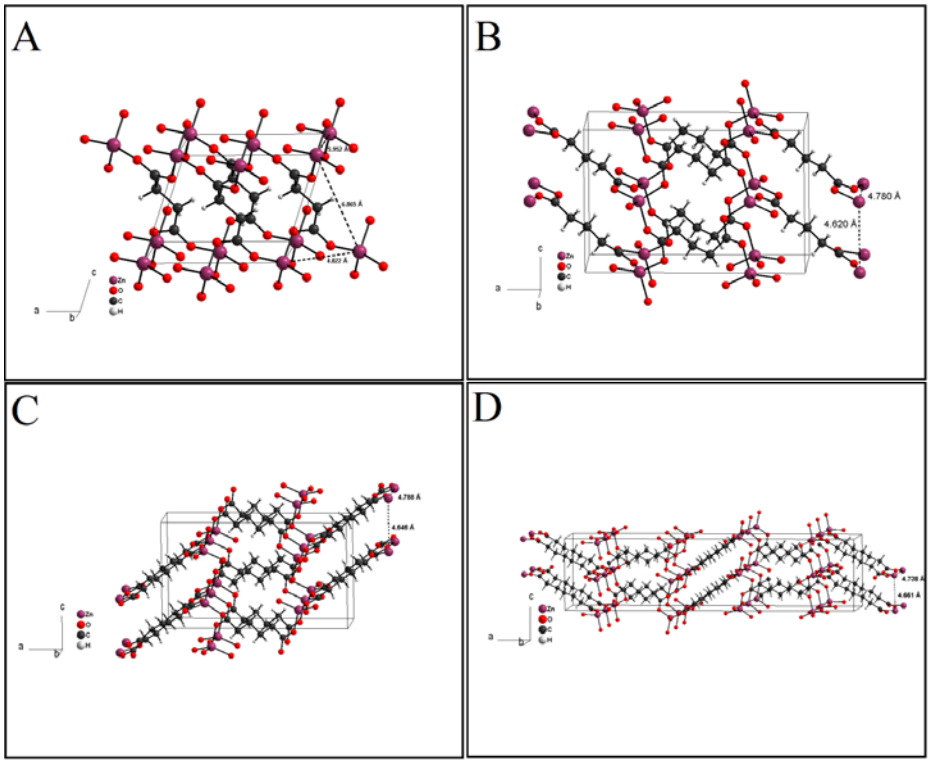


**Figure 42.** Solid state structures of ZnSA[107-108] (A), ZnGA[91-92] (B), ZnAA (C) and ZnPA (D) (Diamond drawing).

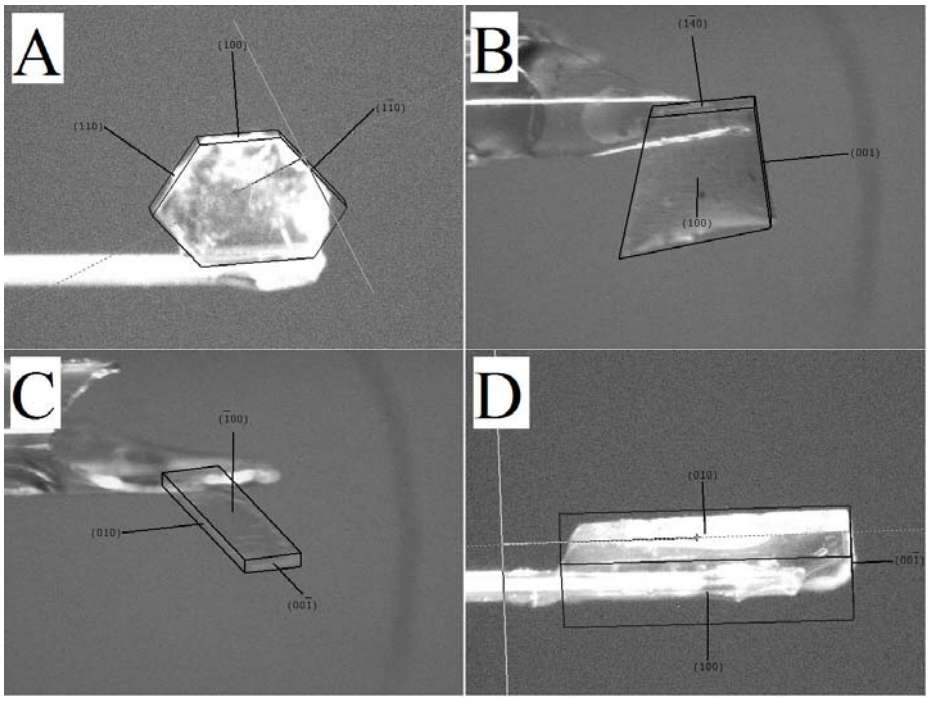


**Figure 43.** Orientation and growth direction of crystals ZnSA[107-108] (A), ZnGA[91-92] (B), ZnAA (C) and ZnPA (D).

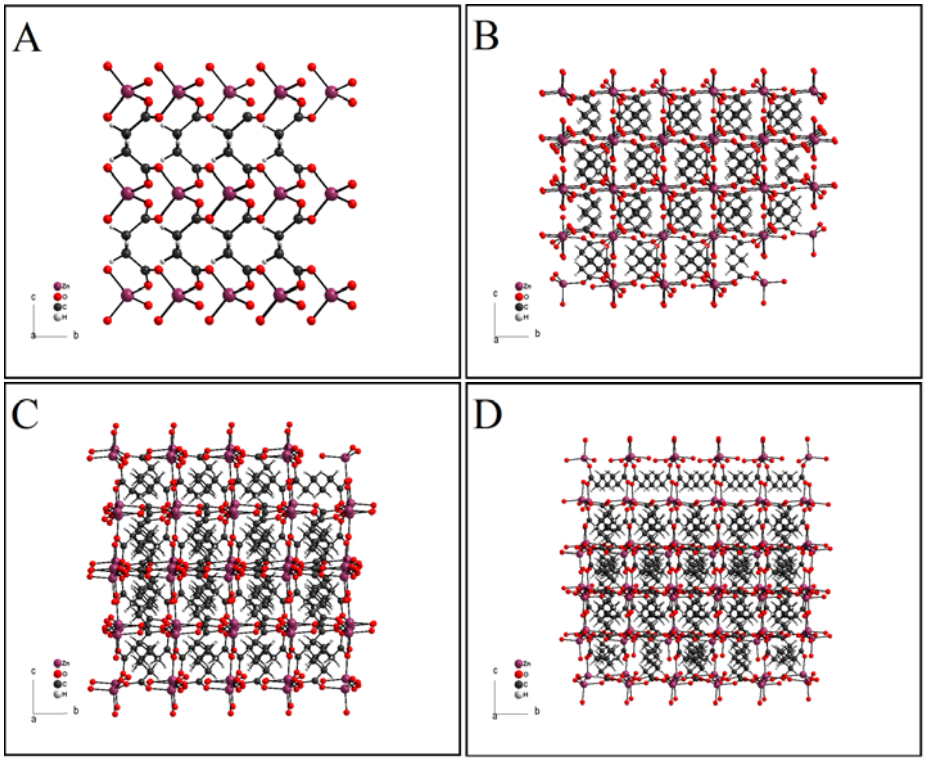


**Figure 44.** View along *a*-axis of ZnSA[107-108] (A), ZnGA[91-92] (B), ZnAA (C) and ZnPA (D)

As expected, ZnGA, ZnAA and ZnPA show the same space group P2/c and a very similar structure, with the cell axes *a* and *c* and all angles having approximately the same axes lengths respectively degrees. Only the cell axis *b* differs considerably in each structure, due to the elongated C-backbone of the higher dicarboxylic acid, which results in a drawn-out unit cell. Most strikingly, the constitution of the hkl-plane [100] remains completely the same in all three structures (ZnGA, ZnAA and ZnPA), with four Zn-atoms in a very defined spatial conformation and a Zn-Zn distance of 4.6 – 4.8 Å (Figure 44). This structural motif however cannot be found in the solid state structure of ZnSA, which could explain the activity difference between ZnSA and its higher homologues, when a bimetallic mechanism is assumed. The distance of 4.6 – 4.8 Å is also situated in the same area as for regular dinuclear homogeneous complexes that are used in $CO_2$/epoxide copolymerization and is therefore considered as necessary for any bimetallic mechanism on a heterogeneous zinc dicarboxylate surface.

When the structures of ZnGA, ZnAA and ZnPA are compared to ZnSA (Figure 42, A), it becomes apparent why this material is much less active than its higher homologues. For an active ZnSA catalyst, the [001] plane needs to have the largest expansion, as on most other [hkl] planes, no Zn-Zn couples can be found (compare Figures 45 and 46 for views along *b*- and *c*-axes). Such a directional growth is rather difficult, which limits the efficiency of ZnSA. When ZnSA is treated with a ball-mill, the breaking events will only expose few new surfaces with the necessary Zn-Zn-couples.

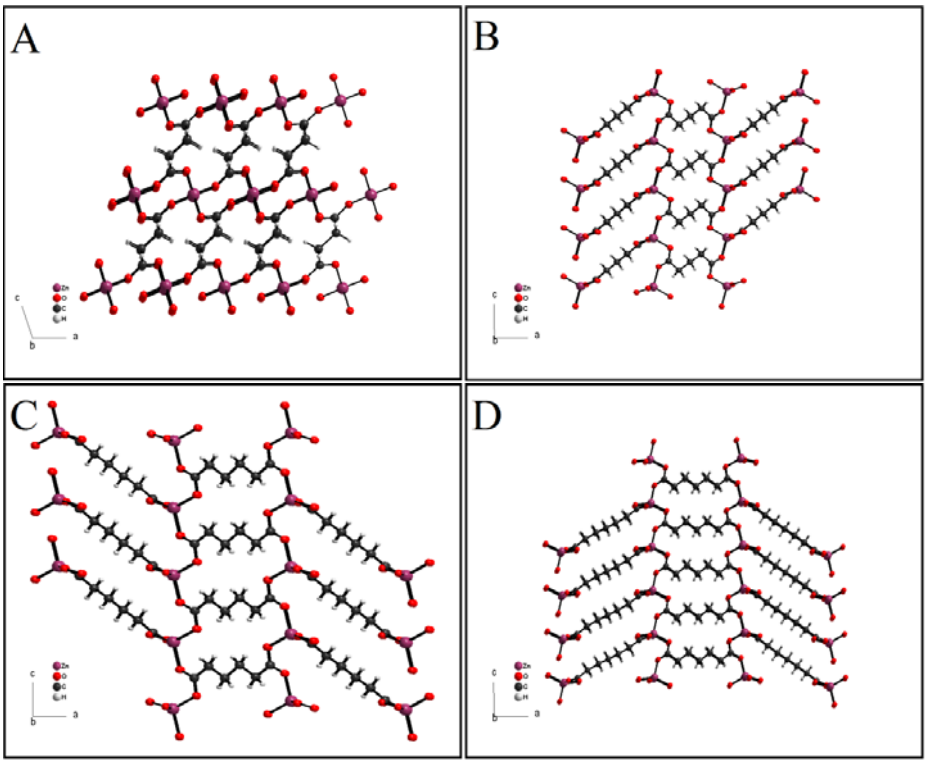


**Figure 45.** View along *b*-axis of ZnSA[107-108] (A), ZnGA[91-92] (B), ZnAA (C) and ZnPA (D).

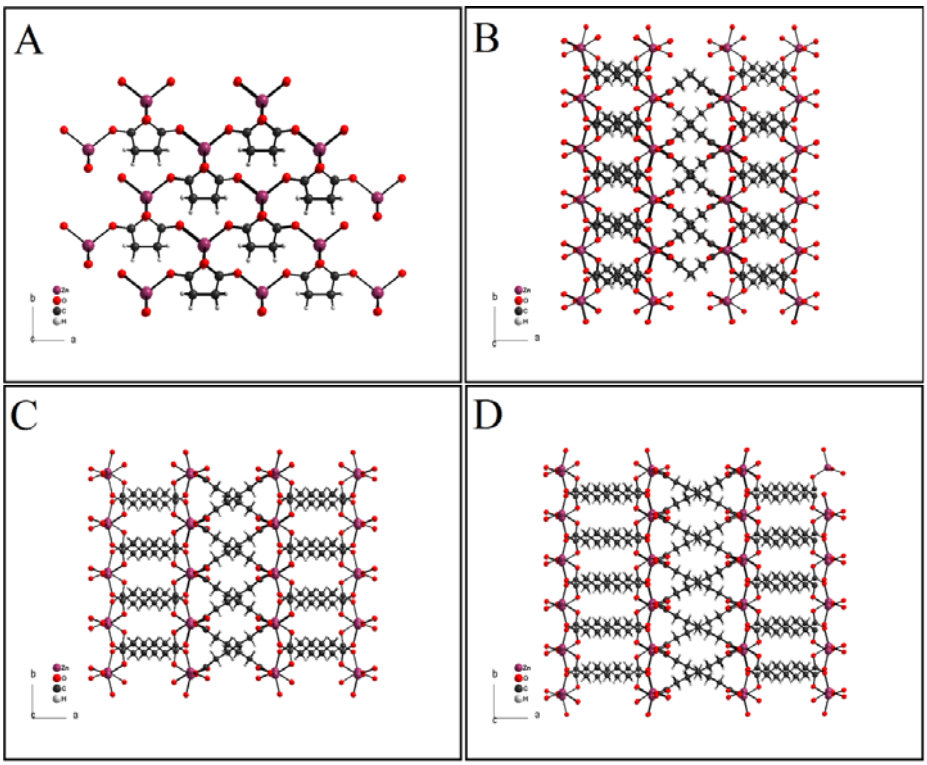


**Figure 46.** View along *c*-axis of ZnSA[107-108] (A), ZnGA[91-92] (B), ZnAA (C) and ZnPA (D).

ZnGA, ZnAA and ZnPA crystals however can be grown or cut in any direction and still have exposed Zn-Zn couples in the right spatial conformation. This means that *e.g.* breaking the

ZnGA along its [100], [010] or [001] plane will always lead to newly exposed Zn-Zn couples with an intermetallic distance of 4.6 – 4.8 Å. For a better comparison, some more selected Zn-Zn-distances on several important [hkl] planes are given for all four treated zinc dicarboxylates (Table 5).

**Table 5.** Zn-Zn-distances on selected [hkl] indiced faces, all values given in Å

| hkl | 100 | 010 | 001 | 110 | 101 | 011 | -110 | 10-1 | 0-11 | 210 | 201 | 120 | 021 | 012 | 102 |
|---|---|---|---|---|---|---|---|---|---|---|---|---|---|---|---|
| **ZnSA** | / | / | 4.83 | 4.83 | / | / | 4.83 | / | / | / | / | / | / | / | / |
| **ZnGA** | 4.78<br>4.64 | 4.64 | 4.78 | 4.64 | 4.78 | / | 4.64 | 4.78 | / | 4.64 | 4.78 | 4.64 | / | / | 4.78 |
| **ZnAA** | 4.78<br>4.64 | 4.64 | 4.78 | 4.64 | 4.78 | / | 4.64 | 4.78 | / | 4.64 | 4.78 | 4.64 | / | / | 4.78 |
| **ZnPA** | 4.74<br>4.66 | 4.66 | 4.74 | 4.66 | 4.74 | / | 4.66 | 4.74 | 4.66 | 4.66 | 4.74 | 4.66 | / | / | 4.74 |

The data given in Table 5 shows that upon growing or cutting ZnGA, ZnAA and ZnPA crystals in most directions, Zn-Zn couples with distances of 4.64 Å or 4.78 Å will be exposed. In contrast, upon growing or cutting ZnSA crystals, only three important hkl-faces will expose new Zn-Zn couples with the relevant distance of 4.83 Å. From a statistical point of view, during ball-milling, ZnGA, ZnAA and ZnPA will be activated to a much larger extend than ZnSA, which explains the polymerization data given in Table 1. A close-up view onto the relevant structure motif in zinc glutarate with the high-lighted Zn-Zn-distances is given in Figure 47.

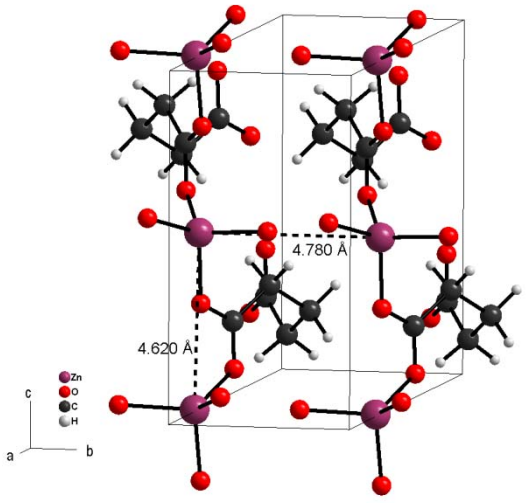


**Figure 47.** Close-up view of metal distances in zinc glutarate (Zn-Zn-distance = 4.6 – 4.8 Å).

This is the first time that a bimetallic $CO_2$/epoxide copolymerization mechanism is suggested for a heterogeneous catalyst. However, it is not clear yet, which intermetallic distance shows an optimum towards copolymerization efficiency and/or selectivity. In order to further investigate the influence of the intermetallic distance, theoretical calculations were conducted (Chapter 4.2.7. Theoretical Investigation). These will also allow to substantiate the conclusions derived in the experimental part and to corroborate the necessity of two closely linked active metal centers on the surface of heterogeneous zinc dicarboxylates, as well as in homogeneous systems.

### 4.2.6. Powder X-Ray Diffraction

PXRD data was taken from the ball-milled samples in order to verify that the solid state structure was not altered by the ball-milling events. Comparison with the calculated diffraction patterns (from the solid state structure *via* Mercury) shows that the solid state structure remains unaltered (Figures 48 – 51).

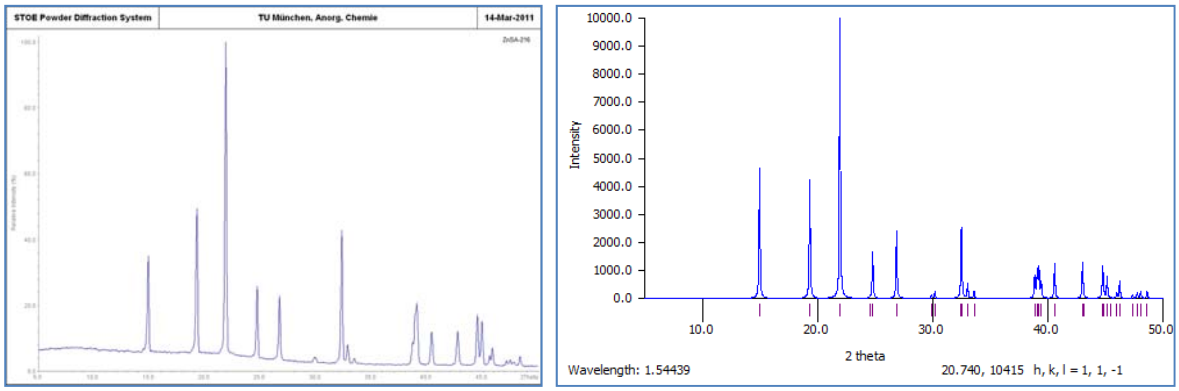


**Figure 48.** PXRD of zinc-succinate (ZnSA) ball-milled for 4 hours and calculated from the solid state structure *via* mercury.

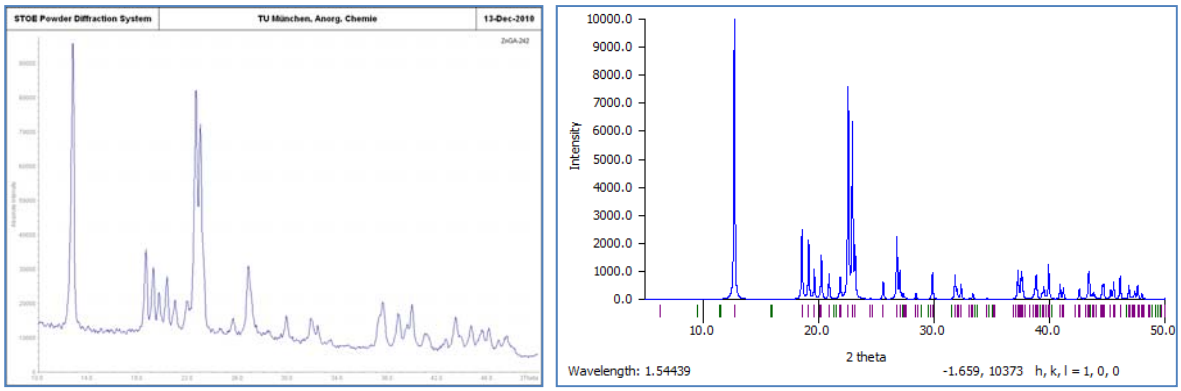


**Figure 49.** PXRD of zinc glutarate (ZnGA) ball-milled for 4 hours and calculated from the solid state structure *via* mercury.

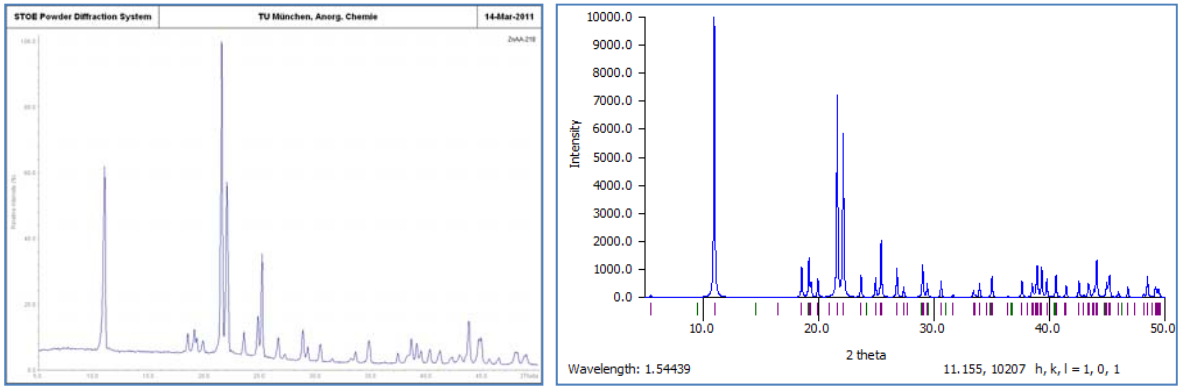


**Figure 50.** PXRD of zinc-adipate (ZnAA) ball-milled for 4 hours and calculated from the solid state structure *via* mercury.

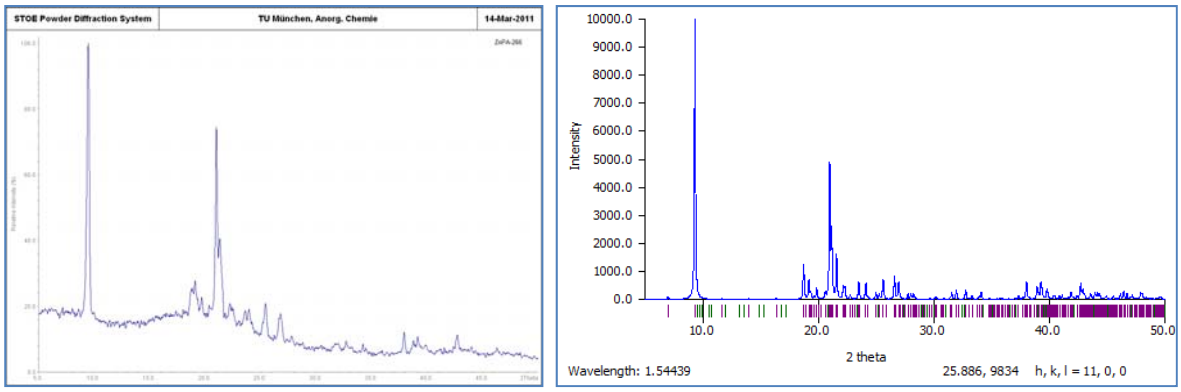


**Figure 51.** PXRD of zinc-pimelate (ZnPA) ball-milled for 4 hours and calculated from the solid state structure *via* mercury.

### 4.2.7. Theoretical Investigation

In order to further investigate the influence of the intermetallic distance suggested by the experimental results, theoretical calculations were conducted.*

The activity of a catalyst in the copolymerization of $CO_2$ and epoxides depends on the activation barrier that has to be overcome. This activation barrier can be defined as the difference between the energetically most favorable species (the catalyst resting state) and the typically rate limiting epoxide ring opening transition state. However, as other reactions compete with the copolymerization and the desired polycarbonate formation, simultaneously the corresponding activation barriers of these side reactions need to be as high as possible for an efficient and selective catalyst. Such side reactions are in particular epoxide homopolymerization and formation of cyclic carbonates.

For PPC catalysts, it can be expected that the major parameters that influence the activation barrier of the main and side reactions are the electrophilicity of the metal centers and the metal-metal distance. As in both side and main reactions, the oxidation states of the reactants and the catalytic centers do not change, general and rather metal independent relations can be assumed to define an optimal distance between two metal sites, *e.g.* with respect to catalyst activity. It was tried to substantiate this idea in the following *via* quantum chemical calculations.

In order to scan the influence of intermetallic distances $d_{MM}$, it is necessary to be able to perform computations over a wide range of $d_{MM}$, which is only possible with a model catalyst. The activation barriers $E_a$, which are obtained by a comparison of energies $E$ of the resting states and the rate limiting transition states of the main or the side reaction, are given by:

$$E_a(d_{MM}) = E^{TS}(d_{MM}) - E^{RS}(d_{MM})$$

It was assumed here, that the actually relevant *Gibbs free energy* curves exhibit a similar behavior as the corresponding pure energy curves given in the following. A critical point in this concept is that it is not trivial to choose a model catalyst that offers a reasonable description of the real zinc carboxylate systems and at the same time exhibits the flexibility to vary $d_{MM}$ over a sufficiently large range. Real, well-designed catalysts with a restricted metal-metal distance around a well defined value can eventually corroborate these results.

*The calculations were conducted by Peter Deglmann, BASF SE, GKT - B001 67056 Ludwigshafen, Germany

Therefore, a number of different model catalysts were studied in order to provide a sound basis for the conclusions derived here. A general feature of the dinuclear sites in zinc carboxylate catalysts is that two neighboring metal centers are connected by one carboxylate bridge. *Via* this bridge a (formally) constant charge is maintained on both reactant and product side and for both Zn atoms involved in the ring opening processes (Figure 52).

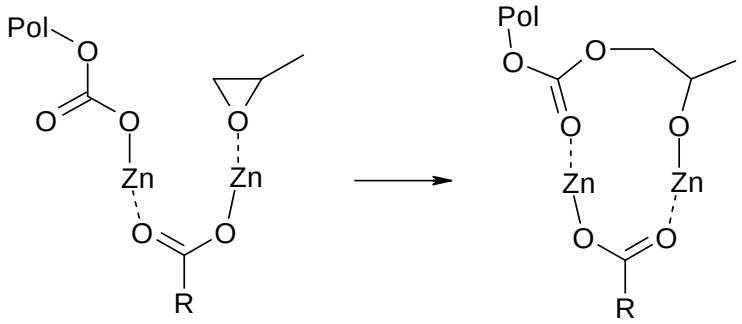


**Figure 52.** Neighboring neutral zinc centers connected *via* a carboxylate bridge maintain their charge upon epoxide ring opening.

This feature was implemented in several model catalysts by incorporating either a chloride or an acetate as anionic bridging ligand. In the case of an acetate bridge (which is closest to the real system investigated), the system switches between an exo- and an endo-conformation depending on the metal-metal distance (Figure 53). This disadvantage can be avoided by introducing a chloride bridge, which is more far away from the real structure, but allows to obtain smooth potential curves at the points, where in either the reactants or the transition states, the bridging carboxylate ligand would jump (typically spontaneously) to the new conformation.

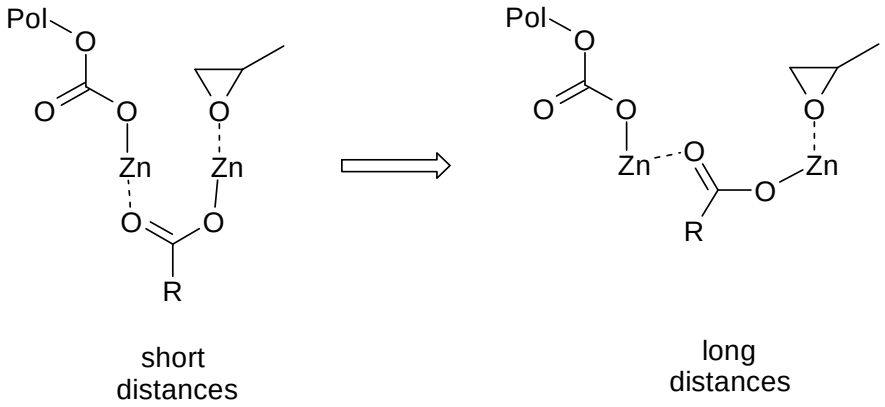


**Figure 53.** Formation of a new bridging conformation.

Besides the bridging unit, there are also multiple choices for the remaining ligands, required to coordinatively saturate the metal centers. Whereas the model ligands closest to the real system would be carboxylates, other monoanionic chelating ligands such as β-diiminates (BDI) offer the advantage of larger and more favorable angles when bidentately coordinating to *one* metal centre (for the two four-coordinate Zn atoms of the considered model catalysts as well as in the heterogeneous Zn dicarboxylates, angles close to the tetrahedron angle of 109° should be preferred). Furthermore, for BDI ligands, there is a reduced tendency to rearrange to multiply bridged structures at shorter metal-metal distances which occurred for terminal carboxylate ligands at 2.5 Å. Apart from this, carboxylate that coordinate with both carboxylic oxygen's to the same zinc atom are also avoided in the bulk structures of zinc dicarboxylates due to the high ring tension.

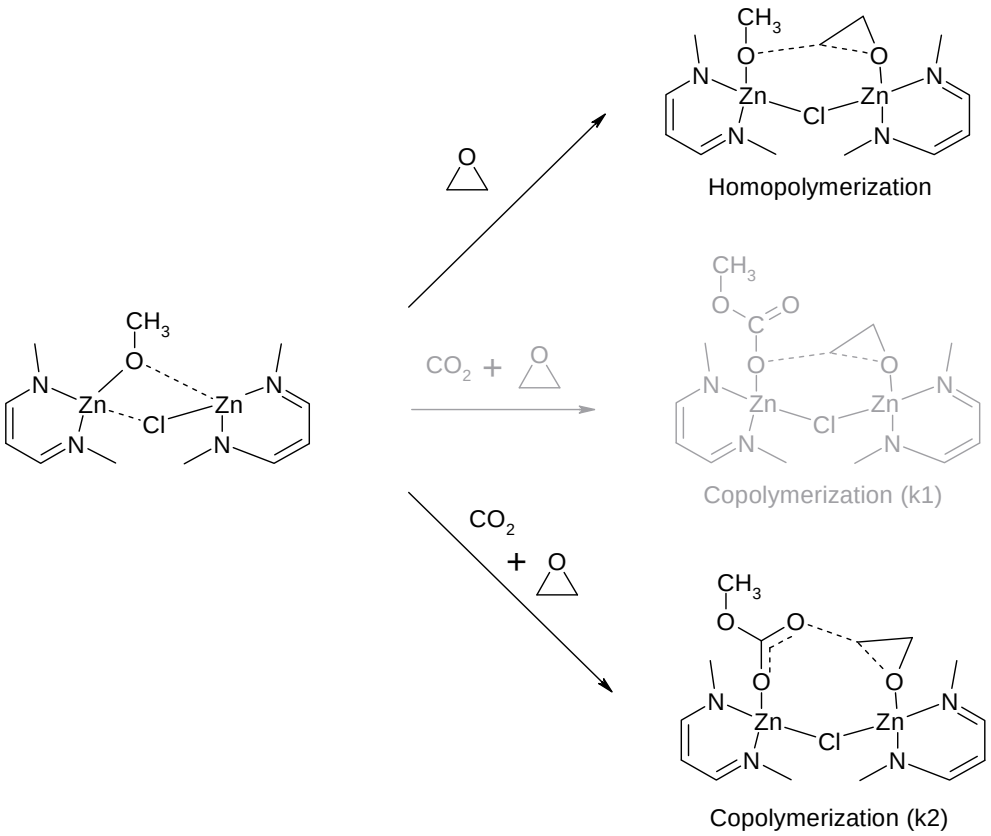


**Figure 54.** Transition states for simplified models to study Zn-Zn-distance dependence of homo- and copolymerization. In Table 3, copolymerization always refers to the $\kappa^2$-case, which was found to be generally favored with respect to $\kappa^1$. Shown here is the system with a chloride bridge and two β-diiminate ligands

From the considerations above, four model catalyst systems can be derived: $(BDI)_2Zn_2(\mu\text{-}Cl)$, $(Ace)_2Zn_2(\mu\text{-}Cl)$, $(BDI)_2Zn_2(\mu\text{-}AcO)$ and $(AcO)_2Zn_2(\mu\text{-}AcO)$. Of these four systems, the $(BDI)_2Zn_2(\mu\text{-}AcO)$ model catalyst is the closest to real catalysts described by Coates, that were already presented in the introduction. The structural parameters of the transition states for homo- and copolymerization (Figure 54) as well as the computed activation barriers are given in Table 3 for metal-metal distances of 2.5, 3.5 and 4.5 Å (as far as it is possible to obtain reasonable reactant and transition state structures).

The energetics show drastic variations depending on the model catalyst. This mainly reflects the binding strengths of the alkoxide ligand in the precursor. This alkoxide ligand may also be the bridging unit between two metal atoms at shorter distances. However, structural parameters of the transition states are rather similar. The O(nucleophile)-C(epoxy) distance is found to be around 2.1 Å (i.e. a factor of 1.5 larger than typical C-O single bond distances),

whereas for the disappearing C(epoxy)-O(epoxy) bond values are situated around 1.8 Å (a factor of 1.3 with respect to C-O single bonds).

For all catalyst systems, it can be observed that copolymerization requires lower activation barriers than homopolymerization. This depends partially on the choice of reference resting states: for both homo- and copolymerization, the same alkoxide species is considered. This means that the copolymerization barriers also reflect the typically exothermic and fast (*i.e.*, not rate limiting) reaction between alkoxides and $CO_2$. The question if alkoxide or carbonate complexes represent the resting state actually depends on both (model) catalyst system as well as process conditions (temperature, $CO_2$ pressure), but is irrelevant if the focus lies on relative differences between reactive pathways, i.e. on catalyst selectivities.

However, with the four dinuclear Zn model catalysts in Table 6, it is only possible to scan distances lower or around those found for bulk structures of heterogeneous Zn dicarboxylates. At larger distances, chloride ligands are not able to bridge anymore, whereas carboxylate bridges tend to drastically interfere with reacting nucleophile and epoxide in the transition state structures, as both the ligand bridge and the actual reacting species strongly prefer to reside as much as possible between the two Zn atoms.

**Table 6.** Dependence of computed structural parameters and activation barriers for homo- and copolymerization on metal-metal-distances. $O^1$ denotes O of the attacking nucleophile (alkoxide or carbonate) and $O^2$ represents the former epoxy O atom.

| | TS (Homopolymerisation) | | | TS (Copolymerisation) | | |
|---|---|---|---|---|---|---|
| $d_{MM}$ [Å] | $d(O^1\text{-}C)$ [Å] | $d(C\text{-}O^2)$ [Å] | $E_a$ [kJ/mol] | $d(O^1\text{-}C)$ [Å] | $d(C\text{-}O^2)$ [Å] | $E_a$ [kJ/mol] |
| $(BDI)_2Zn_2(\mu\text{-}Cl)$ | | | | | | |
| 2.5 | 2.29 | 1.99 | +235.1 | 2.14 | 1.80 | +117.6 |
| 3.5 | 2.18 | 1.78 | +132.2 | 2.07 | 1.80 | +47.5 |
| 4.5 | 2.21 | 1.75 | - | 2.08 | 1.83 | - |
| $(AcO)_2Zn_2(\mu\text{-}Cl)$ | | | | | | |
| 2.5 | - | - | - | - | - | - |
| 3.5 | 2.23 | 1.78 | +66.8 | 2.11 | 1.81 | -8.3 |
| 4.5 | 2.22 | 1.77 | - | 2.11 | 1.82 | - |
| $(BDI)_2Zn_2(\mu\text{-}AcO)$ | | | | | | |
| 2.5 | 2.23 | 1.94 | +257.8 | 2.09 | 1.84 | +102.7 |
| 3.5 | 2.17 | 1.76 | +197.3 | 2.06 | 1.81 | +102.6 |
| 4.5 | 2.20 | 1.73 | 6.7 | 2.04 | 1.85 | -50.1 |
| $(AcO)_2Zn_2(\mu\text{-}AcO)$ | | | | | | |
| 2.5 | - | - | - | - | - | - |
| 3.5 | - | - | - | - | - | - |
| 4.5 | 2.22 | 1.74 | -46.6 | 2.08 | 1.84 | -96.9 |
| $(Cu^+)_2$ | | | | | | |
| 2.5 | 2.33 | 1.97 | +119.9 | 2.21 | 1.77 | +40.3 |
| 3.5 | 2.25 | 1.80 | +92.7 | 2.15 | 1.78 | +27.6 |
| 4.5 | 2.25 | 1.71 | -16.9 | 2.10 | 1.82 | -58.6 |
| 5.5 | 2.24 | 1.71 | -54.6 | 2.16 | 1.81 | -97.0 |

Therefore, an alternative model catalyst was chosen that allows (in principle) to model any metal-metal distance, two $Cu^{+}$ atoms without further ligands were chosen. In this case, overall a monocationic catalyst results, in which every metal centre exhibits the $d^{10}$ electronic configuration, which is also characteristic for $Zn^{2+}$ species. Upon ring opening, the negative counter charge migrates from one side of the dinuclear Cu system to the other side, which however still means no energetic bias (as would be the case if four non-bridging monoanionic ligands, among which would also be the propagating polymer chain, were distributed *e.g.* as 2+2 in the reactant and thus as 3+1 in the product). From the results (also in Table 6), it can be concluded that structural parameters are very similar to the dinuclear Zn complexes. As can be seen, for this model catalyst it was possible to extend metal-metal distances to 5.5 Å and beyond.

For the dinuclear Cu model catalyst, an energetic scan with an increment of 0.05 Å was performed for homo- and copolymerization. Graphical representations of homopolymerization and copolymerization barriers as well as of the resulting energetic differences between these two reactions, are given in Figures 55 and 56, respectively.

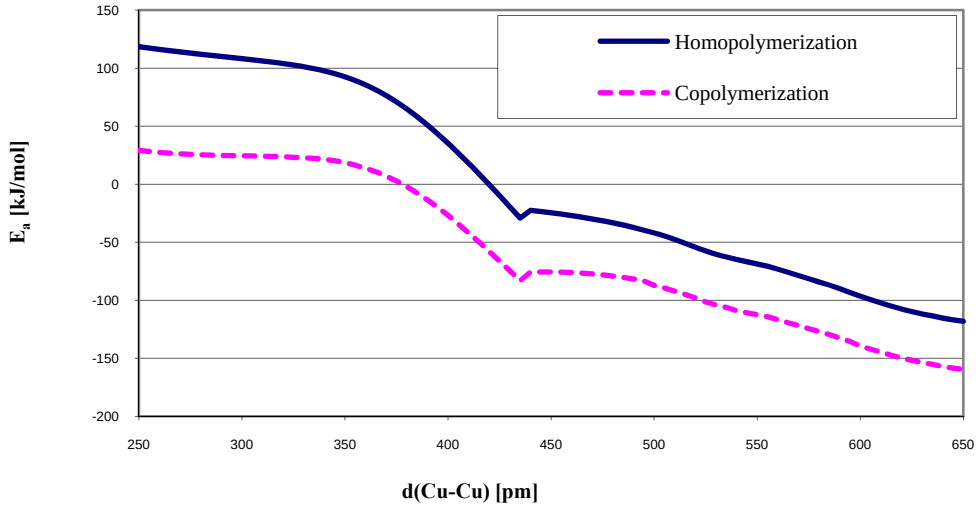


**Figure 55.** Variation of activation barriers of homo- and copolymerization with metal-metal distance, computed for a very simplified catalyst consisting of two $Cu^{+}$ ions.

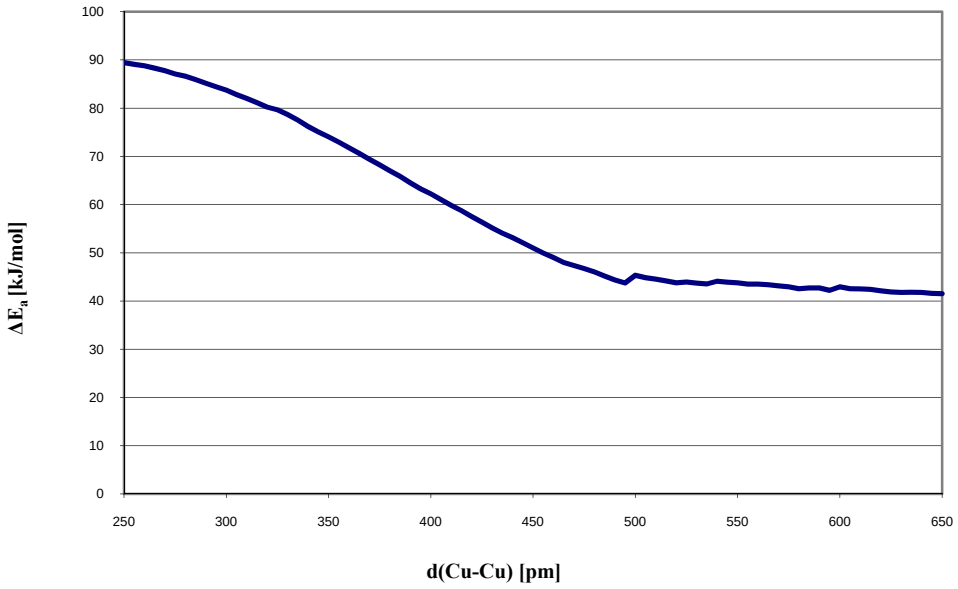


**Figure 56.** Metal-metal distance dependent difference of activation barriers of homo- and copolymerization, computed for a very simplified catalyst consisting of two $Cu^+$ ions.

For dinuclear Zn complexes, the activation barrier of copolymerization (and generally of all ring opening reactions) is lowered upon increasing the metal-metal distance. This can partially be explained by the weaker binding of the alkoxide precursor to the two $Cu^+$ cations. Above 4.35Å the methoxide actually "chooses" one $Cu^+$ and the bridge becomes unsymmetrical, for metal-metal distances below this value the activation barrier for epoxide ring opening increases steeply upon lowering $d_{MM}$. Another important point represents the intrinsic barrier of epoxide ring opening by a nucleophile. For an $S_N2$ like reaction, a linear orientation of O-C-O would be desirable in the transition state. Indeed, part of the lowering of activation barriers for ring opening can be traced back to O-C-O angles being able to come closer to 180° at larger metal-metal distances. This effect becomes even more pronounced for homopolymerization than for copolymerization, as in homopolymerization all three atoms between the two metal centers should assume a linear arrangement, whereas in $\kappa^2$-copolymerization at least five atoms take part and thus a higher structural flexibility is possible. Therefore at short metal-metal distances homopolymerization is more strongly disfavored with respect to copolymerization, whereas at larger metal-metal distances the two competing reactions become closer in energy (Figure 56).

Thus for larger distances, most significantly up to 430 pm, catalytic activity becomes higher, whereas smaller distances below 500 pm offer the advantage to better suppress homopolymerization.

In conclusion, the optimal Zn-Zn-distance for copolymerization of epoxides and $CO_2$ should be located between 4.3 and 5.0 Å. The common distance found in zinc dicarboxylates of 4.6 - 4.8 Å probably leads to a balanced optimum between activity and selectivity. At higher metal-metal distances, homopolymerization and back-biting (which is not discussed here) become more probable, increasing the side-product formation. Therefore, also for homogeneous complexes, the Zn-Zn-distance has to be carefully adjusted to a certain range and cannot be chosen deliberately.

This is the first time that the effect of the intermetallic distance on $CO_2$/epoxide copolymerization has been discussed and calculated. The theoretical investigation corroborates that two cooperating metal centers are necessary for any activity in heterogeneous zinc dicarboxylates. In other words, the more Zn-Zn couples can be found on the surface, the higher the activity of the catalyst will be. In accordance to this, ZnSA will show a reduced activity than its higher homologues as the occurrence of Zn-Zn couples is lower in this catalyst. The effect of intermetallic distance can be extended to homogeneous systems that assume a bimetallic copolymerization pathway.

### 4.2.8. Modification of Surface Active Sites

Besides the intermetallic distance, the nature of the initiating group is determining the catalytic efficiency of the zinc dicarboxylate system. As described previously (Chapter 4.2.3., Post-treatment of Zinc dicarboxylates), activation of the surface sites is crucial for any activity.

Apparently, the post-activation of ball-milled zinc glutarate with water leads to the formation of active sites on the newly generated surface that are able to initiate the copolymerization. In an earlier investigation, it was shown that the functionalization synthesis route also leads to highly active zinc dicarboxylates.[100] In this procedure, a substiochiometric amount of dicarboxylic acid is added to diethyl zinc leading to zinc dicarboxylate with remaining ethyl-groups. These zinc-ethyl-groups are unfavorable to any

$CO_2$/epoxide copolymerization, but post-modification with $SO_2$ leads to highly active ethylsulfinato groups (Scheme 10).

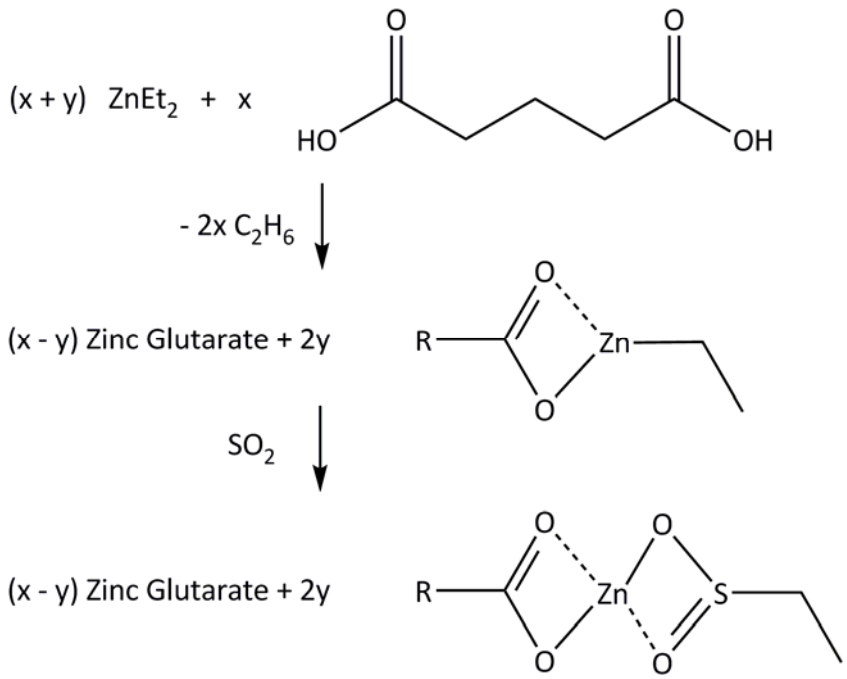


**Scheme 10.** Functionalization route for the synthesis of highly active zinc dicarboxylates.

In this work it was demonstrated that the activity is highest with a TOF = 630 $g \cdot mol^{-1} \cdot h^{-1}$ when the $SO_2$-content is about 17 %. As the nature and the surface concentration of the initiator groups seems to be a crucial factor for the activity of zinc dicarboxylates, several initiator groups were screened (Scheme 11).

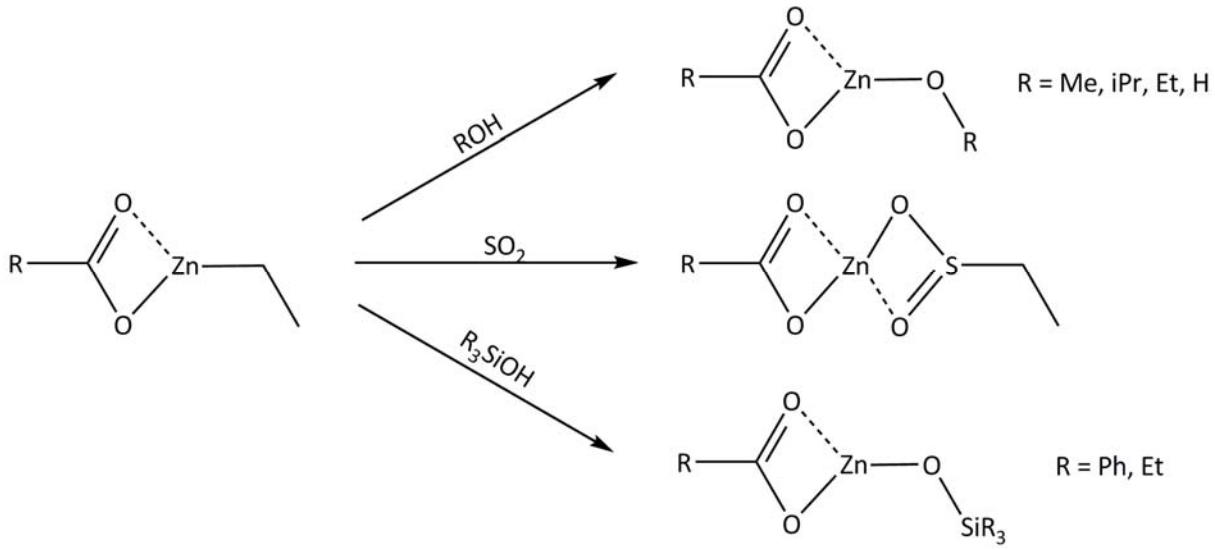


**Scheme 11.** Zinc dicarboxylate with different initiator groups on the surface.

The concentration of these groups was kept constant at 17 % in order to exclude any other effects on activity. As Zn-source, diethyl zinc, dimethyl zinc and diphenyl zinc were chosen and reacted with glutaric acid. The material was then post-treated with isopropanol, diethylsilanol, diphenylsilanol or $SO_2$. The activity data is summarized in Table 7.

**Table 7.** Activity of zinc glutarate post-modified with different initiator groups.[a]

| Entry | catalyst | TON[b] | TOF[c] | % PPC[d] | $M_n$[e] | $M_w/M_n$[e] |
|---|---|---|---|---|---|---|
| 1 | standard ZnGA | 5876 | 294 | 95 | 72 | 4.5 |
| 2 | 17 % $ZnSO_2Et$ | 11148 | 557 | 95 | 41 | 8.6 |
| 3 | 17 % ZnOiPr | 4620 | 231 | 87 | 24 | 2.2 |
| 4 | 17 % $ZnOSiEt_2$ | 2900 | 145 | 83 | 12 | 4.9 |
| 5 | 17 % $ZnOSiPh_2$ | 2236 | 112 | 83 | 6 | 2.0 |
| 6 | 17 % $ZnSO_2Me$ | 6300 | 315 | 71 | 24 | 2.8 |
| 7 | 17 % $ZnSO_2Ph$ | 9000 | 450 | 70 | 22 | 1.9 |

[a] Polymerization conditions: 0.5 mmol cat, 150 mmol PO, 80°C, 20h, 40 bar, 500 rpm. [b] Turnover number in g polymer per mol of zinc. [c] Turnover frequency in g polymer per mol of zinc per hour. [d] Estimated by $^1H$ NMR spectroscopy. [e] Determined by GPC, calibrated with polystyrene standard in THF, $M_n$ given in kg/mol,

It becomes apparent that the best combination in terms of activity and selectivity is found for the ethylsulfinato-modified zinc glutarate. Exchange of the initiator group by any other group (Zn-OiPr, Zn-$OSiEt_2$, Zn-$OSiPh_2$, Zn-OMe, Zn-OPh) leads to less effective catalysts for the $CO_2$/epoxide copolymerization (Table 7, Entries 3-7). However, in terms of industrial application the material gained *via* the functionalization procedure loses its attractiveness, as the precursors are rather expensive and complicated to handle, compared to the standard procedure. Therefore the standard zinc glutarate remains the material of choice for industrial production of polycarbonates out of $CO_2$.

### 4.2.9. Conclusions

Heterogeneous zinc dicarboxylates are – despite over three decades of intensive research activities – limited in their potential for the production of polycarbonates from $CO_2$. Even though huge steps in homogeneous catalysis have been made in the last years, traditional zinc dicarboxylates remain industrially relevant as they are easy to prepare and handle, non-toxic and economically viable. In the first part of this work, several strategies to enhance the activity of zinc glutarate were investigated. It was shown that the crystallization of zinc glutarate can only hardly be controlled *via* additives. The potential of further down-sizing the material (and thereby increasing the surface area and activity) is strongly limited.

In addition to the investigation of the strategies described above, the underlying mechanisms and active species of the heterogeneous zinc dicarboxylates were investigated. A synthesis procedure was designed, which allows comparison of all four zinc dicarboxylates (ZnSA, ZnGA, ZnAA and ZnPA) and their efficiency in $CO_2$/PO copolymerization. Through careful handling in an inert atmosphere it could be proofed that the material needs to be activated in order to generate initiator groups on the surface that are able to copolymerize.

This principle was transferred to a series of experiments in which the initiator group was interchanged. The introduction of zinc-ethylsulfinate species affords the most active material. However, in terms of industrial application, the material obtained *via* the functionalization procedure loses its attractiveness as the precursors are rather expensive and complicated to handle, compared to the standard procedure. Therefore, the standard

zinc glutarate remains the material of choice for industrial production of polycarbonates from $CO_2$.

From the copolymerization experiments conducted, the activity discrepancy between ZnSA and its higher homologues becomes obvious. As this difference can neither be attributed to the surface areas nor to the particle sizes, it can be concluded that the molecular structure is the decisive factor. The major difference between ZnSA and its higher homologues is the occurrence of Zn-Zn surface couples in a well-defined spatial distance between 4.6 and 4.8 Å.

The importance of two closely linked metal sites has already been described for homogeneous complexes in literature. Furthermore, theoretical calculations conducted in this work to identify an “ideal” Zn-Zn-distance suggest an optimal separation of Zn atoms in the range of 4.3 - 5.0 Å, which gives a balanced optimum between activation energy and selectivity towards copolymerization

The combined experimental and theoretical results allow a more complete understanding of the surface processes on zinc dicarboxylates. A well-defined spatial distance and the activation of the surface metal sites are essential to give a catalytically active material. These results strongly indicate that for heterogeneous zinc dicarboxylates, a bimetallic mechanism is at work on the surface.

However, the activities with such catalysts are restricted due to a restrained surface and diffusion limitations. Furthermore, grinding of the material improves its efficiency as expected, even though the increase is strongly limited due to limitations in further down-sizing the material. New strategies should therefore focus on introduction of two metallic species into a molecular framework that does not comprise bulky material, in which no catalysis can take place. Therefore, new strategies have to focus on homogeneous systems that comprise two metal centers (c.f. Chapter 2.4.1 Dinuclear BDI Catalysts and Similar Systems and Chapter 2.4.3. Dinuclear Salen Systems) or a cooperative binary linked ligand system (c.f. Chapter 2.4.2. Binary Linked Salen Systems).

### 4.3. Homogeneous Dinuclear Flexible Linked Salphens

In the investigation of the zinc dicarboxylates, it could be shown that a well-defined spatial distance of the surface metal sites is essential to give a catalytically active material. These results strongly indicate that for heterogeneous zinc dicarboxylates, a bimetallic mechanism is in state. However, as described in Chapter 4.2, the activity of these heterogeneous systems is limited. Therefore, homogeneous complexes were investigated, that introduce two closely linked metal species in one ligand framework.

A set of well-defined, rigid and semi-rigid dinuclear complexes has been designed and applied in the $CO_2$/epoxide copolymerization reactions in the recent years (c.f. Chapter 2.4.1. Dinuclear BDI Catalysts and Similar Systems).[126, 131, 147-153] Other systems are based on the flexibly linked salen-type complexes developed by Jacobsen *et al.*[52-54], which were further investigated by Nozaki *et al.* in 2010 (c.f. Chapter 2.4.3. Dinuclear Salen Systems).[165] Recently, a new synthetic strategy was reported by Rieger *et al.*, which allows an easy modular design of flexibly linked dinuclear salphen-type species.[166]

In this work an extended investigation of the copolymerization reaction and kinetics using the mononuclear complex **51** as well as the flexibly linked dinuclear complex **52** is presented (Figure 57).

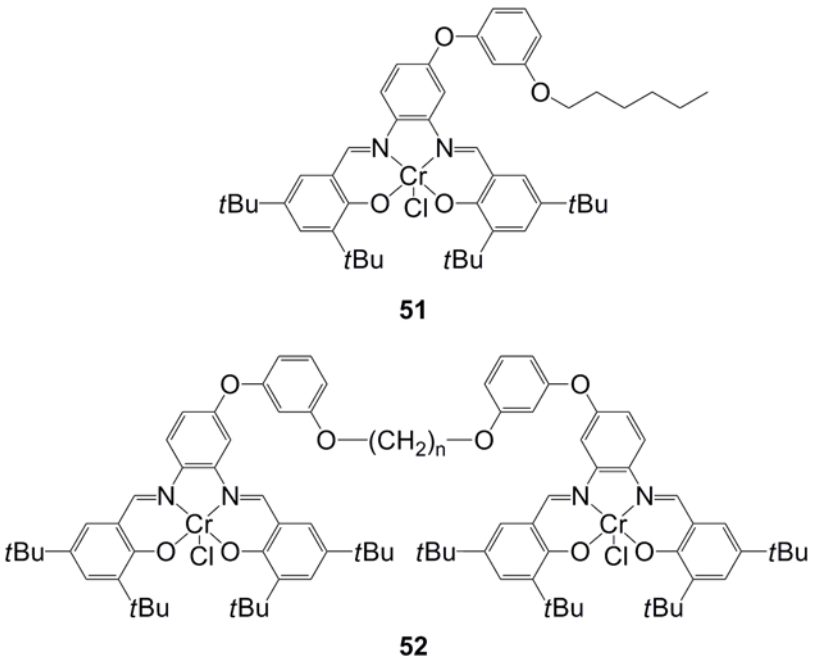


**Figure 57.** Mononuclear and dinuclear salphen-type complexes.

### 4.3.1. General Kinetic Considerations in $CO_2$/Epoxide Copolymerization

In order to proof the bimetallic nature of the homogeneous complexes investigated herein, a detailed kinetic investigation has to be conducted. The catalyst reaction order can deliver additional information on the mechanism of the copolymerization. Formally, the copolymerization rate can be expressed as follows:

$$r_{obs'} = k \cdot [PO]^x \cdot [CO_2]^y \cdot [catalyst]^n \text{ (eq. 1)}$$

As the epoxide and $CO_2$ concentration can be considered as constant over the initial reaction period, both terms can be summarized in a constant term k':

$$r_{obs'} = k \cdot k' \cdot [catalyst]^n \text{ (eq. 2)}$$

Under such conditions the catalyst reaction order can be determined as the slope of the logarithmic plot of r against catalyst concentration n:

$$\ln(r_{obs'}) = n \cdot \ln([catalyst]) + \ln(k \cdot k') \text{ (eq. 3)}$$

For a mononuclear catalyst, which copolymerizes in a bimetallic fashion, a reaction order n = 2 can be expected. For a dinuclear catalyst, where the two interacting metal sites are incorporated into one ligand framework, the reaction order of 1 is predicted in case of intramolecular bimetallic catalysis.

### 4.3.2. Kinetic Investigation with Mononuclear and Dinuclear Catalysts

With a React-IR autoclave system, parallel reactions at different conditions were carried out simultaneously. A series of copolymerization experiments with decreasing catalyst concentration was performed and the growth of the specific carbonyl-band of polypropylene carbonate (PPC) at 1753 $cm^{-1}$ followed *in-situ* (Figure 58).

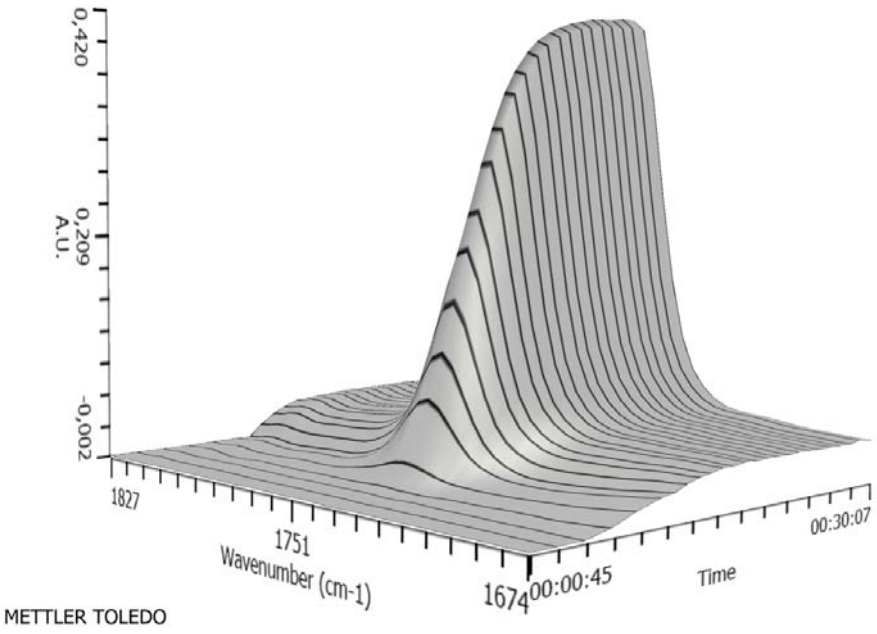


**Figure 58.** Three-dimensional representation of the growth of the specific carbonyl band of PPC at 1753 $cm^{-1}$ with increasing reaction time. The plateau region at prolonged reaction times is due to the saturation of the IR- signal.

The polymerization reaction rates $r_{obs'}$ were obtained from the change of the PPC-signal intensity with time during the initial period of reaction after the temperature stabilization. At prolonged reaction times, artifacts in the measured IR-signal appear, probably due to the raised viscosity and other effects, *e.g.* diffusion limitations or undissolved PPC in the reaction media, leading to a saturation of the IR-signal. For example, a plateau in Figure 58 would indicate that the polymerization has stopped at ca. 30 min, which contradicts the parallel copolymerization experiments in standard autoclave tests (Table 8).

For the mononuclear complex **51**, three initial reaction rates at Cr/PO ratios of 1/500, 1/1000 and 1/4000 were measured (Figure 59). A practically linear dependence of the relative intensity of the PPC signal on reaction time was observed in all experiments. From the slope of the linear approximation of the experimental points the reaction rate $r_{obs}$ could be determined as a relative value. For reasons of clarity, the time scales in Figures 59 and 61 were normalized to the beginning of the linear increase of the IR-signal after temperature stabilization (c.f. Figure 58).

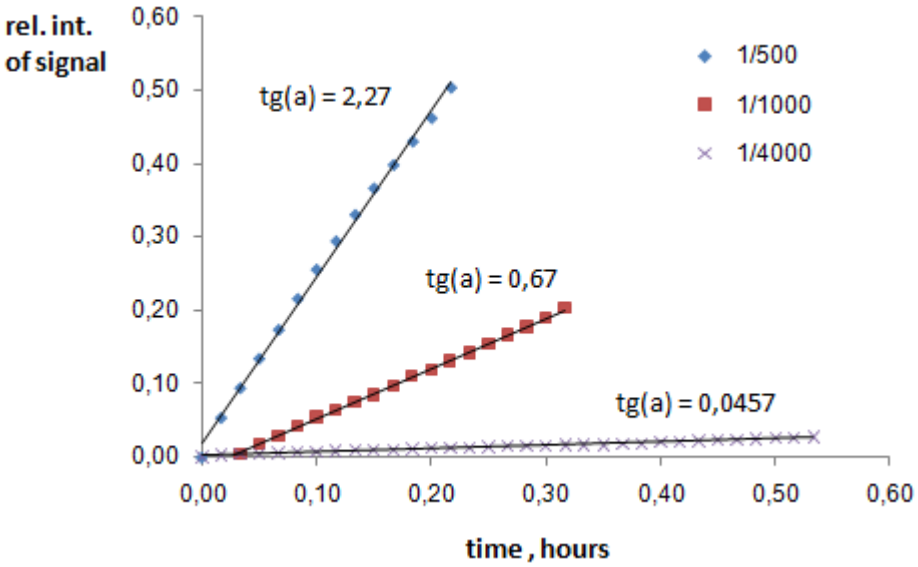


**Figure 59.** Comparison of the initial rates of the polypropylene carbonate formation catalyzed by mononuclear complex **51** at three different catalyst concentrations.

The obtained $r_{obs}$ values show a linear dependence in logarithmic coordinates $\ln(r_{obs})$ against ln([catalyst]) with a slope of 1.89 (Figure 60). Thus, for the monometallic catalyst **51** in the studied copolymerization, the reaction follows the second reaction order (c.f. equation 3).

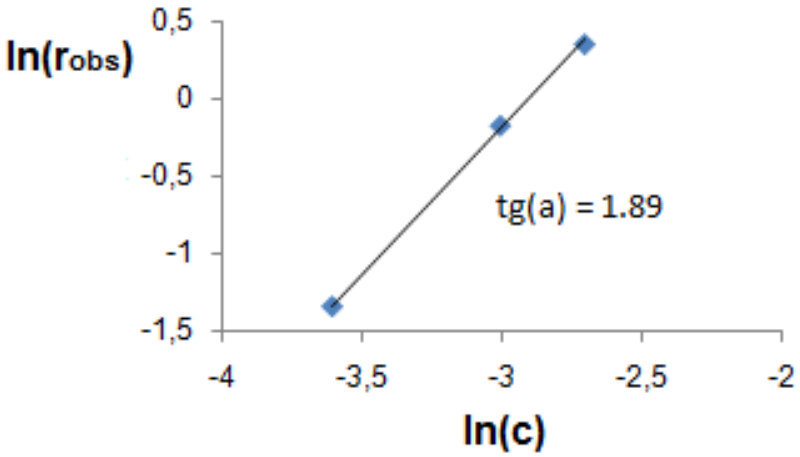


**Figure 60.** Plot of $\ln(k_{obs'})$ against ln([*catalyst)*].

Analogous investigations and data analysis were carried out for the dinuclear catalyst system **52** (Figure 61).

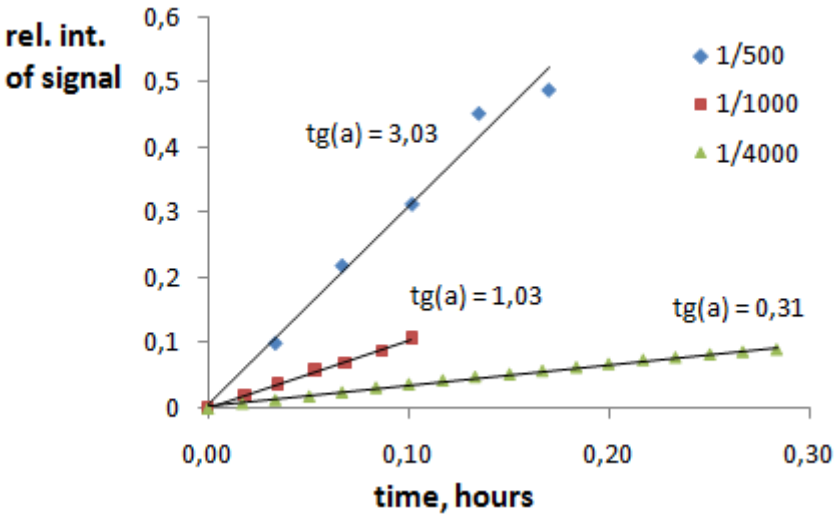


**Figure 61.** Comparison of the initial rates of the polypropylene carbonate synthesis catalyzed by dinuclear complex **52** at different Cr/PO concentrations.

The plot of ln($r_{obs'}$) against ln([catalyst]) shows a linear dependence as well (Figure 62). The adjusted trend line has a slope of 1.06. From equation 3 it can be derived that the reaction order n ≈ 1. The catalyst reaction order found is very close to unity.

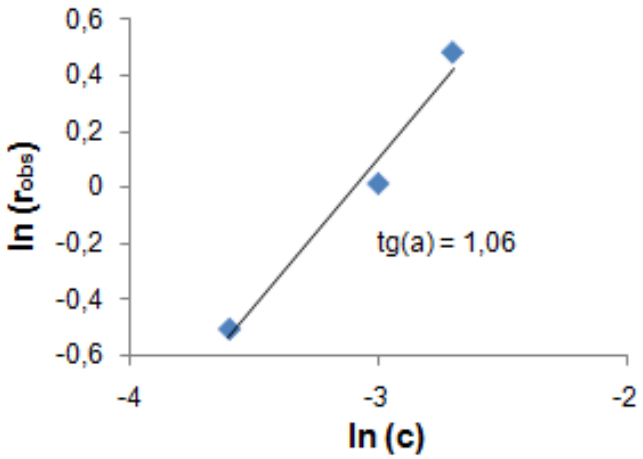


**Figure 62.** Plot of ln[robs'] against ln([catalyst]).

Apparently, both the mononuclear catalyst **51** and the dinuclear catalyst **52** copolymerize $CO_2$ and propylene oxide in a bimetallic fashion. In the case of **51**, two catalytic species need to come spatially close to each other in order to form an active copolymerization system.

Therefore a reaction order n of approximately 2 can be found for this system. In the case of **52**, the two interacting metal species are flexibly tethered and are in close proximity all over the copolymerization period. Therefore the reaction order of slightly beneath 1 is in compliance with a predominantly intramolecular occurrence of the copolymerization catalysis. Interestingly, at high concentration of the catalysts **51** and **52**, the copolymerization proceeds with comparable rates.

These results further back up the mechanistic considerations that predict the copolymerization with salen complexes and similar structures to take place *via* a bimetallic pathway.

### 4.3.3. Copolymerization Experiments

For control purposes, the effect of catalyst concentration and reaction time onto activity was also studied by routine copolymerization experiments without on-line monitoring.

Mononuclear catalyst **51** at a 1:2000 ratio to PO has an average activity of 74 $h^{-1}$ in $CO_2$/epoxide copolymerization at 60°C and 40 bar pressure for 2 hours (Table 8, Entry 1). Extending the reaction period leads to a slight but systematic decrease of the average activity (Table 8, Entries 1-5), which drops to 61 $h^{-1}$ after a reaction time of 24 h.

Diluting the system by a factor of 10 significantly reduces the catalyst efficiency of **51** (Table 8, Entries 6 and 7). A polymerization attempt for 2 hours did not yield any product. Prolonging the reaction time to 24 hours gave a small quantity of PPC with a comparatively high amount (17 %) of cPC as side-product. This observation correlates well with the existence of the bimetallic mechanism. Indeed, besides the strong concentration dependence of the reaction rate, the effect of the catalyst concentration onto the ratio of formed product is very characteristic.

**Table 8.** Effect of catalyst concentration and reaction time on the copolymerization of PO and $CO_2$ with mononuclear catalyst[a]

| Entry | cat | c (PO/Cr) | Time (h) | TON[b] | TOF[c] ($h^{-1}$) | $PO/CO_2$[d] | cPC[d] (mol-%) | $M_n$[e] (kg/mol) | $M_w/M_n$[e] |
|---|---|---|---|---|---|---|---|---|---|
| 1 | **51** | 2000 | 2 | 148 | 74 | 1.37 | 0 | 7.4 | 1.19 |
| 2 | **51** | 2000 | 4 | 284 | 71 | 1.35 | 0 | 13.1 | 1.23 |
| 3 | **51** | 2000 | 8 | 547 | 68 | 1.45 | 0 | 21.1 | 1.33 |
| 4 | **51** | 2000 | 16 | 1045 | 65 | 1.54 | 0 | 24.7 | 1.48 |
| 5 | **51** | 2000 | 24 | 1473 | 61 | 1.96 | 3 | 32.0 | 2.04 |
| 6 | **51** | 20.000 | 2 | 0 | 0 | na | na | na | na |
| 7 | **51** | 20.000 | 24 | 176 | 7 | 1.34 | 17 | 4.0 | 2.00 |
| 8 | **52** | 2000 | 2 | 102 | 51 | 1.69 | 0 | 7.8 | 1.50 |
| 9 | **52** | 2000 | 24 | 1177 | 49 | 2.42 | 0 | 22.2 | 1.83 |
| 10 | **52** | 20.000 | 2 | 182 | 91 | 2.32 | 0 | 1.9 | 3.50 |
| 11 | **52** | 20.000 | 24 | 1975 | 82 | 2.50 | 0 | 15.2 | 2.19 |

[a] Polymerization conditions: propylene oxide (PO, 5 mL, 2000 resp. 20.000 to Cr), 60 °C, 40 bar. [b] Turnover number in mol polymer per mol of Cr. [c] Turnover frequency in mol polymer per mol of Cr per hour. [d] Estimated by $^1$H NMR spectroscopy. $PO/CO_2$ calculated for all products, cPC: cyclic carbonate content. [e] Determined by GPC, calibrated with polystyrene standard in THF.

The high amount of side-product can be attributed to a back-biting reaction (Scheme 6, Chapter 2.1.1. Copolymerization Mechanism). Here, the anionic chain end is released from the metal center and is able to split off a cPC molecule *via* intramolecular nucleophilic attack of the alkoxide (also formed by decarboxylation of the dissociated carbonate chain end at high temperatures) on a neighboring carbonyl atom in the chain. Another possibility for the back-biting is a nucleophilic attack of the carboxylate chain end onto the methylene or methyne carbon atom of the alkoxy-fragment.[51] In case of a bimetallic polymerization mechanism, lower concentration of the mononuclear catalyst increases the average life-time of such uncoordinated polymer species, making the effect of competitive reactions such as back-biting more pronounced. In addition, the dissociation equilibrium at the catalytic center

is shifting toward dissociation products upon dilution, thus again promoting the back-biting reactions. For example, in equilibrium with small dissociation constants, the degree of dissociation increases approximately 3 times upon 10 time dilution.

Besides the decrease in activity of catalyst **51**, the $PO/CO_2$ ratio in the resulting polymer becomes higher for longer reaction times. Both of these effects can be attributed to the drastic lowering of the $CO_2$ concentration in the reaction medium, which undergoes the alteration of composition, viscosity and polarity upon formation of the polymer, thus rendering a PO insertion more favorable. At 10 times lower catalyst concentration, the overall change of the reaction medium remains small and the $CO_2$ concentration practically constant even for 24 h reaction time. Accordingly, the composition of the polymer obtained with **52** in 24 h is very close to the composition of the polymer produced in 2 h at low catalyst concentration (Table 8, Entries 10 and 11). This is also in accordance with observations that the variation of $CO_2$ pressure in 2h polymerization experiments with catalyst **52** has marginal effects on the copolymer composition (c.f. Table 9), whereas longer reaction times (higher conversions) clearly increase the $PO/CO_2$ ratio. In general, the obtained values indicate quite poor selectivity of the studied catalysts toward the formation of alternating polymer (c.f. Scheme 5, Chapter 2.1.2 Factors Influencing Copolymerization).[165] In contrast to catalyst **51**, dilution of system **52** leads to an increase of its efficiency in terms of TOF (Table 8, Entries 8 and 10, resp. 9 and 11), corroborating the necessity of joining two catalytic metal sites into one ligand framework and supporting once again the proposed bimetallic catalysis mechanism.

**Table 9.** Effect of $CO_2$ pressure and temperature on the efficiency of dinuclear complex[a]

| Entry | cat | T (°C) | p (bar) | TON[b] | TOF[c] ($h^{-1}$) | PO/$CO_2$[d] | cPC[d] (mol-%) | $M_n$[e] (kg/mol) | $M_w/M_n$[e] |
|---|---|---|---|---|---|---|---|---|---|
| 1 | **52** | 60 | 20 | 73 | 37 | 1.78 | 0 | 2.8 | 1.53 |
| 2 | **52** | 60 | 40 | 102 | 51 | 1.69 | 0 | 7.8 | 1.50 |
| 3 | **52** | 80 | 20 | 80 | 40 | 1.99 | 0 | 3.0 | 1.62 |
| 4 | **52** | 80 | 40 | 121 | 60 | 1.79 | 0 | 11.0 | 1.57 |

[a] Polymerization conditions: propylene oxide (PO, 5 mL, 2000 to Cr), 2 h. [b] Turnover number in mol polymer per mol of Cr. [c] Turnover frequency in mol polymer per mol of Cr per hour. [d] Estimated by $^1$H NMR spectroscopy. PO/$CO_2$ calculated for all products, cPC: cyclic carbonate content. [e] Determined by GPC, calibrated with polystyrene standard in THF.

The polymer molecular weights obtained with complex **51** in a 2000 excess of PO are rising with reaction time and reach $M_n$ of 32 kg/mol after 24 h (Table 8, Entry 5). The effect of reaction time onto $M_n$ in polymerizations with catalyst **52** is similar (Table 8, Entries 8 and 9, resp. 10 and 11).

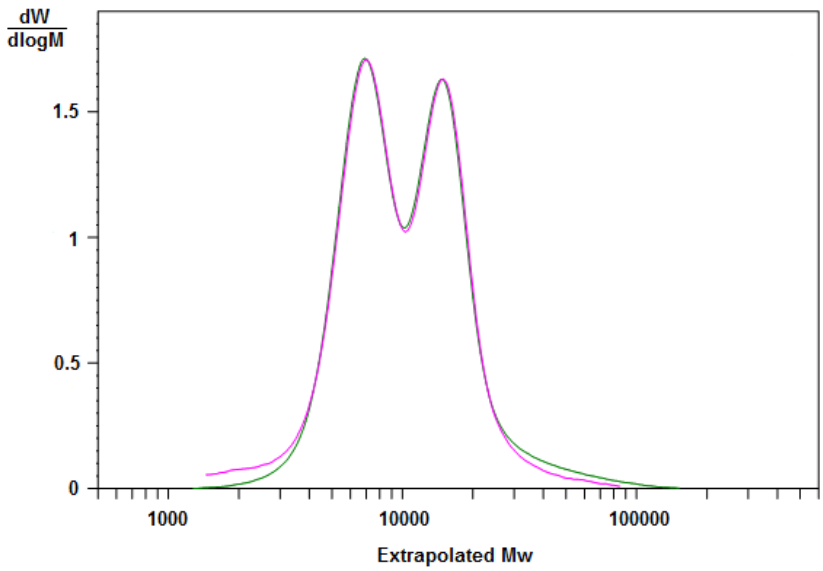


**Figure 63**. Molecular weight distribution of polycarbonate: crude (pink) and treated with $CH_3COOH$ as described (green).

Interestingly, the polymers obtained both with catalyst **51** and **52** show bimodality in their molecular mass distribution in GPC-elugrams, which is pronounced in most cases. The observed peak molecular mass of low-Mw fractions corresponds approximately to a half of that of the high-Mw fractions of the polymer batch. After a major part of catalyst was removed from the polymer by treatment with acetic acid in THF and precipitation with pentane, the GPC-characteristics of polymer remained absolutely identical with the untreated material (c.f. Figure 63).

This fact excludes the possibility of bridging of two polymer chains *via* catalyst molecules under conditions of GPC-analysis. It can speculatively be explained as a result of partial conversion of catalysts into hydroxy-species and μ-oxo dimers, which can, *via* a corresponding initiation of polymerization, lead to a double molecular weight of one polymer fraction compared to the other (Scheme 12).[84]

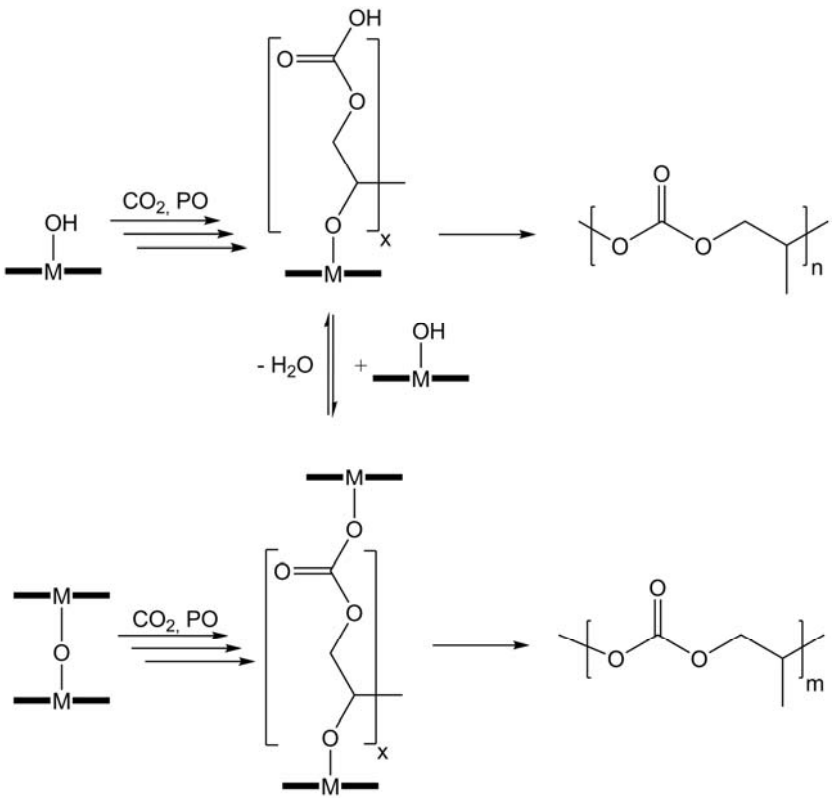


**Scheme 12.** Possible generic pathway for the bimodal copolymerization via hydroxy and μ-oxo catalyst species (m ≈ 2n).

The monomeric species and μ-oxo dimers, as well as μ-oxo trimers have been characterized *via* mass spectra with analogous Cr-salphen complexes in our group (Figure 64).[171]

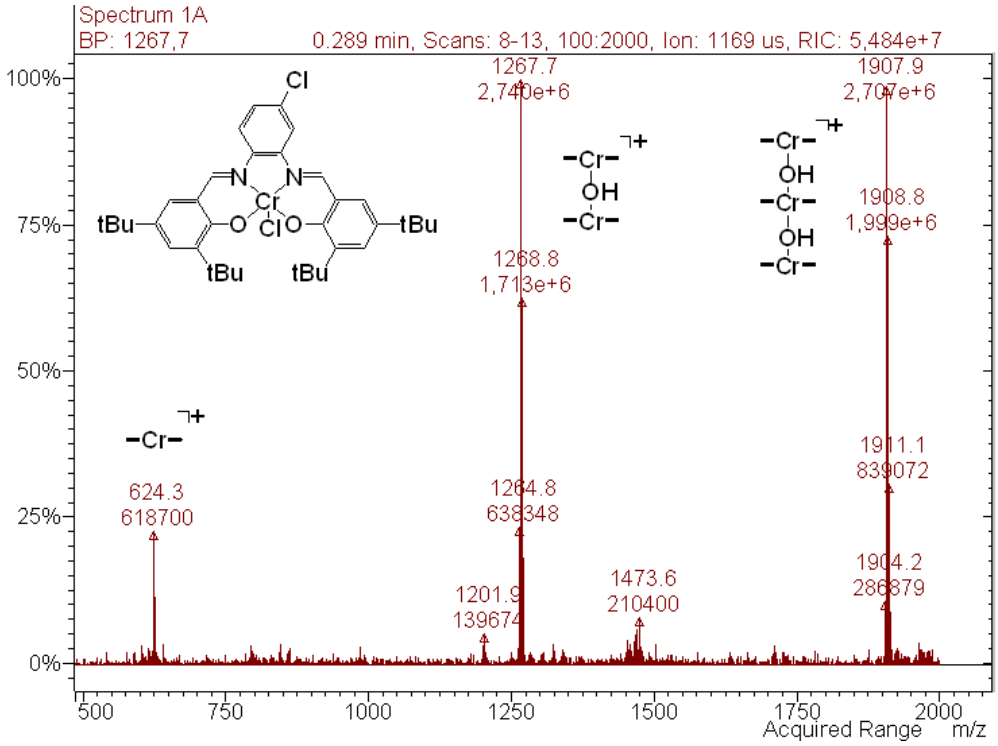


**Figure 64.** MALDI-MS spectrum of monomeric species, μ-oxo dimers and μ-oxo trimers of Cr-salphen complexes.

One of the sources for the formation of such catalytic species can be residual water in the polymerization system. This would also explain the sometimes incongruent molecular weights and weight distributions of polymers from different polymerization batches, which make the exact analysis of polymer growth kinetics difficult.

It is worth to note that polymers obtained with a dimeric catalyst feature a higher PO/$CO_2$ ratio. The dimerization of salphen catalyst renders the homopolymerization of PO more favorable in comparison to the alternated copolymerization with $CO_2$. This seems to be a consequence of the bimetallic catalytic mechanism of PO homopolymerization, reported recently for salen and salphen complexes.[165, 172] A rise of the reaction temperature favors homopolymerization of PO as well (c.f. Table 9). This behavior can presumably be countered by optimization of the dinuclear catalyst design.

Noteworthy, the formation of cPC as side-product is suppressed with the dinuclear system. This is attributed to an effectively decreased life-time of the uncoordinated anionic growing polymer chain-end due to the proximity of a second metal site. In other words, the high local concentration of metal centers decreases the probability of dissociation of the polymer chain end. This increases the probability of interception of the released chain end by the second salphen unit of the dimeric complex, preventing the back-biting to occur.

Optimal conditions allowing to minimize the PO/$CO_2$ ratio in polymers and at the same time to maintain the reasonable activity of the dinuclear catalyst seem to be realized at a reaction temperature of 60 °C and a $CO_2$ pressure of 40 bar. Therefore, these conditions were chosen as standard polymerization conditions throughout this part of the work.

### 4.3.4. Influence of Cocatalyst on $CO_2$/Epoxide Copolymerization

It has widely been discussed in literature that addition of cocatalysts to salen-type catalysts can strongly influence their efficiency.[55, 60-62, 71, 74-75, 77] However, the nature and the amount of cocatalyst added have to be carefully chosen. At first, ionic and neutral cocatalysts must be differentiated. Neutral cocatalysts such as DMAP and *N*-MeIm may weakly coordinate to the metal center, thus promoting the dissociation of anionic ligand from the metal, which is required for the initiation of polymerization. Directly added ionic species such as $Cl^-$ or $Br^-$ with bulky counter-ions are good initiators and are able to open a pre-coordinated epoxide by nucleophilic attack (Scheme 3, Binary Initiation Pathway (C), Chapter 2.1.1. Copolymerization Mechanism).

However, ionic species are also able to strongly coordinate to the metal center, therefore concurring with the monomer addition or polymer coordination to the metal site. When a polymer chain is released from the coordination sphere of the metal, back-biting can occur, followed by the cleavage of polymer to cPC. In this respect, the effects of the cocatalyst nature and of the cocatalyst/catalyst ratio onto polymerization results are very pronounced. To verify these considerations, two different ionic and neutral cocatalysts were tested for copolymerization with the dinuclear catalyst.

**Table 10.** Effect of cocatalyst nature and cocatalyst ratio on the Copolymerization of PO and $CO_2$.[a]

| Entry | cat | cocat[b] | c (PO/Cr) | t (h) | TOF[c] ($h^{-1}$) | $PO/CO_2$[d] | cPC[d] (mol %) | $M_n$[e] (kg/mol) | $M_w/M_n$[e] |
|---|---|---|---|---|---|---|---|---|---|
| 1 | **52** | *N*-MeIm (1/0.5) | 2000 | 2 | 2 | 1.16 | 0 | na | na |
| 2 | **52** | DMAP (1/0.5) | 2000 | 2 | 8 | 1.33 | 0 | na | na |
| 3 | **52** | DMAP (1/5) | 2000 | 2 | 4 | 1.27 | 0 | na | na |
| 4 | **52** | TBAB (1/0.5) | 2000 | 2 | 46 | 1.17 | 6 | 6.9 | 2.19 |
| 5 | **52** | PPNCl (1/0.5) | 2000 | 2 | 82 | 1.21 | 7 | 3.8 | 2.16 |
| 6 | **52** | PPNCl (1/0.5) | 20.000 | 24 | 55 | 1.11 | 10 | 14.6 | 1.82 |
| 7 | **52** | PPNCl (1/1) | 20.000 | 24 | 61 | 1.00 | 100 | / | / |
| 8 | **51** | PPNCl (1/0.5) | 2000 | 2 | 85 | 1.09 | 27 | 5.6 | 1.65 |
| 9 | **51** | PPNCl (1/0.5) | 20.000 | 24 | 68 | 1.07 | 31 | 12.7 | 1.83 |
| 10 | **51** | PPNCl (1/1) | 20.000 | 24 | 67 | 1.00 | 100 | / | / |

[a] Polymerization conditions: propylene oxide (PO, 5 mL, 2000 resp. 20.000 to Cr), 60 °C, 40 bar. [b] equivalent to Cr. [c] Turnover frequency in mol polymer per mol of Cr per hour. [d] Estimated by $^1$H NMR spectroscopy. $PO/CO_2$ calculated for all products, cPC: cyclic carbonate content [e] Determined by GPC, calibrated with polystyrene standard in THF.

The two neutral cocatalysts *N*-MeIm and DMAP render the dinuclear system almost inactive (Table 10, Entries 1 and 2). Probably the neutral species competitively coordinate to the metal site and thereby inhibit monomer addition by simultaneously being incapable of ring-opening an epoxide and initiating copolymerization. As expected, addition of a multiple equivalent per catalyst did not improve the efficiency of the catalyst/cocatalyst system (Table 10, Entry 3).

Comparison of the two ionic cocatalysts TBAB and PPNCl shows that the anionic halogenids render the system more active (Table 10, Entries 4 - 6), with PPNCl being the most efficient cocatalyst. The amount of added cocatalyst is of outmost importance to the product formation. Addition of half an equivalent cocatalyst per Cr-center leads to formation of polypropylene carbonate with high carbonate content for both catalyst systems investigated (Table 10, Entries 4 – 6 for complex **52**, Entries 8 and 9 for complex **51**).

Addition of one equivalent ionic cocatalyst PPNCl per Cr-center noticeably increases the TON and TOF values for low loadings of catalyst **52** (Table 10, Entry 7). However, the activity at high loadings of catalyst **51** as well as of catalyst **52** at any concentration is not much affected. At a 1:1 ratio of catalyst to cocatalyst, cPC is formed as sole product (Table 10, Entries 7 and 10). Apparently, the equilibrium between the coordinated and dissociated growing polymer chain end is effectively shifted to the uncoordinated species and the back-biting reaction is dominating under such conditions.

Addition of 0.5 equivalent of PPNCl per Cr center allows to improve the product selectivity without loss of catalyst activity. The selectivity towards copolymer under such conditions is higher for the dimeric catalyst system **52**, with an amount of formed cPC of only about 10 %. The co-catalytic effect of TBAB onto activity of **52** is not that obvious, therefore the system in combination with this additive was not investigated in detail. However, the PO/$CO_2$ ratio is drastically improved upon addition of both TBAB and PPNCl cocatalysts from almost 2.0 (Table 9) to 1.1 – 1.3 (Table 10).

Apparently, upon addition of cocatalysts, the copolymerization mechanism is optimized towards alternating insertion of PO and $CO_2$. The bimetallic pathway is exchanged against a binary mechanism, where one metal species as well as the PO monomer can interact with an added cocatalyst. In such systems the mononuclear catalyst can even be rendered active at higher dilutions. In other words, salphen-complexes employed solely in the reaction copolymerize *via* a bimetallic pathway. Upon addition of cocatalysts, the complexes are both able to copolymerize at high dilutions supposedly via a previously reported monometallic mechanism.[64] A similar behavior has also been reported for the related dinuclear and mononuclear salen-structures.[165] This idea was subsequently transferred to new complex structures with anchored cocatalyst groups, which are the most active known to date.[159-160] Despite numerous reports on such effects, their mechanistic background is not really understood.

### 4.3.5. Conclusions

The copolymerization of PO with $CO_2$ was investigated by using flexibly linked dinuclear and mononuclear salphen complexes. Kinetic investigations indicate that the reaction occurs *via* a bimetallic mechanism in the absence of cocatalysts for both mono- and dinuclear complexes. The dinuclear system maintains its activity even under highly diluted conditions of [PO]/[M] = 20.000 at which the mononuclear system loses its efficiency. However, the bimetallic and binary pathways need to be distinguished depending on the catalyst/cocatalyst system used. In the presence of cocatalysts, such as onium salts (*e.g.* PPNCl, TBAB) the mechanism shifts to a binary mode, enabling the monomeric catalyst to retain its activity also at high dilution (Scheme 13).

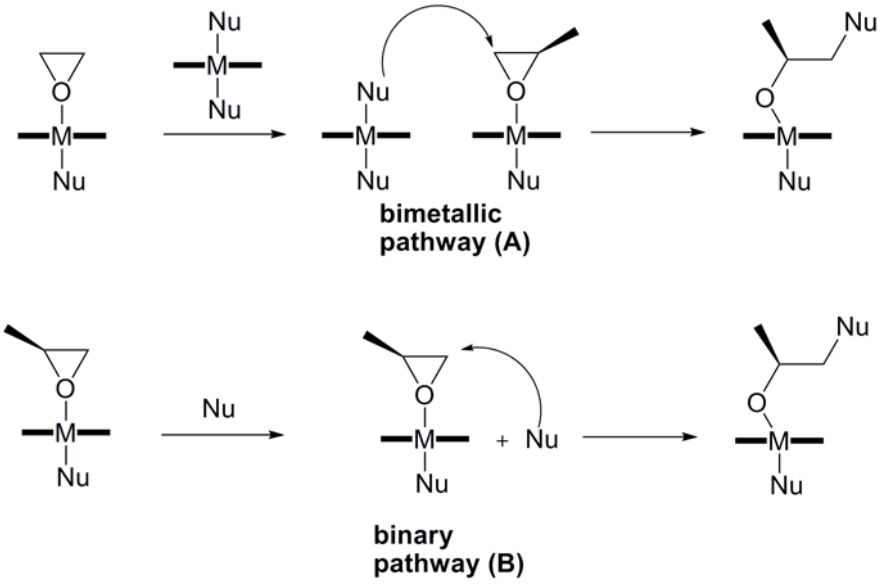


**Scheme 13.** Bimetallic and binary pathways of copolymerization.

The effect of the nature and amount of added cocatalyst on catalytic performance was also investigated, revealing an activating impact of ionic cocatalysts and catalyst inhibition by the typically applied neutral cocatalysts.

## 4.4. Iron-Based Systems

The catalyst systems investigated so far in this work corroborate that a bimetallic mechanism is in state for heterogeneous zinc dicarboxylates and for salen-like complexes. However the activities of both systems are rather low with turn-over frequencies of 5 $h^{-1}$ (≈ 500 g·mol·$h^{-1}$) for zinc glutarate and 200 $h^{-1}$ for the salen complexes.

Rigid dinuclear complexes of the type of **25** (Figure 19) are highly active with TOFs up to 3000 $h^{-1}$ for the copolymerization of cyclohexene oxide and $CO_2$, as the bimetallic mechanism can occur in a much more efficient way with such rigid complexes. However, the catalysts are, up to now, inefficient in the copolymerization of propylene oxide and $CO_2$. As described in the introduction, considerable improvements in terms of activity (for $CO_2$/propylene oxide copolymerization) were achieved with catalysts of the form shown in Figure 26.[159-161] Complex **42** has an activity of up to 26.000 $h^{-1}$, being the highest reported to date for $CO_2$/propylene oxide copolymerization. It is apparent that this catalyst generation does not require two interacting metal species as is the case in the bimetallic mechanism. Instead, the anchored side-groups effectively enhance activity as well as selectivity (c.f. Chapter 2.4.2., Binary Linked Salen Systems for more information). Therefore, besides the strategy of developing efficient dinuclear complexes, catalysts with anchored side-groups can be developed that lead to the desired copolymerization efficiency.

However, complexes of the form **42** introduce several problems. The synthesis route is rather complex with 8 steps, which leads to high process costs. Furthermore, the residual cobalt is toxic and needs to be separated from the crude polymer. Therefore, the search for easy and alternative synthesis routes to such anchored complexes is going on by other members of this project.

Most salen complexes comprise cobalt or chromium centers, which are undesirable from an economical and ecological point of view. Exchange of the toxic metals by unproblematic metals such as zinc, aluminum or iron would lead to a much more ecological way of synthesizing polycarbonates out of $CO_2$. However, complexes containing zinc, aluminum or iron, being active in the coupling reaction of $CO_2$ and propylene oxide are rare in literature.

The focus of this work lies on the development of efficient catalysts for the $CO_2$/epoxide copolymerization reaction. However, the side-product cyclic carbonate, which is often formed, can be used as intermediate for polycarbonate synthesis,[173-174] electrolytes in

lithium ion batteries or as green solvents.[175-176] A multitude of catalysts for the synthesis for cyclic carbonates has been developed in recent years. Among these are onium compounds[26, 177-178], metal halides[179-180], supported metal halides on heterogeneous materials[168, 181-182], salen complexes with aluminum,[51, 183-184] chromium,[51, 73, 185] cobalt,[55, 185-187] zinc[188-191] and tin[192] as well as porphyrin and phthalocyanine complexes of aluminum.[193] Most of these metals are toxic, especially the commonly used cobalt and chromium complexes. For this reason, the complexes generally have to be separated from the resulting products, which limits the potential applications. The development of highly active iron-containing complexes is therefore relevant for both the synthesis of cyclic carbonate as well as of polycarbonates from $CO_2$.

A dinuclear iron(III)-containing complex (Figure 23, complex **34c** with two coordinated iron-centers) was recently reported by Williams *et al.*, producing copolymer from cyclohexene oxide and $CO_2$ with TOFs of 107 $h^{-1}$ at 80°C, 10 bar and a [Fe]/[CHO] ratio of 1/1000. [152-153] The system did not yield copolymer with PO, but introduction of one equivalent PPNCl per Fe-center allowed the conversion of PO into cyclic propylene carbonate (cPC) with TOFs around 25 $h^{-1}$. Recently, Rieger *et al.* presented efficient one-component iron catalysts for the cyclic propylene carbonate synthesis (Figure 65, **35a - b**).[154]

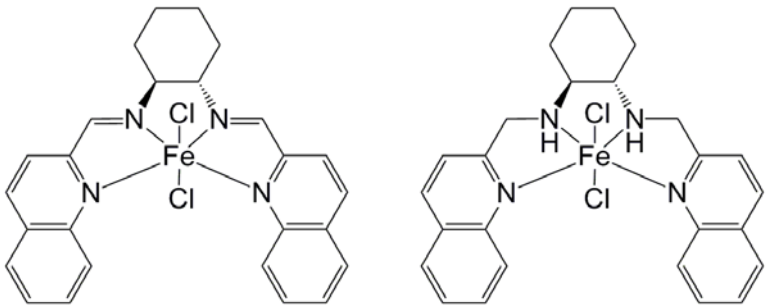


**Figure 65.** Structure of iron(II) complexes showing activity in $CO_2$/epoxide coupling reactions.

Herein, the quadridentate-iron and a new tridentate-iron system are further investigated and a set of different ligand frameworks developed in order to (i) increase the efficiency of cyclic carbonate synthesis and (ii) for the screening of iron(II)- and iron(III)-containing complexes for the possible polycarbonate synthesis from $CO_2$.

### 4.4.1. General Synthesis Procedure

The synthesis of the basic ligand structure of complex **59** can be derived from literature.[194-195] The general procedure for the synthesis of tetradentate ligands and complexes is shown in Scheme 14. Two equivalents of a pyridine carboxaldehyde or a pyrrolecarboxaldehyde are added to a solution of (*S,S*)-cyclohexanediamine or diaminophenylene in ethanol at room temperature. The products either precipitate and can be isolated in analytically pure form by filtration, or can easily be recrystallized from dichloromethane/diethyl in high yields. The diimine ligands are then reduced under mild conditions with sodium borohydride in dry methanol to yield the corresponding diamine. After complexation with $MCl_2$ (for pyridine-containing compounds) or $MCl_3$ (pyrrole-containing compounds), the resulting complexes can be isolated as typically colored products and can be used for $CO_2$/epoxide coupling reactions.

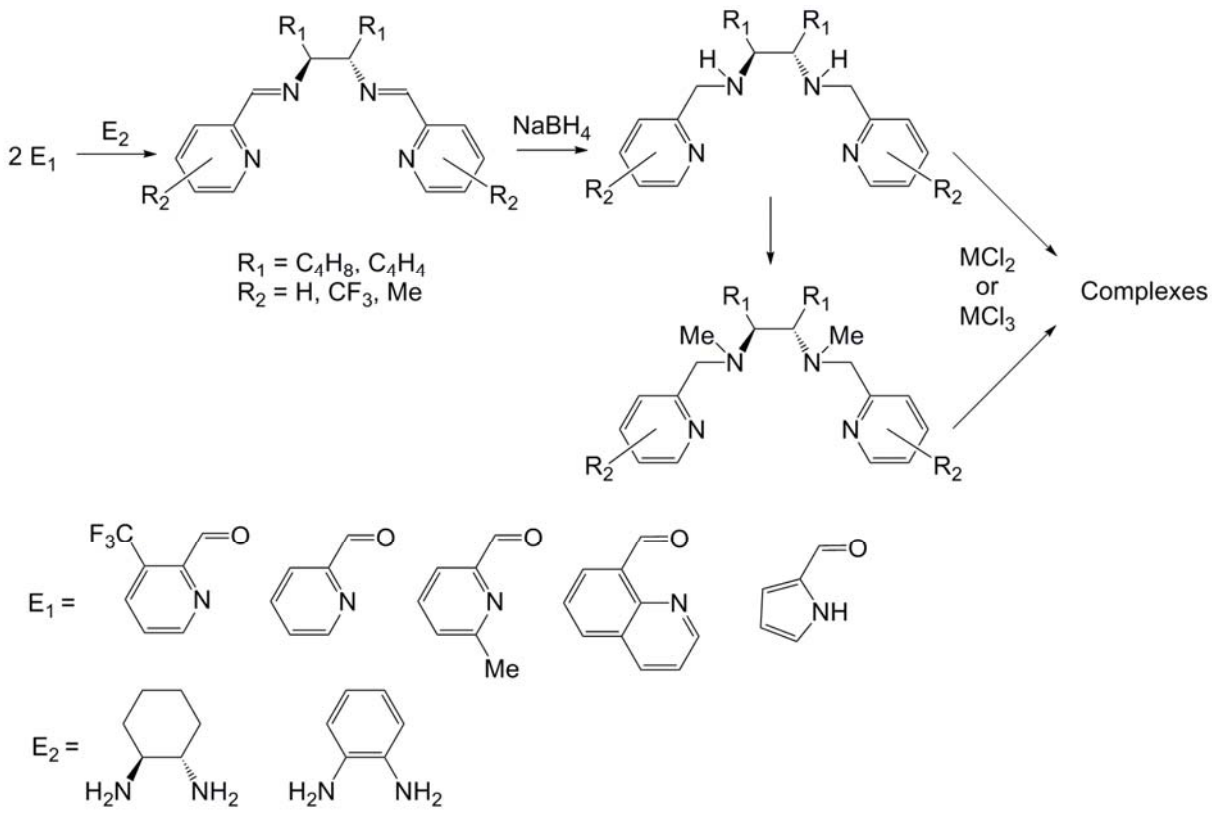


**Scheme 14.** General procedure for synthesis of quadridentate iron- and cobalt-complexes.

### 4.4.2. Activity of Iron(II)-Tetraamine Complexes

In a previous study, Rieger *et al.* investigated the complexes **35a** and **35b** in their reactivity for the coupling reaction of $CO_2$ and propylene oxide. However, so far it was not clear, which structure elements of the ligand were responsible for the high catalytic efficiency. In this work, through systematic variation of the ligand structure, a series of complexes was developed in order to analyze the influence of the ligand environment (sterics and electronics) and the effect of the complexed metal species (Figure 66).

The ligand environment can have substantial influence on the activity and selectivity of a complex. For example, introduction of electron-withdrawing groups into the generalized BDI complex (which is inefficient in the copolymerization of $CO_2$ and propylene oxide), leads to the complex **9**, which is able to copolymerize $CO_2$ and propylene oxide (c.f. Figure 9, Chapter 3.3.1. β-Diiminate Systems).

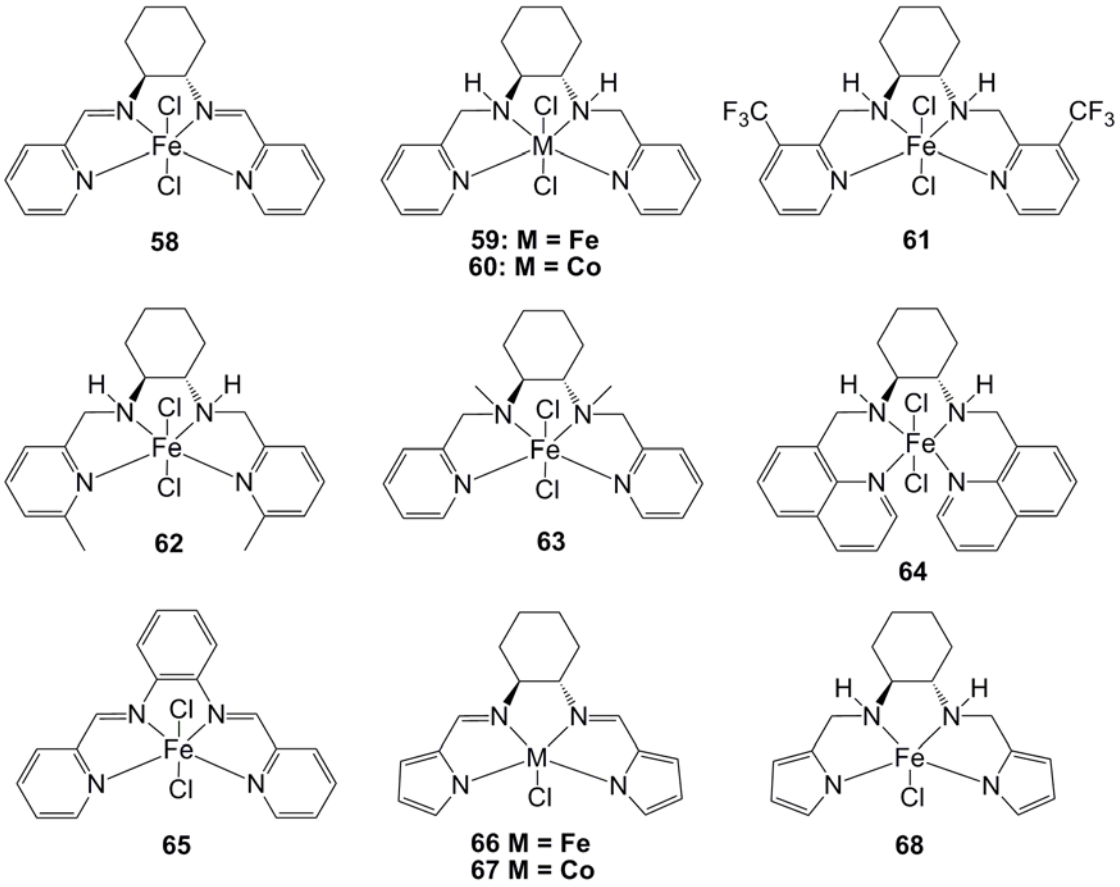


**Figure 66.** Iron- and cobalt-complexes investigated in this work.

Complexes **35a** and **35b** demonstrated good activities in coupling reactions of $CO_2$ and propylene oxide. However, it was not clear, whether the structural motif of the bulky quinoline-ligand is necessary for the activity of the complex. Therefore the corresponding pyridine-derivatives **58** and **59** were synthesized, to reduce the steric demands around the *N*-heteroatomic donors.

Rieger *et al.* previously described for complex **35a**, that no $CO_2$/PO coupling activity is observed, when employed solely for this reaction. The same inefficiency can be found for the analogous diimine-complex **58** (Table 11, Entry 1). However, upon addition of 1 equivalent (Table 11, Entries 2 - 5) resp. 0.5 equivalent (Table 11, Entry 6) cocatalyst per metal center, the activity considerably increases. The cocatalyst nature is of high importance to the degree of activity of the system. Neutral cocatalysts such as *N*-MeIm (*N*-methylimidazolium) and DMAP (dimethylaminopyridine) show little or no effect on the efficiency of the catalyst (Table 11, Entries 2 and 3). Presumably, the *in situ* nucleophilic amines are inefficient ring-openers, but coordinate to the iron centre and are in competitive equilibrium with the epoxide, thereby decelerating the reaction speed. When ionic cocatalysts such as PPNCl (bis(triphenylphosphine)iminium chloride) or TBAB (tetrabutylammonium bromide) are employed, the activity dramatically increases for all complexes tested. The studies indicate that TBAB is the optimum cocatalyst in combination with the iron complexes examined in this study (Table 11, Entry 5).

It is striking that, besides the nature of cocatalyst, the amount of cocatalyst added, respectively the catalyst/cocatalyst ratio is also of outmost importance as well. One equivalent of TBAB per metal center leads to considerable TOF of 66 $h^{-1}$, which can be even increased to 191 $h^{-1}$ by addition of 0.5 equivalents of TBAB per metal center (Table 11, Entries 5 and 6). Presumably, one equivalent of cocatalyst per metal leads to a competitive coordination at the metal center, making an epoxide-coordination unlikely.

**Table 11.** Propylene oxide (PO)/$CO_2$ coupling reactions with different iron(II) tetradentate complexes with and without addition of cocatalysts.[a]

| entry | cat | cocat | T (°C) | p (bar) | TOF[b] | cPC[c] (%) |
|---|---|---|---|---|---|---|
| 1 | **58** | / | 80 | 20 | 0 | / |
| 2 | **58** | *N*-MeIm (1:1) | 80 | 20 | 0 | / |
| 3 | **58** | DMAP (1:1) | 80 | 20 | 7 | 100 |
| 4 | **58** | PPNCl (1:1) | 80 | 20 | 61 | 100 |
| 5 | **58** | TBAB (1:1) | 80 | 20 | 66 | 100 |
| 6 | **58** | TBAB (1:2) | 80 | 20 | 191 | 100 |
| 7 | **59** | / | 40 | 20 | 0 | / |
| 8 | **59** | / | 60 | 20 | 10 | 100 |
| 9 | **59** | / | 80 | 20 | 22 | 100 |
| 10 | **59** | / | 100 | 20 | 18 | 100 |
| 11 | **59** | PPNCl (1:2) | 80 | 20 | 223 | 100 |
| 12 | **59** | TBAB (1:2) | 80 | 20 | 394 | 100 |
| 13 | **60** | TBAB (1:2) | 80 | 20 | 364 | 100 |
| 14 | **61** | TBAB (1:2) | 80 | 20 | 106 | 100 |
| 15 | **62** | TBAB (1:2) | 80 | 20 | 163 | 100 |
| 16 | **63** | TBAB (1:2) | 80 | 20 | 221 | 100 |
| 17 | **63** | PPNCl (1:2) | 80 | 20 | 290 | 100 |
| 18 | **64** | TBAB (1:2) | 80 | 20 | 227 | 100 |
| 19 | **65** | TBAB (1:2) | 80 | 20 | 168 | 100 |

[a] Reaction conditions: 2.5 ml PO, [M]/[PO] = 1000, 2h, 40 - 80 °C, 20 bar $CO_2$ (initial pressure). [b] Turnover frequency in mol converted epoxide per mol of metal per hour. [c] Determined by $^1$H NMR spectroscopy.

In contrast to the diimine-complex **58**, the reduced diamine-complex **59** shows activity even without cocatalyst addition (Table 11, Entries 7 - 10). This behavior has also been demonstrated for complex **35b**.[154] A similar activity difference has been described for analogous salen and salan-complexes.[196-199] SalenCr(III)X complexes show an increased catalyst activity compared to salanCr(III)X complexes in similar $CO_2$ coupling reactions.[197]

This effect can be tentatively ascribed to the presence of $sp^3$-hypridized amino donors in the diamine-structure, which may lead to an increased flexibility of the ligand structure (c.f. Chapter 2.4.3. Salen Systems).[60] Unlike the salen ligand, the salan framework can adopt a *cis*-β-coordination mode with the anion and neutral ligand occupying positions *trans* to oxygen and nitrogen donors, respectively (Scheme 15).[198]

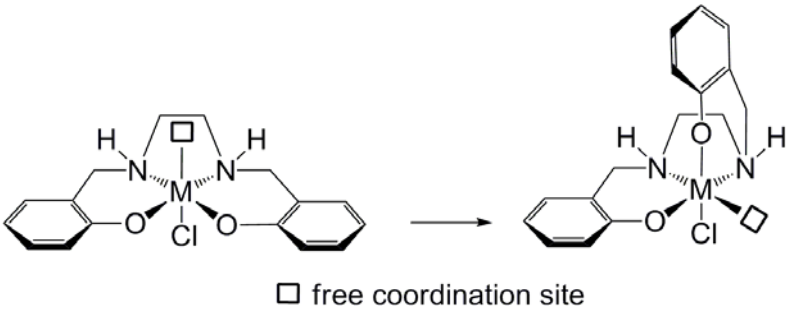


**Scheme 15.** *Trans*- (left) and *cis*-β- (right) configuration of a generalized salanM(III)Cl-complex.

When it comes to substrate coordination, the carboxy-group can coordinate to the metal center in a monodentate and a bidentate binding mode. Considering that a bidentate binding mode is calculated to be more favorable than a monodentate one in some metal-carboxylate complexes, the bidentate binding mode would result in a stabilization of metal-carbonate species.[200] Thus, for an improved $CO_2$ insertion and a higher resistance to decarboxylation, it is desirable to have a complex being able to coordinate carbonate-species in a bidentate mode. This prerequisite is fulfilled when two metal complexes spatially approach each other and “share” a carboxy-species (dinuclear coordination due to bridging of two metal complexes by a carboxy-species) or when one metal-complex possesses two *cis*-coordination sites (Figure 67).

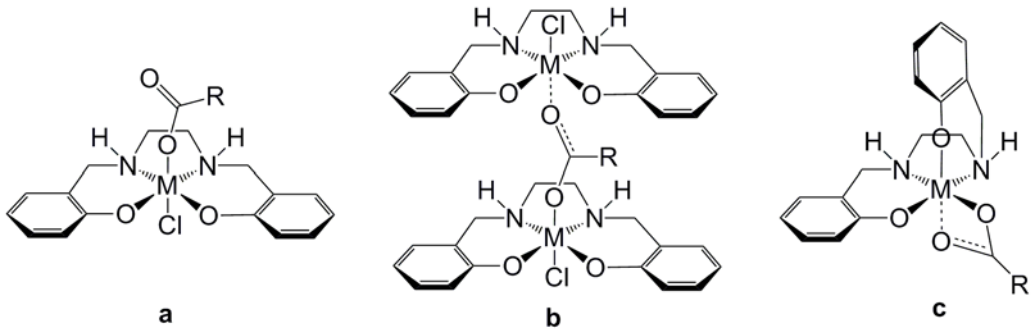


**Figure 67.** (a) monodentate, (b) dinuclear and (c) bidentate coordination of a carboxy-species.

A bidentate coordination would impose a conformational change of the salen-complex which generally tends to coordinate to metal centers in *trans*-configuration. As mentioned above, salan ligands are inherently more flexible than salen ligands. Accordingly, the metal-salan complex should adopt a bidentate binding mode of a carbonate chain end more easily than the metal-salen complex during the coupling reaction. This results in the high catalytic performance and a reduced tendency to dicarboxylate, which may lead to a reduced back-biting mechanism and thereby the formation of copolymer. These considerations are corroborated by the calculations, which indicate that the flexibility of a salan ligand may be favorable to the $CO_2$ insertion step. $CO_2$ insertion into a metal-alkoxide bond in a six-coordinate metal-salen complex first requires an open coordination site.[51] Such a coordination site can only be provided *via* decoordinative rotation of one of the phenoxy-oxygen atoms of the salen ligands, which can be achieved much more easily with salan ligands because of their higher flexibility.

All of these principles also can be transferred to the quadridentate complexes investigated in this study. Such complexes can coordinate in *trans*- or two different *cis*-coordination modi (Figure 68).

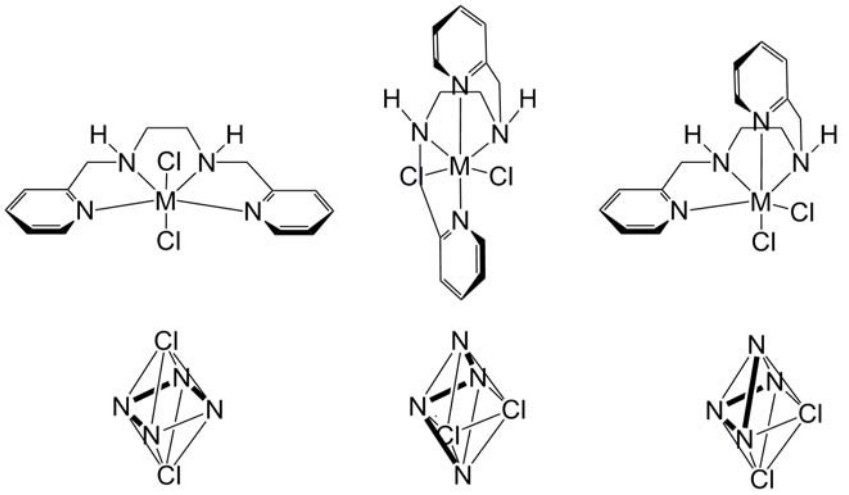

**Figure 68.** *Trans*- (left), *cis*-*α*- (middle) and *cis*-*β*- (right) coordination modi of tetraamine-M(II)-complexes.[154]

Instead of a phenoxy-oxygen atom, the heterocyclic N donor of pyridine must first decoordinate from its regular *trans*-coordination site and recoordinate to a *cis*-coordination position. As a result, the complex is able to offer two *cis*-coordination sites to which the monomers can bind, respectively to which a carboxy-group can bind in a bidentate mode (Scheme 16). These considerations permit an understanding of the difference in catalytic activity of complexes **35a** and **35b** and **58** and **59**, respectively.

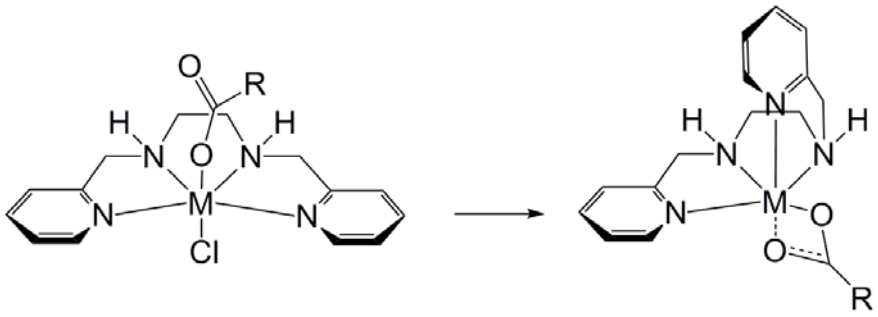

**Scheme 16.** Monodentate and bidentate coordination of a carboxy-species.

### 4.4.3. Influence of Temperature and Cocatalyst on Catalytic Efficiency

In order to determine the optimum temperature for operating the complexes employed herein, the catalyst efficiency of **59** at different reaction conditions without addition of cocatalyst was tested. Catalyst **59** shows an optimum activity at 80 °C, higher or lower temperatures lead to a slightly reduced activity (Table 11, Entries 7 - 10). Presumably, at lower temperatures, the activation barrier is too high, whereas at higher temperatures, the complex presumably is at least partially decomposed. These conditions (80 °C, 20 bar $CO_2$ pressure) were therefore chosen as standard reaction conditions throughout this part of the work, dealing with quadridentate iron-complexes.

When adding 0.5 equivalents of cocatalysts PPNCl or TBAB to **59**, the efficiency of the system dramatically increases to TOFs of 223 and 394 $h^{-1}$, respectively (Table 11, Entries 11 and 12). These values are the highest reported to date for the coupling reaction of $CO_2$ and propylene oxide with iron-based catalysts.

Additionally, the iron-center in **59** was exchanged for a cobalt center to yield the catalyst **60**. As expected, the efficiency of this complex is, with a TOF of 364 $h^{-1}$ (Table 11, Entry 13), comparable to that of complex **59**, thus demonstrating that the commonly applied toxic metal centers cobalt can be exchanged by the less toxic and environmentally more friendly metal iron for successful coupling reactions of $CO_2$ and epoxides.

### 4.4.4. Influence of Electronics on Catalytic Efficiency

It has been shown with β-diiminate (BDI) catalyst systems that alteration of the electronics of the ligand environment can alter the product distribution (cPC vs. PPC) of the catalyst system.[49-50, 128-129] By introduction of electron-withdrawing groups (*e.g.* $CF_3$ or CN) into the ligand framework, the Lewis acidity of the metal center increases. As a result, the polymer chain end may be coordinated more strongly to the metal center, thus inhibiting the back-biting mechanism.[201]

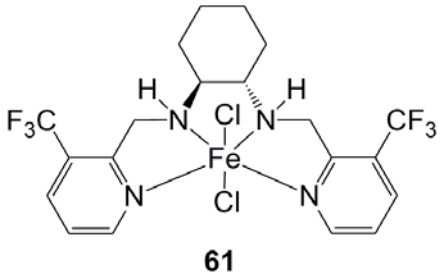


**61**

**Figure 69.** Quadridentate iron complex with electron-withdrawing groups.

This principle was transferred to the iron-containing tetraamine systems employed herein resulting in complex **61** comprising $CF_3$ substituents (Figure 69). However the product formation could not be altered towards PPC formation. Instead, the efficiency of the system even decreased with a TOF of 106 $h^{-1}$ (Table 11, Entry 14).

Presumably, the life-time of complex **61** is too short under the reaction conditions employed and the complex is deteriorated. This effect can also be observed for complex **61**, which is destroyed rapidly upon exposure to air and moisture. Such a fast decomposition of complex **61** could also be observed, when dissolving it under atmospheric conditions, whereas in an inert gas atmosphere, the dissolved complex stays intact for a longer time period. It is most likely that due to the high Lewis acidity of the iron center, the complex reacts with atmospheric oxygen or water, thus leading to the destruction of the complex.

Introduction of more than one electron-withdrawing group could eventually lead to polymer formation; however it is presumed that the activity of such a complex is too low for any industrial application.

### 4.4.5. Influence of Sterics on Catalytic Efficiency

Besides the influence of electronics, the tetraamine framework permits facile introduction of sterically demanding moieties. Thus, methylene-groups on the pyridine (complex **62**) and the diamine-backbone (complex **63**) were introduced (Figure 70). Both catalysts show activity towards $CO_2$/propylene oxide coupling, however with slightly lower activity than for the complex **59** (Table 11, Entries 15 - 17). As described before, traditional salen complexes show lower activities than their corresponding salan-derivatives.

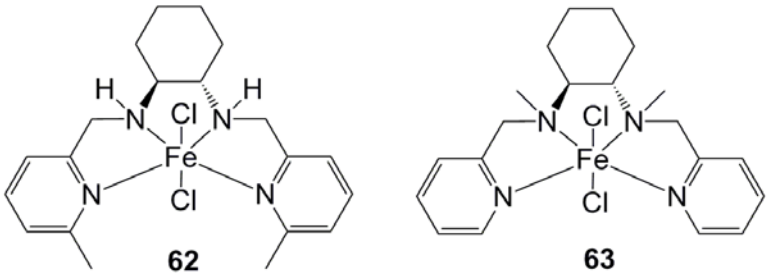


**Figure 70.** Quadridentate iron complex with sterically demanding methylene-groups.

It has also been reported that introduction of bulky groups in the diamine-backbone as in structure **63** can lead to even higher active catalysts.[197, 199-200] Generally, N-H-type salan ligands (Figure 71b) show lower catalytic activity in the epoxide/$CO_2$ copolymerization than the N-Me-type salan ligands (Figure 71c).[199]

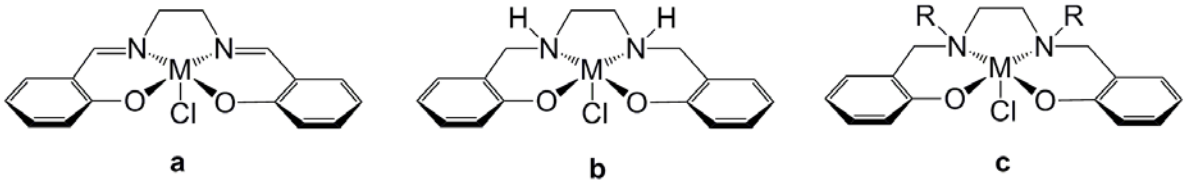


**Figure 71.** Generalized salen (a), N-H-salan (b) and N-R-salan (c) type complexes (R = Me, Et, iPr, Ph).

Complexes with extremely sterically hindered N-R-type salan ligands (R = Et, *i*Pr, Ph) also show lower catalytic activity than their corresponding N-Me-type complexes.[199] It has been proposed that the flexibility of salan ligands is responsible for this high catalytic performance.[199] This would correspond to the considerations discussed earlier for general N-H-type salan complexes. Nevertheless, the increased steric bulk on the nitrogen atom in N-R-type salan ligands may hinder the access of monomers, leading to lower catalytic activity.[199]

This principle was transferred to the tetraamine complexes investigated herein, which show similar properties in $CO_2$/epoxide coupling reactions as salens and salans. The introduced methylene-moiety on the diamine-backbone (complex **63**) leads to a reduced $CO_2$/propylene oxide coupling, compared to the N-H-type complex **59** (Table 11, Entries 15-17).

### 4.4.6. Influence of Iron-Coordination on Catalytic Efficiency

The activity of compounds **35a** and **35b** was proposed to result from the possibility of dissociation of one chloride from the iron centre thereby forming a cationic iron species, being able to coordinate propylene oxide. The released chloride anion is then able to ring-open the epoxide. This theory is supported by the solid state structure of **35b** which exhibits an extremely long and therefore labile iron–chlorine bond[154] and is further corroborated by a bimetallic mechanism of the cyclization reaction (Scheme 17).

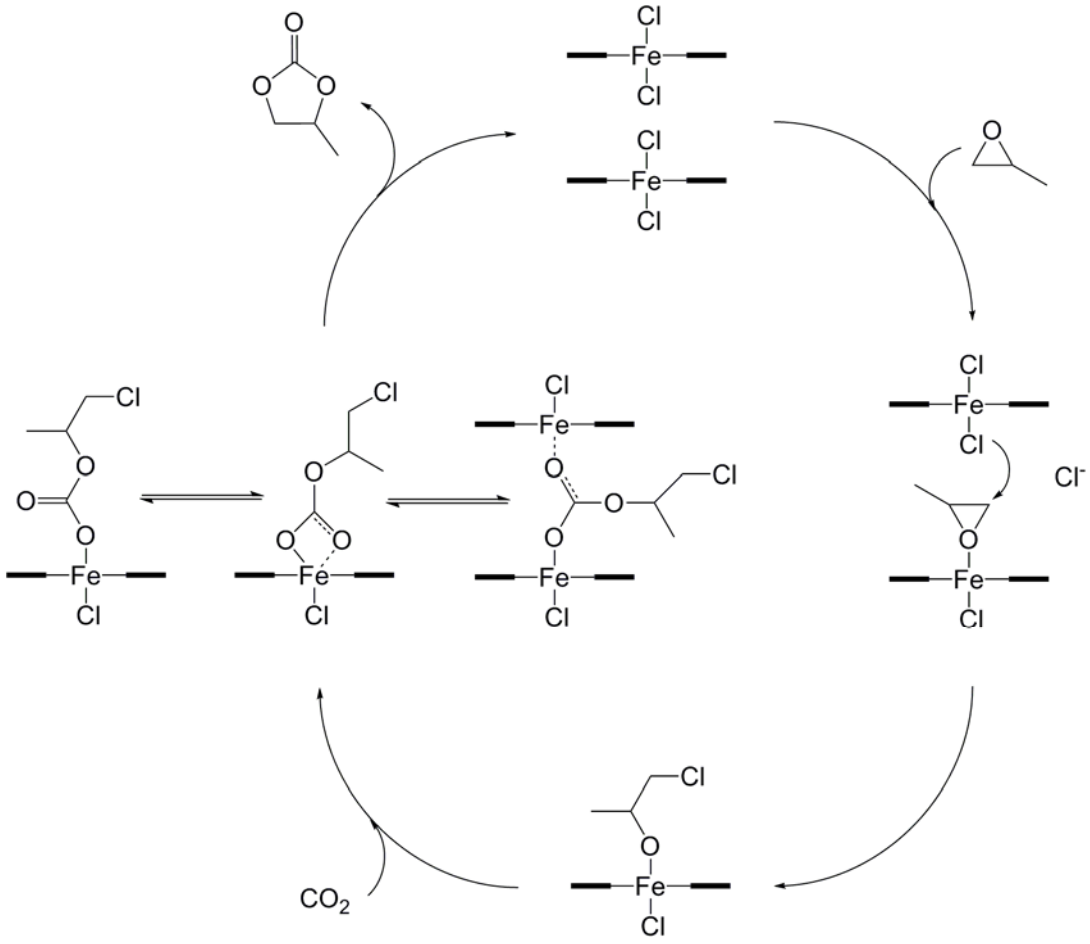


**Scheme 17.** Mechanism for cyclization reaction of propylene oxide and $CO_2$ (analogue to the copolymerization mechanism presented in Scheme 4, Chapter 2.2.1. Copolymerization Mechanism).

The bimetallic nature of the reaction has been confirmed *via* kinetics and has commonly been reported for the coupling reactions of $CO_2$ and epoxides.[52, 54, 56, 202] The weak Fe-Cl

bond of the tetraamine iron complexes presented here allow an attack of the epoxide on the iron center and the opening by a second catalyst molecule.[154] After insertion of one $CO_2$ molecule, one cyclic carbonate is produced and the catalyst reformed. The previously discussed bidentate (and dinuclear) coordination modes of the carboxy-species help to stabilize the intermediate transition state.

However, so far it remained unclear, whether the particular quinoline ligand structures of **35a** and **35b** are essential, or if the activity of the complexes relies primarily on the coordination nature of the tetraamine framework. Complexes **58** and **59** show that the quinoline-moiety can be reduced to a less bulky pyridine one. Furthermore, introduction of side-groups as in complexes **61 – 63** also affords active complex species. To supplement these considerations, the reverse quinoline complex **64** was synthesized, in which the *N*-heterocyclic donor lies in the second aromatic ring, thereby introducing a differing coordination of the iron center (Figure 72).

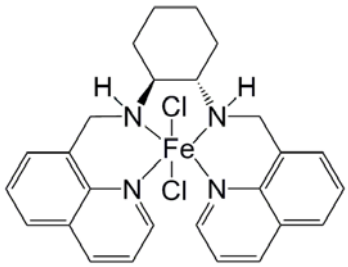


**64**

**Figure 72.** Quadridentate iron complex with quinoline framework.

Again, the activity in $CO_2$/epoxide coupling remains high (and comparable to that of complex **35b**) with a TOF of 227 $h^{-1}$ (Table 11, Entry 18). This indicates that the quinoline-moiety can easily be exchanged and the relevant ligand motif is the tetraamine-chelating structure. These considerations open the field to a new set of tetraamine ligand structures for catalytic reactions.

### 4.4.7. Influence of Tetraamine Backbone on Catalytic Efficiency

Besides the widely investigated salen and salan complexes, salphen systems, where the alkylene diamine backbone is replaced with an aromatic unit, have gained the focus of research activities. [71, 74, 166] An analogous tetraamine iron system has been realized with complex **65** (Figure 73).

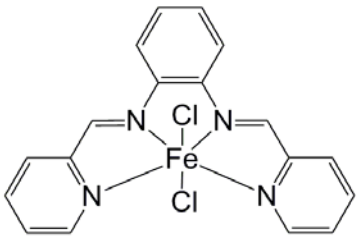


**65**

**Figure 73.** Quadridentate salphen-analogous iron complex.

Again, this system shows catalytic activity in the coupling reaction of $CO_2$ and propylene oxide, showing that also the backbone of such systems can be exchanged, without loss of the reactivity. Similarly to salphen-complexes however, **65** exhibits a reduced activity (Table 11, Entry 19), compared to the salan-analogue complex **59**.

### 4.4.8. Activity of Iron(III)-Tetraamine Complexes

The iron-complexes investigated thus far all contain iron(II) species. Typical salen- and porphyrin-complexes employed in this chemistry generally introduce a metal(III) center, which infers the catalytic activity. This consideration lead us to the design of a new chelating ligand structure, which allows the synthesis of iron(III)-containing complexes. Therefore, the pyridine moiety was exchanged with a pyrrole unit in order to form the complexes **66** – **68** (Figure 74).

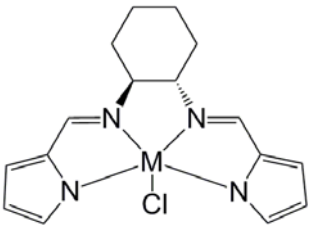


**66 M = Fe**
**67 M = Co**

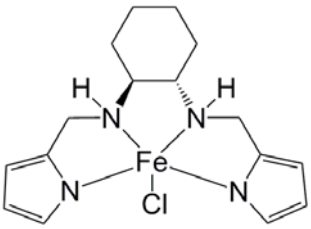


**68**

**Figure 74.** Quadridentate iron(III)-containing complex.

The synthesis is similar to that of the pyridine-complexes, only the coordination behavior is slightly different. Similar to the tetraamine-iron(II) complexes, these catalysts can be synthesized in high yields.

**Table 12.** Propylene oxide (PO)/$CO_2$ coupling reactions with different iron(III) complexes with and without cocatalysts.[a]

| entry | cat | cocat | T (°C) | p (bar) | TOF[b] | cPC[c] (%) |
|---|---|---|---|---|---|---|
| 1 | **66** | / | 80 | 20 | 0 | / |
| 2 | **66** | TBAB (1:2) | 80 | 20 | 13 | 100 |
| 3 | **67** | / | 80 | 20 | 0 | / |
| 4 | **67** | TBAB (1:2) | 80 | 20 | 41 | 100 |
| 5 | **68** | / | 80 | 20 | 0 | / |
| 6 | **68** | TBAB (1:2) | 80 | 20 | 73 | 100 |

[a] Reaction conditions: 2.5 ml PO, [M]/[PO] = 1000, 2h, 80 °C, 20 bar $CO_2$ (initial pressure). [b] Turnover frequency in mol converted epoxide per mol of metal per hour. [c] Determined by $^1$H NMR spectroscopy.

All three iron(III)-catalysts **66** - **68** are inefficient in the coupling reaction of $CO_2$ and propylene oxide, when used in the absence of cocatalyst (Table 12, Entries 1, 3 and 5). Again, only upon addition of 0.5 equivalents of TBAB, can an appreciable activity of the system be noted. Analogous to the iron(II)-complexes, the diimine-structures **66** and **67** (Table 12, Entries 2 and 4) show lower efficiencies, compared to that of the analogous diamine-structure **68** (Table 12, Entry 6). This shows that also a pyrrole containing tetraamine ligand in combination with iron(III)-species is able to catalyze the coupling reaction of $CO_2$ and epoxides. However, the efficiency is lower than for the tetraamine-iron(II) complexes **59** – **65**.

### 4.4.9. Activity of Tridentate Iron Complexes

In the field of olefin polymerization, which is a lot more mature than the field of $CO_2$/epoxide copolymerization, a lot of catalyst systems have been developed. To these systems belong several 2,6-bis(N-arylimino)pyridine ([PDI]) ligands displaying different substituents at the ortho and ortho' positions of the two N-aryl rings.[203] The corresponding paramagnetic iron (II) and cobalt (II) complexes were investigated as precatalysts for the polymerization of ethylene in the presence of modified methylaluminocan (MMAO).[204-207] It was shown that these complexes can exist in a *syn* (meso) and *anti* (chiral) configuration, which interconvert at room temperature *via* rotation of the aryl group.[203] This property is important for their performance as catalysts in the α-olefin polymerization or other catalytic processes susceptible to stereochemical control. The electron effect and positions of the substituent of [PDI] ligands were observed to affect considerably catalyst activity and polymer property.

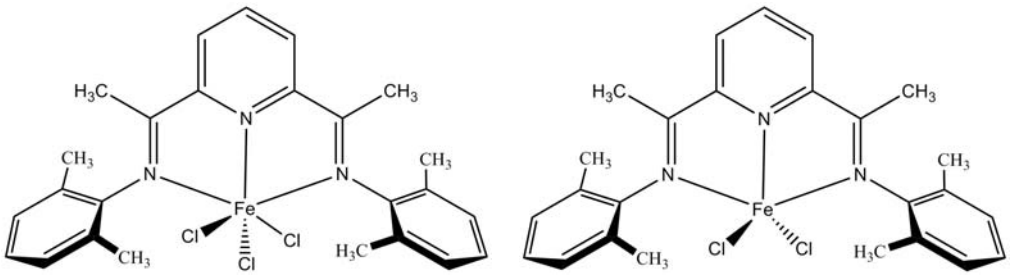


**Figure 75.** Tridentate iron(III) complex **69** (left) and iron(II) complex **70** (right)

This behavior renders the such complexes interesting for the coupling reaction of $CO_2$ and epoxides. The iron complexes **69** and **70** were prepared with a slightly modified procedure according to literature synthesis (Figure 75).[207] After dissolving the 2,6-bis(arylimino)pyridine compound in tetrahydrofurane, water free iron(II) chloride or iron(III) chloride was added, resulting in an immediate color change from yellow to strongly colored. Diethylether was added to the reaction to precipitate the complex and the resultant solids were filtered in air and washed with diethylether and pentane and dried in vacuo. The complexes could be isolated in very high yields (80 - 95 %). Due to the paramagnetism of these complexes, the signals appear as broad singlets over a wide ppm range (-50 ppm to +100 ppm), rendering a useful $^1$H NMR spectroscopy useless. Generally, iron(III)-complexes

show higher polymerization activities with ethylene than their iron(II) analogues.[207] It has been shown that complexes with highly symmetrical ligand frameworks show the sharpest signals in $^1$H NMR spectra than other complexes.[207]

The tridentate complexes **69** and **70** were tested in the coupling reaction of $CO_2$ and propylene oxide (Table 13).

**Table 13.** Propylene oxide (PO)/$CO_2$ coupling reactions with tridentate iron complexes.[a]

| entry | cat | Cocat | T (°C) | P (bar) | TOF[c] ($h^{-1}$) | cPC[d] (%) |
|---|---|---|---|---|---|---|
| 1 | **69** | / | 80 | 20 | 0 | / |
| 2 | **69** | / | 100 | 40 | 0 | / |
| 3 | **69** | TBAB (1:2) | 80 | 20 | 0 | / |
| 4 | **69** | PPNCl (1:2) | 100 | 40 | 138 | 100 |
| 5 | **69** | TBAB (1:2) | 100 | 40 | 148 | 100 |
| 6 | **70** | / | 80 | 20 | 0 | / |
| 7 | **70** | TBAB (1:2) | 80 | 20 | 0 | / |
| 8 | **70** | TBAB (1:2) | 100 | 40 | 176 | 100 |

[a] Reaction conditions: 2.5 ml PO, [M]/[PO] = 1000, 2h, 80 – 100 °C, 20 - 40bar $CO_2$ (initial pressure). [b] Turnover frequency in mol converted epoxide per mol of metal per hour. [c] Estimated by $^1$H NMR spectroscopy.

The iron(III)-[PDI] complex **69** shows no activity when employed solely (Table 13, Entries 1 – 2). Also addition of half an equivalent ionic cocatalyst per metal center at 80 °C and 20 bar $CO_2$ pressure does not lead to an active system (Table 13, Entry 3). Only upon increasing the reaction temperature to 100 °C and the $CO_2$ pressure to 40 bar, cyclic propylene carbonate is formed with TOFs of up to 148 $h^{-1}$ (Table 13, Entries 4 – 5). The iron(II)-[PDI] complex **70** exhibits the same catalytic properties as complex **69**, being only active at reaction conditions of 100 °C, 40 bar and half an equivalent of ionic cocatalyst.

This opens the route to a new class of catalysts for the coupling / copolymerization of $CO_2$ and epoxides. Modifications of the [PDI] ligand system are rather easy and allow to screen a variety of tridentate complexes in their catalytic efficiency.

### 4.4.10. Copolymerization Results with Iron-Complexes.

Williams *et al.* recently presented a dinuclear iron complex, which is able to copolymerize $CO_2$ and cyclohexene oxide with considerable TOFs.[153] The complexes in this work were tested for the copolymerization reaction of $CO_2$ and cyclohexene oxide as well (Table 14).

**Table 14.** Cyclohexene oxide (CHO)/$CO_2$ copolymerization reactions with iron(II)- and iron(III)-complexes.[a]

| entry | cat | cocat | T (°C) | p (bar) | TOF[b] ($h^{-1}$) | Carbonate[c] |
|---|---|---|---|---|---|---|
| 1 | **59** | TBAB (1:2) | 80 | 20 | 12 | 20 |
| 2 | **60** | TBAB (1:2) | 80 | 20 | 11 | 37 |
| 3 | **61** | TBAB (1:2) | 80 | 20 | 18 | 25 |
| 4 | **62** | TBAB (1:2) | 80 | 20 | 18 | 34 |
| 5 | **63** | TBAB (1:2) | 80 | 20 | 17 | 61 |
| 6 | **64** | TBAB (1:2) | 80 | 20 | 9 | 37 |
| 7 | **65** | TBAB (1:2) | 80 | 20 | 30 | 8 |
| 8 | **66** | TBAB (1:2) | 80 | 20 | 4 | 24 |
| 9 | **67** | TBAB (1:2) | 80 | 20 | 5 | 29 |
| 10 | **68** | TBAB (1:2) | 80 | 20 | 12 | 18 |
| 11 | **70** | TBAB (1:2) | 100 | 40 | 18 | 33 |

[a] Reaction conditions: 3.8 ml CHO, [M]/[CHO] = 1000, [TBAB]/[M] = 1/2, 2h, 80 - 100 °C, 20 – 40 bar $CO_2$ (initial pressure). [b] Turnover frequency in mol converted epoxide per mol of metal per hour. [c] Determined by $^1$H NMR spectroscopy.

All catalysts are active in the copolymerization, however with highly reduced TOFs compared to the propylene oxide coupling reaction. At the same time, the carbonate content in the resulting polymer is quite low with only 8 – 61 % and follows no interpretable rule. Analysis of the molecular weights was not possible, because a too high content of residual complex in the crude polymer and too low yields for separation of pure polymer for GPC-analysis. This means that the efficiency in CHO-activation of the systems developed in this work is much lower than their efficiency in PO-activation. The reason for this behavior is not easy to

analyze and can be attributed to many factors. For example, propylene oxide may coordinate more strongly to the iron-center and is preactivated more efficiently. It is also possible that a bidentate binding mode is more unlikely with an incorporated cyclohexene oxide due to the higher sterical demand.

### 4.4.11. Conclusions

In this work, a series of tetraamine iron(II) and tetraamine iron(III) complexes was presented. All complexes show moderate to high activity in $CO_2$/propylene oxide coupling reactions. When adding ionic cocatalysts such as PPNCl or TBAB the efficiency of the system can be increased to approximately 400 $h^{-1}$, which is the highest value reported to date for the coupling reaction of $CO_2$ and propylene oxide with iron-based catalysts.

It could be shown that the commonly applied toxic metal centers, *e.g.* cobalt, can be exchanged by the "green" metal iron for coupling reactions of $CO_2$ and epoxides without loss of catalytic efficiency.

This work also shows that $CO_2$/epoxides can be copolymerized into polycarbonates *via* iron-complexes. In close future, this could allow an ecological as well as economical favorable alternative to the preferentially used toxic metals cobalt and chromium.

So far, it was not clear which structural motif of iron-containing complexes is essential for the catalytic activity. In this study, through systematic variation of the ligand structure, a series of complexes was developed which show that iron complexes can be optimized (i) towards even higher activities in coupling reactions and (ii) towards polycarbonate synthesis out of $CO_2$ and epoxides. Presumably, the strategy described for binary linked salen complexes (Figure 26, complex **42**) can be transferred to such iron-containing complexes to yield untoxic catalysts for the $CO_2$/epoxide copolymerization reaction.

# 5. **Summary and Outlook**

In this work, different catalyst systems were investigated in their catalytic efficiency for $CO_2$/epoxide copolymerization. Furthermore, the underlying pathways and the mechanistic behavior of the catalysts were studied.

Heterogeneous zinc dicarboxylates are – despite over three decades of intensive research activities – limited in their potential for the production of polycarbonates from $CO_2$. Even though huge steps in homogeneous catalysis have been made in the last years, traditional zinc dicarboxylates remain industrially relevant as they are easy to prepare and handle, non-toxic and economically viable. In the first part of this work, several strategies to enhance the activity of zinc glutarate were investigated (Figure 76).

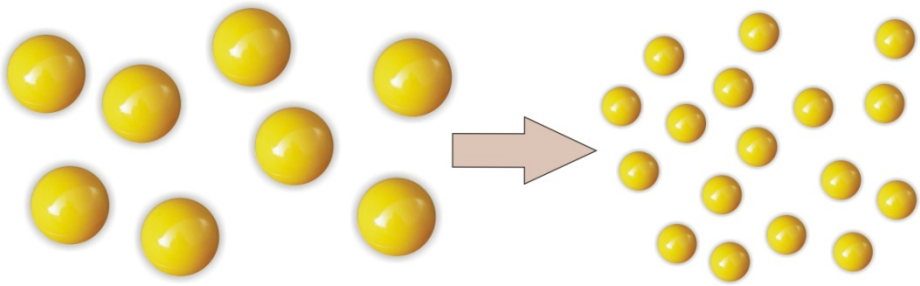

**Figure 76.** Increase of surface area (and activity) *via* down-sizing the material.

Highly disperse silica gel with a surface area of up to 400 $m^2/g$ was added as substrate during the synthesis of zinc glutarate. It was expected that zinc glutarate would form on the substrate surface with similarly high surface areas, thereby leading to a higher activity. Indeed, it was observed that the activity of zinc glutarate increased with increasing silica gel content. However, the activity enhancement was restricted to a factor of 2 – 3 with TOFs of maximum of 5 $mol \cdot mol^{-1} \cdot h^{-1}$ (corresponds to 500 $mol \cdot mol^{-1} \cdot h^{-1}$ or 50 g polymer per g catalyst). Addition of growth controllers (*e.g.* block-copolymers as structuring agent or monoacids for controlled crystal growth) lead to similarly low activities. Also post-treatment of the material *via* ball-milling did not lead to substantial changes in catalytic activity. It was shown that the crystallization of zinc glutarate can only hardly be controlled *via* additives. Presumably, zinc dicarboxylates always tend to crystallize in a platelet-shaped manner, independently of the reaction conditions, making logical modifications of the system

difficult. Concurrently, the particles formed *via* these procedures are already "close" in size to the unit cell with dimensions of less than 1 µm x 1 µm and a thickness of less than 200 nm (Figure 77).

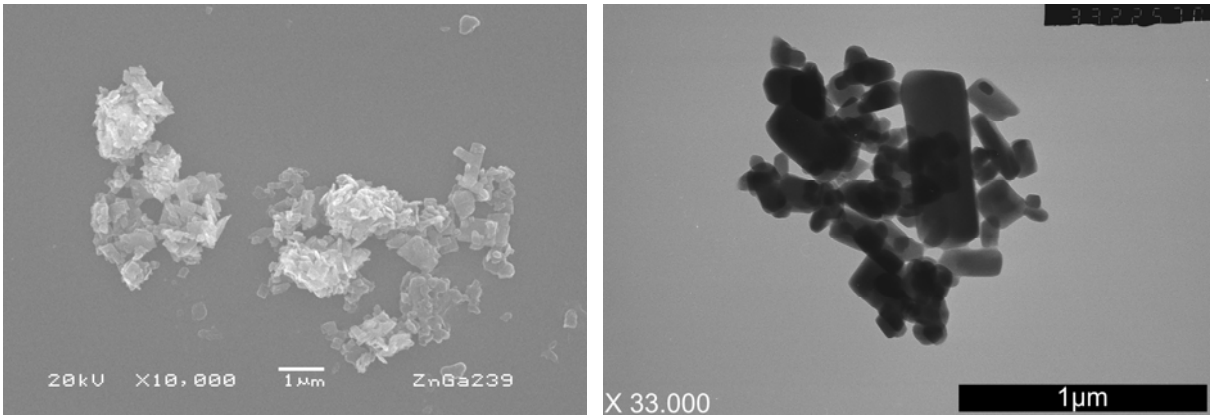


**Figure 77.** SEM (left) and TEM (right) pictures of untreated zinc glutarate showing that the platelet-sized particles have the approximate dimensions 1 µm x 1 µm x 200 nm.

Therefore, the potential of further down-sizing the material (and thereby increasing the surface area and activity) is strongly limited. One possible strategy for the enhancement of catalytic activity, however, could be the addition of a substrate material with a comparable crystal structure to that of zinc glutarate (space group P2/c), on which the catalyst preferentially is able to grow.

In addition to the investigation of the strategies described above, the underlying mechanisms and active species of the heterogeneous zinc dicarboxylates were investigated. It was shown that zinc dicarboxylates need initiator groups on the surface in order to be catalytically active. Through careful handling in an inert atmosphere, it was observed that the heterogeneous material is inactive prior to activation, whereas it can be rendered highly active after activation. This principle was transferred to a series of experiments in which the initiator group was interchanged (Scheme 18).

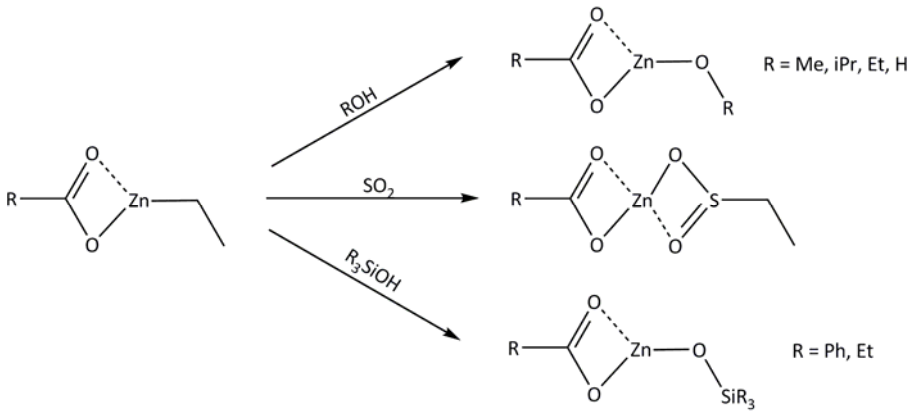


**Scheme 18.** Zinc dicarboxylate with different initiator groups on the surface.

The introduction of zinc-ethylsulfinate species affords the most active material. However, in terms of industrial application, the material obtained *via* the functionalization procedure loses its attractiveness as the precursors are rather expensive and complicated to handle, compared to the standard procedure. Therefore, the standard zinc glutarate remains the material of choice for industrial production of polycarbonates from $CO_2$.

In order to gather further insight into the underlying surface polymerization mechanisms, the solid state structures of several zinc dicarboxylates were compared. It was observed that a specific structure motif needs to be present on the surface of the material in order to render it active (Figure 78).

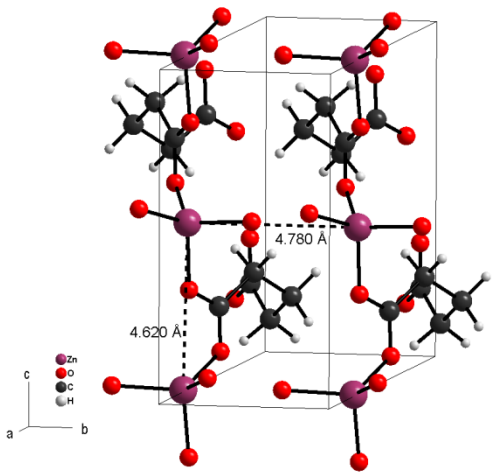


**Figure 78.** Close-up view on the activity-determining structure motif of zinc glutarate with Zn-Zn couples in a defined spatial distance.

For homogeneous catalysts it has been widely discussed that this reaction proceeds by a bimetallic copolymerization mechanism. Supposedly, the heterogeneous zinc dicarboxylates copolymerize in a bimetallic fashion as well, with the necessity of Zn-Zn surface couples in a well-defined spatial distance between 4.6 and 4.8 Å (Scheme 19).

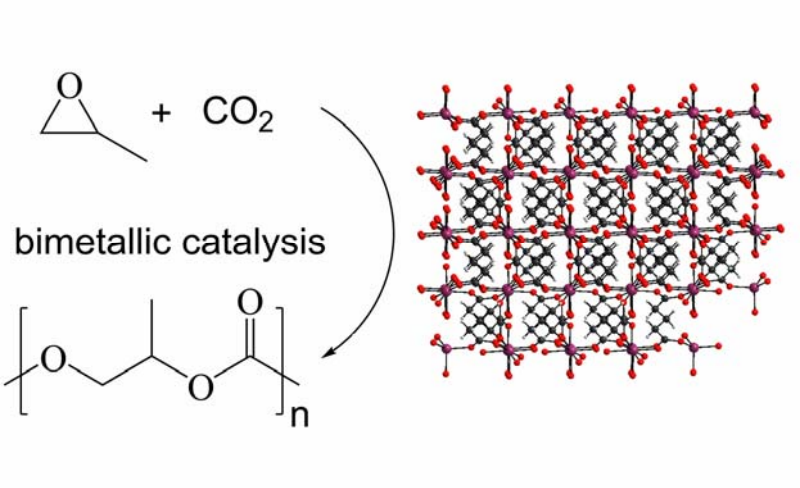


**Scheme 19.** View along *a*-axis of zinc glutarate and proposed bimetallic copolymerization mechanism on the surface.

Theoretical calculations with model systems similar to zinc dicarboxylates were conducted as well, suggesting an optimal separation of Zn atoms in the range of 4.3 - 5.0 Å, which gives a balanced optimum between activation energy and selectivity towards copolymerization. New strategies should therefore focus on introduction of two metallic species into a molecular framework that does not comprise bulky material, in which no catalysis can take place. Therefore, new strategies have to focus on homogeneous systems that comprise two metal centers or a cooperative binary linked ligand system.

The homogeneous flexibly linked dinuclear salphen complexes directly adhere to these considerations. Through kinetic measurements it could be shown that salphen complexes copolymerize $CO_2$ and epoxides in a bimetallic fashion (Scheme 20).

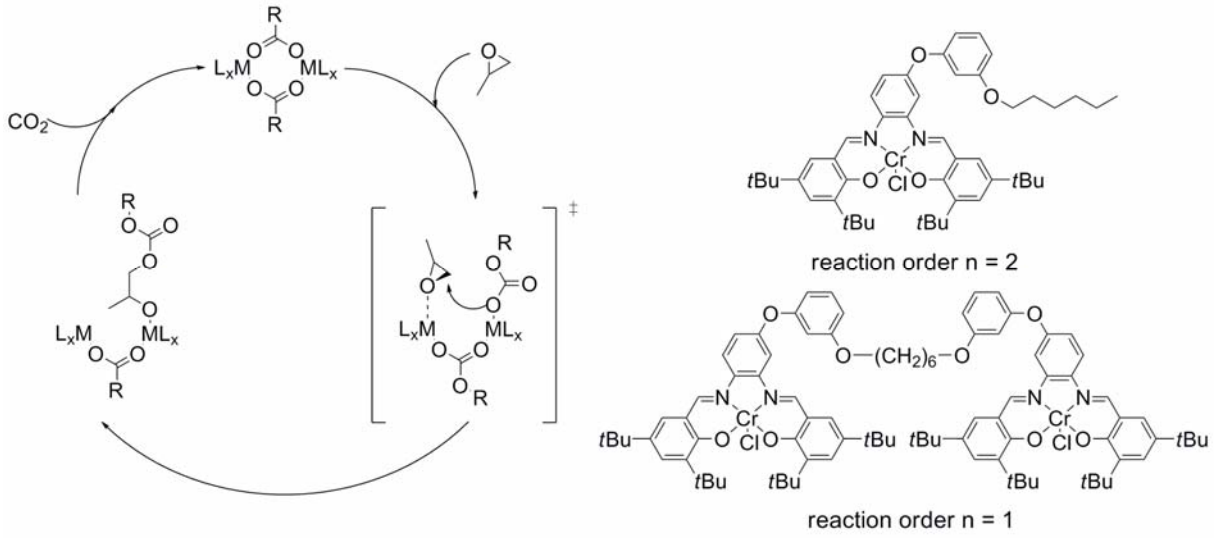


**Scheme 20.** Bimetallic catalytic mechanism for $CO_2$/PO copolymerization with mononuclear and dinuclear salphen-type complexes

Through linking the two interacting metal species, more efficient catalysts that are even able to copolymerize at high dilutions were generated. At such high dilutions, mononuclear catalysts generally lose their activity. However, the bimetallic and binary pathways need to be distinguished depending on the catalyst/cocatalyst system used. The potential of the salphen complexes is restricted to TOFs of less than 100 $h^{-1}$. Recently, Lee *et al.* and Williams *et al.* developed rigid dinuclear complexes which exhibit activities of up to 3000 $h^{-1}$ for the copolymerization of cyclohexene oxide and $CO_2$ (Figure 79, **34a**). These rigid dinuclear systems are currently under investigation and will presumably be optimized towards the copolymerization of propylene oxide and $CO_2$.

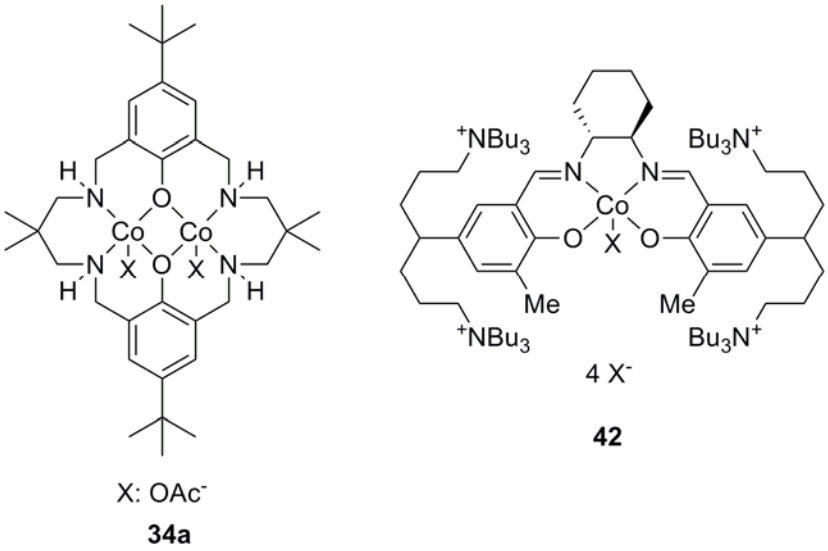


**Figure 79.** Efficient rigid dinuclear complex **34a** and binary anchored salen complex **42**.

In the presence of cocatalysts, such as onium salts (*e.g.* PPNCl, TBAB) the bimetallic mechanism with salphens shifts to a binary mode, enabling the monomeric catalyst to retain activity also at high dilution. This principle has been adopted by Lee *et al.*, who synthesized complexes with anchored cocatalysts (Figure 79, **42**). These systems belong to the most efficient $CO_2$/epoxide copolymerization catalysts known to date with TOF of up to 26.000 $h^{-1}$. However, the cobalt species generally employed in these catalyst systems is toxic and needs to be separated from the resulting polymer. This necessary separation, in addition to the lengthy and expensive catalyst synthesis, restrict the potential of the complex **42**.

Therefore, a set of quadridentate iron(II) and iron(III) complexes was developed and investigated in this work (Figure 80). It could be shown that the commonly applied toxic metal centers such as cobalt can be exchanged against the “green” metal iron for coupling reactions of $CO_2$ and epoxides without losing catalytic efficiency. When adding ionic cocatalysts such as PPNCl or TBAB the efficiency of the system can be increased to approximately 400 $h^{-1}$.

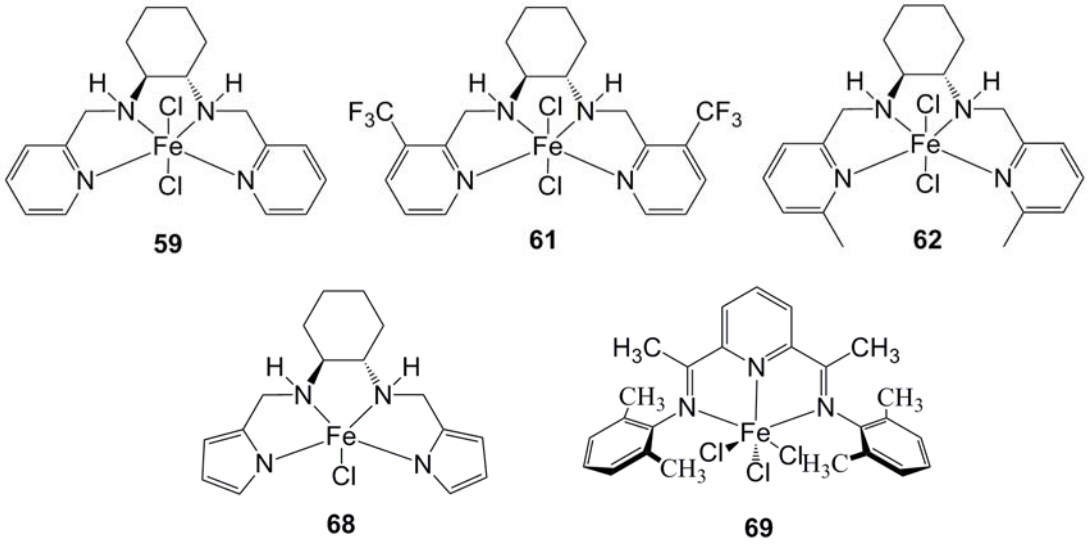


**Figure 80.** Selected iron-containing complexes being active in the $CO_2$/propylene oxide coupling reaction.

In this work, it has been shown that heterogeneous zinc dicarboxylates and metal-salphen complexes copolymerize $CO_2$ and epoxides in a bimetallic fashion. However, their efficiency in the copolymerization reaction is restricted. Therefore, research activities will have to focus on new concepts. The optimization of rigid Zn-containing dinuclear complexes towards $CO_2$/PO copolymerization shows promising results and could lead to the efficiencies desired. Another strategy could be the further enhancement of the binary anchored salen complexes of the form **42**, by (i) finding an alternative and easier synthesis route towards the complex and (ii) exchanging the toxic metal center, circumventing the necessity of separating the catalyst from the polymeric product. The iron complexes presented in this work show that the commonly applied cobalt center can be exchanged by the ecologically unproblematic iron metal and that $CO_2$ and epoxides can be copolymerized into polycarbonates *via* iron-complexes. In close future, this could allow an ecological as well as economical favorable alternative for the industrial production of polycarbonates from $CO_2$.

# 6. **Zusammenfassung und Ausblick**

In dieser Arbeit wurden unterschiedliche Katalysatorsysteme hingehend ihrer katalytischen Effizienz in der Copolymerisation von $CO_2$ und Epoxiden untersucht. Zudem wurden die zugrundeliegenden Reaktions-Pathways und das mechanistische Verhalten der Katalysatoren untersucht.

Heterogene Zinkdicarboxylate sind – trotz über drei Jahrzenten intensiver Forschung – in ihrem Potential für die Produktion von Polycarbonaten aus $CO_2$ limitiert. Obwohl in den letzten Jahren riesige Schritte in der homogenen Katalyse gemacht wurden, werden die traditionellen Zinkdicarboxylate immer noch industriell für die Synthese eingesetzt, da sie einfach herzustellen und zu handeln, sowie untoxisch und ökonomisch praktikabel sind. Im ersten Teil dieser Arbeit wurden verschiedene Strategien für die Aktivitätssteigerung von Zinkglutarat erkundet (Abbildung 81).

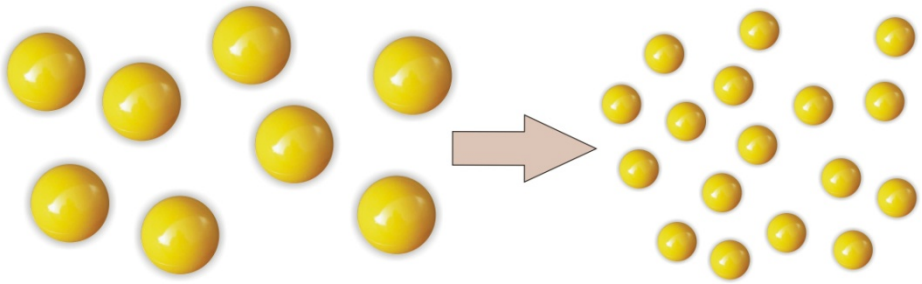

**Abbildung 81.** Erhöhung der Oberfläche (und Aktivität) durch Verkleinerung des Materials.

Hoch disperses Kieselgel mit einer Oberfläche von bis zu 400 $m^2/g$ wurde während der Synthese von Zinkglutarat als Trägermaterial hinzugegeben. Dabei wird erwartet, dass das Zinkglutarat sich auf dem Trägermaterial mit einer ähnlich hohen Oberfläche bilden und somit zu den gewünschten Aktivitäten führen. Zwar wurde eine Aktivitätssteigerung mit steigendem Kieselgelanteil beobachtet, jedoch war diese auf einen Faktor von 2 - 3 limitiert, was einer Aktivität von ca. 5 $mol \cdot mol^{-1} \cdot h^{-1}$ (umgerechnet 500 $g \cdot mol^{-1} \cdot h^{-1}$ oder 50 g Polymer / g Katalysator) entspricht.

Hinzufügen von Wachstumskontrollern (z.B. Blockcopolymeren als Strukturierungs-Agentien oder Monosäuren für das kontrollierte Kristallwachstum) führen zu ähnlich schlechten Aktivitäten. Ebenso führt Nachbehandlung des Materials mit einer Kugelmühle zu einer nur

geringfügigen Erhöhung der katalytischen Aktivität. Es wurde gezeigt, dass die Kristallisation von Zinkglutarat nur schwer über die Zugabe von Additiven kontrolliert werden kann. Es scheint, dass Zinkdicarboxylate, unabhängig von den Reaktionsbedingungen, bevorzugt in einer Plättchen-ähnlichen Form kristallisieren. Dies führt dazu, dass logische Modifizierungen an dem System nur schwer durchzuführen sind. Zudem sind die über diese Methode hergestellten Partikel größentechnisch bereits sehr „nahe“ zur Einheitszelle mit einer Abmessung von weniger als 1 µm x 1 µm und deiner Dicke von weniger als 200 nm (Abbildung 82).

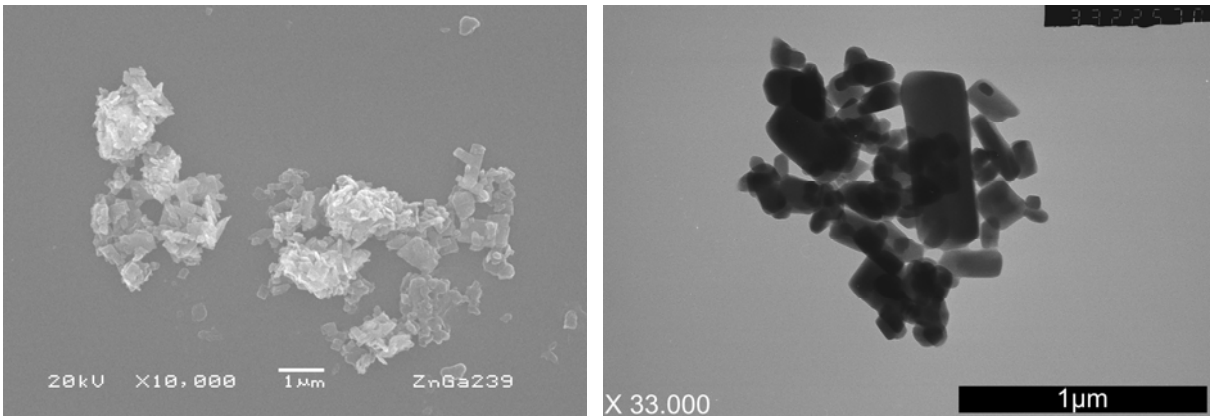


**Abbildung 82.** Rasterelektronenmikroskopie (links) und Tunnelelektronenmikroskopie (rechts) Bilder von unbehandeltem Zinkglutarat. Zu sehen ist die Plättchen-Form der Partikel mit einer ungefähren Abmessung von 1 µm x 1 µm x 200 nm.

Aufgrund dieser Abmessungen ist das Potential des Verkleinerns des Materials (und der damit einhergehenden Oberflächen- und Aktivitätssteigerung) stark limitiert. Eine mögliche Strategie für die Steigerung der katalytischen Aktivität könnte allerdings die Zugabe von Trägermaterialien mit einer zu Zinkglutarat ähnlichen Kristallstruktur (Raumgruppe P2/c) sein, auf welcher der Katalysator bevorzugt wachsen kann.

Zusätzlich zu den oben aufgeführten Strategien wurde eine ausführliche Untersuchung der zugrundeliegenden Mechanismen und der aktiven Spezies auf der heterogenen Zinkdicarboxylat-Oberfläche durchgeführt. Es konnte gezeigt werden, dass Zinkdicarboxylat auf der Oberfläche Initiatorgruppen benötigt, um katalytisch aktiv zu sein. Durch vorsichtige Behandlung in einer inerten Atmosphäre wurde beobachtet, dass das heterogene Material

erst durch Postaktivierung aktiv wird. Dieses Prinzip wurde in einer Serie von Experimenten übernommen, in welche die Initiator-Gruppe ausgetauscht wurde (Schema 21).

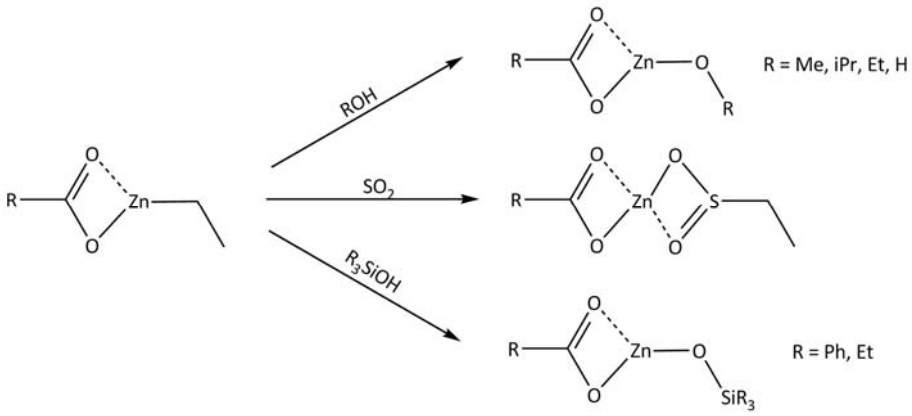


**Schema 21.** Zinkdicarboxylat mit unterschiedlichen Initiator-Gruppen an der Oberfläche.

Die Einführung von Zink-Ethylsulfinat Spezies bringt das aktivste Material hervor. Hinsichtlich einer industriellen Anwendung hingegen ist das Material über diese Funktionalisierungs-Prozedur weniger attaktiv, da die Precursoren – verglichen mit der Standard-Synthese - relativ teuer und kompliziert zu handeln sind. Deswegen bleibt das Standard-Zinkglutarat das Material der Wahl für die industrielle Produktion von Polycarbonaten aus $CO_2$.

Um einen tieferen Einblick in die zugrundeliegenden Polymerisationsmechanismen auf der Oberfläche zu gewinnen, wurden die Kristallstrukturen der unterschiedlichen Zinkdicarboxylate verglichen. Es wurde beobachtet, dass ein spezifisches Strukturmotiv auf der Materialoberfläche vorhanden sein muss, damit das Material aktiv sein kann (Abbildung 83).

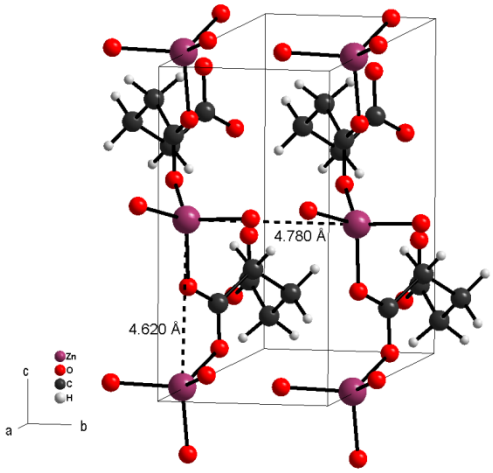


**Abbildung 83.** Nahansicht des aktivitätsbestimmenden Strukturmotivs von Zinkglutarat mit Zn-Zn Pärchen in einem definierten Abstand zueinander.

Für homogene Katalysatoren wurde weithin ein bimetallischer Copolymerisationsmechanismus diskutiert. Es kann davon ausgegangen werden, dass auch heterogene Zinkdicarboxylate in einer ähnlichen bimetallischen Art und Weise Copolymerisieren, wobei Zn-Zn Pärchen in einem definierten Abstand von 4.6 und 4.8 Å zueinander vorhanden sein müssen (Schema 22).

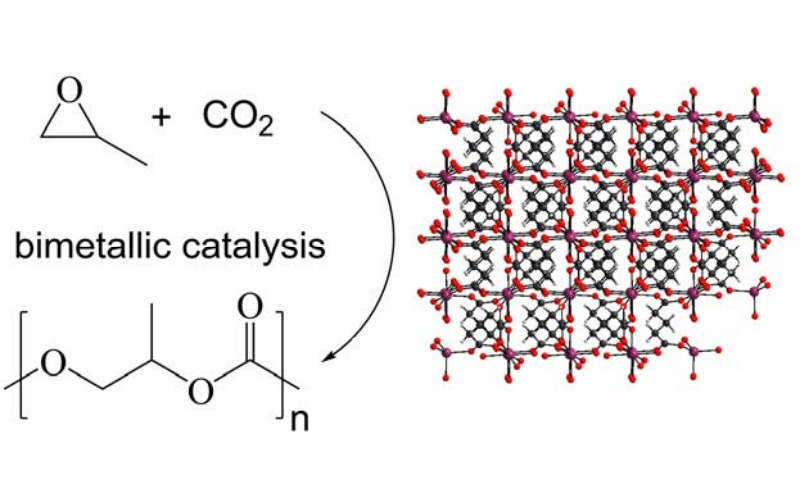


**Schema 22.** Sicht entlang der *a*-Achse von Zinkglutarat und vorgeschlagener bimetallischer Copolymerisations-Mechanismus auf der Oberfläche.

Theoretische Berechnungen mit Zinkdicarboxylat-ähnlichen Modellsystemen weisen ebenso auf einen optimalen Zn-Zn Abstand im Bereich von 4.3 - 5.0 Å hin, in welchem ein ausbalanciertes Optimum zwischen Aktivierungsenergie und Selektivität in Richtung

Copolymer vorhanden ist. Neue Strategien sollten sich daher auf die Einführung von zwei metallischen Spezies in ein molekulares Framework konzentrieren. Dies bedeutet, dass die Forschung sich auf homogene Katalysatorsysteme mit zwei Metallzentren oder den neuartigen binär verknüpften Liganden-Systemen fokussieren sollte.

Die homogenen, flexibel verknüpften Salphen Komplexe knüpfen direkt an diese Überlegungen an. Durch kinetische Messungen wurde gezeigt, dass die Salphen-Komplexe $CO_2$ und Epoxide in einer bimetallischen Art Copolymerisieren (Schema 23).

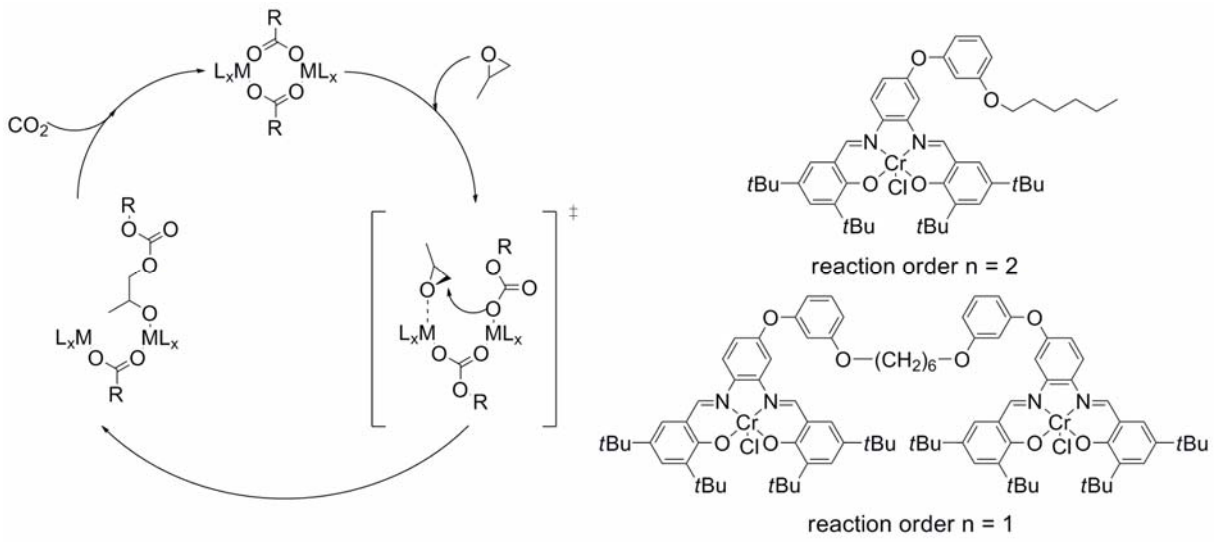


**Schema 23.** Bimetallischer Mechanismus für die Copolymerisation von $CO_2$ und Propylenoxid mit mononuklearem und dinuklearem Salphen-Komplex.

Durch Verknüpfen zweier interagierender Metallspezies konnten effizientere Katalysatoren hergestellt werden, welche selbst bei hohen Verdünnungen, bei denen mononukleare Katalysatoren in der Regel versagen, aktiv sind. Jedoch müssen der bimetallische und der binäre Reaktionspathway voneinander unterschieden werden, je nachdem welches Katalysator/Cokatalysator System benutzt wird. Das Potential von Salphen-Komplexen ist dabei jedoch auf TOFs unter 100 $h^{-1}$ limitiert. Kürzlich haben Lee *et al.* Und Williams *et al.* starre dinukleare Komplexe entwickelt, welche Aktivitäten bis zu 3000 $h^{-1}$ in der Copolymerisation von Cyclohexenoxid und $CO_2$ aufweisen (Abbildung 84, **34a**). Diese starren dinuklearen Systeme werden zurzeit weiter untersucht und können voraussichtlich hinsichtlich der Copolymerisation von Propylenoxid und $CO_2$ optimiert werden.

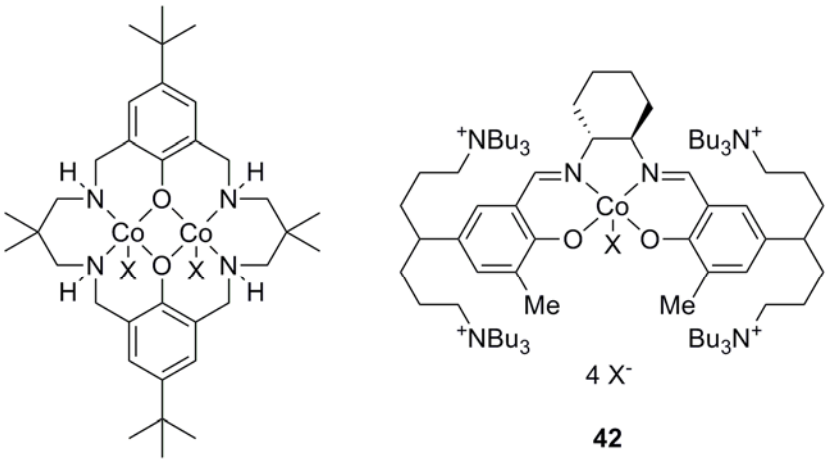


**Abbildung 84.** Effiziente starre dinukleare Komplexe der Form **34a** und binar verknüpfte Salen Komplexe der Form **42**.

In Anwesenheit von Cokatalysatoren wie z.B. Oniumsalzen (z.B. PPNCl, TBAB), schaltet der bimetallische Mechanismus der Salphen in eine binären Modus um, welcher selbst dem mononuklearen Katalysator eine Aktivität bei hohen Verdünnungen erlaubt. Dieses Prinzip wurde von Lee *et al.* Übernommen, welche Komplexe mit verknüpften Cokatalysatoren synthetisiert haben (Abbildung 84, **42**). Diese Systeme gehören zu den bislang effektivsten Katalysatoren für die Copolymerisation von $CO_2$ und Epoxiden mit TOFs von bis zu 26.000 $h^{-1}$. Jedoch sind die Kobalt-Zentren, welche typischerweise in diesen Katalysatoren verwendet werden, toxisch und müssen daher aufwendig von dem entstandenen Polymer abgetrennt werden. Diese notwendige Abtrennung, zusätzlich zu einer aufwendigen und teuren Katalysatorsynthese, engen das Potential von Komplexen der Form **42** stark ein.

Aus dem Grund wurde in dieser Arbeit eine Reihe von quadridentaten Eisen(II)- und Eisen(III)-Komplexen entwickelt und untersucht (Abbildung 85). Es konnte gezeigt werden, dass die üblicherweise in der Kupplungsreaktion von $CO_2$ und Epoxiden verwendeten toxischen Metallzentren wie Kobalt und Chrom durch das „grüne“ Metal Eisen ausgetauscht werden können, ohne Aktivitätsverluste in Kauf nehmen zu müssen. Wenn ionische Cokatalysatoren wie PPNCl oder TBAB hinzugefügt werden, kann die Effizienz bis zu ungefähr 400 $h^{-1}$ erhöht werden.

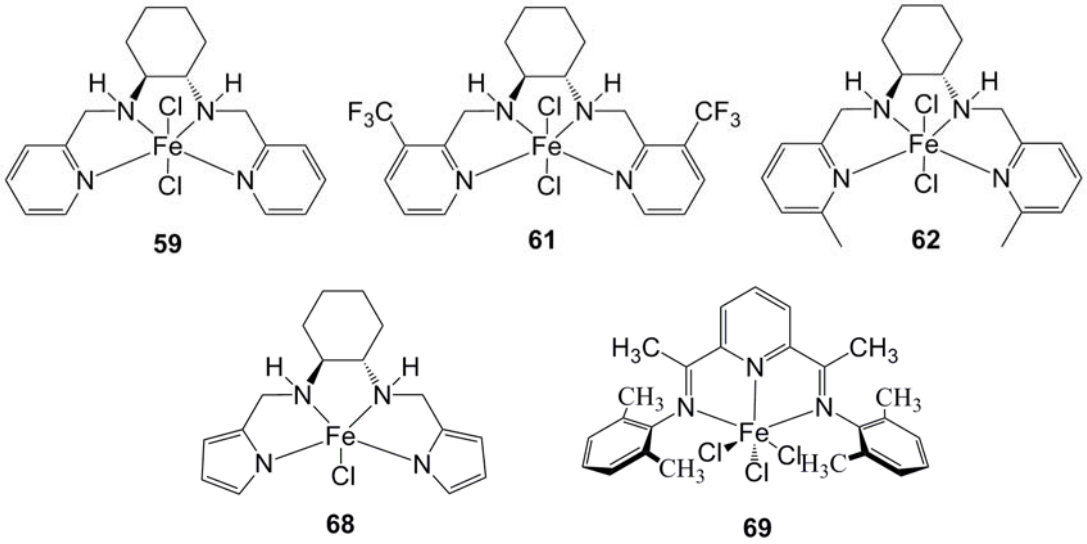


**Abbildung 85.** Ausgewählte Eisen-enthaltende Komplexe, welche in der Kupplungsreaktion von $CO_2$ und Epoxiden aktiv sind.

In dieser Arbeit wurde gezeigt, dass die heterogenen Zinkdicarboxylate und Metal-Salphen Komplexe $CO_2$ und Epoxide in einer bimetallischen Art und Weise Copolymerisieren. Jedoch ist die Effizienz dieser Systeme stark limitiert. Daher sollten zukünftige Forschungsaktivitäten sich auf neue Konzepte fokussieren. Die Optimierung von starren, Zink-enthaltenden dinuklearen Komplexen hinsichtlich der Copolymerisation von $CO_2$ und Propylenoxid sieht vielversprechend aus und könnte bald zu den erwünschten Katalysatoraktivitäten führen. Eine weitere Strategie könnte die Weiterentwicklung der binär verknüpften Salen-Komplexe der Form **42** sein, wobei (i) eine alternative und einfache Syntheseroute zu dem Komplex wünschenswert ist und (ii) das toxische Metallzentrum ausgetauscht werden sollte, um die Notwendigkeit der Katalysatorabtrennung vom polymeren Produkt zu umgehen. Die in dieser Arbeit vorgestellten Eisenkomplexe zeigen, dass das üblicherweise verwendete Kobalt-Zentrum durch das ökologisch unbedenkliche Eisen-Metall ausgetauscht werden kann und dass $CO_2$ und Epoxide mit Eisen-Komplexen zu Polycarbonaten copolymerisiert werden können. In naher Zukunft könnte dies zu einer ökologischen und ökonomischen Alternative für die großindustrielle Herstellung von Polycarbonaten aus $CO_2$ führen.

# 7. Experimental Part

## 7.1. Heterogeneous Zinc Dicarboxylates

### 7.1.1. Standard Synthesis

Zinc dicarboxylates were synthesized with slight variations as reported elsewhere.[87-90] In a heated 250 ml Schlenk-vessel with reflux condenser and dean-stark trap, 2,76 g (34.0 mmol) zinkoxide and 4.49 g (34.0 mmol) glutaric acid were suspended in 200 ml toluene. The mixture was heated several days at 80 °C in an inert argon atmosphere. After cooling down the reaction mixture, the white precipitate was filtered, washed with acetone and the product dried in a vacuum oven at 130 °C, delivering 6.72 g (34 mmol, 100 %) of the product as powder.

**Table 15.** Reagents and reaction conditions for synthesis of different zinc glutarates.

| Catalyst | Reagents | m (g) | n (mmol) | T (°C) | t (h) |
|---|---|---|---|---|---|
| standard ZnGA | ZnO | 3.00 | 34 | 80 | 4 days |
| | glutaric acid | 4.50 | 34 | | |
| ZnGA | ZnO | 2.44 | 30 | 80 | 3 days |
| | glutaric acid | 3.33 | 27 | | |
| | valeric acid | 0.33 (ml) | 3 | | |
| ZnGA | ZnO | 2.44 | 30 | 80 | 3 days |
| | glutaric acid | 3.17 | 24 | | |
| | valeric acid | 0.66 (ml) | 6 | | |
| ZnGA (50 % VA) | ZnO | 2.44 | 30 | 80 | 3 days |
| | glutaric acid | 1.98 | 15 | | |
| | valeric acid | 1.65 (ml) | 15 | | |
| ZnGA (20 % SiO2) | ZnO | 3.00 | 34 | 80 | 4 days |
| | glutaric acid | 4.50 | 34 | | |
| | $SiO_2$ | 0.51 | 8.5 | | |
| ZnGA (50 % SiO2) | ZnO | 2.44 | 30 | 80 | 4 days |
| | glutaric acid | 3.90 | 30 | | |
| | $SiO_2$ | 1.80 | 30 | | |

All other modifications of zinc glutarate (with contents of valeric acid or silica gel) were synthesized the same way, with only the reagents being replaced (c.f. Table 15). The presence of zinc glutarate was verified *via* PXRD and IR and in cases where relevant, SEM and TEM pictures as well as BET-measurements were collected. Standard zinc glutarate was used in this work as reference system for heterogeneous zinc dicarboxylates.

### 7.1.2. Functionalization Synthesis

A solution of diethyl zinc (1.5 M) in toluene was cooled down to 0 °C. A solution of glutaric acid in 50 ml THF was slowly added. During addition, formation of ethane was observed and a white solid precipitated. The reaction mixture was stirred for 18 h at ambient temperature and subsequently cooled down to -10 °C.

**Table 16.** Reagents and reaction conditions for synthesis of different zinc glutarates.

| Catalyst | Reagents | m (g) | n (mmol) | v (ml) |
|---|---|---|---|---|
| ZnGA (17 % $ZnSO_2Et$) | $ZnEt_2$<br>glutaric acid<br>$SO_2$ | 12 (ml)<br>1.98<br>0.2 bar | 18<br>15<br>6 | 60 |
| ZnGA (17 % ZnOiPr) | $ZnEt_2$<br>glutaric acid<br>iPrOH | 12 (ml)<br>1.98 | 18<br>15<br>6 | 60 |
| ZnGA (17 % $ZnOSiEt_2$) | $ZnEt_2$<br>glutaric acid<br>triethylsilanol | 12 (ml)<br>1.98<br>0.92 (ml) | 18<br>15<br>6 | 60 |
| ZnGA (17 % $ZnOSiPh_2$) | $ZnEt_2$<br>glutaric acid<br>triphenylsilanol | 12 (ml)<br>1.98<br>1.66 | 18<br>15<br>6 | 60 |
| ZnGA (17 % $ZnSO_2Me$) | $ZnMe_2$<br>glutaric acid<br>$SO_2$ | 15 (ml)<br>1.98<br>0.2 bar | 18<br>15<br>6 | 100 |
| ZnGA (17 % $ZnSO_2Ph$) | $ZnPh_2$<br>glutaric acid<br>$SO_2$ | 0.5<br>0.25<br>0.2 bar | 4,55 mmol<br>3,79 mmol<br>1,52 mmol | 100 |

An excess of $SO_2$ was added with vigorous stirring and the reaction mixture was allowed to warm up to room temperature. After stirring the heterogeneous mixture for 1 h at 50 °C all volatiles were removed and the remaining white solid was dried for 12 h at 80 °C under vacuum.

Table 16 gives the amount of reactants applied in the synthesis of different zinc dicarboxylates.

The existence of zinc glutarate was verified *via* PXRD and the material constitution characterized with elemental analysis.

| | | |
|---|---|---|
| ZnGA (17 % $ZnSO_2Et$) | EA (theo): | C 28.20 H 3.25 S 5.2 Zn 32.4 O 31.22 |
| | EA (exp): | C 28.22 H 3.1 S 3.46 Zn 31.22 |
| ZnGA (17 % ZnOiPr) | EA (theo): | C 32.06 H 3.79 Zn 33.82 O 30.33 |
| | EA (exp): | C 30.13 H 3.93 Zn 30.7 |
| ZnGA (17 % $ZnOSiEt_2$) | EA (theo): | C 34.03 H 4.60 Zn 30.08 O 26.98 |
| | EA (exp): | C 32.48 H 4.34 Zn 29.5 |
| ZnGA (17 % $ZnOSiPh_2$) | EA (theo): | C 43.40 H 3.95 Zn 25.81 O 23.15 |
| | EA (exp): | C 46.52 H 4.51 Zn 22.9 |
| ZnGA (17 % $ZnSO_2Me$) | EA (theo): | C 26.99 H 3.00 S 5.33 Zn 32.69 O 31,99 |
| | EA (exp): | C 31.01 H 3.24 S 0.8 Zn 30.3 |
| ZnGA (17 % $ZnSO_2Ph$) | EA (theo): | C 33.53 H 3.02 S 4.84 Zn 29.62 O 28.99 |
| | EA (exp): | C 33.18 H 3.33 S 3.72 Zn 28.8 |

### 7.1.3. Solvothermal Synthesis

2.97 g (10.0 mmol) zinc-nitrate-hexahydrate were dissolved together with 10 mmol of the correspondent dicarboxylic acid in 20 ml water, introduced into a glass-autoclave and heated to 180 °C in a heating block. After several hours at this temperature, the glass vessel was interstratified with streaks that eventually form the crystalline particles after one to thirty

days, depending on the dicarboxylic acid used. The reaction mixture was cooled to room temperature and the white crystalline precipitate was filtered, washed with water and acetone and dried in a vacuum oven at 130 °C. Even though this procedure generally suffers from low yields, highly crystalline particles can be gathered in all cases. Several of these crystals were collected for structure determination.

ZnSA: weighed succinic acid: 1,2 g; reaction time: 4 weeks; yield: 33 %.

ZnGA: weighed glutaric acid: 1,3 g; reaction time: 2 weeks; yield: 15 %.

ZnAA: weighed adipic acid: 1,5 g; reaction time: 7 days; yield: 25 %.

ZnPA: weighed pimelic acid: 1,6 g; reaction time: 3 days; yield: 27 %.

### 7.1.4. Ball-milling and Postactivation

The crystalline particles from the hydrothermal synthesis route were introduced into a planetary ball-mill type PM 100 from Retsch GmbH in an inert argon atmosphere. In order to minimize abrasion during the grinding-procedure, a 50 ml $ZrO_2$-beaker and $ZrO_2$-balls (Ø = 2 mm) were used. The ball-milling procedure was conducted for 4 hours at 300 rpm. The beaker was rotated into one direction for 10 minutes and after a five-minute pause rotated into the opposite direction for 10 minutes. This procedure was repeated until the added ball-milling events reached 4 hours.

Additionally, ZnGA was ball-milled for 10 min, 30 min, 1 h, 2h and 4 h in the same manner as previously described.

One part of the powder was taken as is for copolymerization, the rest was activated in a saturated water atmosphere over-night and dried thoroughly in a vacuum oven at 130 °C.

### 7.1.5. Copolymerization with Heterogeneous Zinc Dicarboxylates

All polymerization experiments were performed in 100 ml steel autoclaves equipped with magnetic stirring and oil bath heating. The autoclaves were heated to 130 °C in an oven dried under vacuum prior to use. The autoclave was placed under 40 bar $CO_2$ pressure and

heated to 80 °C. $CO_2$ of purity grade 4.5 was purchased from Westfalen AG and was applied in all experiments. The epoxide was freshly dried over $CaH_2$ and distilled prior to use.

0.025 – 0.050 mmol of catalyst was transferred into an autoclave followed by addition of 300 equivalents of PO. The reactor was closed, pressurized to 40 bars with $CO_2$ and heated to 80°C for 20 hours. After cooling down the reaction vessel to about 0 °C, $CO_2$ was slowly released. The viscous reaction mixture was diluted with $CH_2Cl_2$ and transferred to acidified (HCl) methanol. Immediately, polycarbonate precipitated. The mixture was then stirred for several hours and isolated polycarbonate was dried under vacuum at 60 °C. $^1$H NMR measurement was done from the crude reaction mixture to determine the ratio of cyclic propylene carbonate and poly(propylene carbonate) products. All isolated polycarbonates were analyzed by $^1$H NMR, where protons adjacent to carbonate linkages show a signal at 4.6 ppm and the content of polyether linkages was verified by the signals at 3.5 ppm.

### 7.1.6. Copolymerization with Different Water Contents

The copolymerization with heterogeneous zinc glutarate (from standard procedure) was conducted such as described before for the general procedure with the difference that the corresponding amount of water was added to the pressure vessel prior to copolymerization. The results are summarized in Table 17, a graphical representation of the results can be found in the results and discussion section.

**Table 17.** Propylene oxide/$CO_2$ copolymerization results with standard zinc glutarate and increasing water content[a]

| $H_2O$ | TON[b] | TOF[c] | PPC[d] (%) | $M_w$[e] | $M_n$[e] | PDI[e] |
|---|---|---|---|---|---|---|
| 0 % | 5240 | 262 | 100 | 625 | 178 | 3,51 |
| 1 % | 5876 | 294 | 89 | 420 | 71 | 5,94 |
| 5 % | 8039 | 402 | 87 | 258 | 77 | 3,35 |
| 10 % | 6541 | 327 | 85 | 190 | 46 | 4,17 |
| 20 % | 4500 | 225 | 88 | 260 | 20 | 13,18 |
| 50 % | 286 | 14 | 61 | / | / | / |

[a] Polymerization conditions: 0.5 mmol cat, 150 mmol PO, 80°C, 20h, 40 bar $CO_2$ (initial pressure), 500 rpm. [b] Turnover number in g polymer per mol of zinc. [c] Turnover frequency in

g polymer per mol of zinc per hour. [d] Estimated by $^{1}H$ NMR spectroscopy. Difference corresponds to cyclic carbonate. [e] Determined by GPC, calibrated with polystyrene standard in THF, $M_w$ and $M_n$ given in kg/mol.

### 7.1.7. Theoretical Calculations

Quantum chemical studies were performed at the BP86[208-210] /SV(P)[211] level of theory, employing the solvation model COSMO[212]. (with a dielectric constant of infinity). For the sake of simplicity and the general character of conclusion, as a model for the polymer, a methyl group was used. As an epoxide for copolymerizaion, ethylene oxide was chosen, and a dimethyl β-ketiminato ligand was used to simulate this class of ligands. For the scan of activation barriers with respect to internuclear distances, the reaction coordinate (OCO) was kept fix at the values computed for an intermetallic distance of 3.5Å. Additionally, it turned out to be necessary in the case of the alkoxide intermediate for the model catalyst $[Cu_2]^+$ to keep the C-H bond distances fix (at around 1.10Å) in order to avoid a C-H agostic stabilization for longer metal-metal distances that would markedly bias activation barriers.

The calculations were conducted by Peter Deglmann, BASF SE, GKT - B001 67056 Ludwigshafen, Germany

## 7.2. Homogeneous Dinuclear Flexible Linked Salphens

### 7.2.1. Methods and Materials, Synthesis of Complexes

All manipulations were carried out using a double manifold Schlenk vacuum line under an argon atmosphere or an argon-filled glovebox unless otherwise stated. Propylene oxide was freshly distilled from $CaH_2$ before use. $CO_2$ of purity grade 4.5 was purchased from Westfalen AG and was applied in all experiments without additional purification. Solvents were purified by an MBraun Manual Solvent Purification System packed with Alcoa F200 activated alumina desiccant. The complexes **35a** and **35b** were synthesized according to a previously reported procedure.[166]

### 7.2.2. Kinetic Studies with Homogeneous Salphen Complexes

Copolymerization experiments with *in-situ* monitoring were performed using a React-IR / MultiMax four-autoclave system (Mettler-Toledo). 50 ml Steel autoclaves equipped with a diamond window, a mechanic stirring and a heating device were filled twice with dry toluene and heated to 120 °C for one hour prior to use. The autoclaves were filled with the corresponding amount of catalyst and PO, sealed, placed under 40 bar $CO_2$ pressure and heated to 80 °C. The course of copolymerization at various catalyst concentrations was followed *in-situ* by monitoring the growth of the specific carbonyl-band of polypropylene carbonate (PPC) at 1753 $cm^{-1}$.

### 7.2.3. Standard Copolymerization Procedure with Salphen Complexes

All standard copolymerization experiments were performed in 100 ml steel autoclaves equipped with glass inlay, magnetic stirring and oil bath heating. The autoclaves were heated to 130 °C and dried in an oven under vacuum prior to use.

The catalyst and cocatalyst in a desired ratio were transferred into an autoclave, followed by addition of the calculated amounts of PO. The reactor was closed, pre-pressurized with $CO_2$ and heated to 60 °C, resp. 80 °C. After reaching the temperature, the pressure in the autoclave was adjusted to the desired value and heating was continued for 2 or 24 hours. After cooling down the reaction vessel to 0 °C, $CO_2$ was slowly released. $^1H$ NMR measurement was done from the crude reaction mixture to determine the ratio of cPC and

polymeric products. Protons adjacent to carbonate linkages in poly(propylene carbonate) show a signal at 4.6 ppm and the content of polyether linkages was verified by the signals at 3.5 ppm.

The viscous reaction mixture was diluted with $CH_2Cl_2$ and transferred to acidified (HCl) methanol. Immediately, polycarbonate precipitated. The mixture was then stirred for several hours and isolated polycarbonate was dried under vacuum at 60 °C. All isolated polycarbonates were analyzed by GPC against polystyrene standards in THF.

## 7.3. Synthesis of Iron-Based Systems

### 7.3.1. General

All reactions of air- and/or moisture-sensitive compounds and product manipulations were performed under dry argon using standard Schlenk techniques or in an inert atmosphere in a glovebox. All chemicals were purchased from Aldrich, Acros or ABCR. Solvents were obtained from a MBraun MB-SPS solvent purification system. Solution NMR spectra were collected at room temperature using a Bruker ARX300 spectrometer. $^{1}H$ and $^{13}C$ NMR spectra are referenced to the residual solvent peak of $SiMe_4$. ESI-MS mass spectra were recorded with a Finnigan MAT 8200 spectrometer at 70 eV or an LTQ FT Ultra spectrometer. Infrared spectra were recorded with a Bruker IFS55 FT-IR spectrometer at room temperature.

### 7.3.2. Iron(II)-Tetraamine Complexes

General preparation instructions for synthesis of the ligands can be derived from the general procedure which is given by the preparation of the basic ligand structures **L1** and **L2**. Preparation instructions for synthesis of the complexes can be derived from the general procedure which is given by the preparation of the basic structure 3. NMR-spectra of the complexes were not suitable for analysis due to the paramagnetic property of the iron(II) resp. iron(III) species.

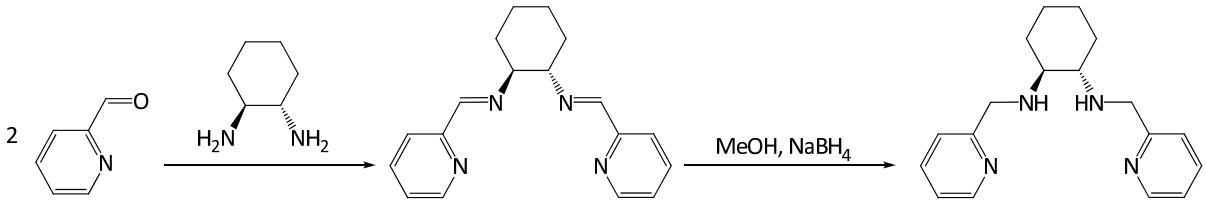


**L1** **L2**

***(1S,2S)*-*N,N'*-bis(pyridin-2-methylene)cyclohexane-1,2-diimine (L1).** To a solution of 1.91 mL pyridine-2-carboxaldehyde (20.0 mmol, 2.0 equiv.) in 40 mL of ethanol, 1.09 g (*S,S*)-cyclohexanediamine (9.5 mmol, 1.0 equiv.) were added. The orange reaction mixture was stirred for 20 h at room temperature. Volatiles were removed in vacuo and the product recrystallized from $CH_2Cl_2/Et_2O$ to yield 1.8 g of a yellow-orange powder (6.16 mmol, 65 %). **FT-IR ($cm^{-1}$):** 2948 s, 2861 s, 2831 s, 1643 s, 1586 s, 1567 s, 1467 s, 1444 m, 1365 s, 1338 s, 1307 s, 1284 s, 1137 s, 1078 s, 1039 m, 991 s, 936 s, 867 s, 840 s, 774 s, 744 s, 666 m, 618 s. **$^{1}H$ NMR** (300 MHz, $CDCl_3$) δ 8.58 – 8.47 (m, 2H), 8.29 (s, 2H), 7.86 (d, *J* = 7.8 Hz, 2H), 7.61 (td,

*J* = 7.8, 1.4 Hz, 2H), 7.19 (ddd, *J* = 7.3, 4.9, 1.4 Hz, 2H), 3.58 – 3.46 (m, 2H), 1.84 (t, *J* = 7.3 Hz, 6H), 1.65 – 1.39 (m, 2H). **$^{13}$C NMR** (75 MHz, $CDCl_3$) δ 161.10, 154.25, 148.90, 136.10, 124.13, 121.00, 73.21, 32.37, 24.00. **ESI-MS** (m/z) calcd. for $C_{18}H_{20}N_4$: 292.17; found 293.1 $(M)^+$, 315.1 $(M + Na)^+$.

**(*1S,2S*)-*N,N'*-bis(pyridin-2-methyl)cyclohexane-1,2-diamine (L2).** 1.20 g of **L1** (4.1 mmol, 1.0 equiv.) were added to a solution of 1.54 g sodium borhydride $NaBH_4$ (41.0 mmol, 10 equiv.) in 60 mL methanol at 0°C. The solution was then stirred for 2 d at room temperature. After adding 5 ml of $H_2O$, the reaction mixture was extracted with 3 x 75 mL of $CH_2Cl_2$ and washed with 3 x 50 mL of $H_2O$. The extract was dried over $Na_2SO_4$ and volatiles were removed in vacuo to yield 0.97 g of a brownish powder (3.3 mmol, 80 %). **FT-IR (cm$^{-1}$):** 2926 s, 2855 s, 1591 s, 1569 s, 1474 s, 1433 m, 1376 m, 1352 m, 1299 m, 1228 m, 1201 m, 1145 m, 1123 m, 1046 s, 993 s, 908 m, 863 s, 832 m, 756 s, 620 s. **$^1$H NMR** (300 MHz, $CDCl_3$) δ 8.48 (dd, *J* = 16.2, 4.4 Hz, 2H), 7.61 (td, *J* = 7.8, 1.7 Hz, 2H), 7.38 (d, *J* = 7.8 Hz, 2H), 7.12 (dd, *J* = 7.0, 5.4 Hz, 2H), 4.02 (d, *J* = 14.2 Hz, 2H), 3.83 (d, *J* = 14.2 Hz, 2H), 2.41 (s, 2H), 2.35 – 2.26 (m, 2H), 2.13 (d, *J* = 13.5 Hz, 2H), 1.77 – 1.60 (m, 2H), 1.22 (dd, *J* = 13.5, 7.0 Hz, 2H), 1.13 – 0.97 (m, 2H). **$^{13}$C NMR** (75 MHz, $CDCl_3$) δ 160.98, 149.35, 136.69, 122.60, 122.04, 61.64, 52.80, 31.86, 25.28. **ESI-MS** (m/z) calcd. for $C_{18}H_{24}N_4$: 296.20; found 297.3 $(M)^+$, 319.2 $(M + Na)^+$.

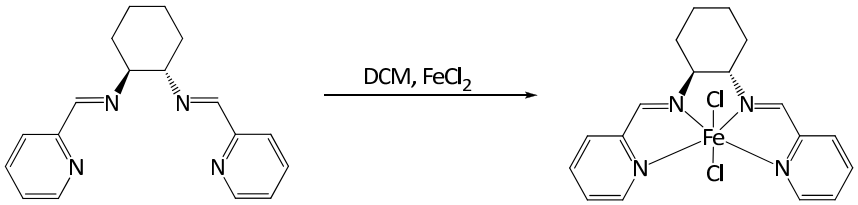


**L2** **58**

**$FeCl_2(C_{18}H_{20}N_4)$ (58).** To a solution of 0.5 g (1.69 mmol, 1.1 equiv) **L1** in 20 ml $CH_2Cl_2$, 0.2 g (1.0 equiv) of $FeCl_2$ was added. After stirring the suspension for 24 h, the green-reddish solution was filtered off in an inert Argon-atmosphere and the solvent removed in vacuo yielding 0.2 g of the desired product as dark-brown powder (0.48 mmol, 28 %). **FT-IR (cm$^{-1}$):** 2928 w, 2856 w, 1647 s, 1596 s, 1444 s, 1302 s, 1223 s, 1155 s, 1105 s, 1050 s, 1017 s, 821 w, 769 s, 731 s, 697 s, 640 s. **ESI-MS** (m/z) calcd. for $C_{18}H_{20}Cl_2FeN_4$: 418.04; found 418.0 $(M)^+$, 383.0 $(M – Cl)^+$.

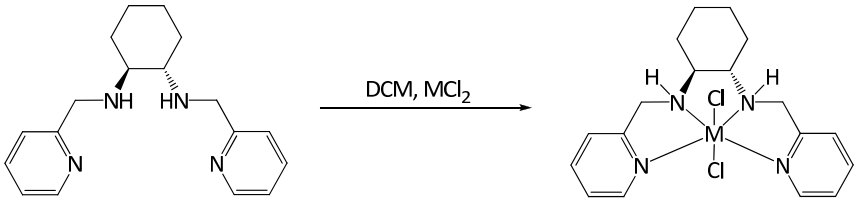


**L2** **59** (M = Fe)

**60** (M = Co)

**$FeCl_2(C_{18}H_{24}N_4)$ (59).** To a solution of 0.2 g (0.68 mmol, 1.1 equiv.) **L2** in 20 ml dry $CH_2Cl_2$, 0.076 g (1.0 equiv.) of $FeCl_2$ was added. After stirring the suspension for 24 h, the dark brown solution was filtered off in an inert Argon-atmosphere and washed with diethylether and pentane. All volatiles were removed in vacuo yielding 0.2 g of **59** as dark-brown powder (0.48 mmol, 70 %). **FT-IR ($cm^{-1}$):** 2930 w, 2859 w, 1605 s, 1570 s, 1480 s, 1441 w, 1280 m, 1154 s, 1101 s, 1050 s, 1017 w, 972 s, 950 s, 882 w, 763 m, 757 s, 642 s. **ESI-MS** (m/z) calcd. for $C_{18}H_{24}Cl_2FeN_4$: 422.07 found 387.0 $(M - Cl)^+$, 350.0 $(M - 2HCl)^+$.

**$CoCl_2(C_{18}H_{24}N_4)$ (60).** To a solution of 0.25 g (0.84 mmol, 1.0 equiv.) **L2** in 20 ml dry $CH_2Cl_2$, 0.54 g (5.0 equiv.) of $CoCl_2$ was added. After stirring the suspension for 24 h, the ultramarin-blue solution was filtered off in an inert Argon-atmosphere and the solvent removed in vacuo. All volatiles were removed in vacuo yielding 0.164 g of the product as dark-blue powder (0.386 mmol, 46 %). **FT-IR** ($cm^{-1}$): 2931 w, 2857 w, 1606 m, 1570 s, 1477 s, 1443 m, 1281 m,1155 s, 1102 s, 1050 s, 1032 s, 975 s, 948 s, 876 m, 764 w, 727 s. **ESI-MS** (m/z) calcd. for $C_{18}H_{24}Cl_2CoN_4$: 425.07, found 390.1 $(M - Cl)^+$, 354.1 $(M - 2HCl)^+$.

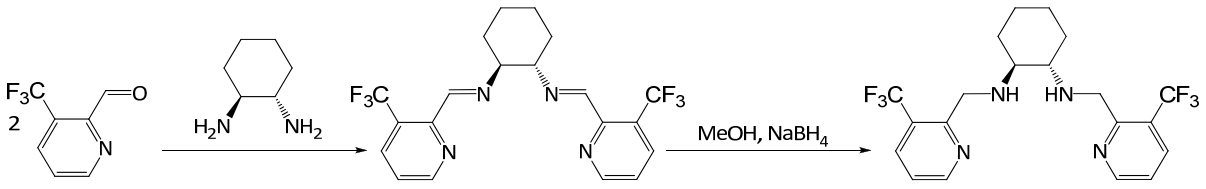


**L3** **L4**

**(1S,2S)-N,N'-bis(3-(trifluoromethyl)pyridin-2-yl)methylen)cyclohexane-1,2-diimine (L3).** 0.70 ml 3-(trifluoromethyl)pyridine-2-carboxaldehyde (5.5 mmol, 2.0 equiv.) were diluted in 30 ml of ethanol and 0.29 g (2.6 mmol, 2.0 equiv.) of 1,2-(*S,S*)-diaminocyclohexane were added. The orange solution was stirred at room temperature and the conversion controlled *via* NMR-samples until completion after 3 days. The solvent was removed in vacuo delivering

an orange oil. The product was recrystallized in $CH_2Cl_2$/$Et_2O$ to yield 0.99 g of a yellow-orange powder (2.3 mmol, 93 %). **FT-IR ($cm^{-1}$):** 2930 m, 2845 m, 1657 s, 1573 m, 1442 s, 1369 s, 1312 s, 1230 m, 1142 s, 1114 s, 1074 m, 1028 s, 988 s, 932 m, 886 m, 811 s, 769 m, 685 s, 623 s. **$^1$H NMR** (300 MHz, $CDCl_3$) δ 8.85 (d, J = 4.3 Hz, 2H), 8.56 (d, J = 1.4 Hz, 2H), 7.90 (dd, J = 8.0, 1.4 Hz, 2H), 7.35 (dd, J = 8.0, 4.3 Hz, 2H), 3.83 – 3.61 (m, 2H), 2.11 – 1.83 (m, 7H), 1.60 – 1.42 (m, 2H). **$^{13}$C NMR** (75 MHz, $CDCl_3$) δ 157.06, 152.81, 150.98, 134.02, 133.95, 123.51, 121.47, 73.73, 32.32, 24.14. **ESI-MS** (m/z) calcd. for $C_{20}H_{18}F_6N_4$: 428.14; found 429.1 $(M^+$, 451.1 $(M + Na)^+$.

**(*1S,2S*)-*N,N'*-bis(3-(trifluoromethyl)pyridin-2-yl)methylen)cyclohexane-1,2-diamine (L4).** 00.30 g of **L3** (0.7 mmol, 1.0 equiv.) were suspended in 20 ml MeOH (dry) and cooled down to 0°C. 0.26 g sodium borohydride (7.0 mmol, 10 equiv.) were added slowly and stirred at room temperature for 12 h. The lightly yellow solution was filtered, washed with water and $CH_2Cl_2$ and the solvent of the united organic phases removed in vacuo. The product was then completely dried in vacuo to yield 0.21 g of a brownish powder (0.49 mmol, 69 %). The compound was spectroscopically clean and used without further purification for complexation. **FT-IR ($cm^{-1}$):** 2826 m, 2855 m, 1666 m, 1575 m, 1440 s, 1363 s, 1315 s, 1260 m, 1114 s, 1075 s, 1029 s, 811 s, 788 m, 690 m, 662 m, 621 s. **$^1$H NMR** (300 MHz, $CDCl_3$) δ 8.71 (d, J = 4.9 Hz, 2H), 7.89 (d, J = 7.5 Hz, 2H), 7.26 (dd, J = 7.5, 4.9 Hz, 2H), 4.15 (d, J = 15.0 Hz, 2H), 4.02 (d, J = 15.0 Hz, 2H), 2.82 (s, 2H), 2.36 (d, J = 7.2 Hz, 2H), 2.09 (d, J = 12.5 Hz, 2H), 1.69 (m, 2H), 1.22 (dd, J = 12.5, 7.2 Hz, 2H), 1.10 (m, 2H). **$^{13}$C NMR** (75 MHz, CDCl3) δ 158.63, 151.81, 133.74, 121.15, 61.29, 49.04, 31.65, 30.95, 24.93. **ESI-MS** (m/z) calcd. for $C_{20}H_{22}F_6N_4$ : 432.18; found 433.1 $(M)^+$, 455.1 $(M + Na)^+$.

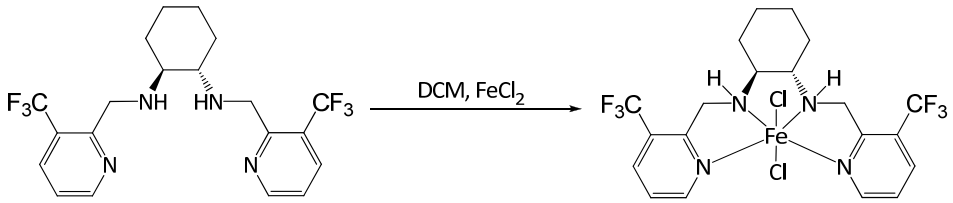


**L4** **61**

**$FeCl_2(C_{20}H_{20}F_6N_4)$ (61).** To a solution of 0.1 g (0.23 mmol, 1.1 equiv.) **L4** in 10 ml $CH_2Cl_2$, 0.028 g of $FeCl_2$ (1.0 equiv.) was added. After stirring the suspension for three days, the deep red solution was filtered off in an inert Argon-atmosphere and the solvent removed in vacuo

yielding 0.1 g of the desired product as dark-brown powder (0.18 mmol, 78 %). **FT-IR ($cm^{-1}$):** 2929 w, 2860 w, 1597 s, 1449 m, 1372 s, 1318 s, 1257 m, 1170 s, 1125 s, 1086 s, 1049 s, 948 s, 815 m, 729 s, 680 s, 657 s. **ESI-MS** (m/z) calcd. for $C_{20}H_{22}Cl_2F_6FeN_4$: 558.05, found 558.0 $(M)^+$, 523.1 $(M - Cl)^+$, 486.1 $(M - 2HCl)^+$.

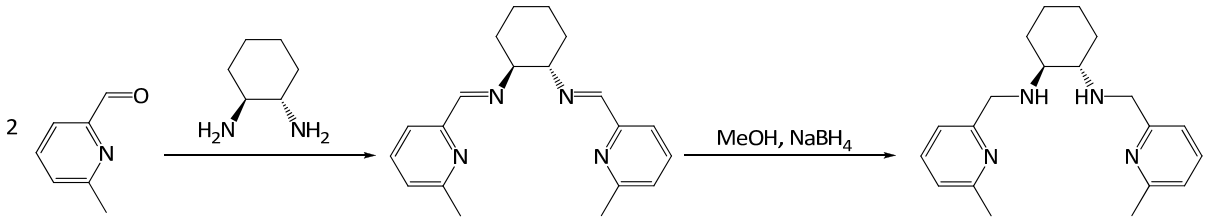


**L5** **L6**

**(*1S,2S*)-*N,N'*-bis(6-methylpyridin-2-yl)methylen)cyclohexane-1,2-diimine (L5).** 4.5 g of 6-Methylpyridine-2-carboxaldehyde (37.0 mmol, 2.0 equiv.) were diluted in 50 ml of ethanol and 2.12 g of *1,2*-(*S,S*)-diaminocyclohexane (18 mmol, 1.0 equiv.) were added. The orange solution was stirred at room temperature for 12 hours and the solvent removed in vacuo delivering an orange oil. The product was recrystallized in $CH_2Cl_2/Et_2O$ to yield 4.8 g of a yellow-orange powder (14.98 mmol, 83 %). **FT-IR ($cm^{-1}$):** 2926 m, 2861 s, 2832 s, 1650 s, 1591 m, 1460 m, 1357 m, 1138 s, 1084 m, 1038 s, 988 s, 934 m, 861 m, 794 s, 736 s, 657 m. **$^1$H NMR** (300 MHz, $CDCl_3$) δ 8.29 (s, 2H), 7.71 (d, *J* = 7.8 Hz, 2H), 7.52 (t, *J* = 7.8 Hz, 2H), 7.07 (d, *J* = 7.8 Hz, 2H), 3.59 – 3.37 (m, 2H), 2.51 (s, 6H), 1.93 – 1.75 (m, 6H), 1.51 (t, *J* = 11.2 Hz, 2H). **$^{13}$C NMR** (75 MHz, $CDCl_3$) δ 161.71, 157.77, 154.21, 137.17, 136.64, 127.71, 124.09, 118.28, 73.61, 32.71, 24.37, 24.29. **ESI-MS** (m/z) calcd. for $C_{20}H_{24}N_4$: 320.20; found 321.3 $(M)^+$, 343.2 $(M + Na)^+$.

**(*1S,2S*)-*N,N'*-bis(6-methylpyridin-2-yl)methylen)cyclohexane-1,2-diamine (L6).** 2.0 g of **L5** (6.24 mmol, 1.0 equiv.) were suspended in 80 ml MeOH (dry) and cooled down to 0 °C. 2.34 g sodium borohydride (62.4 mmol, 10 equiv.) were added slowly and stirred at room temperature for 12 h. The lightly yellow solution was filtered, washed with water and $CH_2Cl_2$ and the solvent of the united organic phases removed in vacuo. The product was then completely dried in vacuo to yield 1.35 g of a yellow powder (4.17 mmol, 67 %). The compound was spectroscopically clean and used without further purification for complexation. **FT-IR ($cm^{-1}$):** 2925 m, 2853 s, 1591 m, 1447 m, 1371 m, 1336 m, 1225 m, 1151 s, 1084 m, 1035 m, 994 m, 880 m, 779 s, 744 s, 630 m. **$^1$H NMR** (300 MHz, $CDCl_3$) δ 7.44 (t, *J*

= 7.6 Hz, 2H), 7.24 – 7.10 (m, 2H), 6.92 (d, *J* = 7.6 Hz, 2H), 3.94 (d, *J* = 14.2 Hz, 2H), 3.73 (d, *J* = 14.2 Hz, 2H), 2.46 (d, *J* = 10.8 Hz, 6H), 2.34 – 2.18 (m, 4H), 2.09 (d, *J* = 12.9 Hz, 2H), 1.65 (d, *J* = 7.5 Hz, 2H), 1.26 – 0.92 (m, 4H). **$^{13}$C NMR** (75 MHz, $CDCl_3$) δ 160.04, 157.59, 136.62, 121.24, 119.11, 61.40, 52.53, 31.65, 25.02, 24.47. **ESI-MS** (m/z) calcd. for $C_{20}H_{28}N_4$: 324.23; found 325.3 $(M)^+$, 347.2 $(M + Na)^+$.

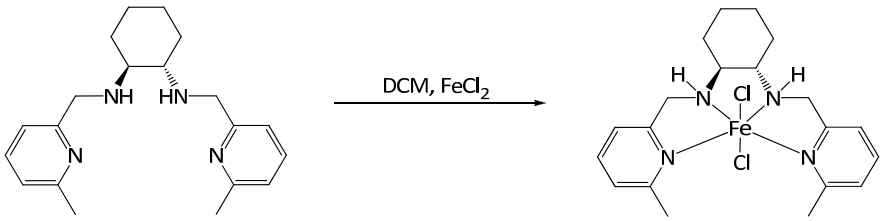


**L6** **62**

**$FeCl_2(C_{20}H_{28}N_4)$ (62).** To a solution of 0.15 g (0.46 mmol, 1.0 equiv.) **L6** in 10 ml $CH_2Cl_2$, 0.6 g of $FeCl_2$ (10.0 equiv) was added. After stirring the suspension for 24 h, the brown-red solution was filtered off in an inert Argon-atmosphere and the solvent removed in vacuo yielding 0.09 g of the desired product as red-brown powder (0.16 mmol, 35 %). **FT-IR ($cm^{-1}$):** 2929 w, 2857 w, 1604 m, 1576 s, 1460 m, 1360 m, 1220 m, 1164 s, 1094 m, 1035 s, 1006 m, 967 s, 835 w, 787 w, 744 s, 717 m, 671 m. **ESI-MS** (m/z) calcd. for $C_{20}H_{28}Cl_2FeN_4$: 450.10, found : 450.1 $(M)^+$, 415.1 $(M – Cl)^+$, 378.1 $(M – 2HCl)^+$.

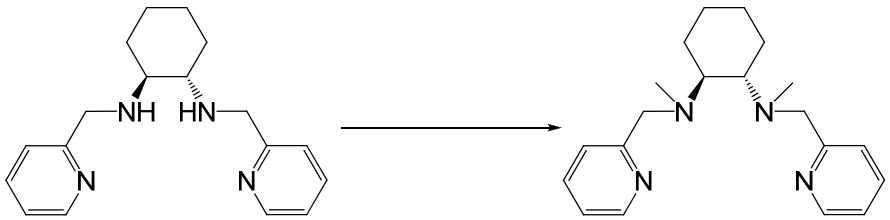


**L2** **L7**

**(*1S,2S*)-*N,N'*-dimethyl-bis(pyridin-2-methyl)cyclohexane-1,2-diamine (L7).** As described in literature.[197, 213] The diamine **L2** (0.4291 g, 1.45 mmol) was dissolved in 37% formaldehyde (2.7 mL) and the resulting solution stirred at RT for 10 min. Aqueous 90% formic acid (3.3 mL) was then added and the mixture stirred and thermally treated at 90 °C for 48 h. The mixture was cooled to 20 °C and the pH adjusted to 12 by addition of aqueous NaOH (3 M) with constant cooling. The aqueous layer was extracted with diethyl ether and the combined

organic layers were dried with anhydrous $Na_2SO_4$, filtered and evaporated to give an oil, which was purified by column chromatography ($Al_2O_3$, ethyl acetate/hexane/triethylamine 10:4:1) to afford the product. **FT-IR ($cm^{-1}$):** 2936 m, 2762 s, 2678 s, 1737 m, 1630 m, 1455 m, 1396 m, 1216 m, 1164 s, 1127 s, 1067 s, 957 s, 896 s, 1031 m, 808 s, 792 s. **$^1$H NMR** (300 MHz, $CDCl_3$) δ 8.55 (d, *J* = 4.8 Hz, 2H), 7.63 (m, 4H), 7.17 (m, 2H), 3.98 (d, *J* = 14.7 Hz, 2H), 3.86 (d, *J* = 14.7 Hz, 2H), 2.71 (m, 2H), 2.33 (s, 6H), 2.02 (m, 2H), 1.81 (m, 2H), 1.26 - 0.92 (m, 4H). **$^{13}$C NMR** (75 MHz, $CDCl_3$) δ 160.98, 149.35, 136.69, 122.60, 122.04, 61.64, 52.80, 31.86, 25.28. **ESI-MS** (m/z) calcd. for $C_{20}H_{28}N_4$: 324.23; found 325.3 $(M)^+$, 347.2 $(M + Na)^+$.

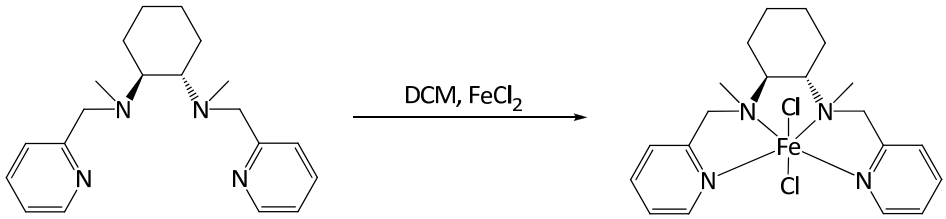


**L7** **63**

**$FeCl_2(C_{20}H_{28}N_4)$ (63).** To a solution of 0.2 g (0.62 mmol, 1.1 equiv.) **L7** in 10 ml $CH_2Cl_2$, 0.078 g of $FeCl_2$ (1.0 equiv) was added. After stirring the suspension for 24 h, the brown solution was filtered off in an inert Argon-atmosphere and the solvent removed in vacuo yielding 0.17 g of the desired product as red-brown powder (0.38 mmol, 61 %). **FT-IR ($cm^{-1}$):** 2933 w, 2857 w, 1602 s, 1569 s, 1476 s, 1440 m, 1368 m, 1303 m, 1257 m, 1228 m, 1151 m, 1085 m, 1051 s, 1016 m, 973 s, 933 ss, 969 s, 762 m, 730 s, 641 m. **ESI-MS** (m/z) calcd. for $C_{20}H_{28}Cl_2FeN_4$: 450.10, found 450.0 $(M)^+$, 415.1 $(M - Cl)^+$.

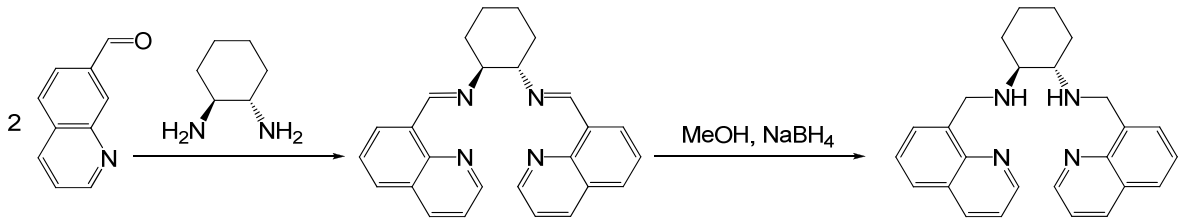


**L8** **L9**

**(*1S,2S*)-*N,N'*-bis(methylpyridin-8-methylen)cyclohexane-1,2-diimine (L8).** 3.14 g 8-quinoline-carboxaldehyde (20.0 mmol, 2.0 equiv.) were diluted in 120 ml of ethanol and 1.14 g of 1.2-(*S,S*)-diaminocyclohexane (10.0 mmol, 1.0 equiv.) were added. The orange solution

was stirred at room temperature for 12 hours and the solvent removed in vacuo delivering white powder. The product was recrystallized in $CH_2Cl_2/Et_2O$ to yield 3 g of a white powder (7.64 mmol, 81 %). **FT-IR ($cm^{-1}$):** 2920 m, 2855 s, 1633 s, 1572 s, 1496 s, 1441 s, 1395 s, 1365 s, 1331 s, 1303 s, 1254 s, 1141 s, 1091 m, 1027 m, 978 s, 936 m, 873 m, 826 s, 788 s, 767 m, 649 s, 628 s. **$^1$H NMR** (300 MHz, $CDCl_3$) δ 9.62 (s, 2H), 8.97 – 8.84 (m, 2H), 8.28 (dd, *J* = 11.9, 6.5 Hz, 2H), 8.06 (dd, *J* = 8.3, 1.6 Hz, 2H), 7.72 (dt, *J* = 9.0, 4.5 Hz, 2H), 7.49 – 7.31 (m, 4H), 3.73 (dd, *J* = 11.9, 6.5 Hz, 2H), 1.96 (dd, *J* = 27.2, 9.0 Hz, 6H), 1.56 (t, *J* = 9.5 Hz, 2H). **$^{13}$C NMR** (75 MHz, $CDCl_3$) δ 159.12, 149.75, 146.62, 136.05, 133.71, 129.70, 127.95, 127.79, 126.42, 121.02, 74.33, 33.11, 24.62. **ESI-MS** (m/z) calcd. for $C_{26}H_{24}N_4$: 392.50; found 393.0 $(M)^+$.

**(*1S,2S*)-*N,N'*-bis(methylpyridin-8-methylen)cyclohexane-1,2-diamine (L9).** 2.9 g of **L8** (7.5 mmol, 1.0 equiv.) were suspended in 100 ml MeOH (dry) and cooled down to 0°C. 2.9 g sodium borohydride (75.0 mmol, 10 equiv.) were added slowly and stirred at room temperature for 12 h. The lightly yellow solution was filtered, washed with water and $CH_2Cl_2$ and the solvent of the united organic phases removed in vacuo. The product was then completely dried in vacuo to yield 2.4 g of a white powder (6.0 mmol, 80 %). The compound was spectroscopically clean and used without further purification for complexation. **FT-IR ($cm^{-1}$):** 2928 m, 2856 s, 1594 m, 1498 s, 1446 m, 1369 m, 1334 m, 1262 m, 1166 s, 1130 m, 1071 s, 1027 s, 936 m, 873 m, 823 s, 788 s, 729 s, 696 s. **$^1$H NMR** (300 MHz, $CDCl_3$) δ 8.71 (d, *J* = 2.6 Hz, 2H), 8.09 (dd, *J* = 8.2, 1.5 Hz, 2H), 7.77 – 7.63 (m, 4H), 7.53 – 7.40 (m, 2H), 7.30 (dd, *J* = 8.2, 4.2 Hz, 2H), 4.52 (d, *J* = 13.8 Hz, 2H), 4.27 (d, *J* = 13.8 Hz, 2H), 2.49 (d, *J* = 7.8 Hz, 2H), 2.25 (d, *J* = 11.0 Hz, 2H), 1.73 (s, 2H), 1.24 (d, *J* = 5.2 Hz, 4H). **$^{13}$C NMR** (75 MHz, $CDCl_3$) δ 149.25, 146.75, 136.20, 128.45, 128.20, 126.64, 126.33, 120.79, 61.20, 47.24, 31.61, 25.17. **ESI-MS** (m/z) calcd. for $C_{26}H_{28}N_4$: 396.53; found 396.9 $(M)^+$.

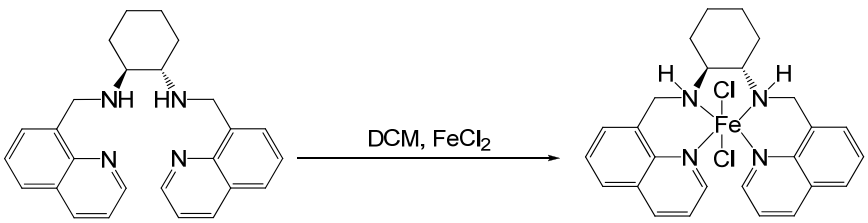


**L9** **64**

**$FeCl_2(C_{26}H_{28}N_4)$ (64).** To a solution of 0.20 g (0.50 mmol, 1.1 equiv.) **L9** in 20 ml $CH_2Cl_2$, 0.060 g (1.0 equiv) of $FeCl_2$ was added. After stirring the suspension for 24 h, the deep-violet

solution was filtered off in an inert Argon-atmosphere and the solvent removed in vacuo yielding 0.080 g of the desired product as dark-violet powder (0.15 mmol, 61 %). **FT-IR ($cm^{-1}$):** 2924 m, 2854 m, 1605 s, 1571 s, 1480 s, 1443 m, 1291 m, 1260 m, 1156 s, 1099 m, 1052 s, 1020 m, 822 m, 763 m, 729 s, 644 s. **ESI-MS** (m/z) calcd. for $C_{26}H_{28}Cl_2FeN_4$: 522.10, found 487.1 $(M - Cl)^+$, 450.1 $(M - 2HCl)^+$.

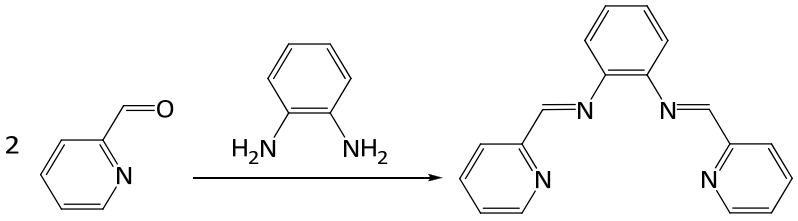

**L10**

**(*1S,2S*)-*N,N'*-bis(pyridine-2-methyl)phenylene-1,2-diimine (L10).** 2.50 ml (26 mmol) 2-pyridine-carboxaldehyde were diluted in 100 ml of ethanol and 1.41 g (13 mmol mmol) of diaminophenylene were added. The deep-orange solution was stirred at room temperature for 12 hours and the solvent removed in vacuo delivering an orange oil. The product was recrystallized in $CH_2Cl_2/Et_2O$ to yield 1.8 g of a yellow-orange powder (6.16 mmol, 65 %). **FT-IR ($cm^{-1}$):** 2911 m, 2852 m, 1630 s, 1556 s, 1445 s, 1418 s, 1377 m, 1316 m, 1135 m, 1087 m, 1029 m, 967 s, 938 s, 883 s, 829 m, 729 m, 658 s. **$^1$H NMR** (300 MHz, $CDCl_3$) δ 8.64 (d, *J* = 4.4 Hz, 2H), 8.43 (d, *J* = 7.7 Hz, 2H), 7.90 – 7.83 (m, 4H), 7.50 (dd, *J* = 6.3, 2.7 Hz, 2H), 7.37 (ddd, *J* = 7.7, 4.4, 1.1 Hz, 2H), 7.33 – 7.28 (m, 4H). **$^{13}$C NMR** (75 MHz, $CDCl_3$) δ 149.20, 148.23, 137.27, 124.61, 123.97, 122.72, 121.52, 120.19, 111.20. **ESI-MS** (m/z) calcd. for $C_{18}H_{14}N_4$: 286.33; found 287.0 $(M)^+$.

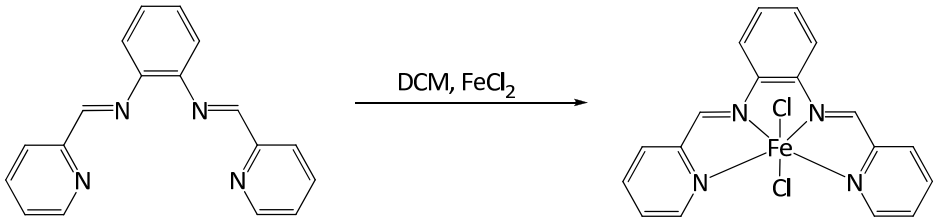


**L10** **65**

**$FeCl_2(C_{18}H_{14}N_4)$ (65).** To a solution of 0.1 g (0.35 mmol, 1.1 equiv.) **L10** in 10 ml DCM, 0.044 g (1.0 equiv.) of $FeCl_2$ was added. After stirring the suspension for 24 h, the violet solution was

dried and washed with diethylether and pentane. 0.086 g of the desired product was isolated as dark-violet powder (0.21 mmol, 60 %). **FT-IR ($cm^{-1}$):** 2922 m, 2852 m, 1592 m, 1476 s, 1429 s, 1335 m, 1298 s, 1260 s, 1152 m, 1091 m, 1014 m, 790 m, 745 w, 697 s, 635 s. **ESI-MS** (m/z) calcd. for $C_{18}H_{14}Cl_2FeN_4$: 411.99, found 378.1 $(M - Cl)^+$, 394.3 $(M - Cl + OH)^+$.

### 7.3.3. Iron(III)-Tetraamine Complexes

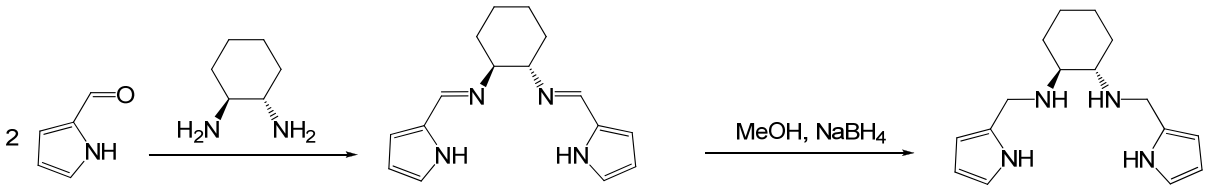


**L11** **L12**

**(*1S,2S*)-*N,N'*-bis(pyrrol-2-methyl)cyclohexane-1,2-diimine (L11).** 5.00 g (52.6 mmol) pyrrol-2-carboxaldehyde were diluted in 40 ml of ethanol and 2.84 g (26.3 mmol) of 1,2-(S,S)-diaminocyclohexane were added. After a short time, a white precipitate formed. The mixture was stirred for one day and the precipitate filtered off. The product was dried to yield 5.80 g of a yellowish powder (21.6 mmol, 82 %). **FT-IR ($cm^{-1}$):** 2911 s, 2852 s, 1629 s, 1556 s, 1445 s, 1418 s, 1376 s, 1359 m, 1316 m, 1246 s, 1199 s, 1148 m, 1087 s, 1029 s, 967 s, 938 m, 829 m, 729 m, 604 s. **$^1$H NMR** (300 MHz, $CDCl_3$) δ 7.65 (s, 2H), 6.84 (s, 2H), 6.39 (d, *J* = 2.6 Hz, 2H), 6.20 (t, *J* = 3.0 Hz, 2H), 3.06 – 2.94 (m, 2H), 1.73 (dd, *J* = 23.4, 11.4 Hz, 4H), 1.52 (d, *J* = 10.5 Hz, 2H), 1.33 (dd, *J* = 23.4, 11.4 Hz, 2H). **$^{13}$C NMR** (75 MHz, $CDCl_3$) δ 152.43, 130.46, 122.16, 114.69, 109.82, 109.61, 72.49, 34.27, 25.08, 24.80. **ESI-MS** (m/z) calcd. for $C_{16}H_{20}N_4$: 268.17; found 269.0 $(M)^+$.

**(*1S,2S*)-*N,N'*-bis(pyrrol-2-methyl)cyclohexane-1,2-diamine (L12).** 0.3 g (1.14 mmol) of **L11** were suspended in 20 ml MeOH (dry) and cooled down to 0°C. 0.43 g (11.4 mmol) sodium borohydride were added slowly and stirred at room temperature for 12 h. The lightly yellow solution was filtered, washed with water and DCM and the solvent of the united organic phases removed in vacuo. The product was then completely dried in vacuo to yield 0.14 g of a yellow powder (0.51 mmol, 45 %). The compound was spectroscopically clean and used without further purification for complexation. **FT-IR ($cm^{-1}$):** 2927 s, 2855 s, 1630 m, 1446 m, 1341 m, 1287 s, 1239 s, 1094 m, 1025 s, 974 m, 791 s, 714 s. **$^1$H NMR** (300 MHz, $CDCl_3$) δ 6.59 (d, *J* = 11.6 Hz, 2H), 6.02 (dt, *J* = 11.6, 2.8 Hz, 2H), 5.92 (s, 2H), 3.83 (t, *J* = 13.4 Hz, 2H),

3.62 (t, *J* = 13.4 Hz, 2H), 2.16 (dd, *J* = 5.4, 3.6 Hz, 2H), 2.12 – 2.03 (m, 2H), 1.66 (d, *J* = 8.4 Hz, 2H), 1.13 (dd, *J* = 20.2, 10.0 Hz, 2H), 0.94 (d, *J* = 10.0 Hz, 2H). **$^{13}$C NMR** (75 MHz, $CDCl_3$) δ 130.49, 117.28, 107.96, 106.01, 60.84, 43.61, 31.49, 24.98. **ESI-MS** (m/z) calcd. for $C_{16}H_{24}N_4$: 272.20; found 295.0 $(M+ Na)^+$.

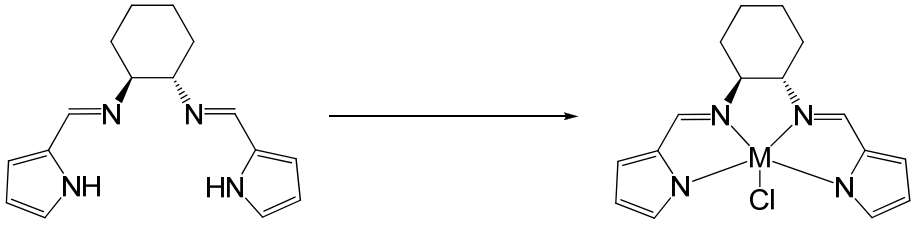


**L11** **66 (M = Fe)**

**67 (M = Co)**

**FeCl($C_{16}H_{18}N_4$) (66).** To a solution of 0.1 g (0.38 mmol, 1.1 equiv.) **L11** in 10 ml DCM, 0.062 g (1.0 equiv.) of $FeCl_3$ was added. The dark-green suspension was stirred for 24 hours. The solution was dried in vacuo and the residue washed with diethylether and pentane. 0.067 g of the desired product was isolated as dark-brown powder (0.19 mmol, 50 %). **FT-IR ($cm^{-1}$):** 2929 m, 2810 m, 1648 m, 1548 s, 1432 m, 1401 s, 1376 s, 1341 m, 1258 s, 1131 m, 1087 s, 1038 m, 965 m, 913 m, 759 m. **ESI-MS** (m/z) calcd. for $C_{16}H_{18}ClFeN_4$: 357.0, found 322.1 $(M – Cl)^+$.

**CoCl($C_{16}H_{18}N_4$) (67).** The procedure was derived from the synthesis of analogous Co(III)(salen)X (X = Cl, Br) complexes.[214] To a solution of 0.1 g (0.38 mmol, 1.1 equiv.) **L11** in 10 ml dry MeOH, 0.067 g (1.0 equiv.) of anhydrous $Co(OAc)_2$ was added. The blue suspension turned reddish after a few seconds and was stirred for another 24 hours. 0.033 g LiCl (0.76 mmol) were added. The mixture turned deep-blue after a few seconds and the resulting mixture was exposed to air and stirred for an additional 48 hours. After 48 hours, the solvent was removed under reduced pressure, and the residual was extracted with DCM. The extract was washed with distilled water, dried over anhydrous $Na_2SO_4$ and filtrated. The filtrate was dried under reduced pressure to leave 0.6 g of dark blue powder (0.17 mmol, 44 %). **FT-IR ($cm^{-1}$):** 2926 m, 2854 m, 1649 m, 1577 s, 1442 s, 1404 s, 1384 s, 1353 s, 1294 s, 1261 s, 1129 m, 1090 s, 1033 m, 862 m, 730 m, 671 m. **ESI-MS** (m/z) calcd. for $C_{16}H_{18}ClCoN_4$: 360.05, found 325.1 $(M – Cl)^+$.

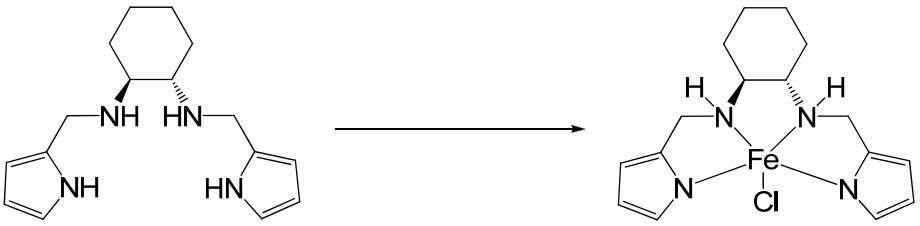


**L12** **68**

**FeCl($C_{16}H_{22}N_4$) (68).** To a solution of 0.1 g (0.37 mmol, 1.1 equiv.) **L12** in 10 ml DCM, 0,060 g (1.0 equiv.) of $FeCl_3$ was added. The dark-green suspension was stirred for 24 hours. The solution was dried in vacuo and the residue washed with diethylether and pentane. 0.082 g of the desired product was isolated as dark-brown powder (0.23 mmol, 61 %). **FT-IR ($cm^{-1}$):** 2935 m, 2864 m, 1595 m, 1507 m, 1448 s, 1405 m, 1338 s, 1246 m, 1162 m, 1024 m, 774 m, 646 m. **ESI-MS** (m/z) calcd. for $C_{16}H_{22}ClFeN_4$: 361.09, found: 325.2 $(M - Cl)^+$.

### 7.3.4. Tridentate Iron(II) and Iron(III) Complexes

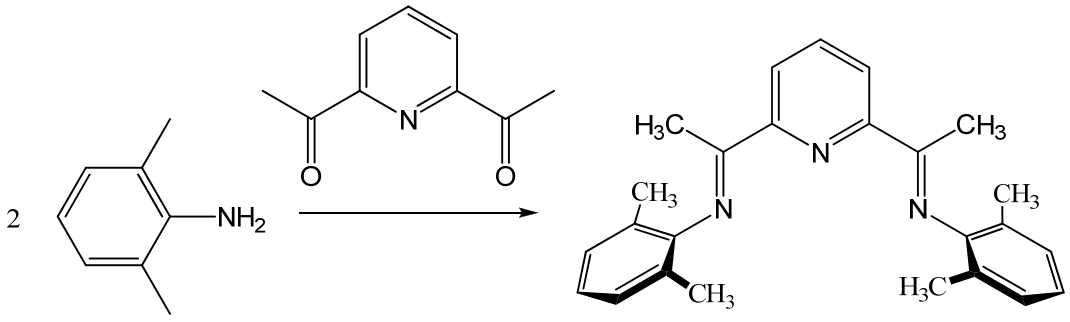


**L13**

**2,6-bis-[1-(2,6-dimethylphenylimino)ethyl]pyridine (L13)**

1 g (6.13 mmol) of 2,6-diacetylpyridine were dissolved in 20 ml MeOH and 1.51 ml (12.26 mmol) 2,6-dimethylaniline were added. A few drops of 97 % formic acid were added and the sealed solution stirred several days at 50°C. The solution was cooled in an ice bath, resulting in the formation of 2.016 g of a light yellow precipitate that was isolated by filtration (5.46 mmol, 89 %). **FT-IR ($cm^{-1}$):** 2942 s, 2918 s, 1644 s, 1593 s, 1567 m, 1466 m, 1364 s, 1297 m, 1247 s, 1202 s, 1093 m, 990 m, 817 m, 761 m, 691 s. **$^1$H NMR** (300 MHz, $CDCl_3$) δ 8.51 (d, *J* = 7.8 Hz, 2H), 7.92 (t, *J* = 7.8 Hz, 1H), 7.07 (d, *J* = 7.5 Hz, 4H), 6.98 – 6.90 (m, 2H), 2.24 (s, 6H),

2.05 (s, 12H). **$^{13}$C NMR** (75 MHz, $CDCl_3$) δ 155.00, 148.46, 136.94, 127.94, 125.56, 123.19, 122.49, 17.97, 16.51. **ESI-MS** (m/z) calcd. for $C_{25}H_{27}N_3$: 369.22; found 370.1 $(M)^+$.

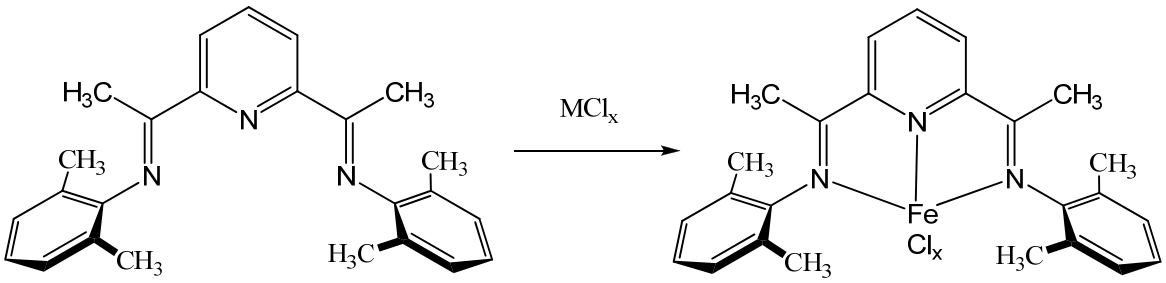


**L13**

**69** (x = 3)

**70** (x = 2)

**$FeCl_3(C_{25}H_{27}N_3)$ (69).** 0.2 g of the ligand (0.54 mmol, 1.05 eq.), 10 ml THF and 0.084 g (0.52 mmol) of $FeCl_3$ were added together under Schlenk conditions. After 18 hours, $Et_2O$ was added to the reaction to precipitate the complex and the dark-violet solid filtered in air and washed with $Et_2O$ and pentane and dried in vacuo to yield 0.14 g of the desired product (0.26 mmol, 49 %). **FT-IR ($cm^{-1}$):** 2914 w, 2855 w, 1738 m, 1626 s, 1588 s, 1471 m, 1372 m, 1264 s, 1217 m, 1094 m, 1059 m, 919 m, 820 w, 768 m, 695 s. **ESI-MS** (m/z) calcd. For $C_{25}H_{27}Cl_3FeN_3$ (530.06), found 460.1 $(M - 2Cl)^+$.

**$FeCl_2(C_{25}H_{27}N_3)$ (70).** 0.2 g of the ligand (0.54 mmol, 1.05 eq.), 10 ml THF and 0.065 g (0.52 mmol) of $FeCl_2$ were added together under Schlenk conditions. After 18 hours, $Et_2O$ was added to the reaction to precipitate the complex and the dark-blue solid filtered in air and washed with $Et_2O$ and pentane and dried in vacuo to yield 0.16 g of the desired product (0.32 mmol, 60 %). **FT-IR ($cm^{-1}$):** 2915 w, 2862 w, 1738 m, 1626 s, 1588 s, 1470 m, 1372 m, 1263 s, 1216 m, 1094 m, 1059 m, 920 m, 819 w, 768 m, 695 s. **ESI-MS** (m/z) calcd. For $C_{25}H_{27}Cl_2FeN_3$ (495.09), found 460.1 $(M - Cl)^+$.

### 7.3.5. Coupling Reactions with Iron-Based Systems

A 100 mL stainless-steel autoclave was heated to 130 °C in an oven and allowed to cool to room temperature under vacuum. The autoclave was filled with the iron or cobalt complex and propylene oxide / cyclohexene oxide and pressurized with $CO_2$ to the desired pressure. The reactor was then heated to the 40 – 100 °C and the reaction stirred for 2 h. After cooling

the mixture to 0 °C, the reactor was opened and the crude product filled into a glass vessel. Residual propylene oxide was allowed to evaporate and the turn-over frequency determined from the weight of the remaining product. The product was analyzed with $^{1}H$ NMR spectroscopy in deuteriated chloroform. Analysis of the molecular weights was not possible, because a too high content of residual complex in the crude polymer and too low yields for separation of pure polymer for GPC-analysis.

# 8. **Abbreviations**

| | | |
|---|---|---|
| BDI | | β-diiminate |
| CHC | | cyclohexene carbonate |
| CHO | | cyclohexene oxide |
| cPC | | cyclic propylene carbonate |
| DMAP | | 4-(dimethylamino)pyridine |
| DNP | | 2,4-dinitrophenolate |
| ESI | | electrospray ionization |
| $M_n$ | | molecular weight, number average |
| MS | | mass spectrometry |
| $M_w$ | | molecular weight, weight average |
| NMR | | nuclear magnetic resonance |
| | d | doublet |
| | dd | doublet of doublets |
| | ddd | doublet of doublet of doublets |
| | j | coupling constant |
| | m | multiplet |
| | ppm | chemical shift |
| | q | quartet |
| | s | singlet |
| | t | triplet |
| *N*-MeIm | | *N*-methylimidazole |
| OAc | | acetate |
| cPC | | propylene carbonate |
| PCHC | | poly(cyclohexene carbonate) |
| [PDI] | | 2,6-bis(N-arylimino)pyridine |
| PDI | | polydispersity index |
| PO | | propylene oxide |
| PPC | | poly(propylene carbonate) |
| PPNCl | | *bis*(triphenylphosphine)iminium chloride |
| TOF | | turn-over frequency |
| TON | | turn-over number |

| | |
|---|---|
| tpp | tetraphenylporphyrin, porphyrin |
| ZnAA | zinc adipate |
| ZnGA | zinc glutarate |
| ZnPA | zinc pimelate |
| ZnSA | zinc succinate |

# 9. **References**

[1] H. Danner, R. Braun, *Chem. Soc. Rev.* **1999**, *28*, 395.
[2] T.U. Gerngross, S.C. Slater, *Sci. Am.* **2000**, *283*, 37.
[3] R. A. Gross, B. Kalra, *Science* **2002**, *297*, 803.
[4] M. Okada, *Prog. Polym. Sci.* **2001**, *27*, 87.
[5] B. D. Santer, K. E. Taylor, T. M. L. Wigley, T. C. Johns, P. D. Jones, D. J. Karoly, J. F. B. Mitchell, A. H. Oort, J. E. Penner, V. Ramaswamy, M. D. Schwarzkopf, R. J. Stouffer, S. Tett, *Nature* **1996**, *382*, 39.
[6] W. S. Broecker, *Science* **1997**, *278*, 1582.
[7] G. A. Meehl, W. M. Washington, *Nature* **1996**, *382*, 56.
[8] K. Kacholia, R.A. Reck, *Climatic Change* **1997**, *35*, 53.
[9] *Department of Energy (US), International Energy Agency Report* **2009**, *0484*.
[10] *Wissenschaftlicher Beirat der Bundesregierung Globale Umweltveränderungen, Sequestrierung von $CO_2$: Technologien, Potenziale, Kosten und Umweltauswirkungen* **2003**.
[11] J. Paul, C.-M. Pradier, *Carbon Dioxide Chemistry: Environmental Issues, R. Soc. Chem.* **1994**.
[12] W. Keim, A. Behr, G. Schmitt, *Principles of Industrial Chemistry. Industrial Products and Processes, Sale und Sauerlander, Frankfurt* **1986**.
[13] R. Dittmeyer, W. Keim, G. Kreysa, A. Oberholz, *Winnacker-Küchler: Chemische Technik* **2005**, *4*
[14] T. Sakakura, K. Kohno, *Chem. Commun.* **2009**, 1312.
[15] B. Schäffner, F. Schäffner, S.P. Verevkin, A. Börner, *Chem. Rev.* **2010**, *110*, 4554.
[16] S. Klaus, M. W. Lehenmeier, Carly E. Anderson, B. Rieger, *Coord. Chem. Rev.* **2011**, *25*, 1460.
[17] H. Arakawa et al., *Chem. Rev.* **2001**, *101*, 953.
[18] A.I. Cooper, *J. Mat. Chem.* **2000**, *10*, 207.
[19] C. Bolm, O. Beckmann, O.A.G. Dabard, *Angew. Chem. Int. Ed.* **1999**, *38*, 907.
[20] C. Bruckmeier, M. W. Lehenmeier, R. Reichardt, S. Vagin, B. Rieger, *Organometallics* **2010**, *29*, 2199.
[21] T. Sakakura, J. -C. Choi, H. Yasuda, *Chem. Rev.* **2007**, *107*, 2365.
[22] M.S. Super, E.J. Beckman, *Trends Polym. Sci.* **1997**, *5*, 236.
[23] S. Inoue, *CHEMTECH* **1976**, *6*, 588.
[24] E. J. Beckman, *Science* **1999**, *283*, 946.
[25] W. Kuran, *Prog. Polym. Sci.* **1998**, *23*, 919.
[26] D. J. Darensbourg, M. W. Holtcamp, *Coord. Chem. Rev.* **1996**, *153*, 155.
[27] G. W. Coates, D. R. Moore, *Angew. Chem.* **2004**, *43*, 6618.
[28] D. J. Darensbourg, *Chem. Rev.* **2007**, *107*, 2388.
[29] H. Sugimoto, S. Inoue, *J. Polym. Sci., Part A: Polym. Chem.* **2004**, *42*, 5561.
[30] M. R. Kember, A. Buchard, C. K. Williams, *Chem. Commun.* **2010**, DOI: 10.1039/c0cc02207a.
[31] D. J. Darensbourg, R. M. Mackiewicz, A. L. Phelps, D. R. Billodeaux, *Acc. Chem. Res.* **2004**, *37*, 836.
[32] K. Nozaki, *Pure and Applied Chemistry* **2004**, *76*, 541.
[33] S. Inoue, H. Koinuma, T. Tsuruta, *Makromol. Chem.* **1969**, *130*, 210.
[34] M. Kobayashi, S. Inoue, T. Tsuruta, *Macromolecules* **1971**, *4*, 658.
[35] M. Kobayashi, Y.-L. Tang, T. Tsuruta, S. Inoue, *Makromol. Chem.* **1973**, *169*, 69.

[36] M. Kobayashi, S. Inoue, T. Tsuruta, *J. Polym. Sci. Polym. Chem. Ed.* **1973**, *11*, 2383.
[37] S. Inoue, M. Kobayashi, H. Koinuma, T. Tsuruta, *Makromol. Chem.* **1972**, *155*, 61.
[38] W. Kuran, S. Pasynkiewicz, J. Skupinska, *Macromol. Chem. Phys.* **1976**, *177*, 1283.
[39] W. Kuran, S. Pasynkiewicz, J. Skupinska, *Makromol. Chem.* **1977**, *178*, 2149.
[40] W. Kuran, T. Listos, *Macromol. Chem. Phys.* **1994**, *195*, 977.
[41] K. Soga, E. Imai, I. Hattori, *Polym. J.* **1981**, *13*, 407.
[42] W. Kuran, S. Pasynkiewicz, J. Skupinska, A. Rokicki, *Makromol. Chem.* **1976**, *177*, 11.
[43] A. Rokicki, W. Kuran, *Makromol. Chem.* **1979**, *180*, 2153.
[44] T. Aida, M. Ishikawa, S. Inoue, *Macromolecules* **1986**, *19*, 8.
[45] D. J. Darensbourg, M. W. Holtcamp, *Macromolecules* **1995**, *28*, 7577.
[46] D. J. Darensbourg, M. W. Holtcamp, G. E. Struck, M. S. Zimmer, S. A. Niezgoda, P. Rainey, J. B. Robertson, J. D. Draper, J. H. Reibenspies, *J. Am. Chem. Soc.* **1999**, *121*, 107.
[47] C. Koning, J. Wildeson, R. Parton, B. Plum, P. Steeman, D. J. Darensbourg, *Polymer* **2001**, *42*, 3995.
[48] M. Cheng, E. B. Lobkovsky, G. W. Coates, *J. Am. Chem. Soc.* **1998**, *120*, 11018.
[49] D. R. Moore, M. Cheng, E. B. Lobkovsky, G. W. Coates, *Angew. Chem. Int. Ed.* **2002**, *41*, 2599.
[50] S. D. Allen, D. R. Moore, E. B. Lobkovsky, G. W. Coates, *J. Am. Chem. Soc.* **2002**, *124*, 14284.
[51] G. A. Luinstra, G. R. Haas, F. Molnar, V. Bernhart, R. Eberhardt, B. Rieger, *Chem. Eur. J.* **2005**, *11*, 6298.
[52] E. N. Jacobsen, *Acc. Chem. Res.* **2000**, *33*, 421.
[53] L. P. C. Nielsen, C. P. Stevenson, D. G. Blackmond, E. N. Jacobsen, *J. Am. Chem. Soc.* **2004**, *126*, 1360.
[54] K. B. Hansen, J. L. Leighton, E. N. Jacobsen, *J. Am. Chem. Soc.* **1996**, *118*, 10924.
[55] C. T. Cohen, T. Chu, G. W. Coates, *J. Am. Chem. Soc.* **2005**, *127*, 10869.
[56] D. J. Darensbourg, J. C. Yarbrough, *J. Am. Chem. Soc.* **2002**, *124*, 6335.
[57] D. J. Darensbourg, J. C. Yarbrough, C. Ortiz, C. C. Fang, *J. Am. Chem. Soc.* **2003**, *125*, 7586.
[58] D. J. Darensbourg, J. L. Rodgers, R. M. Mackiewicz, A. L. Phelps, *Catal. Today* **2004**, *98*, 485.
[59] M. H. Chisholm, Z. Zhou, *J. Am. Chem. Soc.* **2004**, *126*, 11030.
[60] D.-Y. Rao, B. Li, R. Zhang, H. Wang, X.-B. Lu, *Inorg. Chem.* **2009**, *48*, 2830.
[61] X.-B. Lu, Y. Wang, *Angew. Chem. Int. Ed.* **2004**, *43*, 3574.
[62] X.-B. Lu, L. Shi, Y.-M. Wang, R. Zhang, Y.-J. Zhang, X.-J. Peng, Z.-C. Zhang, B. Li, *J. Am. Chem. Soc.* **2006**, *128*, 1664.
[63] L. Shi, X.-B. Lu, R. Zhang, X.-J. Peng, C.-Q. Zhang, J.-F. Li, X.-M. Peng, *Macromolecules* **2006**, *39*, 5679.
[64] C. T. Cohen, G. W. Coates, *J. Polym. Sci., Part A Polym. Chem.* **2006**, *44*, 5182.
[65] R. L. Paddock, S. T. Nguyen, *Macromolecules* **2005**, *38*, 6251.
[66] Y. Niu, W. Zhang, X. Pang, X. Chen, X. Zhuang, X. Jing, *J. Polym. Sci., Part A Polym. Chem.* **2007**, *45*, 5050.
[67] C. T. Cohen, C. M. Thomas, K. L. Peretti, E. B. Lobkovsky, G. W. Coates, *Dalton Trans.* **2005**, 237.
[68] Z. Q. Qin, C. M. Thomas, S. Lee, G. W. Coates, *Angew. Chem. Int. Ed.* **2003**, *42*, 5484.
[69] H. Sugimoto, K. Kuroda, *Macromolecules* **2008**, *41*, 312.
[70] L. Guo, C. Wang, W. Zhao, H. Li, W. Sun, Z. Shen, *Dalton Trans.* **2009**, 5406.
[71] D. J. Darensbourg, P. Bottarelli, J. R. Andreatta, *Macromolecules* **2007**, *40*, 7727.

[72] D.J. Darensbourg, A.L. Phelps, *Inorg. Chem.* **2005**, *44*, 4622.
[73] D. J. Darensbourg, R. M. Mackiewicz, *J. Am. Chem. Soc.* **2005**, *127*, 14026.
[74] R. Eberhardt, M. Allmendinger, B. Rieger, *Macromol. Rapid Commun.* **2003**, *24*, 194.
[75] D.J. Darensbourg, R.M. Mackiewicz, J.L. Rodgers, C.C. Fang, D.R. Billodeaux, J.H. Reibenspies, *Inorg. Chem.* **2004**, *43*, 6024.
[76] D.J. Darensbourg, R.M. Mackiewicz , J.L. Rodgers, A.L. Phelps, *Inorg. Chem.* **2004**, *43*, 1831.
[77] B. Li, G.-P. Wu, W.-M. Ren, Y.-M. Wang, D.-Y. Rao, X.-B. Lu, *J. Polym. Sci., Part A Polym. Chem.* **2008**, *46*, 6102.
[78] D.R. Moore, M. Cheng, E.B. Lobkovsky, G.W. Coates, *J. Am. Chem. Soc.* **2003**, *125*, 11911.
[79] Y. Hino, Y. Yoshida, S. Inoue, *Polym. J.* **1984**, *16*, 159.
[80] T. Tsuruta, *Makromol. Chem.* **1986**, *6*, 23.
[81] W. Kuran, *Appl. Organomet. Chem.* **1991**, *5*, 191.
[82] W. Kuran, T. Listos, *Pol. J. Chem.* **1994**, *68*, 1071.
[83] K. Nakano, T. Kamada, K. Nozaki, *Angew. Chem. Int. Ed.* **2006**, *45*, 7274.
[84] H. Sugimoto, H. Ohtsuka, S. Inoue, *J. Polym. Sci., Part A: Polym. Chem.* **2005**, *43*, 4172.
[85] L. J. Gao, M. Xiao, S. J. Wang, F. G. Du, Y. Z. Meng, *J. Appl. Polym. Sci.* **2007**, *104*, 15.
[86] G. A. Luinstra, *Polymer Rev.* **2008**, *48*, 192.
[87] M. Ree, Y. Hwang, J.-S. Kim, H. Kim, G. Kim, H. Kim, *Catal. Today* **2006**, *115*, 134.
[88] M. Ree, J. Y. Bae, J. H. Jung, T. J. Shin, *J. Polym. Sci. Part A* **1999**, *37*, 1863.
[89] J.-S. Kim, M. Ree, T. J. Shin, O. H. Han, S. J. Cho, Y.-T. Hwang, J. Y. Bae, J. M. Lee, R. Ryoo, H. Kim, *J. Catal.* **2003**, *218*, 209.
[90] Y. Z. Meng, L. C. Du, S. C. Tiong, Q. Zhu, A. S. Hay, *J. Polym. Sci. Part A* **2002**, *40*, 3579.
[91] Y. Q. Zheng, J. L. Lin, H. L. Zhang, *Z. Kristallogr. - New Cryst. Struct.* **2000**, *215*, 535.
[92] J.-S. Kim, H. Kim, M. Ree, *Chem. Mater.* **2004**, *16*, 2981.
[93] M. Ree, J. Y. Bae, J. H. Jung, T. J. Shin, *Kor. Polym. J.* **1999**, *7*, 333.
[94] J. T. Wang, Q. Zhu, X. L. Lu, Y. Z. Meng, *Eur. Polym. J.* **2005**, *41*, 1108.
[95] J.-S. Kim, H. Kim, J. Yoon, K. Heo, M. Ree, *J. Polym. Sci., Part A: Polym. Chem.* **2005**, *43*, 4079.
[96] S. J. Wang, L. C. Du, X. S. Zhao, Y. Z. Meng, S. C. Tjong, *J. Appl. Polym. Sci.* **2002**, *85*, 2327.
[97] Caroll W. E., Motika S. A., *US Patent 4.960.862* **1990**.
[98] M. H. Chisholm, D. Navarro-Llobet, Z. Zhou, *Macromolecules* **2002**, *35*, 6494.
[99] R. Eberhardt, M. Allmendinger, G. A. Luinstra, B. Rieger, *Organometallics* **2003**, *22*, 211.
[100] R. Eberhardt, M. Allmendinger, M. Zintl, C. Troll, G. A. Luinstra, B. Rieger, *Macromol. Chem. Phys.* **2004**, *205*, 42.
[101] J. S. Kim, M. Ree, S. W. Lee, W. Oh, S. Baek, B. Lee, T. J. Shin, K. J. Kim, B. Kim, J. Luning, *J. Catal. Journal of Catalysis* **2003**, *218*, 386.
[102] Q. Zhu, Y. Z. Meng, S. C. Tjong, Y. M. Zhang, W. Wan, *Polym. Int. Polymer International* **2003**, *52*, 799.
[103] S. Inoue, T. Takada, H. Tatsu, *Makromol. Chem., Rapid Commun.* **1980**, *1*, 775.
[104] M. Ree, J. Y. Bae, J. H. Jung, T. J. Shin, Y. T. Hwang, T. Chang, *Polym. Eng. Sci.* **2000**, *40*, 1542.
[105] J. T. Wang, D. Shu, M. Xiao, Y. Z. Meng, *J. Appl. Polym. Sci.* **2006**, *99*, 200.
[106] A.M. Sakharov, V.V. Il'in, V.V. Rusak, Z.N. Nysenko, S.A. Klimov, *Russ. Chem. Bull. Int. Ed.* **2002**, *51*, 1451.
[107] T.A. Bowden, H.L. Milton, A.M.Z. Slawin, P. Lightfoot, *Dalton Trans.* **2003**, 936.
[108] Pan J., Zhang G., Zheng Y., Lin J., Xu W., *J. Cryst. Growth* **2007**, *308*, 89.

[109] W. J. Kruper, D. V. Dellar, *J. Org. Chem.* **1995**, *60*, 725.
[110] T. Aida, S. Inoue, *J. Am. Chem. Soc.* **1985**, *107*, 1358.
[111] F. Kojima, T. Aida, S. Inoue, *J. Am. Chem. Soc.* **1986**, *108*, 391.
[112] Y. Qin, X. Wang, S. Zhang, X. Zhao, F. Wang, *J. Polym. Sci. Part A* **2008**, *46*, 5959.
[113] P. Chen, M. H. Chisholm, J. C. Gallucci, X. Zhang, Z. Zhou, *Inorg. Chem.* **2005**, *44*, 2588.
[114] R. L. Paddock, Y. Hiyama, J. M. McKay, S. T. Nguyen, *Tetrahedron Lett.* **2004**, *45*, 2023.
[115] L. Jin, H. Jing, T. Chang, X. Bu, L. Wang, Z. Liu, *J. Mol. Cat. A* **2007**, *261*, 262.
[116] R. L. Geerts, J. C. Huffman, K. G. Caulton, *Inorg. Chem.* **1986**, *25*, 1803.
[117] D.J. Darensbourg, S.A. Niezgoda, J.D. Draper, J.H. Reibenspies, *J. Am. Chem. Soc.* **1998**, *120*, 4690
[118] D. J. Darensbourg, J. R. Wildeson, J. C. Yarbrough, J. H. Reibenspies, *J. Am. Chem. Soc.* **2000**, *122*, 12487.
[119] D. J. Darensbourg, M. S. Zimmer, P. Rainey, D. L. Larkins, *Inorg. Chem.* **2000**, *39*, 1578.
[120] D. J. Darensbourg, M. W. Holtcamp, B. Khandelwal, K. K. Klausmeyer, J. H. Reibenspies, *J. Am. Chem. Soc.* **1995**, *117*, 538.
[121] D. J. Darensbourg, S. A. Niezgoda, M. W. Holtcamp, J. D. Draper, J. H. Reibenspies, *Inorg. Chem.* **1997**, *36*, 2426.
[122] L. Bourget-Merle, M. F. Lappert, J. R. Severn, *Chem. Rev.* **2002**, *102*, 3031.
[123] M. Cheng, D. R. Moore, J. J. Reczek, B. M. Chamberlain, E. B. Lobkovsky, G. W. Coates, *J. Am. Chem. Soc.* **2001**, *123*, 8738.
[124] M. Cheng, N. A. Darling, E. B. Lobkovsky, G. W. Coates, *Chem. Commun.* **2000**, 2007.
[125] G. W. Coates, M. Cheng, *US Pat. Appl.* **2000**, *US 6,133,402*.
[126] S. D. Allen, D. R. Moore, E. B. Lobkovsky, G. W. Coates, *J. Organomet. Chem.* **2003**, *683*, 137.
[127] M. Kroeger, M. Doering, *Catal. Today* **2006**, *115*, 146.
[128] C. M. Byrne, S. D. Allen, E. B. Lobkovsky, G. W. Coates, *J. Am. Chem. Soc.* **2004**, *126*, 11404.
[129] M. Kroeger, C. Folli, O. Walter, M. Doering, *Advanced Synthesis & Catalysis* **2005**, *347*, 1325.
[130] M. Kroeger, C. Folli, O. Walter, M. Doering, *J. Organomet. Chem.* **2006**, *691*, 3397.
[131] B. Y. Lee, H. Y. Kwon, S. Y. Lee, S. J. Na, S. Han, H. Yun, H. Lee, Y.-W. Park, *J. Am. Chem. Soc.* **2005**, *127*, 3031.
[132] W. J. van Meerendonk, R. Duchateau, C. E. Koning, G.-J. M. Gruter, *Macromol. Rapid Commun.* **2004**, *25*, 382.
[133] M. H. Chisholm, J. C. Huffman, K. Phomphrai, *J. Chem. Soc. Dalton Trans.* **2001**, 222.
[134] M. H. Chisholm, J. Gallucci, K. Phomphrai, *Inorg. Chem.* **2002**, *41*, 2785.
[135] Rieth L. R., Moore D. R., Lobkovsky E. B., Coates G. W., *J. Am. Chem. Soc.* **2002**, *124*, 15239.
[136] B. Liu, C. Tian, L. Zhang, W. Yan, W. Zhang, *J. Polym. Sci., Part A Polym. Chem.* **2006**, *44*, 6243.
[137] M. Walther, K. Wermann, M. Lutsche, W. Gnther, H. Grls, E. Anders, *J. Org. Chem.* **2006**, *71*, 1399.
[138] D. V. Vitanova, F. Hampel, K. C. Hultzsch, *J. Organomet. Chem.* **2005**, *690*, 5182.
[139] B. B. Lazarov, F. Hampel, K. C. Hultzsch, *Z. Anorg. Allg. Chem.* **2007**, *633*, 2367.
[140] B. Liu, X. Zhao, H. Guo, Y. Gao, M. Yang, X. Wang, *Polymer* **2009**, *50*, 5071.
[141] D.J. Darensbourg, R.M. Mackiewicz, D.R. Billodeaux, *Organometallics* **2005**, *24*, 144.
[142] K. Nozaki, K. Nakano, T. Hiyama, *J. Am. Chem. Soc.* **1999**, *121*, 11008.
[143] K. Nakano, K. Nozaki, T. Hiyama, *J. Am. Chem. Soc.* **2003**, *125*, 5501.

[144] K. Nakano, T. Hiyama, K. Nozaki, *Chem. Commun.* **2005**, 1871.
[145] Y. Xiao, Z. Wang, K. Ding, *Chem. Eur. J.* **2005**, 3668.
[146] Y. Xiao, Z. Wang, K. Ding, *Macromolecules* **2006**, *39*, 128.
[147] T. Bok, H. Yun, B. Y. Lee, *Inorg. Chem.* **2006**, *45*, 4228.
[148] M. F. Pilz, C. Limberg, B. B. Lazarov, K. C. Hultzsch, B. Ziemer, *Organometallics* **2007**, *26*, 3668.
[149] D. Piesik, S. Range, S. Harder, *Organometallics* **2008**, *27*, 6178.
[150] M.R. Kember, P.D. Knight, P.T. Reung, C.K. Williams, *Angew. Chem.* **2009**, *121*, 949.
[151] M.R. Kember, A.J.P. White, C.K. Williams, *Inorg. Chem.* **2009**, *48*, 9535.
[152] M. R. Kember, A. J. P. White, C. K. Williams, *Macromolecules* **2010**, *43*, 2291.
[153] A. Buchard, M. R. Kember, K. Sandeman, C. K. Williams, *Chem. Commun.* **2010**, *46*, DOI: 10.1039/c0cc02205e.
[154] J. E. Dengler, M. W. Lehenmeier, S. Klaus, C. E. Anderson, E. Herdtweck, B. Rieger, *Eur. J. Inorg. Chem.* **2010**, DOI: 10.1002/ejic.201000861.
[155] W. M. Ren, Z. W. Liu, Y. Q. Wen, R. Zhang, X. B. Lu, *J. Am. Chem. Soc.* **2009**, *131*, 11509.
[156] W. M. Ren, X. Zhang, Y. Liu, J. F. Li, H. Wang, X. B. Lu, *Macromolecules* **2010**, *43*, 1396.
[157] E. K. Noh, S. J. Na, S. Sujith, S. W. Kim, B. Y. Lee, *J. Am. Chem. Soc.* **2007**, *129*, 8082.
[158] J. E. Seong, S. J. Na, A. Cyriac, B. W. Kim, B. Y. Lee, *Macromolecules* **2010**, *43*, 903.
[159] S. Sujith, J. K. Min, J. E. Seong, S. J. Na, B. Y. Lee, *Angew. Chem. Int. Ed.* **2008**, *47*, 7306.
[160] J. Na Sung, S. Sujith, A. Cyriac, E. Kim Bo, J. Yoo, K. Kang Youn, J. Han Su, C. Lee, Y. Lee Bun, *Inorg. Chem.* **2009**, *48*, 10455.
[161] J. Yoo, S. J. Na, H. C. Park, A. Cyriac, B. Y. Lee, *Dalton Trans.* **2010**, *39*, 2622.
[162] C. Hongfa, J. Tian, J. Andreatta, D.J. Darensbourg, D.E. Bergbreiter, *Chem. Commun.* **2008**, 975.
[163] R.G. Konsler, J. Karl, E. N. Jacobsen, *J. Am. Chem. Soc.* **1998**, *120*, 10780.
[164] E. Schön, X. Zhang, Z. Zhou, M. H. Chisholm, P. Chen, *Inorg. Chem.* **2004**, *43*, 7278.
[165] K. Nakano, S. Hashimotoa, K. Nozaki, *Chem. Sci.* **2010**, *1*, 369.
[166] S. I. Vagin, R. Reichardt, S. Klaus, B. Rieger, *J. Am. Chem. Soc.* **2010**, *132*, 14367.
[167] K. Yu, C. W. Jones, *Organometallics* **2003**, *22*, 2571.
[168] M. Alvaro, C. Baleizao, D. Das, E. Carbonell, J. Garcia, *J. Catal.* **2004**, *228*, 254.
[169] M. Alvaro, C. Baleizao, E. Carbonell, M.E. Ghoul, H. García, B. Gigante, *Tetrahedron* **2005**, *61*, 12131.
[170] Bowden T. A., Milton H. L., Slawin A. M. Z., Lightfoot P., *Dalton Trans.* **2003**, 936.
[171] Robert Reichardt, *Dissertation* **2011**.
[172] R. M. Thomas, P. C. B. Widger, S. Mé. Ahmed, R. C. Jeske, W. Hirahata, E. B. Lobkovsky, G. W. Coates, *J. Am. Chem. Soc.* **2010**, *132*, 16520.
[173] S. Fukuoka, M. Kawamura, K. Komiya, M.Tojo, H. Hachiya, K. Hasegawa, M. Aminaka, H. Okamoto, I. Fukawa, S. Konno, *Green Chem.* **2003**, *5*, 497.
[174] G. Rokicki, *Progr. Polym. Sci.* **2000**, *25*, 259.
[175] J. H. Clements, *Ind. Eng. Chem. Res.* **2003**, *42*, 663.
[176] A.-A. G. Shaikh, S. Sivaram, *Chem. Rev.* **1996**, *96*, 951.
[177] L. Han, S.-W. Park, D.-W. Park, *Energy Environ. Sci.* **2009**, *2*, 1286.
[178] A. Sibaouih, P. Ryan, M. Leskelä, B. Rieger, T. Repo, *Appl. Catal. A* **2009**, *365*, 194.
[179] N. Kihara, N. Hara, T. Endo, *J. Org. Chem.* **1993**, *58*, 6198.
[180] D. J. Darensbourg, S. J. Lewis, J. L. Rodgers, J. C. Yarbrough, *Inorg. Chem.* **2003**, *42*, 581.
[181] R. Srivastava, D. Srinivas, P. Ratnasamy, *Appl. Catal. A* **2005**, *289*, 128.
[182] T. Zhao, Y. Han, Y. Sun, *Phys. Chem. Chem. Phys.* **1999**, *1*, 3047.
[183] X. B. Lu, R. He, C. X. Bai, *J. Mol. Catal. A* **2002**, *186*, 1.

[184] X.-B. Lu, Y.-J. Zhang, K. Jin, L.-M. Luo, H. Wang, *J. Catal. A* **2004**, *210*.
[185] R. L. Paddock, S. T. Nguyen, *J. Am. Chem. Soc.* **2001**, *123*, 11498.
[186] T. Chang, L. Jin, H. Jing, *ChemCatChem* **2009**, *1*, 379.
[187] A. Sibaouih, P. Ryan, K. V. Axenov, M. R. Sundberg, M. Leskelä, T. Repo, *J. Mol. Cat. A* **2009**, *312*, 87.
[188] A. Decortes, M. M. Belmonte, J. Benet-Buchholz, A. W. Kleij, *Chem. Comm.* **2010**, *46*, 4580.
[189] S.-I. Fujita, M. Nishiura, M. Arai, *Catal. Lett.* **2010**, *135*, 263.
[190] J. Meléndez, M. North, P. Villuendas, *Chem. Comm.* **2009**, 2577.
[191] M. North, R. Pasquale, *Angew. Chem. Int. Ed.* **2009**, *48*, 2946.
[192] H. Jing, S. K. Edulji, J. M. Gibbs, C. L. Stern, H. Zhou, S. T. Nguyen, *Inorg. Chem.* **2004**, *43*, 4315.
[193] D. Ji, X. Lu, R. He, *Appl. Catal. A* **2000**, *203*, 329.
[194] V. Amendola, L. Fabbrizzi, E. Mundum, P. Pallavicini, *Dalton Trans.* **2003**, 773.
[195] P. Pallavicini, V. Amendola, C. Massera, E. Mundum, A. Taglietti, *Chem. Commun.* **2002**, 2452.
[196] D.-Y. Rao, B. Li, R. Zhang, H. Wang, X.-B. Lu, *Inorg. Chem.* **2009**, *48*, 2830.
[197] B. Li, G.-P. Wu, W.-M. Ren, Y.-M. Wang, D.-Y. Rao, X.-B. Lu, *J. Pol. Sci.: Part A: Polymer Chemistry* **2008**, *46*, 6102.
[198] D. J. Darensbourg, M. Ulusoy, O. Karroonnirum, R. R. Poland, J. H. Reibenspies, B. Cetinkaya, *Macromolecules* **2009**, *42*, 6992.
[199] K. Nakano, M. Nakamura, K. Nozaki, *Macromolecules* **2009**, *42*, 6972.
[200] T. Dudev, C. Lim, *J. Phys. Chem. B* **2004**, *108*, 4546.
[201] M. W. Lehenmeier, C. Bruckmeier, S. Klaus, J. E. Dengler, P. Deglmann, A. K. Ott, B. Rieger, *Chem. Eur. J.* **2011**, 10.1002/chem.201100578.
[202] L. E. Martinez, J. L. Leighton, D. H. Carsten, E. N. Jacobsen, *J. Am. Chem. Soc.* **1995**, *117*, 5897.
[203] J. Cámpora, M. Á. Cartes, A. Rodríguez-Delgado, A. Marcos Naz, P. Palma, C. M. Pérez, *Inorg. Chem.* **2009**, *48*, 3679.
[204] J.-Y. Liu, Y. Zheng, Y.-G. Li, L. Pan, Y.-S. Li, N.-H. Hu, *J. Organomet. Chem.* **2005**, *690*, 1233.
[205] J.-Y. Liu, Y. Zheng, N.-H. Hu, Y.-S. Li, *Chin. J. Chem.* **2006**, *24*, 1447.
[206] L.-H. Guo, H.-Y. Gao, L. Zhang, F.-M. Zhu, Q. Wu, *Organometallics* **2010**, *29*, 2118.
[207] C. Görl, H. G. Alt, *J. Mol. Cat. A* **2007**, *273*, 118.
[208] A. D. Becke, *Phys. Rev. A* **1988**, *38*, 3098.
[209] J. Perdew, *Phys. Rev. B* **1986**, *33*, 8822.
[210] S. H. Vosko, L. Wilk, M. Nusair, *Can. J. Phys.* **1980**, *58*, 1200.
[211] A. Schäfer, H. Horn, R. Ahlrichs, *J. Chem. Phys.* **1992**, *97*, 2571.
[212] A. Klamt, G. Schüürmann, *J. Chem. Soc. Perkin Trans II* **1993**, 799.
[213] T. Soundiressane, S. Selvakumar, S. Ménage, O. Hamelin, M. Fonceave, A. P. Singh, *J. Mol. Cat. A* **2007**, *270*, 132.
[214] B. Liu, X. Zhao, H.Guo, Y. Gao, M. Yang, X. Wang, *Polymer* **2009**, *50*, 5071.